A STUDY OF CATALYTIC REACTIONS OF SULPHUR DIOXIDE AND CARBON MONOXIDE ON PEROVSKITE-TYPE COMPOUNDS OF THE FORMULA $La_{1-x}Sr_xCoO_3$

By

Rosemary Helen Campbell

A Thesis submitted to the University of London

for the degree of

Doctor of Philosophy in the Faculty of Science

CHEMISTRY DEPARTMENT
Royal Holloway and Bedford New College

October 1986

ABSTRACT

This work investigates the use of the perovskite-type compound $La_{1-x}Sr_xCoO_3$ (x = 0.3, 0.5, 0.6, 0.7) as a catalyst for the reaction

$$SO_2 + 2CO \longrightarrow \frac{1}{x} S_x + 2CO_2$$

Adsorption of SO_2 and CO separately on the degassed catalysts at several temperatures, was followed by TPD (temperature programmed desorption), with mass spectroscopic detection of the desorbed species. Trends in the mass changes on adsorption are explained in terms of the changes in reducibility of $La_{1-x}Sr_xCoO_3$ on changing x.

Computation of the SO_2 TPD results, which showed two and sometimes three adsorbed species, yielded desorption energies of the range 30-200 kJ mol^{-1}.

Several SO_2 and CO mixtures were allowed to flow over $La_{1-x}Sr_xCoO_3$ at various temperatures and flow rates. The removal of SO_2 and production of CO_2 were followed using gas chromatography and sulphur was collected in a cold trap. $La_{0.7}Sr_{0.3}CoO_3$ at 550^oC removed SO_2 from a stoichiometric mixture of SO_2 and CO very efficiently without producing COS. COS production, if it occurs, may be problematical in a commercial SO_2 removal application.

XRD (X-ray diffraction) revealed that the fresh compounds all had the perovskite-type structure, those exposed to either SO_2 or CO retained this structure and those exposed to SO_2 and CO together were no longer $La_{1-x}Sr_xCoO_3$. XRD of the used catalysts showed the presence of $SrSO_4$ on those exposed to only SO_2 and the presence of sulphides of La, Sr and Co, on those exposed to SO_2 and CO.
XPS (X-ray photoelectron spectroscopy) of catalysts exposed to SO_2 and CO indicated sulphidation, with some sulphate species also present.

The results may be explained in terms of the relative oxidizibilities of the SO_2, CO,'SO_2 reduced catalyst', 'CO reduced catalyst', 'reaction reduced catalyst' and $La_{1-x}Sr_xCoO_3$.

The continuation of the operation of the material for the removal of SO_2 suggests that in this instance the active catalyst is no longer a perovskite-type oxide, but possibly a metal sulphide.

ACKNOWLEDGEMENTS

The author wishes to thank

Dr D B Hibbert for his helpful and encouraging supervision.

Mr J Turner the departmental glassblower and the other technical staff for their assistance.

Dr G F M Marriner of the Geology Department for her help with the XRD analyses.

Mr R J B Jakeman of the Chemical Crystallography Department of Oxford University for doing some of the XRD analyses.

The staff of the ETC at Brunel University for doing the ESCA analyses.

Dr L H Sutcliffe for doing the e.s.r. measurements.

The Department of Education for Northern Ireland for financing the project.

Mrs E I Kearsey for typing the thesis.

CONTENTS

Page No.

FIGURES

ABBREVIATIONS

Chemical abbreviations

[S]	sulphur in an unspecified chemical state
HC	hydrocarbon
Co^{3+}	high spin trivalent cobalt
Co^{III}	low spin trivalent cobalt
Co^{IV}	low spin tetravalent cobalt
dpph	1,1-diphenylpicrylhydrazyl

Technical abbreviations

MS	mass spectrometer
GC	gas chromatograph
XRD	X-ray diffraction
XPS	X-ray photoelectron spectroscopy
ESCA	electron spectroscopy for chemical analysis
ESR	electron spin resonance

General abbreviations

r.t.	room temperature
TDP	temperature programmed desorption
s.s.a.	specific surface area
b.e.	binding energy
k.e.	kinetic energy

mmHg is the pressure unit used throughout the thesis

1 mmHg ≡ 133.3 Nm^{-2}

CHAPTER 1

INTRODUCTION AND LITERATURE REVIEW

Sulphur dioxide (SO_2) emissions from coal and oil burning power stations are widely blamed for contributing to acidification of rainfall and the subsequent damage to flora, fauna and architecture. It is therefore imperative that research into methods of desulphurization, of either flue gases or fuel, is carried out.

In the present work the potential desulphurization of flue gases by the reduction of SO_2 to elemental sulphur is investigated. The reduction is accomplished by reaction of the SO_2 with carbonmonoxide (CO), as shown in equation 1.

$$SO_2 + 2CO \rightleftharpoons \frac{1}{x}S_x + 2CO_2 \qquad 1$$

The aim of the present work is to characterize the role of the perovskite-type compound $La_{1-x}Sr_xCoO_3$ ($x = 0.3, 0.5, 0.6, 0.7$), as a catalyst for the above reaction. By gaining an understanding of the mechanism of the reaction plus that an unwanted side reaction, shown in equation 2, which produces carbonyl sulphide (COS), it may be possible to modify the catalyst to give maximum SO_2 removal and minimize the side reaction.

$$CO + [S] \longrightarrow COS \qquad 2$$

Before introducing the experimental procedure adopted in this thesis a very brief example of some of the effects of acid rain will be presented; followed by an introduction to alternative methods of flue gas desulphurization; a brief description of perovskite-type compounds and a review of earlier work done in the research area.

1.1 SOME EFFECTS OF ACID RAIN ON THE ENVIRONMENT

In a recent report (1), the Royal Commission for Environmental Pollution state that acid deposition is one of the most important pollution issues of the present time. They recommend that high priority be given to research on acid deposition and that the CEGB (Central Electricity Generating Board) should introduce, on a pilot basis, certain SO_2 abatement options that are already available.

In the report they state that there is evidence of increasing acidity over the last few decades in parts of Britain, Scandanavia and the United States. They quote pH readings from a survey between 1978 and 1980 in Britain. The mean acidity varied from pH 4.7 in north west Scotland to about pH 4.2 in north east England and south east Scotland. The most acid rain with a pH of 4.1 was detected in southern England. Taking volume into account it seems that the largest inputs of acid rain are in Cumbria, and parts of Scotland. The acidity is comparable with the worst affected areas in Scandanavia and North America, where fish stocks have been severely depleted. They quote references to increasing evidence of acidity affecting fresh-water fish stocks in the United Kingdom. They state that some effects on forest tree growth and performance have been reported, but that the trends are either unclear or too small to be separated from climatic influences. The Forestry Commission are reported to have stated that acid deposition is unlikely to pose an immediate threat to forestry in the United Kingdom.

In a review of a video made by the CEGB (2), entitled Acid Rain, Fry et al (3) describe the history of the effects of acid rain in Norway.

Britain has been widely blamed for acid rain in Norway. This is because of the High Stack Policy of the CEGB which prevents deposition of pollutants in the locality of power stations, but directs it into higher air streams, where the prevailing south westerly winds carry it towards Norway.

During the 1920s salmon and brown trout numbers declined in lakes in southern Norway. By the 1970s major rivers had deteriorated and many salmon, sea trout and brown trout were lost. The first losses were in inland lakes which had low concentrations of dissolved salts. The presence of salts provides a buffer to neutralize acids. By 1983, 1631 lakes had lost their brown trout populations and 141 had lost their perch. Even the lakes with relatively high salt content were suffering. Fry et al claim that below pH 5.5 the fish can no longer regulate their salt balance. The acidity releases aluminium (Al) which is toxic to the fish. In areas of Norway where the effects of acid rain are not yet detected fish survive in acidic lakes. This is because the acidity is due to humic acid from decaying vegetation. Al is bound to the humus and is not toxic to the fish.

The CEGB suggest that liming the lakes will cure the problem. This, however, is expensive, particularly in remote areas and where it must be continuous, such as in rivers. Liming accelerates the breakdown of organic matter and this can cause secondary problems.

As a business enterprize the CEGB naturally want a cost effective solution. Fry et al point out, however, the difficulty of quantifying damage to materials, buildings, health, wildlife, crops, forests and fish.

1.2 METHODS OF FLUE GAS DESULPHURIZATION (FGD)

Of the methods of FGD patented, the majority appear to be based on the use of lime ($CaCO_3$) to remove the SO_2 in the form of calcium sulphate ($CaSO_4$). This by-product, known as gypsum, has many uses and can be sold commercially and used, for example, in building, Plaster of Paris and paper filler.

Leimkuehler (4) has patented FGD apparatus which includes several stages, these are, a spray scrubbing tower with scrubbing solution sump, raw gas inlet and clean gas outlet; a scrubbing solution cycle with a circulatory pump over the sump; a device for adding the scrubbing solution to the sump; a regulatory device for addition, in which SO_2 concentrations are monitored to control the addition device and a by-pass line which is connected between the addition device and the scrubbing solution sump. When the SO_2 concentration in the flue gas exceeds a given threshold the additive is directly added to the scrubbing solution cycle over the by-pass line to ensure that the SO_2 is removed.

Mitsubishi Heavy Industries Ltd., have patented several methods. One of these (5) removes SO_2, dust, hydrogen chloride (HCl) and hydrogen fluoride (HF). The gases are passed over an absorber slurry, containing a calcium compound. Sulphates, carbonates and sulphites of calcium are produced. Highly concentrated slurry is then passed on to an oxidation reactor, containing oxygen (O_2) and sulphuric acid (H_2SO_4), where gypsum is produced. Low concentration slurry from the absorber is returned there to adjust the slurry concentration. The desulphurization is 95% and the gypsum by-product is free from unreacted $CaCO_3$.

Margraf (6) has also patented a method which removes HCl and HF as well as SO_2. The gases can be removed from raw or flue gases by being passed transversely through a bed of granular limestone or other basic materials, which are moving downwards either continuously or periodically. Water is injected through distributing tubes or nozzles either directly upstream or within the limestone bed. It is claimed that SO_2 can be removed at temperatures less than $400^{o}C$.

In the method patented by Krigmont et al (6) the SO_2 containing gas is simultaneously sprayed and dried and a dry powder is produced.

Processes such as that of Margraf (6), where the product appears as a slurry are known as wet scrubber processes and those like that described by Krigmont et al (7) are called dry scrubber processes. The slurries produced in the former are usually dried in order to extract the gypsum.

Cross (8) describes a method in which the product is calcium sulphite ($CaSO_3$). The flue gas leaves the power plant and at the top of a process tower it meets an atomized flow of lime slurry,then $CaSO_3$ and water are formed. The water evaporates and the powder is conveyed pneumatically to a filter.

Unlike the method of SO_2 removal in the present work all of these involve oxidation of the SO_2.

1.3 PEROVSKITE-TYPE COMPOUNDS

Perovskite-type compounds have a structure which closely resembles that of the mineral perovskite ($CaTiO_3$). The structure of the mineral is shown in Figure 1.1.

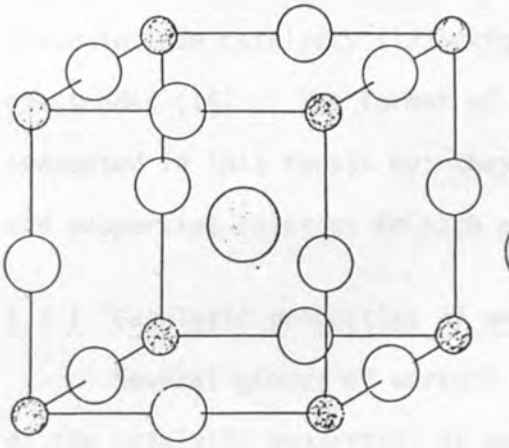

Fig. 1.1 The structure of the perovskite mineral (11)

The Ti cation is at the cube corners, the Ca cation is in the body centred position and the oxygen anions are at the midpoint of the cube edges. The transition metal ion is octahedrally coordinated by oxygen and oxygen is linearly coordinated by transition metal ions (9). The general formula of a perovskite-type compound is ABO_3. A may be a dipositive or tripositive alkaline earth or alkali cation and B is a transition metal of oxidation state 3 or 4. The B cation must have +3 as one of its oxidation states (10). A and B cations can be present as more than one element. Mixed A cation crystals may have oxygen vacancies which are present in order to maintain electrical neutrality when, for example, a dipositive cation is present in the A site of a predominately tripositive cation. In this case a more

accurate general formula is $A_{1-x}A'_xBO_{3-\lambda}$. Voorhoeve et al (11) state that the oxygen vacancies in the perovskite structure play an important role in the catalytic activity.

Several uses for perovskite-type compounds have been explored. These include catalysts (12) oxygen electrodes (13) and laser electrodes (14). The former of these is the basis for the work presented in this thesis but they will all be introduced as the structure and properties relevant to each are interrelated.

1.3.1 Catalytic properties of perovskite-type compounds

Several groups of workers have investigated the research area of the catalytic properties of perovskite-type compounds. Some workers have carried out reactions with and on the surface, while others have provided electronic and magnetic information which with the structural information available about perovskites have served to help to explain the observed results.

Voorhoeve et al (15) state that because of the wide range of ions and valencies which the perovskite structure can accommodate they lend themselves to chemical tailoring. They are relatively simple to synthesize. By appropriate formulation many desirable properties can be tailored. These include the valence state of the transition metal ions, the binding energy and diffusion of oxygen in the lattice, the distance between active sites and the magnetic and conductive properties of the solid.

For the purposes of this review the perovskites have been divided between $La_{1-x}Sr_xCoO_3$, which was studied in the present work and other

perovskite-type compounds. Work involving $La_{1-x}Sr_xCoO_3$ will be reviewed first and because of its direct relevance, in greater detail than the other species which are included to show the scope of the topic.

1.3.1.1 $La_{1-x}Sr_xCoO_3$

$La_{1-x}Sr_xCoO_3$ compounds have been studied for values of $0 \leq x \leq 1$. It has been observed by Askham et al (16) from X-ray diffraction (XRD) that at values of x = 0 to x = 0.5 the structure shows a rhombohedral distortion. From about x = 0.5 onwards splitting of the X-ray lines was no longer visible, indicating the cubic perovskite structure is present. At x = 1 the brown millerite structure exists and not that of perovskite (16, 17).

Jonker and van Santen (18) found that on preparation of $La_{1-x}Sr_xCoO_3$, those compounds with high values of x appeared to contain less oxygen, but maintained the perovskite structure. By substitution of Sr^{2+} for La^{3+} in the lattice the charge change was compensated for by both loss of oxygen and by the formation of tetravalent Co instead of trivalent Co. They observed that when x = 0.6 a maximum of 45% tetravalent Co existed. Beyond x = 0.6 charge compensation took place by an increased loss of oxygen from the lattice and less tetravalent Co was formed. The change in tetravalent Co with x is shown in Fig. 1.2.

Goodenough (19) deduced from magnetic measurements that the introduction of low spin Co^{IV} into the $LaCoO_3$ lattice should increase the crystalline field sufficiently to induce neighbouring high spin

FIGURE 1.2 PERCENTAGE OF TOTAL Co As Co^{IV} AGAINST PERCENTAGE OF (La, Sr) AS Sr (FROM JONKER AND VAN SANTEN (18)) AND CALCULATED δ IN $La_{1-x}Sr_xCoO_3$ AGAINST (La, Sr) AS Sr

e.g. of calculation of δ

$La^{3+}_{0.3}$ $Sr^{2+}_{0.7}$ $Co^{IV}_{0.35}$ $Co^{III/3+}_{0.65}$ $O_{3-\delta}$

(0.3x3) (0.7x2) (0.35x4) (0.65x3)

+ 0.9 +1.4 +1.4 +1.95

Charge due to O^{2-} = -5.65 for neutrality

$$\delta = \frac{6-5.65}{2} \simeq 0.18$$

therefore write $La_{0.3}Sr_{0.7}CoO_{2.82}$

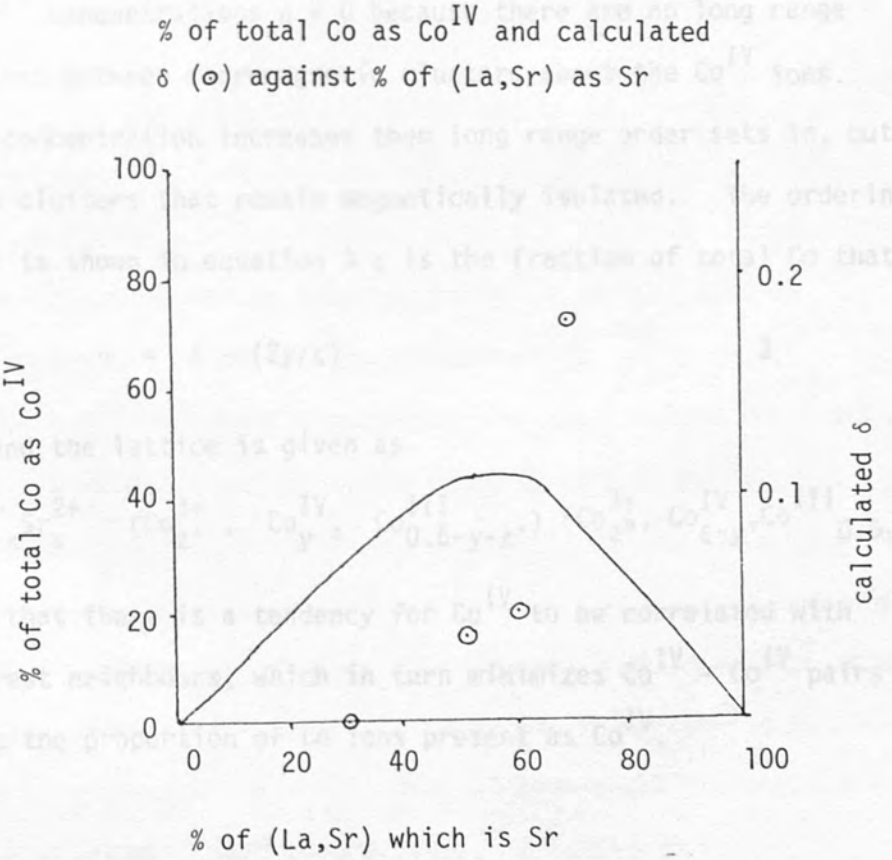

Co^{3+} ions to their low spin Co^{III} equivalents. This can have the effect of creating magnetically isolated clusters in the lattice. At low concentrations of Co^{IV} most of the trivalent Co is high spin Co^{3+}. As the concentration of Co^{IV} increases then so does that of low spin Co^{III}. The Co ions interact across the intervening O^{2-} ion. Co^{3+} - Co^{3+} interactions lead to antiferromagnetism and Co^{IV}- Co^{3+} interactions lead to ferromagnetism, therefore across the $0 \leqslant x \leqslant 1$ range the magnetic properties of the structure change. Co^{III} is diamagnetic and therefore does not interact magnetically with Co^{3+} or Co^{IV}.

Goodenough introduces the idea of an ordering parameter η. At low Sr^{2+} concentrations $\eta = 0$ because there are no long range interactions between ferromagnetic clusters about the Co^{IV} ions. As the Co^{IV} concentration increases then long range order sets in, but there are clusters that remain magnetically isolated. The ordering parameter is shown in equation 3 ζ is the fraction of total Co that

$$\eta = 1 - (2y/\zeta) \qquad 3$$

is Co^{IV} and the lattice is given as

$$La^{3+}_{1-x}Sr^{2+}_{x} \quad (Co^{3+}_{z'}, \ Co^{IV}_{y}, \ Co^{III}_{0.5-y-z'}) \ (Co^{3+}_{z''}, \ Co^{IV}_{\xi-y}, Co^{III}_{0.5-\xi+y-z''})$$

The fact that there is a tendency for Co^{IV} to be correlated with Co^{3+} nearest neighbours, which in turn minimizes Co^{IV} - Co^{IV} pairs may limit the proportion of Co ions present as Co^{IV}.

Sis et al (9) investigated magnetic properties of $LaCoO_3$. They found that trivalent Co existed predominately in its low spin form below 125°C. Above this the high spin state increased and at 375°C a rapid increase in high spin Co^{3+} appeared, due to long range ordering occurring at that temperature.

Yakel (20) looked at the way which structural properties of $La_{1-x}Sr_xCoO_3$ changed on Sr^{2+} substitution. Yakel noted an increase in cell volume when Sr^{2+} was substituted for La^{3+}. Lattice expansion occurs on substitution of the similarly sized Sr^{2+} for La^{3+} and consequent change to the smaller Co^{IV} from Co^{3+}. A possible explanation given was that the percentage charge decrease at A sites was greater than the increase at B sites; this may, Yakel postulates, decrease the partial covalent character of the bonds involving oxygen ions and cause lattice expansion.

Gai and Rao (21) studied the structure of $La_{1-x}Sr_xCoO_3$, using electron diffraction. Their work shows evidence for a doubling of the cubic cell when x = 0.5 compared to x = 0.3. They suggested that this could be attributed to ordering of La^{3+} and Sr^{2+} ions on alternate sites due to strict charge neutrality.

Temperature programmed desorption (TPD) experiments have been carried out on samples which have been pretreated by exposure to O_2.

Yamazoe et al (17) adsorbed O_2 on samples with a range of x values, at 100 mm Hg and 800°C. The samples were then cooled and evacuated before TPD. Oxygen was detected by a thermal conductivity detector (TCD). Two peaks were observed, a broad one below 800°C and a sharp one above this temperature. The size of both peaks increased with increasing x value. The surface states were examined using XPS.

Two oxygen species were identified. The peak observed with the lowest binding energy was assigned to oxygen in the crystal lattice. The other peak was assigned to adsorbed oxygen and this increased in size with increasing x value. The amount adsorbed and subsequently desorbed was shown therefore, by XPS and TPD, to increase with increasing Sr^{2+} content. On looking at evacuated samples at room temperature, 300°C, 500°C and 800°C the XPS peak assigned to surface oxygen diminished and became narrower. The narrowing of the peak was said to be due to the heterogeniety of adsorbed oxygen at low temperatures and the removal of species with lower binding energies as the temperature was increased. At 800°C the lower binding energy XPS peak was observed to broaden, it was speculated that this may be due to the loss of lattice oxygen at this temperature causing a new defect lattice.

No change was observed in the Co $2p_{3/2}$ and La $3d_{5/2}$ levels but a slight increase in the binding energy of Sr $3p_{3/2}$ after evacuation at 500°C suggested that adsorbed oxygen may have been desorbed from sites adjacent to Sr^{2+} ions.

Sieyama et al (22) continued investigations into the desorbed oxygen species discussed above. By plotting the specific reactivity of oxygen, obtained by pulsing hydrogen over samples with differing x values and taking their initial oxygen reduction rate and plotting this against x; it was observed that the reactivity appears to decrease with increasing x. The amount of oxygen reduced, however, was shown to increase with x. The total reactivity was taken as a product of the specific reactivity and the amount of oxygen, it therefore peaked between $x = 0.2$ and $x = 0.4$.

George and Viswanathan (23) carried out a TPD of oxygen adsorbed at 100°C on $La_{0.9}Sr_{0.1}CoO_3$. They observed two peaks between 400°C and 500°C. They attributed these to a resolution of the TPD peak assigned by Yamazoe et al (17), to adsorbed oxygen below 800°C. The fact that there were two peaks observed they concluded was a confirmation of the assumption that the broadness of the XPS peaks presented by Yamazee et al indicated more than one type of oxygen adsorption.

Nakamura et al (24) also carried out some TPD experiments on $La_{1-x}Sr_xCoO_3$ which had been exposed to 100 mm Hg O_2 at 300°C and cooled to 150°C and then evacuated. In agreement with the work cited above by Yamazoe et al, the rate of O_2 desorbed increased with Sr^{2+} content in the $La_{1-x}Sr_xCoO_3$, between x = 0 and x = 0.6. Nakamura et al, however, did not attribute most of the oxygen to adsorbed oxygen. They observed that some amount of the oxygen desorbed at high temperatures was certainly lattice oxygen as its amount was comparable to greater than a monolayer of oxygen. The continuity between the low and high temperature desorption made it seem impossible to distinguish whether the desorption at low temperature was of weakly held lattice oxygen or adsorbed oxygen. The high temperature desorption was at temperatures lower than those which Yamazoe et al attributed to desorption of lattice oxygen.

Misono and Nitadori (25) preadsorbed oxygen at 300°C then cooled $La_{1-x}Sr_xCoO_3$ to room temperature and substituted a helium (He) stream. TPD experiments carried out were in agreement with the other works cited in this review. The rate of desorption increased with increasing x.

All of the work done on TPD of oxygen from $La_{1-x}Sr_xCoO_3$ may not be directly comparable due to the different conditions of oxygen adsorption before TPD. A conclusion, however, which is common to all of the workers was that reducibility of the $La_{1-x}Sr_xCoO_3$ increased with increasing x.

Isotopic exchange and equilibration of oxygen experiments were carried out by Misono and Nitadori (25). Prior to the reaction the samples were heated with 100 mm Hg pure circulating O_2 at 300°C and then evacuated for 1 h at 300°C. The samples were then exposed to a mixture of $^{18}O_2$ and $^{16}O_2$. A decrease in $^{18}O_2$ remaining in the gas phase was observed with increasing x, from x = 0 to x = 0.6. This was presumed to represent the capability of the catalysts to dissociate O_2 in the gas phase and to represent the mobility of oxygen in the crystal lattice. Increasing mobility would ensure that the recombination of ^{18}O atoms would be less likely.

Tseung et al (26) also looked at the dissociation of $^{18}O_2$ over $La_{0.5}Sr_{0.5}CoO_3$. They passed a 3.75/1 mixture of $^{16}O_2$ and $^{18}O_2$ through a reactor containing $La_{0.5}Sr_{0.5}CoO_3$ with a surface saturated with oxygen at 180°C. The detection of mass 34 confirmed that dissociative chemisorption had taken place.

The catalytic activity of $La_{1-x}Sr_xCoO_3$ with regard to CO oxidation has been investigated by several groups of workers.

Nakamura et al (24) allowed stoichiometric amounts of CO and O_2 over catalysts, some of which had been pretreated with O_2 and others which had not. It was observed that catalytic activity was always higher for those catalysts which had been pre-exposed to O_2. This is

in agreement with the work on CO oxidation done by George and Viswanathan (23), who looked at CO oxidation over $La_{0.9}Sr_{0.1}CoO_3$ and $La_{0.7}Sr_{0.3}CoO_3$. They too allowed stoichiometric amounts of CO and O_2 over the catalysts with and without oxygen pretreatment. Those with oxygen pretreatment showed the highest catalytic activity. Viswanathan and George (27) found that except for $LaCoO_3$ the conductivity increased in an O_2 atmosphere and decreased in a CO atmosphere. From this and infrared (IR) observations they postulated a mechanism involving CO reacting with activated lattice oxygen and oxygen adsorbed in oxygen vacancies giving intermediate carbonate (CO_3^{2-}) species before these decomposed to produce CO_2.

Nakamura et al (24) observed that catalytic activity appeared to increase with x until x = 0.2 and then to decrease with x. Re-oxidation of the catalyst by oxygen after reduction by CO was also investigated. The rate of re-oxidation decreased with increase in x. When the rate of reduction of the catalyst by CO and rate of re-oxidation by O_2 were plotted against the degree of reduction the crossover points of the two rates for different values of x showed a trend comparable to that of the catalytic activity.

The coincidence of these two trends suggested to Nakamura et al that a redox mechanism existed where the CO reduced the surface and it was re-oxidized by oxygen. At values of x greater than x = 0.4 this reduction and re-oxidation were both slow. For the reaction in the presence and absence of oxygen little difference was noted between the rates of CO oxidation at x = 0.6, but the rate increased when oxygen was present for lower values of x. This indicated that in addition

the redox mechanism, adsorbed oxygen had to be accounted for in the CO oxidation. Iwamoto et al (28) suggest that metal oxides which catalyse partial oxidation are poor adsorbents while those which are good adsorbents catalyse total oxidation.

In a later paper, Nakamura et al (29) declare that the oxidation state of catalysts during CO oxidation can be found from the difference between the total amount of CO_2 formed and the amount of CO_2 accounted for by the reaction of gaseous oxygen. The difference is the amount of CO_2 formed by lattice oxygen and is therefore proportional to the degree of reduction which they stated was equivalent to the oxidation state. For experiments with x = 0, 0.2 and 0.6 the results indicated that the catalyst was in a lower oxidation state as x increased. When the partial pressure of oxygen increased then the reduction was less but still increased with x.

Nakamura et al (30) endeavoured to discover what was the rate determining step (RDS) for the redox cycle of $La_{1-x}Sr_xCoO_3$. They suggest two possible steps. The first is the surface reaction and the second is diffusion of oxygen in the bulk. They decided that it could not be the first because the rates at 2% and 5% reduction were different showing that diffusion could not be fast. They also observed (31) that equilibration of oxygen in the gas phase is much quicker than the bulk oxygen which did not support the hypothesis of rapid diffusion. The fact that reoxidation became slower with increasing x cannot be explained by a diffusion controlled RDS, since the rate of oxygen diffusion in the bulk should increase with the

concentration of ion defects and therefore with x. They noted (31) that release of oxygen from the bulk became more difficult at higher calcination temperatures and that this was in conformity with the trend of catalytic activity. It was concluded that neither of the two steps was rate determining, they both contributed.

Viswanathan and George (27) plotted the activation energy for oxidation of CO over $LaCoO_{3-\delta}$ against δ for δ = 0 to 0.07. It was found that the activation energy decreased with increasing δ. This was interpreted as meaning that the ease of oxidation of CO was related to the ease of oxygen removal, whether adsorbed or from the lattice.

Misono and Nitadori (25) found that increasing the calcination temperature of $La_{1-x}Sr_xCoO_3$ led to better catalytic activity, except for $LaCoO_3$, where the effect was minimal. This agrees with Nakamura et al (29) who found that activity increased up to a calcination temperature of 850°C. Above this temperature the activity per unit weight decreased,apparently due to surface area effects.

Voorhoeve et al (32) found that $LaCoO_3$ was an active catalyst for CO oxidation.

Tascon and Gonzalez-Tejuca (33) looked at straightforward adsorption of CO on $LaCoO_3$ (x = 0). They observed two adsorbed species, one below 375°C and the other above this temperature. Above 375°C adsorption is slow and the amount adsorbed exceeds a monolayer and it is concluded that the CO penetrates the oxide surface. 375°C is also a significant magnetic threshold according to Sis et al (9). Heats of adsorption were calculated. Low temperature adsorption was found

to be physisorption, with adsorption heats calculated between 15 - 5 kJ mol^{-1}, that above 375^{o}C was chemisorption, with a heat of adsorption of 49 kJ mol^{-1}. Tascon and Gonzalez-Tejuca suggest that the high temperature species takes part in surface reduction which is controlled by the diffusion of oxygen through the lattice. IR spectroscopy revealed CO_3^{2-} ions on the surface as observed by Viswanathan and George (27), which suggested that the CO adsorbed on oxygen sites. CO and CO_2 appeared to compete for sites but O_2 did not.

The simultaneous oxidation of CO and reduction of SO_2 has also been investigated, and is of particular relevance to the present work. Hibbert and Tseung (12) have shown that $La_{0.5}Sr_{0.5}CoO_3$ catalyses the reaction which is shown in equation 1, page 20 . At temperatures greater than 550^{o}C a mixture of 1% SO_2, 2% CO in nitrogen (N_2) was allowed to flow over $La_{0.5}Sr_{0.5}CoO_3$. Total removal of gas phase sulphur was noted for an initial period of 30 min. Then the concentration of gas phase sulphur increased and steady state values were attained in about 1 h. The catalytic activity remained stable for at least 36 h. XRD analysis of used catalysts showed no substantial difference in structure after 6 h or 36 h. If an excess of CO was present then carbonyl sulphide (COS) was produced. 3-4% O_2 added to the feed gas when there was less than the stoichiometric amount of CO present led to a drop in SO_2 conversion efficiency by up to 10%. O_2 affected the conversion efficiency only if there was insufficient CO to react with it. The efficiency always recovered if the feed gas was adjusted to provide sufficient CO to react with any O_2 or SO_2 present. At no time was sulphur trioxide (SO_3) detected. In the presence of water (H_2O)

hydrogen sulphide (H_2S) was detected but always at a concentration of an order of magnitude less than COS. Equations 4 and 5 show the probable reactions for production of H_2S.

$$CO + H_2O \rightleftharpoons H_2 + CO_2 \qquad 4$$

$$H_2 + \tfrac{1}{2} S_2 \longrightarrow H_2S \qquad 5$$

The most efficient conversion observed was for a flow rate of 100 cm^3min^{-1} and a contact time of 0.25s. Contact times both above and below this were less efficient. Long contact times led to increases in COS and H_2S formation. XRD and sulphide analysis suggested that the catalyst had altered during the reaction. All sulphur present appeared to be as sulphide and there was evidence for Co and Sr sulphides. Metal sulphides, however, are known to catalyse the production of COS (34).

Bazes et al (35) studied the oxidation of CO and reduction of SO_2 over $LaCoO_3$. They found that for complete reduction of SO_2, greater than the stoichiometric amount of CO was required otherwise COS was produced, this disagrees with the observations by Hibbert and Tseung for $La_{0.5}Sr_{0.5}CoO_3$. The maximum temperature for no production of COS in the work of Bazes et al was found to be 344^oC, which is close again to the 375^oC temperature which appeared so important in the work of Sis et al (9) and Tascon and Gonzalez-Tejuca (33).

Investigations into the reaction involving nitrogen oxides, equivalent to equation 1, have been done, bearing in mind the applications

in the automobile industry. Nitrogen oxides and CO are produced during fuel combustion and are then emitted to the atmosphere. They take part in photochemical reactions and therefore contribute to photochemical smog which is possibly best known for its presence over Los Angeles.

The reaction between nitrogen oxide (NO) and CO is given in equation 6.

$$CO + NO \longrightarrow CO_2 + \tfrac{1}{2}N_2 \qquad 6$$

Voorhoeve et al (36) state that introduction of Sr^{2+} for La^{3+} into the $LaCoO_3$ lattice leads to a decrease in activity. The La^{3+}:Sr^{2+} ratios were not given but other workers quoted in this review including Nakamura et al (24) found that catalytic activity for CO oxidation reached a maximum between x = 0.2 and x = 0.4. After investigating several active perovskite-type catalysts which all had similar electronic configurations, it was suggested that the CO oxidation took place by a suprafacial process involving the electronic configuration of Co. The catalyst surface appeared to provide orbitals of the correct energy and symmetry for bond formation with reactions and intermediates.

In the same publication (36) Voorhoeve et al suggest that NO reduction was intrafacial. The reduction was carried out over $LaCoO_3$ at temperatures where it was claimed by Sorenson et al (37) that reduction of the $LaCoO_3$ surface occurred by loss of oxygen. Sorenson et al observed that weight loss started at 500°C and attributed this to loss of oxygen. They found that temperatures

exceeding 600^{o}C were required to initiate reduction of NO in the presence of exhaust gases containing NO, CO and hydrocarbons (HC). Equations 7 and 8 have been suggested by Mars and van Krevelen (38), for reduction reactions on oxide catalysts.

Aromatic compound + oxidized catalyst $\longrightarrow$ oxidation products + reduced catalyst 7

Reduced catalyst + oxygen $\longrightarrow$ oxidized catalyst 8

These equations have been adapted by Voorhoeve et al to illustrate the intrafacial reduction of NO, in equations 9 and 10.

$$M - O - M + CO \longrightarrow M - V_o - M + CO_2 \quad 9$$

$$M - V_o - M + NO \longrightarrow M - O - M + \tfrac{1}{2}N_2 \quad 10$$

Lauder (39) also found that $LaCoO_3$ was an efficient catalyst for NO reduction and CO oxidation.

Bauerle et al (40) studied CO oxidation and NO reduction over $LaCoO_3$ and $La_{0.85}Sr_{0.15}CoO_3$. NO reduction was greater after CO pretreatment. This supports the mechanism suggested in equations 9 and 10. The Sr^{2+} substituted compound was more efficient than the $LaCoO_3$. This agrees with other workers such as Nakamura et al (24) who stated that at low x values Sr^{2+} substitution increased catalytic activity.

Sorenson et al (37) suggested two reasons for the catalytic activity of $LaCoO_3$. One was the presence of oxygen defects the other the presence of Co metal. The increase in activity caused by substitution of Sr^{2+} for La^{3+} and subsequent increase in oxygen defects, but not the formation of Co metal observed by Sis et al (9), confirmed that the oxygen defects enhanced catalytic activity.

Sorenson et al (37) looked at HC oxidation as well as the removal of NO and CO. Removal of all of these was dependent on the overall composition of the inlet gas.

Sekido et al (41) studied the oxidation of CO and HC and reduction of NO_2 in exhaust gases over $La_{1-x}Sr_xCoO_3$ at 600°C. For a mixture of 50 ppm HC, 50 ppm CO and 50 ppm NO_2 in N_2 it was found that maximum CO oxidation was favoured at low values of x, that is, between x = 0.15 to x = 0.2. Removal of HC or NO_2 was favoured at high x values of x = 0.8 to x = 0.9. It was therefore suggested that x in an $La_{1-x}Sr_xCoO_3$ catalyst ought to be chosen, depending on the composition of the feed gas, for example, for a high percentage of CO a low x value should be used.

Nakamura et al (24) looked at the oxidation of propane (C_3H_8) and methanol (CH_3OH) as well as CO, which was discussed earlier on page 33, with reference to the catalyst oxidation state. The catalytic oxidation of C_3H_8 was found to increase as x increased up to x = 0.2, then to become constant or decrease slightly with further increase in x. When, however, C_3H_8 or CH_3OH were in a pulsed system, in the absence of oxygen, the extent of CO_2 formation which reflects oxidation power of the catalyst increased as x increased. Only CO_2 and H_2O were formed. When C_3H_8 was copulsed with O_2 the amounts of CO_2 formed increased with x up until x = 0.2, but decreased when $x \geq 0.4$. This closely resembles the catalytic activity in a flow system.

Nakamura et al (24) suggest that as stated earlier for CO oxidation, the oxidation of C_3H_8 and CH_3OH occurs via a redox mechanism. They state that at low values of x the supply of gaseous oxygen is probably faster than that from the bulk. They suggest that the surface is on average in a higher oxidation state and becomes more reactive in the presence of gaseous oxygen than in its absence.

The results of Nakamura et al (24, 29) contradict those of Sekido et al (41) with respect to removal of HC. Nakamura et al state that low values of x are suitable for removal of HC and Sekido et al quote high x values. It is not clear however, from the latter work which HC are referred to and in what form they are removed. Between x = 0 and x = 0.4 inclusive, C_3H_8 at 227°C, CH_4 at 352°C and CO at 100°C all had a maximum oxidation rate at x = 0.2, although C_3H_8 virtually levelled off at x = 0.1, at a rate an order of magnitude greater than for x = 0 (21).

1.3.1.2 Catalytic properties of perovskite-type compounds excluding $La_{1-x}Sr_xCoO_3$

A brief review of some of the effects on catalytic activity of perovskite-type compounds with differing A and B cations will be presented.

Several workers have attempted to show a relationship between the mobility of oxygen in perovskite-type structures and catalytic activity. A reference to work by Nakamura et al (20) has been made in the previous section.

Chauvin et al (42) compared three compounds; $La_3Ba_3Cu_6O_{14+\delta}$ which has a perovskite-type structure and K_2NiF_4 and $Sr_3Ti_2O_7$ which have perovskite related structures. The compounds were heated in flowing argon and the oxygen evolved was detected by a MS. The MS results were in accord with thermogravimetric analysis (TGA) results. The MS data provide a differential of the oxygen loss and therefore indicate oxygen mobility. Oxygen loss was greatest and most rapid from $La_3Ba_3Cu_6O_{14+\delta}$. Oxygen was recovered on cooling $La_3Ba_3Cu_6O_{14+\delta}$. The catalytic activity of the compounds with respect to CO oxidation was also investigated. The perovskite-type structure showed the best catalytic activity and this was attributed to the mobility of the bulk oxygen.

Teraoka et al (43) prepared sintered discs of $La_{1-x}Sr_xCo_{0.4}Fe_{0.6}O_{3-\delta}$ where x = 0.0, 0.4, 0.8 and 1.0. They looked at the permeation of oxygen through these over the temperature range 300 - 1150 K (7 - 877^{o}C). The temperature of onset of permeation decreased as x increased and the rate of oxygen permeation increased with x for a given constant temperature. They refer to works by Yamazoe et al (44) and Ishigaki et al (45) and thereby conclude that the oxygen permeation is due to the creation of oxygen vacancies formed by substitution of La^{3+} for Sr^{2+} and that this allows diffusion of oxygen. The driving force for this diffusion was only the oxygen partial pressure. They also found that a low proportion of Fe compared to Co led to increased permeability and attributed this to the smaller ionic radius of Co^{3+} compared to Fe^{3+} and lower bonding energy of Co and oxygen than Fe and oxygen. Teraoka et al (46) state that a little

Fe at high Sr content helps to maintain the perovskite-type structure so important to the oxygen permeation. $SrCoO_{2.5}$ has poorer permeation properties possibly because of its brown millerite structure (41).

Teraoka et al (43) found that at temperatures greater than 1073 K (800^{o}C) oxygen permeation followed Ficks Law but below this temperature deviations occurred. This was said to show that the processes of oxygen sorption and desorption were also important in the mechanism of oxygen permeation. If indeed as is suggested by Chauvin et al (42), oxygen mobility is related to catalytic activity, then the suggestion by Teraoka et al (43) agrees with that of Nakamura et al (31), that the RDS of the redox cycle of $La_{1-x}Sr_xCoO_3$ is a combination of surface reactions and oxygen diffusion.

Tascon and Gonzalez-Tejuca (47) studied the catalytic activity with respect to CO oxidation of $LaMeO_3$ (Me^{3+} = V^{3+}, Cr^{3+}, Mn^{3+}, Fe^{3+}, Co^{3+} and Ni^{3+}). They found that activity for CO oxidation decreased in the order $Co^{3+} > Ni^{3+} > Mn^{3+} > Fe^{3+} > Cr^{3+} > V^{3+}$, as a function of temperature. The log of the catalytic activities at 500 K (237^{o}C) were plotted against the number of d electrons of the transition metal cation. The order of activity was shown as above but maxima appeared at $LaMnO_3$ (d^4) and $LaCoO_3$ (d^6). Iwamoto et al (28) looked at the equivalent transition metal oxides and found maxima for oxygen chemisorption at the equivalent oxides to those perovskites which showed high catalytic activity. Iwamoto et al. (28) state that less stable oxides which therefore readily

form surface defects (like perovskite-type oxides) exhibited higher catalytic activity.

Fierro and Gonzalez-Tejuca (48) found that $LaCoO_3$ was a better catalyst for oxidation of CO than $LaCrO_3$. They stated that this may be due to $LaCrO_3$ being more difficult to reduce or to $LaCrO_3$ being a p-type semiconductor and $LaCoO_3$ being able to exist as suggested by Meadowcroft (49) as a p or n type semiconductor. This property of $LaCoO_3$, they postulated, may account for a high oxygen adsorption and ready reducibility.

Voorhoeve et al (36) relate that partial substitution, in the ABO_3 perovskite-type structure, of A atoms which cause B atoms to change their oxidation state in order to compensate for charge changes have different effects on different B atoms. They summarized some data as follows: (a) introduction of Cr^{2+} and Cr^{4+} in $LaCrO_3$ has large effects on the catalytic activity, (b) introduction of Co^{2+} (formed, they said, by electron transfer from Co^{III} to Co^{3+}) and Co^{4+} in $LaCoO_3$ has smaller more equivocal effects and (c) introduction of Mn^{4+} in $LaMnO_3$ or Fe^{4+} in $LaFeO_3$ has effects contrary to the introduction of Cr^{4+} in $LaCrO_3$, after CO oxidation. The results cannot be explained in terms of conductivity. In keeping with the hypothesis referred to earlier about suprafacial catalysis, Voorhoeve et al suggest that investigations into energy levels and symmetry are carried out.

In the same publication as cited above, Voorhoeve et al discuss perovskite oxides where A = La, Sr, Ca, Bi, K, Rb, Na and Nb. They found that the range of catalytic activities for CO oxidation

depend on the stoichiometry of the feed gas. $LaFeO_3$, for example, was found to be inactive with high partial pressures of oxygen, but near the stoichiometric ratio of CO and O_2 it had fair activity.

Particular A cations appear to have specific qualities in the structure for given reactions in different environments. Inclusion of lead (Pb) in catalysts intended for use in automobile engines has been found by Voorhoeve et al (32) to reduce catalyst poisoning by lead. Lead is present in petrol as lead tetraethyl. $La_{1-x}Pb_xMnO_3$, $Pr_{1-x}Pb_xMnO_3$ and particularly $Nd_{1-x}Pb_xMnO_3$ ($0.4<x<0.6$) showed less severe poisoning by lead than other catalysts.

Doping perovskite-type catalysts with platinum (Pt) has also led to increased catalytic activity (50, 51, 52). Gallagher et al (51) investigated the oxidation of CO in the presence of SO_2, using $La_{0.7}Pb_{0.3}MnO_3$ as a catalyst. The catalytic activity was found to increase with the amount of platinum in the catalyst. It was concluded that as little as 200 ppm of platinum in the catalyst increased its resistance to poisoning by SO_2. It appeared that a Pt/Pb alloy formed but that lead sulphate ($PbSO_4$) was produced in the presence of SO_2 causing the Pt to be released.

Croat and Tibbets (53) also looked at $La_{0.7}Pb_{0.3}MnO_3$ with respect to CO oxidation and found that only those samples prepared in a Pt crucible had high catalytic activity. 75 ppm Pt was found to increase catalytic activity by an order of magnitude. The activity was said to be higher than for free Pt crystals due to the segregation of Pt on the surface. The perovskite structure was confirmed by XRD.

Addition of Pt to $La_{0.5}Cu_{0.5}MnO_3$ did not lead to increased catalytic efficiency. Johnson et al (51) found that Pt poisoned the catalyst in the absence of SO_2. It was suggested that a Pt/Cu alloy formed. In the presence of SO_2 the activity did increase but it was less than, for example, $La_{0.5}Sr_{0.5}MnO_3$.

Happel et al (10) looked at the oxidation of CO and reduction of SO_2 over $Ca_{0.1}La_{0.9}TiO_3$. As in the case of $La_{1-x}Sr_xCoO_3$ excess CO reacted with sulphur produced from the reduction of SO_2 to form COS.

$LaMnO_{3.15}$ was found to be a more active catalyst for NO reduction than $LaMnO_{3.01}$. Voorhoeve et al (32) found however, that the oxygen rich compound produces ammonia (NH_3) as well as the N_2 and N_2O produced by the other catalyst. In another publication (11) Voorhoeve and his co-workers found that the effective reduction rate for NO in the series $(AA')MnO_3$ decreased in the order (Bi,K)>La>(La,Rb)≃ (La,K)≃(La,Na)>(La,Pb)≳(La,Sr). They suggest that the catalytic activity is determined by molecular adsorption of NO on a transition metal ion of low valence, combined with dissociative adsorption of NO on lattice oxygen.

The $La_{1-x}Sr_xCo_{1-y}Fe_yO_3$ discussed on page 43 has been tested for its catalytic efficiency by Tachibana et al (54). 40 mol % $La_{0.35}Sr_{0.65}Co_{0.7}Fe_{0.3}O_3$ and 60 mol % $SrTiO_3$ were mixed, baked for 3 h at 1300° in air and pulverized. 0.3 g of this was deposited on 0.4 g Al_2O_3 - SiO_2 fibre, packed in a quartz glass tube and used to treat a gas containing a mixture of 42 ppm NO_2 and 15 ppm CO in N_2. The gas was fed at a superficial velocity of 3000 h^{-1} at 900° and removal of CO was 64.5% and N_2 production was 69.0%.

Madgavkar and Vogel (55) investigated the possibility of using $La_{0.6}Sr_{0.4}Pt_{0.1}Co_{0.9}O_3$ as a catalyst for the combustion of hydrogen (H_2), CO and aliphatic HC with up to 7 carbons. They have patented a method which utilizes the heat produced from the combustion, before the waste gases are vented to the atmosphere. By always providing a constant substoichiometric amount of O_2 they state that the heat produced will be constant. They claim that this will prevent damage to turbines caused by heating and cooling cycles. The provision of insufficient O_2 for complete combustion, they say, will allow the other gases to be preferentially combusted before CH_4. This they would emit as it is not regarded as a pollutant in moderate amounts. They suggest that this would be useful in a plant where preferably 5 mol % and most preferably 10 mol % of the combustible component is CH_4. The main object of the exercise was to decrease the CO_2:CO ratio emitted. The perovskite gave a ratio of 18.8 - 47.3:1 CO_2:CO as compared to 0.56-3.64:1 CO_2:CO for Co-Pt catalysts.

For the catalyst Madgavkar and Vogel recommend that the lanthanide selected is La or cerium (Ce) because they are available relatively cheaply. They suggest that the B cation is 80 - 99% and preferably 90 - 99% from a non Pt group. They select Fe, Co or Ni. They stress the importance of the provskite-type structure.

1.3.2 Use of $La_{1-x}Sr_xCoO_3$ as an oxygen electrode

It is of interest here to review work done to investigate the way in which $La_{1-x}Sr_xCoO_3$ works as an oxygen electrode, because the

mechanisms suggested may bear some relationship to those reactions which occur when $La_{1-x}Sr_xCoO_3$ is employed as a catalyst in gas phase reactions.

The earliest mention of such work appears to be that of Meadowcroft (49) in 1970 and the study by Tseung and Bevan (56) gives an adequate summary of the topic. Meadowcroft perceived the development of high energy density batteries which would be particularly useful as an energy source. He visualized that these could be used in, for example, urban transport; they could be recharged overnight and thereby level out demand for electricity. He recognised the need for a material like Pt which could reduce oxygen from the air to hydroxide ion (OH^-) in a concentrated alkaline solution and to perform the reverse process for recharging. Tseung and Bevan (56) in addition suggest that the development of a reversible oxygen electrode could cheapen the manufacture of oxygen.

The activity of $LaCoO_3$ was discovered by Meadocroft (49) because he investigated semiconducting oxides with high conductivities. He looked at NiO, CoO, SnO_2, InO_2, $LaCrO_3$, $LaCoO_3$, $PrCoO_3$ and $SrMoO_4$, all of which, except $SrMoO_4$, he doped with impurities. Only $LaCoO_3$ and $PrCoO_3$ were promising and of these $LaCoO_3$ was cheaper. He found that the conductivity of $LaCoO_3$ could be increased by doping Sr and Ni for La and Co respectively. The high activity which these compounds exhibited was attributed to the Co because increasing both Sr and Ni increased the activity and $PrCoO_3$ was active whereas $LaCrO_3$ was not. In an attempt to explain the activity Meadowcroft cited two differences between $LaCoO_3$ and $LaCrO_3$. The first was that $LaCoO_3$ could exist as

a p or n type semiconductor and that $LaCrO_3$ exists only as a p type. The $LaCoO_3$ band gap was given by Meadowcroft as 0.30 eV. He suggests that the amphoteric behaviour and narrow band gap may aid the adsorption of oxygen and subsequent release of ions. The second difference was that $LaCrO_3$ is antiferromagnetic and has a Neél temperature of 320 K (47^oC). $LaCoO_3$ was reported to have no long range magnetic order. The activity of $LaCrO_3$ was said to improve above its Neél point.

Tseung and Bevan (56) state that the overall reduction of oxygen is written as in equation 11

$$2H_2O + O_2 + 4e^- \rightleftharpoons 4OH^- \qquad 11$$

For a reversible electrode they state that for the anodic evolution of O_2 gas and cathodic reduction of O_2 to OH^- to occur, they must occur just above and below the reversible point. The reaction requires dissociative adsorption of O_2 and therefore "side on", as opposed to "end on" adsorption of the O_2 molecule.

Winter (57) found that above its Neél temperature, nickel oxide (NiO) dissociatively adsorbed O_2, but below this temperature it only non-dissociatively chemisorbed it. It, therefore, seemed likely that above the Neél point, side on adsorption, which required an electron to be transferred to each end of the O_2 molecule simultaneously, occurred. It, therefore, appears likely that Meadowcroft's hypothesis about the Neél temperature may be correct.

Tseung et al (58) found that the reversible oxygen electrode potential could be achieved for NiO doped with lithium (Li) in 75% potassium hydroxide (KOH), above the Neél point. This showed that the electrochemical reaction was comparable with that done by Winter, in the gas phase. It was therefore assumed that this is true for $La_{1-x}Sr_xCoO_3$.

Tseung and Bevan (56) realized that the reaction given in equation 11 required that there always be a continuous layer of OH^- ions on the electrolyte and that this would only be possible in a strongly alkaline solution. They therefore looked at alkali resistant conducting oxides whose room temperature magnetic qualities are like those of paramagnetic NiO. They looked at $(La,Sr)(Ni,Co)O_3$ as Meadowcroft had done. They too attributed the properties specifically to the Co ion. Meadowcroft suggests that the activity is due to either the type of semiconductor or the magnetism of the compound. Tseung and Bevan propose that the trivalent Co ion in an octahedral perovskite interstice of O^{2-} anions, exhibits a crystal field splitting approximately equal to the exchange energy. They believe that the spin state of Co is crucial to O_2 adsorption. The existence of the ferromagnetic exchange between Co^{3+} and Co^{IV} discussed in section 1.3.1, with reference to work by Goodenough (19) satisfies the important criterion for "side on" chemisorption of O_2. They acknowledge that the substitution of 50% Sr^{2+} for La^{3+} will produce more Co^{IV}. They claim that the electron hopping between Co^{3+} and Co^{IV} by double exchange via intermediate O^{2-} anions enhanced the conductivity and magnetic character.

Tseung and Bevan prepared $La_{1-x}Sr_xCoO_3$ with x = 0, 0.2 and 0.5, by freeze drying (56). The perovskite structure was confirmed by XRD. The Sr^{2+} doped electrodes showed the theoretical current-potential relationship at 25°C, for the O_2 reduction and showed no change of slope of the current-potential curve on changing from the cathodic to the anodic mode or vice versa. The latter observation was deemed the proof that the reaction was truly reversible. Equivalent experiments with $LaCoO_3$ and Pt black were not reversible. The current density increased linearly with temperature for the perovskites but not for the Pt black. The relationship between the rate of oxygen chemisorption and the partial pressure of O_2 was as expected for the system where for every O_2 molecule adsorbed "side on" there will be two electron transfer centres, at particular temperatures, even though the electrodes were porous. This relationship was not found for teflon bonded Pt black electrodes. The performance of $La_{0.5}Sr_{0.5}CoO_3$ was better than that of Pt black at the temperature of the experiment, that is, 170°C.

The magnetic susceptibility of $La_{0.5}Sr_{0.5}CoO_3$ was reliant on the magnetic state of Co which in turn depended on the La^{3+}:Sr^{2+} ratio. The magnetic susceptibility was shown to decrease with increasing temperature, indicating that $La_{0.5}Sr_{0.5}CoO_3$ behaves like a normal paramagnetic material above its Neél temperature.

It is proposed by Tseung and Bevan that the performance of the reversible electrode is controlled by the population of active sites at the interface and that such sites are few at 25°C, but their number increases with temperature. This, they state, may be due to the resultant expansion of the lattice causing the interaction

between cations in the bulk and the surface to decrease. This may lead to a decrease in the magnetic susceptibility and increase the availability of surface sites to associate with chemisorbed oxygen and to facilitate electron transfer.

Meadowcroft (49) and Tseung and Bevan (56) do not refer to the participation of lattice oxygen in the reversible reaction shown in equation 11. Nakamura et al (30), page 36, state that the RDS of the gas phase reactions on $La_{1-x}Sr_xCoO_3$ involves lattice oxygen diffusion and the surface reaction.

Matsuki and Kamadu (59) looked at oxygen reduction on a mixture of the perovskite-type $La_{0.6}Sr_{0.4}MnO_3$ and $CaMnO_{3-x}$ and carbon, used as the electrocatalyst. The activity decreased by repeating the cathodic and anodic cycles of the steady state polarization. XRD and XPS evidence suggested to them that lattice oxygen was cathodically reduced and that this led to the formation of oxygen defects at the electrode surface. Bearing in mind the work of Nakamura et al (30) and the fact that no such decrease in activity was observed for $La_{1-x}Sr_xCoO_3$ by Tseung and Bevan (56), it appears that the diffusion rate of oxygen in the $La_{0.6}Sr_{0.4}MnO_3/CaMnO_{3-x}$ mixture may be insufficient to maintain a prolonged use of such an electrode for the reaction under discussion.

Viswanathan and Charkey (60) looked at $La_{0.5}Sr_{0.5}CoO_3$ with respect to its properties as a cathode for oxygen reduction. Like Matsuki and Kamadu (59), they mixed their perovskite with carbon. They said that the graphite stabilizes electrode potentials during cycling.

The type of electrolyte was shown to be important by Vondrák and Doležal (13). They studied $La_{1-x}Sr_xCoO_3$ for x = 0.02, 0.04 and 0.5 at pH 5. They discovered that some strong oxidants including, for example, the peroxodisulphate ion ($S_2O_8^{2-}$) were reduced on the perovskite surface and that this was accompanied by O_2 evolution. On provision of a sufficient voltage, an anodic current was evidently flowing. Strong oxidants are expected to be reduced and therefore to accept electrons, giving the reaction shown in equation 12, where O_2 is consumed and not evolved.

$$2H_2O + O_2 + 4e^- \longrightarrow 4OH^- \qquad 12$$

It therefore appeared to Vondrák and Doležal that during the reduction of the $S_2O_8^{2-}$ ion, intermediates which reacted in such a way as to produce O_2 were formed. They suggest that the reactions shown in equations 13 and 14 occurred and that the OH_{ads} reacted with the OH^-, in the alkaline solution and followed the mechanism suggested by Kobussen and Broers (61) which led to O_2 evolution.

$$S_2O_8^{2-} \rightleftharpoons SO_4^{2-} + SO_{4ad} \qquad 13$$

$$SO_{4ad} + H_2O + e^- \rightleftharpoons HSO_4^- + OH_{ad} \qquad 14$$

They represented the overall reaction by equation 15

$$S_2O_8^{2-} = 4OH^- \rightleftharpoons 2SO_4^{2-} + O_2 + 2H_2O + 2e^- \qquad 15$$

Equation 15 explains why the current produced was anodic.

Perrault and Reby (62) found, contrary to the work by Tseung and Bevan (56) that oxygen was irreversibly reduced at $La_{1-x}Sr_xCoO_3$, x = 0 to x = 1, electrodes, in an alkaline solution. This illustrates

the importance of having the correct concentration of alkali and the correct voltage range for reversibility. Interestingly, they found that at x = 0.2 the catalytic activity showed a maximum, this agrees with much of the gaseous work reviewed in section 1.3.1.1.

Once a suitable material for a reversible oxygen electrode has been established, then the conditions under which it will work appear to be quite specific. The electrolyte must have the ability to support the cathodic and anodic reactions when necessary without the interference by intermediates such as in the work by Vondrák and Doležal. The limiting voltage for the anodic and cathodic potentials of the electrode must have a sharp clearly defined crossover point in a given electrolyte, as shown for $La_{1-x}Sr_xCoO_3$ by Tseung and Bevan (56).

1.3.3 Use of $La_{1-x}Sr_xCoO_3$ as a laser cathode

Iehisha et al (14) have recognized the potential of $La_{1-x}Sr_xCoO_3$ as a cathode in a CO_2 laser. These lasers are increasingly being used in medical applications as well as in science. It is therefore essential that they are developed to give maximum efficiency and lifetime.

One of the main problems encountered with CO_2 lasers, is the dissociation of CO_2, as shown in equation 16. This dissociation

$$CO_2 \rightleftharpoons CO + \tfrac{1}{2} O_2 \qquad 16$$

can be up to 60 - 70% and causes a significant decrease in output power.

An electrode is required which is chemically inert, particularly from oxidation, as this depletes the O_2 and the equilibrium of equation 16 consequently moves to the right. The electrode must possess a low sputtering rate as O_2 will adsorb on to a sputtered film.

Iehisha et al listed the advantages of using $La_{1-x}Sr_xMO_3$, where M = Co or Mn. They stated that the exchange of electrons between M^{3+} and M^{4+} enhanced the conductivity sufficiently for use as an electrode. The catalytic activity for oxidation of CO and therefore suppression of CO_2 dissociation weighs much in their favour. The fact that they do not consume oxygen by oxidation fulfilled another requirement and their oxygen emissivity, which is discussed by Nakamura et al (31), gives them an added advantage. The low sputtering rate which Iehisha et al found, together with the catalytic activity for CO oxidation ensured a long operating life for the laser.

$La_{0.7}Sr_{0.3}CoO_3$ was found to be the best of the series due to the catalytic activity for the CO oxidation being highest at this value of x. The conductivity it was stated, increased with x until x = 0.3 and then saturated. The oxygen emissivity too, seemed to be suitable at this x value. They avoided high x values because, they said, enhanced adsorption and desorption occurred. This disagreed with work on adsorption and desorption of oxygen done by Nakamura et al (30), who found that desorption increased with increasing x but re-oxidation decreased. Iehisha et al found that sintering the $La_{0.7}Sr_{0.3}CoO_3$ at 1150^{o}C optimized the perovskite phase and the catalytic activity.

14Ni-16Cr-Fe alloy which is not catalytically active for prevention of CO_2 dissociation, showed a lower output power than $La_{0.7}Sr_{0.3}CoO_3$. The power enhancement appeared to be due to the presence of O_2. This forced equation 16 to the left. It was shown that $La_{0.8}Sr_{0.2}CoO_3$ which is not such a good emitter of O_2 as $La_{0.7}Sr_{0.3}CoO_3$, functioned well when 2 mm Hg of O_2 was present in the laser gas.

H_2 and H_2O were known to suppress CO_2 dissociation but adding these did not increase the efficiency of the perovskite-type cathode as it in itself was sufficient to suppress the dissocation. The dissociation was found to be as low as 1.3%.

The laser cathode displays yet another use for this versatile perovskite-type compound.

1.4 CATALYTIC REACTIONS OF CARBON MONOXIDE, SULPHUR DIOXIDE AND NITROGEN OXIDES WHICH DO NOT INVOLVE PEROVSKITE-TYPE COMPOUNDS

Several potential catalysts for removal from exhaust gases and flue gases of CO by oxidation and SO_2 and NO_x by reduction have been investigated. The compounds researched have tended to be metals on oxide supports or metal oxides. Much of the work pre-dates that done on perovskite-type compounds.

Copper on alumina supports (Cu/Al_2O_3) appears to have been well investigated. A number of workers have published results which reflect its efficiency as a catalyst under various conditions of, for example, temperature or SO_2:CO ratio.

Dautzenberg et al (63) found that on passing SO_2 and oxygen (O_2) over Cu then copper sulphate ($CuSO_4$) was formed. The Cu catalyst was regenerated using hydrogen (H_2) or CO and an SO_2 rich gas was

produced. This was reduced to sulphur by H_2S which was added to the process or produced from a reduction step. Up to 90% SO_2 removal was attained.

Querido and Short (64) found that by passing SO_2 and CO over Cu/Al_2O_3, production of COS increased by increasing either the CO ratio or the temperature. At high CO ratios 80 - 100% SO_2 was converted to COS. This evidence for excess CO causing COS production agrees with results quoted by Hibbert and Tseung (12) for a $La_{0.5}Sr_{0.5}CoO_3$ catalyst.

Okay and Short (65) looked at the reaction between SO_2 and CO in the presence of water. They found that water had an adverse effect on the catalytic reaction. They found that the water gas shift reaction shown as equation 4 page 38 did not occur between 426°C and 493°C. Water did not appear to affect COS production.

Mohadi (66) also looked at the reaction in the presence of water over Cu/Al_2O_3 and Cu on silica (Cu/SiO_2). When the experiment was carried out below the dew point of sulphur vapour, then COS production was virtually zero and H_2S diminished dramatically. Working at this temperature range may allow any elemental sulphur produced to be retained in the catalyst. Mohadi did not explain why the side reactions were not favoured.

Quinlan et al (67) also investigated the Cu/Al_2O_3 system. They attempted to recreate the SO_2 content in a flue gas. For a 90% conversion of SO_2 they found no condition where more than 75-80% of the entering SO_2 could be removed as elemental sulphur. As the SO_2 conversion approached 100% the amount of COS production

increased to 40 - 100%, dependent on the temperature, CO ratio and contact time.

Hibbert and Tseung (68) found that sulphur was taken up into the Cu/Al_2O_3 catalyst during the reaction of SO_2 with CO at 557-582^oC. CuS was formed in the presence of water. In agreement with Hibbert and Tseung (12) and Querido and Short (64) it was found that an excess of CO led to COS production, it also led to the formation of H_2S. Hibbert and Tseung found that O_2 poisoned the catalyst yet Dautzenberg et al (63) actually used O_2 in their process.

Quinlan et al (69) looked at the reduction of both NO and SO_2 by CO over Cu/Al_2O_3. The catalyst was found to be less active for the combined reduction than the separate reductions. Sulphur produced was removed by electrostatic precipitation and by an ice trap. Complete conversion of NO to N_2 occurred above 260^oC. It was suggested that NO oxidized the Cu to a less active state, as the decrease in SO_2 reduction was greater than that expected for straightforward competition between SO_2 and NO for CO. For reduction of both of the oxides, higher temperatures, higher contact times and greater CO ratios were necessary.

Goetz et al (70) compared the activities of Cu/Al_2O_3 and an iron/chromia(Fe/Cr_2O_3)catalyst. There appeared to be more COS produced over the Fe/Cr_2O_3 catalyst.

Fe/Cr_2O_3 investigations into the removal of SO_2 and CO have tended to involve a two stage process.

Khalafalla and Haas (71) looked at a two stage system where the first stage was at 430^oC and H_2S was produced. This was removed

in the second stage at temperatures below 250°C via the Claus reaction, shown in equation 17

$$2H_2S + SO_2 \rightleftharpoons 2H_2O + 3/x\ S_x \qquad 17$$

It was suggested that sulphur produced in the first reactor be condensed out of the system before the gases passed through the so called Claus reactor to prevent it being plugged by elemental sulphur. (The boiling point of sulphur is 446°C so it is in fact likely that it would be condensed in the first reactor).

Sood and Kittrel (72) experimented with a dual bed system. CO and SO_2 first passed through an Fe/Cr_2O_3 catalyst and COS was produced, as found by Goetz et al (70). The COS was then passed over activated Al_2O_3 to yield sulphur. At 370°C greater than 90% reduction of both SO_2 and NO to sulphur and N_2 respectively, occurred.

George and Tower (73) dismissed another possible candidate for the catalysis, that is, cobalt molybdate, as unsuitable. They suggest that a more selective catalyst be used, to minimize COS production.

Bazes et al (35) found substantial COS production at high temperatures and excess CO for both cerium oxide-cobalt oxide (CeO_2 - Co_3O_4) and copper cobaltale ($CuCo_2O_4$). The yield was lessened by decreasing the CO to SO_2 ratio.

COS production appears to be a major setback for most of the catalysts discussed. It seems to be less of a problem for the perovskite-type catalysts, although COS is produced if excessive amounts of CO are present.

CHAPTER 2

EXPERIMENTAL PROCEDURE

The $La_{1-x}Sr_xCoO_3$ compounds investigated were all prepared in the laboratory by freeze drying. They were then characterized by surface area analysis, XRD, ESCA and their conductivity was measured. The density of $La_{0.4}Sr_{0.6}CoO_3$ was measured. The e.s.r. spectrum was run to see if Co^{IV} could be identified by this method.

Before the reaction between SO_2 and CO over the catalysts was studied, the gases were individually adsorbed on the catalyst surface. This was followed by TPD from which the heats of desorption of the various adsorbed species could be determined. This data, it was expected, would be helpful when attempting to deduce the mechanism of the catalytic reduction of SO_2 and oxidation of CO. From reactions between CO and catalysts pre-exposed to SO_2 or SO_2 and CO it was expected that the mechanism of COS production could be understood.

Finally, the flow rig experiments were carried out. Several mixtures of SO_2 and CO were passed over the catalysts at different temperatures and contact times. The catalytic efficiency was thereby investigated under various conditions.

The used catalysts were then re-examined.

2.1 PREPARATION OF $La_{1-x}Sr_xCoO_3$

The perovskite-type catalysts were prepared by the freeze drying method used by Tseung and Bevan (74).

A solution of $La(NO_3)_3.6H_2O$ (lanthanum nitrate), $Sr(NO_3)_2$ (strontium nitrate) and $Co(NO_3)_2.6H_2O$ (cobalt(II)nitrate) was made

up in distilled water, which fulfilled the solvent requirements stated by Hibbert and Tseung (75). The solution was made to 0.25 mol dm^{-3} in Co and to the ratios of La, Sr and Co required which depended on the specific $La_{1-x}Sr_xCoO_3$ being prepared. The nitrates used were BDH $La(NO_3)_3.6H_2O$, BDH $Sr(NO_3)_2$ and BDH $Co(NO_3)_2.6H_2O$.

The deep red solution was sprayed into liquid nitrogen using an atomiser spray. The instant freezing thus achieved, ensured that fractional crystallization did not occur and therefore the intimate mixture of the nitrates present in the liquid was maintained in the solid phase.

The solid solution was then freeze-dried under vacuum. At low pressures the water from the solid solution sublimed leaving,as before, the atomic mixture of the nitrates. Kelly et al (76) calculated that the heat applied to the surface of the solid solution was below that required for maximum rate of sublimation. In compliance with the suggestion made by Kelly et al an IR lamp was shone on the solid solution to speed up the rate of sublimation. Hibbert and Tseung (75), however, report that the IR lamp cannot be used to its full advantage when subliming aqueous solutions containing, for example, cobalt nitrate, due to the high risk of melting. During the sublimation the pale pink solid solution changed to a purple powder.

The next step of the process was the decomposition of the mixture of nitrates to form the oxides. The nitrates were retained under vacuum in the freeze-drying apparatus and heated to $300^{o}C$, with a heating mantle. As the decomposition proceeded the powder became black and the pressure within the system increased, due to the

evolution of the gaseous decomposition products. A blue/green ring formed on the inside of the liquid nitrogen trap which was used to collect water during the sublimation. This may have been due to the presence of NO or O_2. When the pressure fell again the decomposition was shown to be complete. The black powder was allowed to cool and was then allowed up to atmospheric pressure. At atmospheric pressure the blue/green ring disappeared and a brown gas was evolved. This suggests that the ring was indicative of NO, which reacted with oxygen at atmospheric pressure to produce NO_2 (nitrogen dioxide), which is brown.

The solid decomposition product was then transferred to a muffle furnace and heated to 550°C in air for 16 h to give the perovskite-type structure.

2.1.1 Decomposition of $Co(NO_3)_2.6H_2O$, to identify the decomposition products

In order to identify the decomposition products of one of the nitrates used for the preparation of $La_{1-x}Sr_xCoO_3$, the decomposition of $Co(NO_3)_2.6H_2O$ under vacuum was recorded gravimetrically and mass spectrometrically.

Two samples were investigated. The first sample of the orange/brown $Co(NO_3)_2.6H_2O$ was weighed and then placed on the microbalance in the vacuum line. The vacuum line is described in section 2.3.1.1. During evacuation the colour of the sample changed. It first acquired a whitish tinge and then changed to the pink colour observed during freeze-drying of the nitrate mixture used to make the $La_{1-x}Sr_xCoO_3$.

When the evacuation of the system had been achieved the mass was allowed to equilibriate and was noted. On allowing the system up to atmospheric pressure no weight change was observed.

The system was re-evacuated and the needle value between the vacuum line and the already evacuated MS was opened. The MS was set in the scanning mode in the range 17 to 48 a.m.u. Each scan took approximately 30s and covered the range of the anticipated possible gaseous products, that is, 18 a.m.u. (H_2O), 30 a.m.u. (NO), 32 a.m.u.(O_2)and 46 a.m.u. (NO_2). It was also expected that N_2 (28 a.m.u.) and CO_2 (44 a.m.u.) might be detected. The sample was heated with a cylindrical furnace and the temperature was read from a chromel-alumel thermocouple. The sample was heated to 186^{o}C. When constant mass was attained this was noted.

The procedure for the second sample was similar, apart from the omission of the step where the sample was allowed up to atmospheric pressure and then re-evacuated. The initial, evacuated and final sample masses were noted.

2.2 CHARACTERIZATION OF $La_{1-x}Sr_xCoO_3$

The methods used to investigate the fresh and used catalysts will be described then their application to this work will be related.

2.2.1 Introduction to the catalyst characterization methods

2.2.1.1 Surface area analysis

The specific surface areas of the catalysts were measured so that it could be ascertained whether or not results of experiments were surface area controlled or dictated by, for example, the value of x in $La_{1-x}Sr_xCoO_3$.

The surface area of a given sample of powder, of known mass is measured by determining how much adsorbed N_2 is required to form a monolayer on its surface. Adsorption of N_2 is strong at liquid N_2 temperatures so, such conditions are suitable.

N_2 is the most frequently used adsorbate for surface area analysis (77). The surface coverage per N_2 molecule is known and it is readily available as a dry gas. High purity liquid N_2 is also readily obtained.

The surface areas of each of the catalysts was measured automatically and that of $La_{0.5}Sr_{0.5}CoO_3$ was also measured using a vacuum line and microbalance. This was to show that both methods gave a result of the same magnitude.

Both methods employ a form of the B.E.T. equation, which derives its name from three early workers in the field of surface area analysis, they are, Brunauer, Emmett and Teller.

2.2.1.1.1 Introduction to analysis of surface area using the single point automatic technique

The automatic surface area analyser consists essentially of three sample holders; three two-stage valves; two pressure sensors, one of which is set slightly above atmospheric pressure and one at the pressure of monolayer formation; a variable volume cell; three sorption pumps connected to the variable volume by a solenoid valve and the associated piping and connectors (77).

The powder samples are outgassed by heating and simultaneous purging with nitrogen gas to drive off gases released by heating. When outgassing is complete the sample is cooled using an ice bath initially and then liquid N_2. The analyser automatically measures the surface area from the change in pressure due to adsorption of N_2. The sample tube containing the sample is then removed, stoppered and weighed. The specific surface area may be calculated by dividing the surface area by the mass.

The form of the B.E.T. equation used by the Surface Area Analyser is given in equation 18

$$\frac{P/Ps}{V\left[1-(P/Ps)\right]} = \frac{1}{VmC} + \left[\frac{C-1}{VmC}\right]\frac{P}{Ps} \qquad 18$$

V is the volume (s.t.p.) of gas adsorbed at pressure P, Ps is the saturation pressure (the vapour pressure of liquefied gas at the adsorbing temperature), Vm is the volume of gas required to form an adsorbed monolayer and C is a constant related to the energy of adsorption. The area covered by an adsorbed N_2 molecule is assumed to be 16.2 $\mathring{A}^2$, from an evaluation by Brunauer et al (78).

2.2.1.1.2 Introduction to surface area analysis using a vacuum line and microbalance

For this method of measuring surface area the vacuum line shown inPlate 2.1 in section 2.3.1.1 was used.

Unlike the automatic surface area analyser, where the calculation is based on one pressure reading, this method requires several points.

The surface area is calculated from the change of mass due to absorption of N_2, with pressure of N_2.

The surface area is calculated using the form of the B.E.T. equation shown in equation 19.

$$\frac{p}{Ma\ (Po-p)} = \frac{1}{MmC} + \frac{C-1}{VmC}\ \frac{p}{Po} \qquad 19$$

Mm = mass of gas able to cover the whole surface of adsorbent with a unimolecular layer of gas (monolayer capacity) (s.t.p.).

Ma = mass of gas adsorbed (s.t.p.).

Po = saturated pressure of adsorbate at the adsorbing temperature.

p = the equilibrium pressure.

C = a constant = $\exp\left[\frac{E_1 - E_2}{RT}\right]$

$E_1 - E_2$ is the difference between the heat of adsorption of the first layer and that of the second and subsequent layers.

P/Ma (Po - p) is plotted against p/Po.

From the slope and intercept the monolayer capacity was obtained, as shown in equation 20.

$$Mm = \frac{1}{\frac{C-1}{MmC} + \frac{1}{MmC}} \qquad 20$$

From this the specific surface area (s.s.a.) was calculated using equation 21.

$$s.s.a. = \frac{aNMm}{MW} \qquad 21$$

a = cross sectional area of an adsorbed molecule.

N = Avogadro number.

W = mass of powder (catalyst) in sample pan.

M = molecular weight of adsorbate gas.

2.2.1.2 Density measurements

The density was measured in order to work out the number of unit cells present in a given mass of catalyst. The volume per unit cell was obtained from unpublished X-ray measurements by Hibbert.

The density measurements are made by measuring the volume of a bottle filled with water, then weighing the bottle plus catalyst and bottle plus catalyst and water. From the mass (m) and volume (v) of catalyst, the density (ρ) is calculated using equation 22.

$$\rho = \frac{m}{v} \qquad 22$$

2.2.1.3 X-ray diffraction

X.R.D. analysis of the $La_{1-x}Sr_xCoO_3$ was done prior to and after the vacuum line and flow line investigations. The purpose of the analysis was first of all to confirm that the starting material was indeed the perovskite-type structure which had been prepared similarly by Tseung and Bevan (74) and Hibbert and Tseung (75). Analysis of the compounds after experimentation helped to identify what changes to the bulk structure, if any, had occurred.

X-rays are produced by bombarding a metal with high energy electrons. A broad continuum of differing wavelengths is produced by the initial impact of the electrons with the crystal and superimposed on this are some sharp peaks arising from interactions with the electrons of the metal, these are characteristic of the metal.

X-rays have wavelengths similar to interatomic distances in crystals and they can be diffracted if passed through crystals.

Von Laue passed a beam of X-rays of a broad range of wavelengths into a single crystal and recorded the diffraction pattern on a photographic plate. In this way the Bragg equation, shown in equation 23 was satisfied by using differing wavelengths.

$$n\lambda = 2d \sin \theta \qquad 23$$

n is an integer and denotes the order of diffraction.
λ is the wavelength of X radiation.
d is the spacing between the lattice planes.
θ is the angle between the incident rays and lattice planes.

The method used in this work involved powder samples. These are inherently randomly orientated. A monochromatic X-ray source is used and the sample is rotated, thereby changing θ. Every plane gives use to a diffraction peak of characteristic d value, which can be calculated from 2θ for a given λ and has a characteristic intensity for a given crystal. The unit cell, that is, the smallest repeating unit which shows the full symmetry of the crystal structure, for a

perovskite-type crystal is cubic. The particular plane which corresponds to a given peak on an intensity versus d spacing, for a cubic structure, can be identified using equation 24.

$$d = \frac{a}{\sqrt{h^2 + k^2 + l^2}} \qquad 24$$

a is the length of a unit cell. h, k and l are the Miller indices which are the reciprocals of the fractional intersections of a given plane in the three dimensions a, b and c of the unit cell. For a cubic structure a = b = c.

Tables of d values and relative intensities for the most significant planes of crystals, which have been characterized are available. From these, unknown species may be identified.

2.2.1.4 Electron spectroscopy for chemical analysis

E.S.C.A. or X-ray photoelectron spectroscopy (XPS) as it is also called was carried out before and after the flow rig experiments.

This technique is an excellent tool for identifying surface elements and theiroxidation states. In the field of surface chemistry and therefore in the present work, involving heterogeneous catalysis, it is particularly useful. Chemical changes involving only the surface and not the bulk, which might not be detected by X.R.D., may be identified using E.S.C.A.

Photoelectron spectroscopy involves the measurement of the energy required to remove an electron from an orbital in a given atom,

that is, the binding energy or ionization potential of that electron. If ultraviolet radiation is used then a valence electron is removed; if, as in this work, X-rays are used then a core electron is ejected. The binding energy (b.e.) is characteristic of the atom and is calculated using equation 25.

$$b.e. = h\nu - k.e. - \emptyset \qquad 25$$

$h\nu$ is the incident photoelectron energy.

k.e. is the kinetic energy of the ejected electron.

$\emptyset$ is a correction factor related to the work function.

The binding energy is not only characteristic of the element from which it is ejected, but of the environment in which the atom exists. Small but significant shifts in the energy, therefore, enable the oxidation state to be identified. The resolution is about 1eV.

The technique is confined to surface analysis due to the potential escape depth of electrons through the bulk. The escape depth depends on the nature of the material in question and is usually of the order 10^{-9}m.

It is essential that the radiation source is monochromatic, so that definition of the incident radiation is sufficient for reliable calculation of the binding energy. The kinetic energies of the electrons ejected are measured by passing them between the poles of an electromagnetic or electrostatic analyser, the masses being equal

means that the extent of deflection depends on their velocity. The electron flux is measured for each field strength. The technique is therefore quantitative as well as qualitative.

A reservation held about the use of E.S.C.A. is that at the high vacuums at which measurements are made,desorption from the surface may occur. It is essential, however, to have a good vacuum, to ensure that the surface is clean and to minimize scattering of the emitted photoelectrons.

It must be borne in mind that the electron ejected is from a molecular,as opposed to atomic orbital and that the energy is an approximation, this is called Koopmans' Theorem. Also, ideally single electrons should not be considered, but instead the overall states of the given molecule or ion should be considered. In spite of these limitations, the technique is very sensitive.

2.2.1.5 Conductivity measurements

The $La_{1-x}Sr_xCoO_3$ group of compounds have been reported to be semiconductors (13) and it is understood that their conductivity influences their properties as catalysts (12), electrocatalysts (13) and electrodes (14,62). It was therefore interesting to measure the conductivities of the compounds and to see how they related to chemical trends across the series.

The conductivities of the powder samples were obtained by measuring their resistances when compressed and calculating the conductivity (K) by using equation 26.

$$K = \frac{l}{\rho a} \qquad 26$$

l is the length of catalyst present.

a is the cross sectional area of catalyst.

ρ is the resistance.

2.2.1.6 Electron spin resonance

$La_{1-x}Sr_xCoO_3$, where $0<x<1$, contains Co^{IV} (19), which is uncommon. Jonker and van Santen (18) have calculated the amount of Co^{IV} present in a series of $La_{1-x}Sr_xCoO_3$ compounds by measuring their oxygen contents. In certain environments, depending on the position of the unpaired electron the Co^{IV} ought to be capable of producing an e.s.r. signal. It was therefore decided to attempt the first characterization of Co^{IV} in $La_{1-x}Sr_xCoO_3$.

The presence of an unpaired electron in a molecule or ion allows energy levels to be produced from the interaction of the magnetic moment of the electron with an applied magnetic field. If a given sample is bathed in radiation of frequency ν, the unpaired electron spins of the sample have energy levels, that come into resonance with the radiation, when the magnetic field has been adjusted so that equation 27 holds.

$$h\nu = 2\mu_B B \qquad 27$$

h is Planck's constant.

μ_B is the Bohr magneton.

B is the applied magnetic field.

When this condition is satisfied the energy levels are in resonance with the surrounding radiation and the spins may absorb its energy strongly. Hence, e.s.r. is the study of the properties of molecules containing unpaired electrons by observing the magnetic fields at which they resonate with an applied radiation field of definite frequency.

It is found that when a magnetic field of 3000G is used, the spacing between levels with different spin orientation relative to this field is such that transitions are caused by radiation of wavelength about 30 mm, which corresponds to microwave radiation.

A klystron generator produces microwaves which are then passed through the sample to a detector. The absorption of radiation by the sample is monitored as the field is swept. The first derivative of the signal is plotted and this is analysed to measure the g values, which are characteristic of the sample. The value of g depends on the electronic structure of the species because the applied field has to be able to move the electron through the molecule, and so a knowledge of its value gives some structural information (79).

The value of g is close to 2 and equation 27 may be modified to give equation 28.

$$h\nu = g\mu_B B \qquad 28$$

Hyperfine splitting of the spectrum is caused by the interaction of electron magnetic moments with nuclear magnetic moments. Like

electrons, protons have a spin of $\frac{1}{2}$ and their magnetic moment can add to the applied field or subtract from it. If 'a' is the hyperfine coupling constant, then for one proton instead of a single line the spectrum will show two lines separated by a magnetic field of magnitude 'a', equally disposed about the original centre of the spectrum, each having half the total intensity. Hence, when an electron is located near a particular nucleus orseveral nuclei, the splitting is unique to that species. Since the magnitude of the splitting depends on the distribution of the unpaired electron into the vicinities of the magnetic nuclei present, the measured splittings can be used to map the molecular orbital it occupies.

E.s.r. is an extremely sensitive technique and can detect as few as 10" spins. It has important applications in the detection of intermediate reaction radicals.

2.2.2 Procedure of $La_{1-x}Sr_xCoO_3$ characterization

Some of the characterization methods which have been introduced in section 2.2.1 were used before and after experimentation. Fig. 2.1 shows in the form of a flow diagram what the procedure followed was.

2.2.2.1 B.E.T. surface area analyses

2.2.2.1.1 Analysis of surface area using the single point automatic technique

A Micromeritics Surface Area Analyser was used for the single point automatic analyses. The surface areas of samples of each of the perovskite-type compounds used were measured. Each sample was outgassed in a stream of N_2 as described in section 2.2.1.1.1, at

FIGURE 2.1 FLOW DIAGRAM OF EXPERIMENTAL PROCEDURE

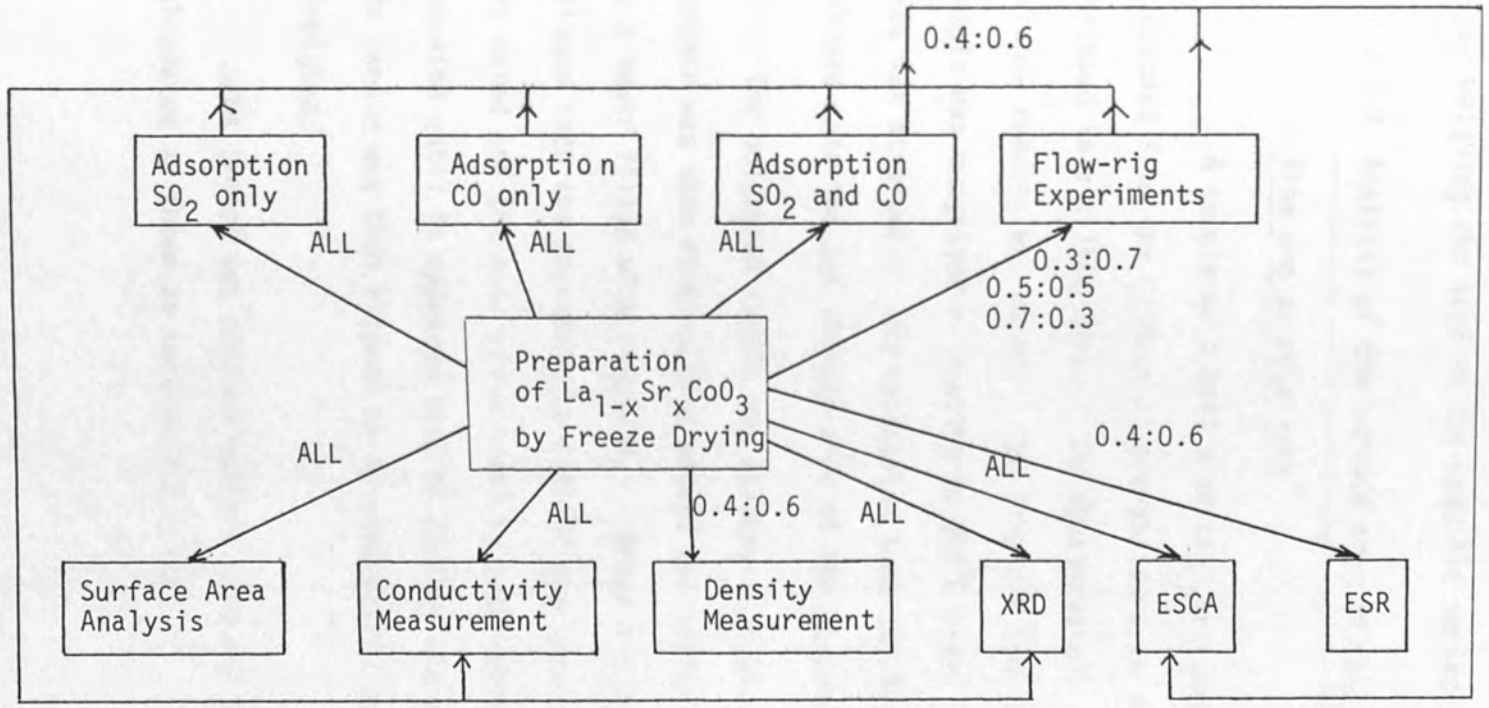

0.3:0.7 = $La_{0.3}Sr_{0.7}CoO_3$

0.4:0.6 = $La_{0.4}Sr_{0.6}CoO_3$

0.5:0.5 = $La_{0.5}Sr_{0.5}CoO_3$

0.7:0.3 = $La_{0.7}Sr_{0.3}CoO_3$

ALL = each of above

200°C for about 1 h. The adsorption of N_2 was then carried out at liquid N_2 temperatures and the total surface area was measured. After weighing the samples the specific surface areas were calculated.

2.2.2.1.2 Analysis of the surface area of $La_{1-x}Sr_xCoO_3$ using a vacuum line and microbalance

A sample of 0.0973 g of $La_{0.5}Sr_{0.5}CoO_3$ was weighed out and suspended from the CI Mark II microbalance in the vacuum line and enclosed in a silica tube. The counterweight was adjusted and the balance reading was noted. The line was then evacuated. The sample was outgassed by heating to 200°C under vacuum until a constant mass was attained. The outgassing time was 4h. Meanwhile N_2 was allowed into the gas storage side of the vacuum line.

The outgassed sample was allowed to cool. The cylindrical furnace was then removed from around the silica tube and replaced by a Dewar filled with liquid N_2. After 1 h 7 mm Hg of N_2 was allowed into the microbalance side of the vacuum line. The pressure was noted and the mass was allowed to equilibrate. This was repeated until it appeared that no further change in mass would occur. The sample was then allowed up to atmospheric pressure and quickly reweighed.

p/Ma (Po-p) was plotted against p/Po and the surface area was calculated as shown in section 2.2.1.1.2.

2.2.2.2 Measurement of the density of $La_{0.4}Sr_{0.6}CoO_3$

The density of $La_{0.4}Sr_{0.6}CoO_3$ was measured by the method described in section 2.2.1.2. The mass of the empty stoppered bottle was measured. The bottle was then reweighed with a sample of $La_{0.4}Sr_{0.6}CoO_3$. This was then topped up with water, stoppered and reweighed. The bottle was then emptied, rinsed out and the outside was dried. The bottle was then filled with water, stoppered and weighed. From the known mass and density of water, the volume of the bottle was calculated. From the mass and density of the water present with the sample the volume of water present then was calculated. The volume occupied by the known mass of catalyst was therefore easily worked out and from the mass and volume the density was calculated.

2.2.2.3 X-ray diffraction measurements to determine the bulk properties of $La_{1-x}Sr_xCoO_3$

The fresh and used catalysts were examined using a Philips PW 1010 X-ray diffractometer and an Automated Philips PW 1710 X-ray diffractometer. The voltage used was 40 kV and the current was 20 mA. The X radiation was CuKα of wavelength 1.542 Å and collimating slits of angles 1^o, 0.2^o and 1^o were used.

The 2θ range scanned was 10^o to 100^o, in order to include the perovskite-type d spacings and to ensure that if any reaction with SO_2 to produce sulphides or sulphates occurred the patterns belonging to these could be detected.

For each sample the scattering intensity was recorded as a function of 2θ. The 2θ values of the peaks were converted to d values, using the Bragg equation, shown in equation 23. The peaks were then assigned by d value and relative intensity, using the Selected Powder Diffraction Data for Minerals (80). The d values of peaks which did not correspond to those of $La_{1-x}Sr_xCoO_3$ were compared to values for sulphur compounds of La, Sr and Co and were assigned accordingly. Where evidence existed of compounds other than $La_{1-x}Sr_xCoO_3$, it was used to support the suggested mechanisms of the reactions between the reactant gases and between the gases and catalysts.

2.2.2.4 Use of electron spectroscopy for chemical analysis to determine the surface characteristics of $La_{1-x}Sr_xCoO_3$

The fresh catalysts and those exposed to SO_2 and CO in the flow rig, plus $La_{0.4}Sr_{0.6}CoO_3$ which had been exposed to SO_2 and CO in the vacuum line, were examined, using a Kratos ES300 photoelectron spectrometer. The operating pressure was 2×10^{-7} mm Hg and AlKα radiation of energy ($h\nu$) 1486.6 eV was used. The voltage was 14 kV and the current was 10 mA.

The kinetic energy (k.e.) ranges scanned were chosen to include the principal peaks of all of the elements which could be present, that is, La, Sr, Co, O and S. The binding energies (b.e.) were then calculated using equation 25. $\emptyset$ for each sample was calculated by identifying the k.e. of the Cls peak from the Sellotape® used to support the sample, The Cls b.e. is used as a standard.

The binding energy values obtained were then compared to tables (81) of measured values for each element for known oxidation states of that element. In this way it could be deduced whether or not the oxidation state of a given element had changed during an experiment. By comparison between elements it was possible to work out if any products had been deposited on the catalyst and to postulate what they might be. Catalysts which had been exposed to SO_2 were examined for the presence of the S2p peak. The O1s peaks were compared to those presented by Yamazoe et al (17) from their studies on E.S.C.A. of adsorbed and lattice oxygen.

2.2.2.5 Measurement of the conducitivies of fresh and used $La_{1-x}Sr_xCoO_3$

The conductivities of the powder samples were measured by compressing a small amount of each between two steel rods, in a Salter Pocket Balance, to a 20 kg equivalent pressure. The resistance was measured using a Fluke 8020A multimeter. The resistance across the steel rods and connecting wires was measured first and subsequently subtracted from the catalyst resistance. The length of catalyst plus steel rods was measured by a micrometer and l, the length of catalyst was calculated from the difference in length with no catalyst present. The cross sectional area of the steel rods and therefore the catalyst sample was measured using the micrometer.

The conductivities of the catalysts were measured before exposure to SO_2, CO or both, to ensure that they did have semiconducting properties. The conducting properties of the used catalysts were

measured to see if any change took place during interactions with the gases. If any changes did take place, they could be considered in the wider context of other characterization experiments.

2.2.2.6 Electron spin resonance of $La_{0.4}Sr_{0.6}CoO_3$

As stated in section 2.2.1.6 the purpose of this experiment was to characterize Co^{IV}.

The sample of $La_{0.4}Sr_{0.6}CoO_3$ was investigated using a Varian E-4 e.p.r. spectrometer. The microwave frequency was 3260G.

To characterize Co^{IV} $La_{0.4}Sr_{0.6}CoO_3$ was chosen from the range of $La_{1-x}Sr_xCoO_3$ compounds prepared. This was chosen, in spite of the fact that e.s.r. is extremely sensitive, because according to Jonker and van Santen (18), it has the highest Co^{IV} content.

A small sample of the $La_{0.4}Sr_{0.6}CoO_3$ was placed in a glass e.s.r. tube and the spectrum was run at 19.6°C for a 100G scan. A signal was obtained. The scan was then run with $La_{0.7}Sr_{0.3}CoO_3$ at 20.0°C to check whether or not the signal was characteristic of $La_{1-x}Sr_xCoO_3$.

The $La_{0.4}Sr_{0.6}CoO_3$ was then replaced in the e.s.r. spectrometer for investigation at lower temperatures. The signal was expected to sharpen on lowering the temperatures due to the Boltzmann distribution. The spectrum was re-run as the sample was cooled to -143.5°C. The sample was then heated to 180°C and scanned again. The scan at room temperature was then repeated to see if any irreversible changes were observed due to the thermal changes. The $La_{0.4}Sr_{0.6}CoO_3$ was then heated once again to 272°C and another spectrum was run.

A 1000G scan was run at room temperature, to make certain that all of the signals due to $La_{0.4}Sr_{0.6}CoO_3$ had been detected.

A spectrum of $La(NO_3)_3.6H_2O$ was also run to check whether the signal found for $La_{0.4}Sr_{0.6}CoO_3$ might be due to a lanthanide impurity.

The reference standard used for calculation of g values was dpph (1,1-diphenylpicrylhydrazyl), which is a common e.s.r. standard, that has been characterized by Adams et al (82).

g is calculated using equation 29.

$$g = g_{ref}\left(1 \pm \frac{\Delta B_{ab}}{Bo}\right) \qquad 29$$

where g_{ref} is $g_{dpph} = 2.00358$.

B_{ab} is the magnetic sweep between the reference peak and the unknown. Bo is the set field. The $\frac{\Delta B_{ab}}{Bo}$ term is added or subtracted if the unknown peak is up or down field, respectively, of the reference. For a given species the g value is the average of the g values obtained for each peak.

2.3 ADSORPTION AND DESORPTION EXPERIMENTS

Adsorption of SO_2 and CO was carried out on $La_{1-x}Sr_xCoO_3$ (x = 0.3, 0.5 and 0.7) in a vacuum at room temperature, 100°C, 300°C and 500°C. For $La_{0.4}Sr_{0.6}CoO_3$ the adsorption experiments were done at 500°C only.

Each adsorption was followed by TPD to 650°C. The range of temperature studied was chosen because earlier work on $La_{0.5}Sr_{0.5}CoO_3$ by Hibbert and Tseung (12) indicated favourable results for the reaction between SO_2 and CO at around the 550 - 650°C range. The lower temperatures were studied in order to see whether the temperature at which adsorption of SO_2 and, or CO would occur, was related to the temperature at which they reacted in the presence of $La_{1-x}Sr_xCoO_3$. It was of interest to know whether or not adsorption was reversible in the experimental conditions. If irreversible adsorption took place then subsequent investigations would show whether the gases had reacted with the surface or if further heating would remove adsorbed SO_2.

2.3.1 The vacuum line used for the adsorption and desorption experiments

2.3.1.1 Description of the vacuum line and associated equipment

The vacuum line used to investigate the adsorption and desorption experiments is shown in Plate 2.1. The line is made of glass apart from the silica tube which enclosed the $La_{1-x}Sr_xCoO_3$ samples and is heated to 650°C. The joint above the silica tube is water cooled, to prevent the grease from melting and to protect the microbalance from the high temperatures of the furnace.

The line consists of two sections. One section can be used as a gas storage vessel and contains a mercury manometer to measure the pressure of gas therein. The other contains the microbalance, it too has a mercury manometer. Each section can be evacuated independently of the other.

PLATE 2.1 VACUUM LINE APPARATUS

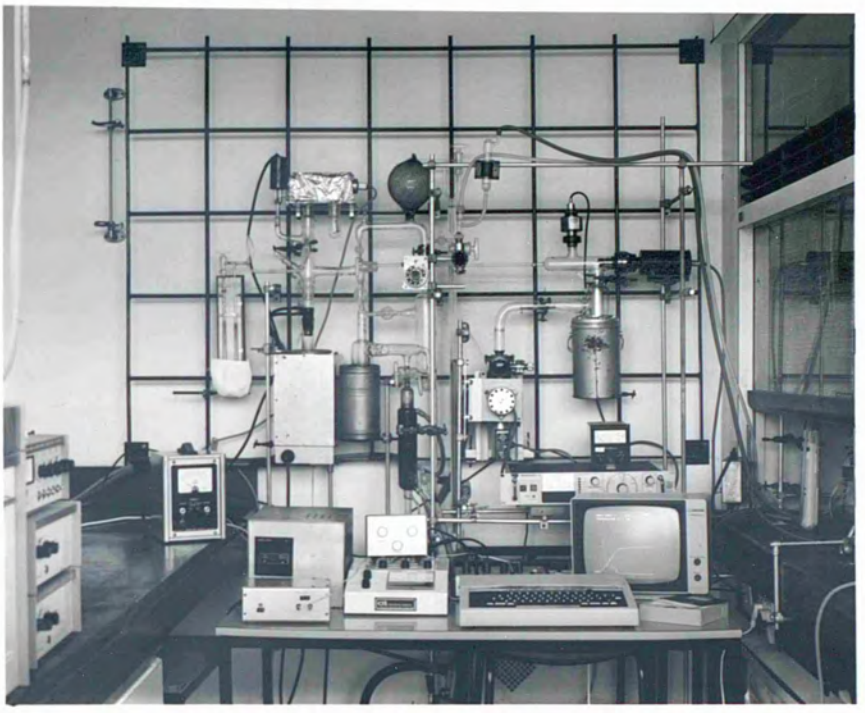

The line is pumped by an Edwards rotary pump and a water cooled Jencons mercury diffusion pump. In order to bring the vacuum below the vapour pressure of mercury and to protect the line, particularly the microbalance and catalyst sample from mercury, there was a liquid N_2 trap between the diffusion pump and the line. The pressure during evacuation was monitored with a Pirani Type Vacuum Gauge Model 8/2.

Accessories of the vacuum line also shown in Plate 2.1 include the CI Mark II resettable microbalance which could measure with an accuracy of $\pm$ 0.01 mg. This was used to measure changes of mass during adsorption and desorption experiments. A Eurotherm Microprocessor Based PID Controller, Type 810 temperature controller was used to regulate a Lindberg Cylindrical Heating furnace. Temperatures for adsorption and rates of heating for desorption could therefore be set.

Also shown in Plate 2.1 is the VG Micromass Anavac - 2 Quadrupole Mass Analyser, which is referred to throughout this text as the MS. The MS was connected to the vacuum line via an Edwards High Vacuum Ltd. Model LB2B needle valve. The mass spectrometer enabled species desorbed from the catalyst surface to be identified and monitored. This system was evacuated by an Edwards rotary pump and an air cooled oil Edwards E01 Vapour Diffusion Pump. As in the vacuum line there was a liquid nitrogen trap between the diffusion pump and the line. The pressure was monitored by an Edwards Penning 8 gauge.

The microbalance, temperature controller and MS output were recorded using a BBC microcomputer via a Philip Harris 4 channel A.D.A. unit. This set-up enabled the three outputs to be recorded simultaneously, for a length of time dictated by the time interval chosen between the 1024 datapoints which could be recorded.
A program written for the BBC microcomputer enabled the recorded data of each of the channels to be plotted simultaneously on the V.D.U. (visual display unit). It was also possible to look at the values of each of the plots on a scale of 0 - 255, for each of the 1024 data points. From this information the temperature at, for example, a maximum peak height could be calculated.

T.P.D. data recorded on the BBC were processed and activation energies of desorption were calculated using the Fortran computer program, MASS1, shown in Appendix 1 , on the VAX11/780 computer of Royal Holloway and Bedford New College.

2.3.1.2 Calibration of the vacuum line for gas transfer between the gas handling side and the microbalance section

The volumes of each side of the vacuum line were measured so that a given pressure of gas could be allowed into the gas handling side and when the tap leading to the microbalance side was opened the required pressure was obtained.

The vacuum line was opened to the atmosphere. The 1000cm^3 bulb at the top of the gas handling side was isolated from the remainder of the vacuum line. The vacuum line, excluding the bulb

was then evacuated. The gas handling line was then isolated, the manometer was closed and the air from the bulb was leaked into the line. The pressure was noted from the manometer. The volume of the gas handling section was then calculated using equation 30.

$$P_1V_1 = P_2V_2 \qquad 30$$

P_1 = pressure in the bulb (760 mm Hg).

V_1 = volume of bulb (1000 cm^3).

P_2 = pressure in gas handling side (including bulb).

The section containing the microbalance was then isolated from the pumps. The manometer was closed and the procedure was repeated. The volume calculated was then the total volume of the line. From these volumes the required pressure in the gas handling line could easily be calculated.

2.3.1.3 Calibration of the temperature in the vacuum line with that of the furnace

The temperature of the $La_{1-x}Sr_xCoO_3$ samples inside the vacuum line could not be measured during adsorption or TPD. A temperature measuring device, such as a thermocouple, might adsorb and subsequently desorb SO_2 or CO, thereby giving spurious peaks on the MS. The gases might interfere with the conductivity of the thermocouple and give inaccurate temperature readings. It was therefore decided that the temperature in the vacuum line at the position the $La_{1-x}Sr_xCoO_3$

would occupy in the furnace should be calibrated independently with the furnace in the absence of the gases.

A chromel-alumel thermocouple was lowered into the silica tube inside which the sample of $La_{1-x}Sr_xCoO_3$ being examined would be placed. The thermocouple was passed through a side arm, which can be seen in Plate 2.1, above the furnace and cooling jacket, via a glass stopper which had been modified for this purpose. The thermocouple was placed in a sample of $La_{0.5}Sr_{0.5}CoO_3$.

The vacuum line was evacuated so that the pressure was lower than what could be read on the Pirani gauge. The furnace was set at the maximum heating rate and the voltage of the thermocouple was recorded as the temperature increased. This was repeated several times with the temperature being set at 300°C and 650°C. When reproducibility of results proved difficult with and without $La_{0.5}Sr_{0.5}CoO_3$ present a set-up whereby the cold junction of the thermocouple was inside the vacuum line was attempted. The temperature of this was followed with a thermometer.

The calibration at lower temperatures, that is, up to 300°C was also attempted, using a mercury thermometer suspended in the silica tube.

2.3.2 Preparation of catalyst samples for adsorption and TPD

The procedure of preparation was similar for all of the adsorption experiments.

Samples of the catalysts were weighed out in silica weighing pans which could be suspended from the microbalance in the vacuum line. The samples were weighed on a Stantan Instruments 4 figure balance.

Once the samples were suspended from the microbalance, it was set on its most sensitive scale, that is, the 1mg scale. The balance was set in such a way that if mass was lost due to evacuation and heating, before adsorption, the system could be rebalanced on this scale.

When the microbalance had settled to a steady reading, this was noted and the vacuum line was evacuated. The mass was allowed to equilibrate again. When the mass attained a constant value, it was noted, as it was after each step of each experiment.

During evacuation of the vacuum line, the MS was also evacuated.

The needle valve between the vacuum line and MS was opened. The MS was switched on and set to detect a mass of 32 a.m.u., that is, the molecular mass of O_2. When the filament had heated and a constant reading of the background partial pressure of O_2 was attained, then the catalyst was heated to 650^{o}C. During this experiment the maximum heating rate was set and the time interval for recording on the BBC was 1.5s, which gave the temperature sufficient time to settle at 650^{o}C.

The desorption of O_2 was monitored so that it could be shown whether O_2 desorbed was preadsorbed from the atmosphere or if it was lattice oxygen.

When the temperature settled at 650°C the mass was allowed to equilibrate before being noted. When constant mass was reached the furnace was allowed to cool to room temperature. The mass was then noted again and the catalyst was re-heated to 650°C. This heating and cooling cycle was repeated until on cooling a constant mass was attained. This mass was then noted and defined as the starting mass for the adsorption experiments.

2.3.3 Adsorption of SO_2 on $La_{1-x}Sr_xCoO_3$

It was decided to expose the catalysts to 7.6 mm Hg SO_2. This figure was chosen because the flow-rig experiments involving SO_2 and CO would study several ratios of SO_2 to CO with a 1% input of SO_2 in each. 7.6 mm Hg is 1% of atmospheric pressure.

The mass was allowed to come to equilibrium at room temperature after the heating and cooling cycles described in section 2.3.2. The gas handling side of the vacuum line was isolated from the microbalance and the pumping system and the manometer tap was shut. Approximately the amount of SO_2, calculated to give 7.6 mm Hg SO_2 in the entire system, that is, 12.9 mm Hg was allowed into the gas handling section. The source of SO_2 was a canister of liquefied SO_2 supplied by BDH Chemicals Ltd. The catalyst was then isolated from the pumping system and the manometer tap was shut. The SO_2 was then slowly allowed into this section of the line. The mass reading was kept on scale by the resetting controls and range changes were made when necessary. The adsorption was considered to be complete when the mass was shown to be constant on a recording by the BBC microcomputer.

The system was re-evacuated in preparation for the TPD. The weight change which occurred during re-evacuation was considered to be due to the desorption of physisorbed SO_2.

TPD was then carried out using the procedure described later in section 2.3.6.

After TPD the adsorption and evacuation were repeated once and sometimes twice, to see if the results were repeatable, or if there was a change in weight due to, for example, some irreversible adsorption of SO_2.

The same samples were used for the adsorption experiments at 100°C, 300°C and 500°C. Before adsorption at a given temperature the catalyst was allowed to cool from 650°C, after the previous TPD. The mass was allowed to settle and the adsorption process was repeated as above.

The above procedure was carried out for x = 0.3, 0.5 and 0.7. Adsorption at x = 0.6 was only done at 500°C.

2.3.3.1 Scavenging experiments with O_2 and CO over catalysts pre-exposed to SO_2 at 500°C

Whenever a catalyst was not restored to its mass before adsorption, by TPD to 650°C, then it was decided that chemical methods of removing the adsorbed SO_2 or reaction product would be investigated.

Adsorption of SO_2 at 500°C on $La_{0.5}Sr_{0.5}CoO_3$, the first catalyst examined by this method, led to a large mass increase which did not

recover on heating to 650°C. It was decided to allow O_2 into the system and when this had no effect to introduce CO, to see if it would react with the surface. The other catalysts were then exposed to CO, after the same treatment.

2.3.3.1.1 Exposure to O_2 of $La_{0.5}Sr_{0.5}CoO_3$ pre-exposed to SO_2 at 500°C

The $La_{0.5}Sr_{0.5}CoO_3$ sample gained a significant weight on exposure to SO_2 at 500°C. This weight was not lost on heating to 650°C, so it was postulated that if, for example, sulphur or sulphides had been formed that they might react with O_2 to produce SO_2 which might then be desorbed.

It was also considered that a possible reaction which might cause a further weight increase on exposure to O_2, might be the formation of sulphates by oxidation of sulphides if these were present.

Initially O_2 supplied to the catalyst surface was present in 40 mm Hg dried air, that is about 8.4 mm Hg O_2, from the laboratory atmosphere, with the catalyst temperature at 500°C. This led to a significant increase in mass. Subsequent evacuation led to no mass change. TPD to 650°C gave a small mass decrease and the MS detected a species of molecular mass 64, which was believed to be SO_2, although this is also the molecular mass of S_2, which would not have required the presence of O_2 for desorption, if it was present, but which would have been expected to desorb after the initial TPD after adsorption of SO_2.

Due to a fault with the microbalance, the catalyst was cooled and allowed up to atmospheric pressure for 36 h, then returned to the

microbalance and re-evacuated. It was heated to 500°C. Exposure to air at 500°C and then to pure O_2 at 500°C, 550°C and 650°C led to very small inconsistent increases and decreases in mass, which did not lead to any significant change. There was certainly no recovery to the mass before exposure to SO_2. This method of retrieving the original mass was abandoned.

2.3.3.1.2 Exposure to CO of catalysts pre-exposed to SO_2 at 500°C

Hibbert and Tseung (12) found that $La_{0.5}Sr_{0.5}CoO_3$ which had been used in the SO_2/CO reaction was sulphided. They found that on passing CO in N_2 over the sulphided catalyst, that sulphur was removed from the used catalyst as COS, by reaction with CO.

It was therefore decided to allow CO on to samples of $La_{1-x}Sr_xCoO_3$ which had had irreversible mass increases on exposure to SO_2.

The first attempt at this experiment was for the $La_{0.5}Sr_{0.5}CoO_3$ sample described in section 2.3.3.1.1. A sample of 71 mm Hg 8% CO in N_2, that is, 5.7 mm Hg CO, was allowed into the system at room temperature. This caused a slight increase in mass. The system was then re-evacuated and heated to 650°C. This method of scavenging sulphur was unsuccessful and was abandoned.

For the other catalysts exposed to SO_2, scavenging of sulphur was attempted by allowing about 2% of atmospheric pressure of CO into the vacuum line, that is, about 15.2 mm Hg. This was done at either room temperature or 600°C or both, and was followed by heating to 650°C in the presence of CO. The procedure for each catalyst is given in Chapter 3. Changes in mass were noted.

The needle valve to the MS was opened, only slightly due to the relatively high pressure of gas in the vacuum line. The MS was set at 60 a.m.u. to detect any COS which may have been formed.

The final procedure described here was repeated for all of the catalysts exposed to SO_2 at 500°C, although $La_{0.3}Sr_{0.7}CoO_3$ and $La_{0.7}Sr_{0.3}CoO_3$ had been exposed to SO_2 and CO together after the SO_2 experiments and before adsorption of CO alone.

2.3.4 Adsorption of CO on $La_{1-x}Sr_xCoO_3$

It was decided to expose the catalysts to 15.2 mm Hg CO, that is, 2% of atmospheric pressure and of the correct stoichiometric ratio which would theoretically react with the 7.6 mm Hg SO_2 used in the SO_2 adsorption experiments described in section 2.3.3. This pressure of CO also gives comparable exposure of the catalyst to that in the flow-rig experiment.

The adsorption of CO was done by the same procedure as that of SO_2 with 25.8 mm Hg of CO being allowed into the gas handling side of the vacuum line. TPD experiments were carried out between each desorption.

The CO was supplied by BDH Chemicals Ltd.

No chemical methods were used to attempt to identify products of any large mass changes which occurred during adsorption.

2.3.5 Simultaneous adsorption of SO_2 and CO on $La_{1-x}Sr_xCoO_3$

Simultaneous adsorption of the reactant gases was carried out in order to compare mass changes due to exposure to both gases, with the individual adsorptions. From this such information as whether there appeared to be competition for adsorption sites, or whether the SO_2/CO reaction recorded in a flow experiment by Hibbert and Tseung (12), appeared to take place. It was expected that if the gases adsorbed at different sites then an additive effect of the mass changes caused by each would be observed. This, however, may be an invalid assumption, as adsorption of say SO_2 on a given site may block a neighbouring CO site of a different nature. If the reaction producing sulphur and CO_2 proceeded then evidence apart from change in mass may be available. Reduction of SO_2 to elemental sulphur on the surface would be expected to be followed by desorption of the sulphur at the temperature of adsorption, that is, 600^{o}C, particularly at the low pressures of the experiment. The sulphur if produced would be expected to be deposited on the cooling jacket above the furnace.

Adsorption of SO_2 and CO on $La_{1-x}Sr_xCoO_3$ was carried out on two of the catalysts which had already been exposed to the full range of SO_2 adsorptions, that is, $La_{0.3}Sr_{0.7}CoO_3$ and $La_{0.7}Sr_{0.3}CoO_3$. All of the $La_{1-x}Sr_xCoO_3$ catalysts studied were also exposed to SO_2 and CO at 600^{o}C after only the preliminary heating and cooling cycles.

The SO_2 and CO gases were admitted to the gas handling section of the vacuum line in the correct amounts to give approximately 7.6 mm Hg SO_2 and 15.2 mm Hg CO exposure to the catalyst when the tap

between the two sections was opened. After the catalyst was exposed to the gases and the mass reached equilibrium then the system was re-evacuated before cooling the catalyst to room temperature. At room temperature approximately 15.2 mm Hg CO was admitted and the samples were heated to 650°C in the presence of CO at 50% of the maximum heating rate. As in the experiments described in section 2.3.3.1.2 the mass spectrometer was set up at 60 a.m.u. to detect any COS which may be produced.

2.3.6 Temperature programmed desorption experiments

The procedure for the TPD experiments was the same after the SO_2 adsorption and CO adsorption experiments.

After adsorption of the gas and equilibration of the mass at the temperature of adsorption then the system was re-evacuated. The MS was evacuated and set up at 64 a.m.u. for SO_2 desorption or at 44 a.m.u. for desorption of CO_2 from the catalysts on which CO was adsorbed. There were two reasons for the detection of CO_2 and not CO. When CO is adsorbed on an oxide when desorption is attempted only CO_2 can be obtained (83). Even if there was desorption of some CO from the catalyst surface the MS would not have detected it. The Anavac-2 MS has a maximum resolution of 1 a.m.u., therefore it could not distinguish between CO and N_2 which both have a molecular mass of 28. The background pressure of N_2 of less than 10^{-7} mm Hg is two orders of magnitude higher than the lowest detectable partial pressure so pressures of greater than 10^{-7} mm Hg CO would be required for detection by the MS.

The needle valve between the MS and the vacuum line was opened and the MS reading was allowed to reach equilibrium. For detection of 64 a.m.u. there was no initial signal, however for CO_2 a low background level was allowed to settle.

When the mass and MS readings were constant the recording of these and the temperature was started. After one minute the TPD was started. The maximum heating rate was always used, that is, about $30^{o}C\ min^{-1}$.

During heating mass losses were compensated for when necessary by adjusting the balance accordingly and the reading was kept on scale, with each change being noted so that the final temperature could be calculated.

Changes in MS scale were also noted. The MS output was used to calculate the desorption energies using the Fortran computer program, MASS1, shown in Appendix 1.

The temperature was allowed to settle at $650^{o}C$, then when the mass was at equilibrium it was recorded before allowing the sample to cool to the temperature required for the next adsorption.

2.3.7 Control experiment with no catalyst present

A control experiment was set up to find out whether there was significant adsorption of either SO_2 or CO by the silica balance pan in which the catalysts were placed during adsorption and TPD.

The vacuum line was set up with the microbalance balanced but with no catalyst present. The line was evacuated and then the furnace

was set to 650°C and the glassware was degassed. The furnace was allowed to cool to room temperature.

When the mass was steady 7.6 mm Hg SO_2 was allowed into the microbalance side of the vacuum line. When the mass had settled the line was re-evacuated. The MS had been evacuated and set at 64 a.m.u. The needle valve was opened and TPD was carried out.

The furnace was allowed to cool to room temperature. The balance pan returned to its mass before SO_2 adsorption and 15.2 mm Hg of CO was allowed into the microbalance side of the vacuum line. The vacuum line was re-evacuated and heated to 650°C.

Mass changes were noted throughout the experiment.

2.4 FLOW-RIG EXPERIMENTS

The reaction of SO_2 and CO over $La_{1-x}Sr_xCoO_3$ (x = 0.3, 0.5, 0.7) was studied at four temperatures with three ratios of the gases and at two flowrates. The reactant and product gases were monitored by gas chromatography. Sulphur was collected in a cold trap.

2.4.1 The flow-rig

2.4.1.1 Description of the flow-rig and associated equipment

The flow-rig which was used to investigate the reaction of SO_2 with CO is represented in Fig. 2.2. The rig was made of glass apart from those parts which were exposed to high temperatures, which were silica. Three flowmeters led to a glass wool filled compartment where the gases could be mixed. From the mixing compartment the gases could either be directed through a sintered silica disc on which the

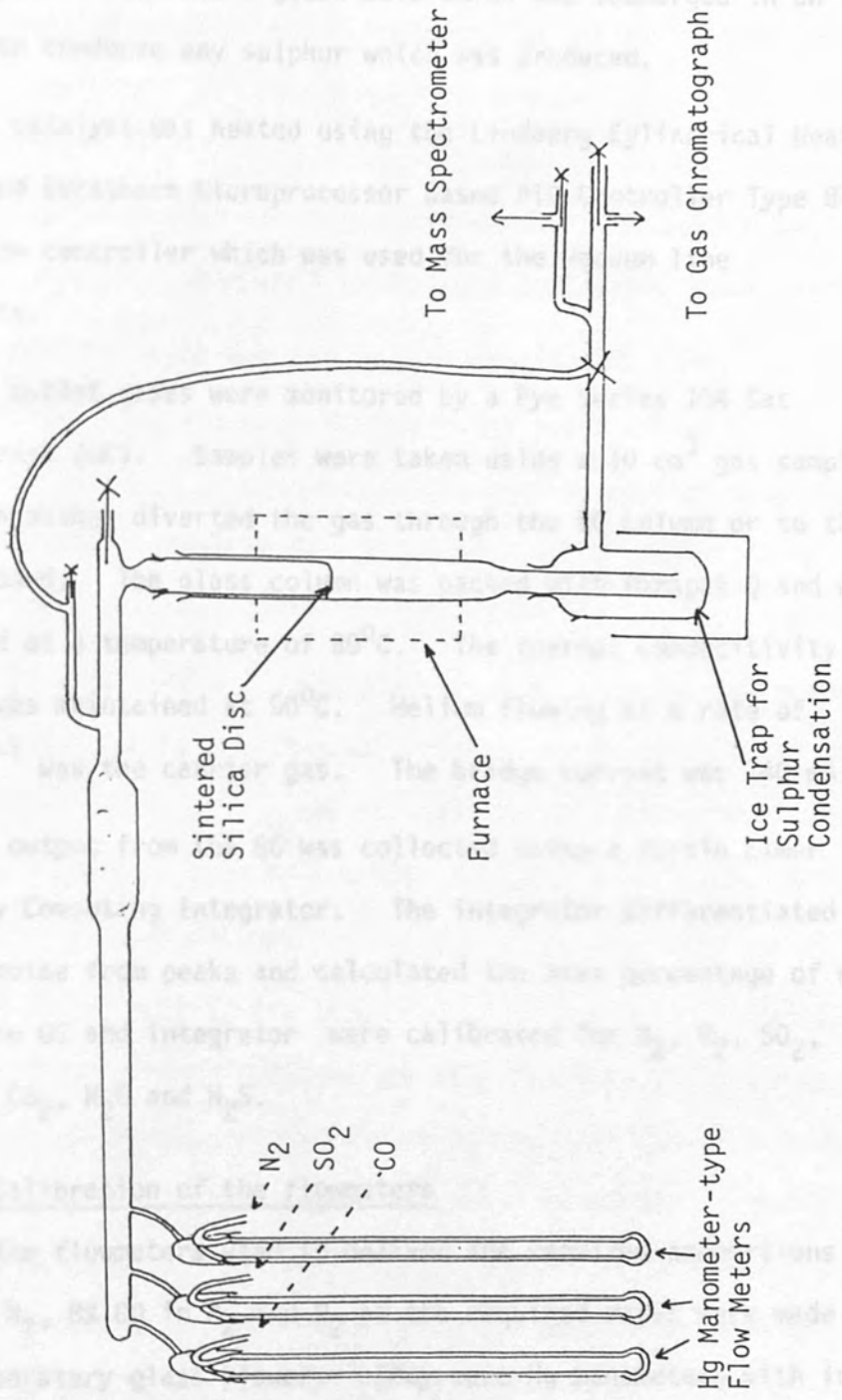

FIGURE 2.2 GAS FLOW-RIG APPARATUS

catalyst was supported or via by-pass tubing, directly to the GC and or to the MS. The tube through which gases flowed over the catalyst fitted into a glass bulb which was submerged in an ice bath to condense any sulphur which was produced.

The catalyst was heated using the Lindberg Cylindrical Heating furnace and Eurotherm Microprocessor Based PID Controller Type 810 temperature controller which was used for the vacuum line experiments.

The outlet gases were monitored by a Pye Series 104 Gas Chromatograph (GC). Samples were taken using a 10 cm^3 gas sampling loop which either diverted the gas through the GC column or to the fume cupboard. The glass column was packed with Porapak Q and was maintained at a temperature of 80^oC. The thermal conducitivity detector was maintained at 90^oC. Helium flowing at a rate of 60 cm^3min^{-1} was the carrier gas. The bridge current was 140 mA.

The output from the GC was collected using a Perkin Elmer Laboratory Computing Integrator. The integrator differentiated baseline noise from peaks and calculated the area percentage of each peak. The GC and integrator were calibrated for N_2, O_2, SO_2, CO_2, COS, CS_2, H_2O and H_2S.

2.4.1.2 Calibration of the flowmeters

The flowmeters used to deliver the required proportions of 5% SO_2 in N_2, 8% CO in N_2 and N_2 at the required rates were made by the laboratory glass blower. They were Hg manometers with inlets from the gas cylinders and capillary outlets to the flow rig.

Each flowmeter had to be calibrated for the range of flow rates of the specific gas for which it was used.

The calibrations were carried out by measuring the length of time in seconds for 5 cm^3 of gas to flow between two points in a bubble flowmeter, for a range of Hg displacements in the manometer. The upper and lower flow rates required were calculated beforehand and the calibrations were done accordingly to include these limits.

The SO_2 flowmeter was calibrated using 5% SO_2 in N_2, which was used in the flow rig experiments. The rates obtained were converted so that $P_{SO_2+N_2}$/mm Hg could be plotted against time for 1 cm^3 SO_2 to flow/s. From this graph the $P_{SO_2+N_2}$ required for the two flow rates to give 1% SO_2 could easily be seen.

The CO flowmeter was calibrated using N_2 although the actual mixture used in the SO_2 and CO reaction experiments was 8% CO in N_2. The rates were converted so that P_{CO+N_2}/mm Hg could be plotted against time for 2 cm^3 CO to flow/s. From this graph the P_{CO+N_2} for 1% CO, 2% CO and 4% CO could easily be derived.

In order to make up the volume of inlet gas to, for example, 1% SO_2 and 2% CO a third inlet to the flow rig from an oxygen free N_2 cylinder was employed. The amount of N_2 required varied considerably depending on whether, for example, a total flow of 100 cm^3 for a 1% SO_2 and 2% CO mixture or total flow of 50 cm^3 for a 1% SO_2 4% CO mixture was required. The amount of N_2 was calculated from the difference in the total flows of the 5% SO_2 in N_2 and 8% CO in N_2. The flow rate of N_2 was plotted as P_{N_2}/mm Hg against N_2 flow/$cm^3 min^{-1}$.

2.4.2 Investigation of the reaction between SO_2 and CO using the flow-rig apparatus

2.4.2.1 Experimental conditions for the SO_2 and CO reaction study

Several catalysts, SO_2:CO ratios, temperatures and contact times were investigated to see which conditions were most suitable for the reaction.

Three catalysts were studied. $La_{0.3}Sr_{0.7}CoO_3$, $La_{0.5}Sr_{0.5}CoO_3$ and $La_{0.7}Sr_{0.3}CoO_3$ were chosen because this gave quite a wide range of La:Sr ratios.

Three ratios of SO_2:CO were chosen. The theoretical stoichiometric ratio was given by 1% SO_2 and 2% CO. A mixture with an excess of CO was made up with 1% SO_2 and 4% CO. A deficiency of CO was given by 1% SO_2 and 1% CO.

Four temperatures were chosen, these were 500°C, 550°C, 600°C and 650°C. Hibbert and Tseung (12) had found that $La_{0.5}Sr_{0.5}CoO_3$ was quite a good catalyst at temperatures of this range. The temperatures were also chosen, bearing in mind the results of the adsorption and TPD experiments.

The effect of contact time was looked at by changing the total flow rate of the gases. For a flow rate of 100 cm^3 min^{-1} each of the catalysts was investigated for the three SO_2:CO ratios and the complete temperature range. Only the 1% SO_2/2% CO and 1% SO_2/4% CO experiments were done at the higher contact time and hence lower flow rate of 50 cm^3 min^{-1}.

2.4.2.2 Experimental procedure for the SO_2 and CO reaction study

The procedure for the investigation of the SO_2 and CO reaction was similar for all of the conditions outlined in section 2.4.1.1.

A sample of the catalyst of known mass was placed on the sintered disc in the flow rig. The furnace was replaced and the coldtrap was refitted and placed in an ice bath.

The gases used were 5% SO_2 in N_2 and 8% CO in N_2, both of which were supplied by BOC. The N_2 which made up the total bulk of the gas was 'white spot' N_2, also supplied by BOC.

The gas flows were set up at the required ratios and rates. The flowmeters took some time to settle so about 1 h was spent regulating and stabilizing the gas flow. The GC was always preset at the conditions described in 2.4.1.1. and several samples of the outlet gas were always analysed at room temperature before heating the catalyst.

The catalyst was heated at 50% of the maximum heating rate, that is, about $15^{o}C\ min.^{-1}$, to $500^{o}C$. During heating the outlet gases were analysed initially using the GC and MS and then using the GC only. It was hoped that following the initial stages of the experiment with the MS set at 64 a.m.u., it would be possible to obtain kinetic data from the change in SO_2 output. This, however, proved impossible as the MS detected no change in the partial pressure of SO_2. The MS was therefore not used in subsequent experiments. The temperature of the furnace was noted for each injection of sample. The data

collected from this range of temperatures was then considered with reference to the changes noted on adsorption of the reactant gases throughout the temperature range from room temperature to 500^{o}C.

The temperature was allowed to equilibrate and the outlet gases were continuously monitored. When several readings gave constant results then the reaction was believed to have reached equilibrium.

The next step of the reaction was to set the temperature controller at 550^{o}C, and allow the temperature to rise to this value. Continuous monitoring of the outlet gases was carried on until equilibration of temperature and then reaction, were achieved.

This process was repeated at 600^{o}C and 650^{o}C. All of the GC output was recorded and printed by the integrator.

For some of the experiments the four temperatures were not investigated during one day. In such a case the procedure was the same as that when a series of four temperatures were studied in sequence. The gases were allowed to continue flowing. The temperature controller was set at 25^{o}C and the furnace was allowed to cool. During cooling the monitoring of the gases by the GC was continued until COS production, if it was occurring had ceased, the detection of SO_2 was steadily increasing and that of CO_2 was steadily decreasing. As always the temperature was noted for each sample taken. When the reaction had evidently completely ceased the SO_2 and CO sources were stopped and a slow flow of N_2 was left passing through the catalyst bed. The furnnace was switched off.

The setting up procedure for a different flow rate or SO_2:CO ratio a higher temperature was identical to that just described and the same sample of catalyst was used throughout the twenty combinations of conditions for each catalyst.

2.4.2.3 Control experiment with no catalyst present

To ascertain whether at the elevated temperatures at which the reaction of SO_2 and CO, to give CO_2 and sulphur takes place, any reaction occurs in the absence of a catalyst, a control was set up.

The flowrig was set up as it was for the catalyst experiments but with no catalyst on the sintered disc. A mixture of 1% SO_2 and 2% CO in N_2 flowing at 100 cm^3 min^{-1} was allowed to flow through the rig. As in the catalyst experiments the outlet gases were continuously monitored and the cold trap was maintained.

When the gas flow was constant and correct the area in which the catalyst would have been and through which the gases flowed was heated to 600°C. The gases were monitored throughout heating and temperature equilibration.

At 600°C the mixture was changed to 1% SO_2 and 4% CO flowing at 100 cm^3 min^{-1}. The furnace was allowed to cool to room temperature with this mixture flowing and constant monitoring of the output by the GC was continued.

At about 250°C the SO_2, CO and N_2 flows were stopped.

CHAPTER 3

EXPERIMENTAL RESULTS

In this chapter the observations made on the interactions between SO_2, CO and $La_{1-x}Sr_xCoO_3$ are reported.

Initially the decomposition of one of the nitrates used to make $La_{1-x}Sr_xCoO_3$ is studied.

The properties of the fresh catalysts are then reported. These include their surface areas, the density of $La_{0.4}Sr_{0.6}CoO_3$, their XRD and ESCA patterns, their conductivities and the e.s.r. spectrum of $La_{0.4}Sr_{0.6}CoO_3$.

Next, the results of the adsorption and desorption studies are included. The setting up of each catalyst for adsorption, the adsorption and desorption cycles and subsequent scavenging reactions of those exposed to SO_2 are related.

The flowrig results are then examined. These are divided according to the value of x in $La_{1-x}Sr_xCoO_3$ and then described with respect to SO_2:CO ratio temperature and total flow rate of the reactant gases.

The properties of the used catalysts are then reported.

3.1 IDENTIFICATION OF PRODUCTS OF DECOMPOSITION OF $Co(NO_3)_2.6H_2O$

During the decomposition of $Co(NO_3)_2.6H_2O$ by evacuation and heating the changes in mass were noted and are shown in Table 3.1.

During heating the gaseous decomposition products were recorded using the MS. The gases H_2O, N_2, NO, O_2 and CO_2 were detected.

Table 3.1

Mass changes during the decomposition of $Co(NO_3)_2.6H_2O$

	Sample 1		Sample 2	
	mass/g ±0.0001	total % change	mass/g ±0.0001	total % change
Initial mass	0.1071	-	0.1098	-
Mass after evacuation	0.0737	31.2	0.0773	29.6
Mass after heating	0.0310	71.1	0.0317	71.1

By using the scanning facility on the MS the relative concentrations of each of these gases and their change with time was followed. The gases are shown in order of abundance for the latter part of the experiment in Fig. 3.1. A peak at 36 a.m.u. appears consistently and has not been assigned. The other peaks were detected on the 10^{-7} mbar range of the MS,this allowed some of the larger peaks to go off scale but ensured that low concentrations of gases were detected.

3.2 PROPERTIES OF FRESH $La_{1-x}Sr_xCoO_3$

The properties of the catalysts, as prepared, are reported as these may dictate the efficiency of the catalytic reaction.

3.2.1 Surface areas of fresh $La_{1-x}Sr_xCoO_3$

The results of surface area measurements by both the automatic single point surface area analysis and the vacuum line and micro-balance multipoint measurement are reported.

FIGURE 3.1 ORDER OF ABUNDANCE OF GASES EVOLVED DURING THE DECOMPOSITION OF $Co(NO_3)_2.6H_2O$ AGAINST TIME

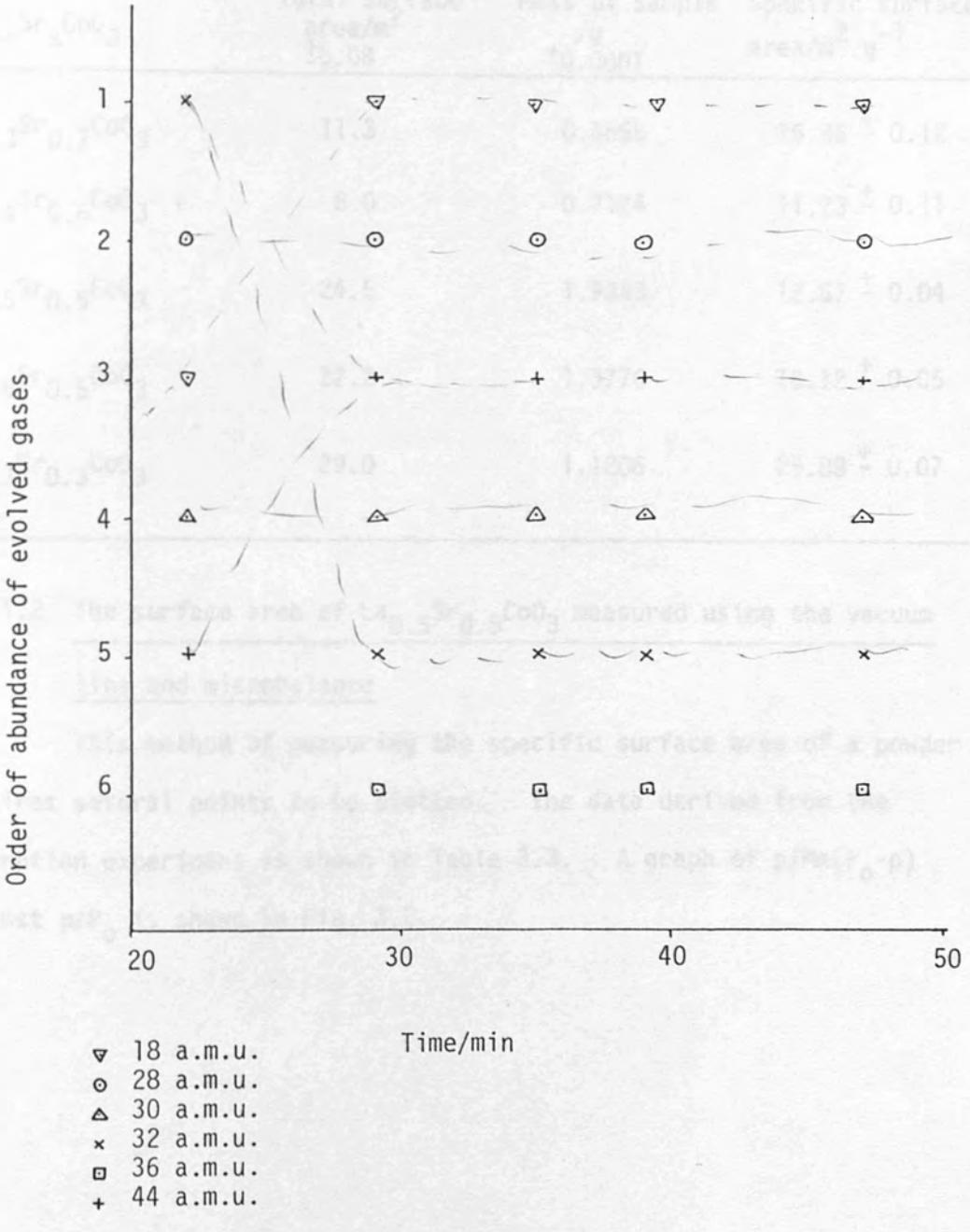

3.2.1.1 Surface areas measured by automatic analysis

The specific surface areas of catalysts measured by the Micromeritics Surface Area Analyser are shown in Table 3.2.

Table 3.2

Specific surface areas of $La_{1-x}Sr_xCoO_3$

$La_{1-x}Sr_xCoO_3$	Total surface area/m^2 ±0.08	Mass of sample /g ±0.0001	Specific surface area/$m^2\ g^{-1}$
$La_{0.3}Sr_{0.7}CoO_3$	11.3	0.6656	16.98 ± 0.12
$La_{0.4}Sr_{0.6}CoO_3$	8.0	0.7124	11.23 ± 0.11
$La_{0.5}Sr_{0.5}CoO_3$	24.5	1.9343	12.67 ± 0.04
$La_{0.5}Sr_{0.5}CoO_3$ 1	22.2	1.3776	16.12 ± 0.05
$La_{0.7}Sr_{0.3}CoO_3$ 2	29.0	1.1206	25.88 ± 0.07

3.2.1.2 The surface area of $La_{0.5}Sr_{0.5}CoO_3$ measured using the vacuum line and microbalance

This method of measuring the specific surface area of a powder requires several points to be plotted. The data derived from the adsorption experiment is shown in Table 3.3. A graph of $p/Ma(P_o-p)$ against p/P_o is shown in Fig. 3.2.

FIGURE 3.2 B.E.T. PLOT OF $p/Ma(P_0 - p)$ against P/P_o FOR ADSORPTION OF N_2 ON $La_{0.5}Sr_{0.5}CoO_3$

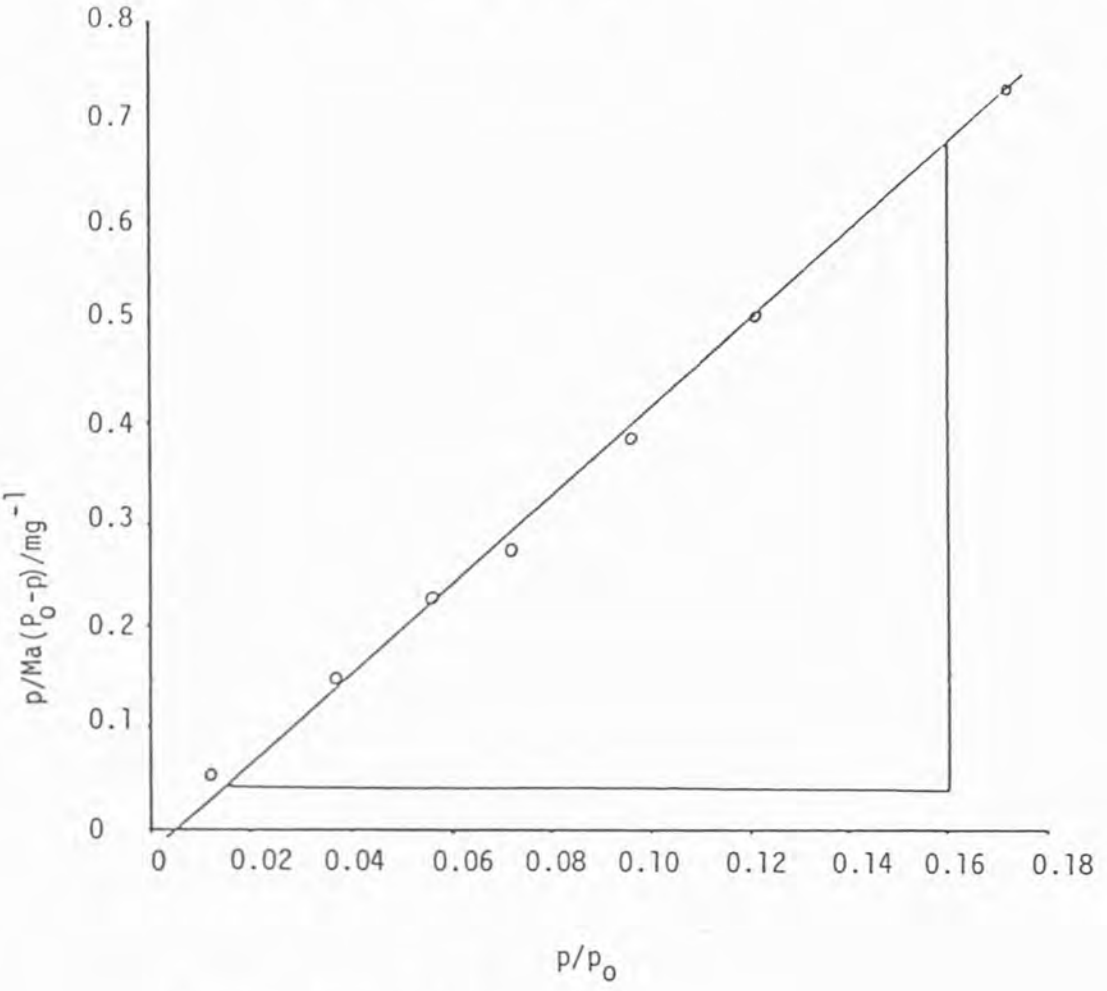

slope = 4.329 ± 0.010

intercept = -0.015 ± 0.009

$$M_m = \frac{1}{\text{slope + intercept}} = \frac{1}{4.329 - 0.015}$$

$= 0.232 \pm 0.013$ mg

$$\text{s.s.a.} = \frac{16.2 \times 10^{-20} \times 6.02252 \times 10^{23} \times 0.232 \times 10^{-3}}{28 \times 0.0963}$$

$= 8.39 \pm 0.56\ m^2g^{-1}$

Table 3.3

Mass and pressure data collected for the calculation of the specific surface area of $La_{0.5}Sr_{0.5}CoO_3$ by the B.E.T. method

N_2 transfer No.	Ma/mg ±0.005	P_{N_2}/mm Hg (p) ±0.7	P_o-p/ mm Hg ±0.7	Ma(P_o-p) ±0.02	p/Ma(P_o-p) ±0.005	p/P_o ±0.001
1	0.24	7	563	135.12	0.052	0.012
2	0.26	21	549	142.74	0.147	0.037
3	0.26	32	538	139.88	0.229	0.056
4	0.28	41	529	148.12	0.277	0.072
5	0.275	55	515	141.62	0.388	0.096
6	0.27	69	501	135.27	0.510	0.121
7	0.28	98	472	132.16	0.742	0.172

Ma = mass of gas adsorbed

P_o = saturated pressure of the adsorbed gas, that is, 570 mm Hg for N_2 at 75 K (77).

From Fig. 3.2 the specific surface area of $La_{0.5}Sr_{0.5}CoO_3$ is calculated to be 8.39 m^2g^{-1} which compares very favourably with the value of 12.67 m^2g^{-1} measured by the automatic method for the same batch of catalyst.

3.2.2 Density of $La_{0.4}Sr_{0.6}CoO_3$

The calculation of the density of $La_{0.4}Sr_{0.6}CoO_3$ is presented below.

Density of water (ρ_w) = 1.00 g cm^{-3}

Mass of bottle plus stopper (empty) (M_{be}) = 5.5679 g

Mass of bottle, stopper and catalyst (M_{bc}) = 6.5528 g

Mass of bottle, stopper and catalyst filled with water (M_{bcw}) = 8.7648 g

Mass of bottle plus stopper, filled with water only (M_{bw}) = 8.0245 g

The volume of the bottle (V_b) is calculated

$$V_b = \frac{M_w}{\rho_w} = \frac{M_{bw} - M_{be}}{\rho_w} = 2.4566 \pm 1.4 \times 10^{-4} cm^3$$

Mass errors = $\pm$ 1 x 10^{-4} g

The volume of water used to fill the bottle when the catalyst is present (V_{cw}) is calculated

$$V_{cw} = \frac{M_{bcw} - M_{bc}}{\rho_w} = = 2.2120 \pm 1.4 \times 10^{-4} cm^3$$

The volume of catalyst present (V_c) is calculated using

$$V_c = V_b - V_{cw} = 0.2446 \pm 2 \times 10^{-4} cm^3$$

The mass of catalyst present (M_c) is calculated

$$M_c = M_{bc} - M_{be} = 0.9849 \pm 1.4 \times 10^{-4} cm^3$$

The density of catalyst ρ_c is calculated

$$\rho_c = \frac{M_c}{V_c} = \frac{0.9849}{0.2446} = 4.0266 \pm 1.5 \times 10^{-4} cm^{-3}$$

$$\simeq 4.03\ gcm^{-3}$$

3.2.3 Bulk properties of fresh $La_{1-x}Sr_xCoO_3$ determined by XRD

The XRD patterns of the fresh catalysts were examined before any exposure to SO_2 or CO, to ensure that they had the perovskite-type structure. The diffraction patterns were compared to unpublished results obtained by Hibbert and Tseung (84) and some peaks were identified using a powder diffraction data manual (80).

The 2θ values of the peaks are shown in Table 3.4.

The major peaks compare well with unpublished work by Hibbert and Tseung (84). $LaCoO_3$ has peaks at 2θ values of 33.01, 33.44 and 47.61 (80) and is closely related to $La_{1-x}Sr_xCoO_3$. Peaks with approximately these values are among the strongest present.

The 2θ values of the fresh $La_{1-x}Sr_xCoO_3$ are of greatest interest when compared to those of the used catalysts.

3.2.4 Surface properties of fresh $La_{1-x}Sr_xCoO_3$, determined by ESCA

The main purpose of studying the ESCA spectra of fresh $La_{1-x}Sr_xCoO_3$ was to measure the binding energies of La, Sr, Co and O so that these could be compared with the values for the used catalysts. If the chemical environment of an atom changes then this may be detected by a change in the binding energy of an electron in a particular energy level.

The binding energies may also be used to confirm the oxidation states of the elements at the surface of $La_{1-x}Sr_xCoO_3$.

The binding energies of the fresh samples are shown in Table 3.5. The value of $\emptyset$ was calculated for each sample from the C1s peak which has a binding energy of 1186 eV.

Table 3.4

XRD of fresh $La_{1-x}Sr_xCoO_3$ (λ = 1.542 Å)

A $La_{0.3}Sr_{0.7}CoO_3$		B $La_{0.4}Sr_{0.6}CoO_3$		A $La_{0.5}Sr_{0.5}CoO_3$		A $La_{0.7}Sr_{0.3}CoO_3$		Major perov-skite peaks
2θ	Intensity	2θ	Intensity	2θ	Intensity	2θ	Intensity	
		10.8	w					
				15.7w	w	15.8	w	
18.4	w							
20.4	w							
23.2	w							
23.5	w							
						24+	bw	
				25	w	25.2	vw	
25.4	m	25.8	m	25.7	w			
27.6	w					27.6	vvw	
28.4	w	28.9	s	28.3	w	28.2	w	
				29.5	w			
31.8	w							
33.1	m	33.2	s	32.9	s	33.1	s	✓
		33.9	m					
36.8	vw							
37.1	vw	37.1		37	w	37.3	w	
						39.9	w	
						41		
		43.8	w	43.8	w			
44.3	vw	44.2	w/m	44.5	vvw	44.5	vw	
48	b	47.6	s			47.5	s	✓
58.6	vb	59	m	59	w	59	m	✓

s = strong m = medium w = weak vs = very strong

vw = very weak.

A = Philips PW 1010 X-ray diffractometer used.

B = Philips PW 1710 X-ray diffractometer used.

✓ indicates the peaks attributed to the perovskite-type structure.

2θ error = $\pm$ 0.05°

Table 3.5

Binding energies of fresh $La_{1-x}Sr_xCoO_3$

	Binding energy/eV			
Energy level	$La_{0.3}Sr_{0.7}CoO_3$	$La_{0.4}Sr_{0.6}CoO_3$	$La_{0.5}Sr_{0.5}CoO_3$	$La_{0.7}Sr_{0.3}CoO_3$
La $3d_{5/2}$	836.5	836.5	836.5	835.9
Sr $3d_{5/2}$	133.7	133.3	133.7	133.1
Co $2p_{3/2}$	780.8	781.3	781.2	780.9
O 1s	532.4	531.8	532	531.6
	531.1*	530.2*	530.4*	529.7

* = shoulder. b.e. error = $\pm$ 0.3eV

The oxidation states of La and Sr are +3 and +2 as expected. Although trivalent and tetravalent Co are present only one peak is present for the Co $2p_{3/2}$ spectrum. According to the Handbook of X-ray photoelectron spectroscopy (81) the binding energies of many Co compounds are very close. The difficulty in distinguishing the two oxidation states and three Co species, that is, Co^{3+}, Co^{III} and Co^{IV} may also be related to the conductivity of $La_{1-x}Sr_xCoO_3$. Two O species are evident, these may be lattice oxygen and adsorbed oxygen.

3.2.5 Conductivities of fresh $La_{1-x}Sr_xCoO_3$

The conductivities of fresh $La_{1-x}Sr_xCoO_3$ samples were measured, to check that they were semiconductors, to see if there was a trend

that changed with the value of x and to compare with used catalysts.

The resistance of the steel bars and connecting wires without any catalyst was 0.1 Ω. The length of the bars under 20 kg equivalent pressure was 86.2 mm. The cross sectional area was 5.73 ± 0.005 mm^2.

The conductivities of the fresh catalysts are shown in Table 3.6. Conducitivity (κ) is calculated using equation 26 shown in section 2.2.1.5 that is,

$$\kappa = \frac{l}{\rho a} \qquad 26$$

l = length of catalyst sample under 20 kg equivalent pressure.

ρ = resistance of catalyst.

a = cross sectional area of catalyst.

Table 3.6

Conductivities of fresh $La_{1-x}Sr_xCoO_3$

$La_{1-x}Sr_xCoO_3$	$l+l_i$/mm ± 0.005	l/mm ± 0.007	$\rho + \rho_l$/Ω ± 0.1	ρ/Ω ± 0.14	κ/Ω^{-1}m^{-1}
$La_{0.3}Sr_{0.7}CoO_3$	86.6	0.4	169.8	169.7	0.4 ± 0.02
$La_{0.4}Sr_{0.6}CoO_3$	86.35	0.15	1.2	1.1	23.8 ± 0.14
$La_{0.5}Sr_{0.5}CoO_3$	86.8	0.6	6	5.9	17.8 ± 0.03
$La_{0.7}Sr_{0.3}CoO_3$	86.8	0.6	6.1	6	17.4 ± 0.03

The conductivity limits which define semiconductors are 10^{-5} - 10^{4} $\Omega^{-1}m^{-1}$. The $La_{1-x}Sr_xCoO_3$ samples fall well within these limits.

The conductivity increases significantly from $La_{0.3}Sr_{0.7}CoO_3$ to $La_{0.4}Sr_{0.6}CoO_3$, that is, from x = 0.7 to x = 0.6, in comparison to the changes observed from x = 0.6 to x = 0.3. The gradual decrease in conductivity on decrease of x from x = 0.6 to x = 0.3 may be real but the closeness of the values suggests that there is a levelling off of the conductivity of $La_{1-x}Sr_xCoO_3$ at high concentrations of La.

3.2.6 E.s.r. studies of $La_{0.4}Sr_{0.6}CoO_3$

The purpose of the e.s.r. study was to attempt a characterization of Co^{IV}.

The e.s.r. spectrum shown in Fig. 3.3 is that of $La_{0.4}Sr_{0.6}CoO_3$ at 19.6°C. The signal is not typical of that produced for a d^5 system of the type to which Co^{IV} would be expected to belong. Fig. 3.4 shows the spectrum produced for $La_{0.7}Sr_{0.3}CoO_3$ at 20.0°C. The signal is similar to that for $La_{0.4}Sr_{0.6}CoO_3$ but it is considerably weaker.

During cooling of the $La_{0.4}Sr_{0.6}CoO_3$ sample to -143.5°C the spectrum became steadily weaker and disappeared. On reheating the signal returned and on further heating to 180°C a sharpening of the signal was observed. In order to determine whether the effects of cooling and heating were reversible another spectrum was run at 21.2°C. The result was the same as that for the previous room temperature

FIGURE 3.3 E.S.R. SPECTRUM OF $La_{0.4}Sr_{0.6}CoO_3$

Temperature = +19.6°C

Field = 3263.9 ± 100G

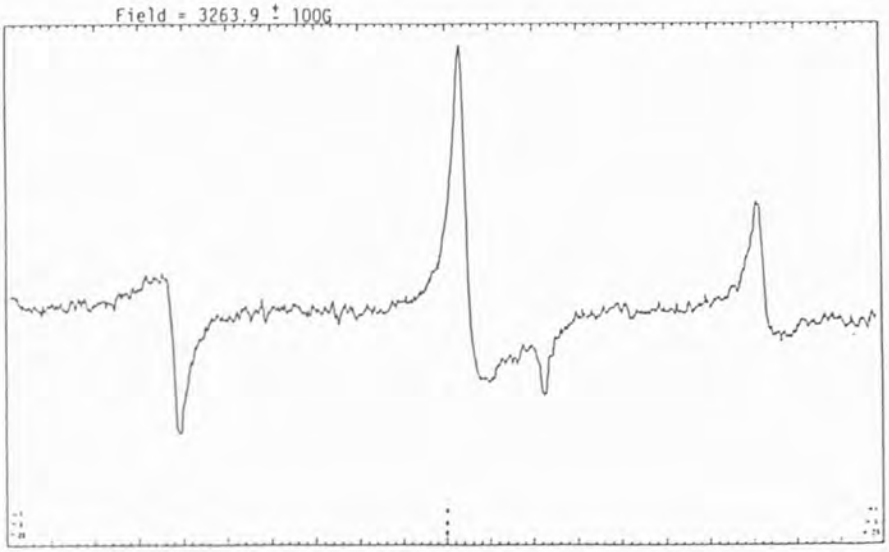

FIGURE 3.4 E.S.R. SPECTRUM OF $La_{0.7}Sr_{0.3}CoO_3$

Temperature = +20.0°C

Field = 3263.9 ± 100G

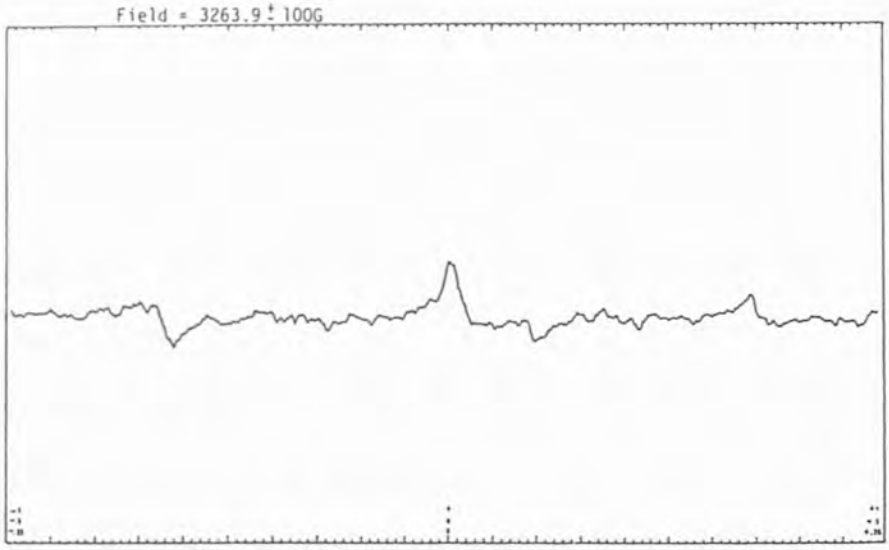

FIGURE 3.5 E.S.R. SPECTRUM OF $La_{0.4}Sr_{0.6}CoO_3$

Temperature = +272.2°C

Field = 3263.9 ± 100G

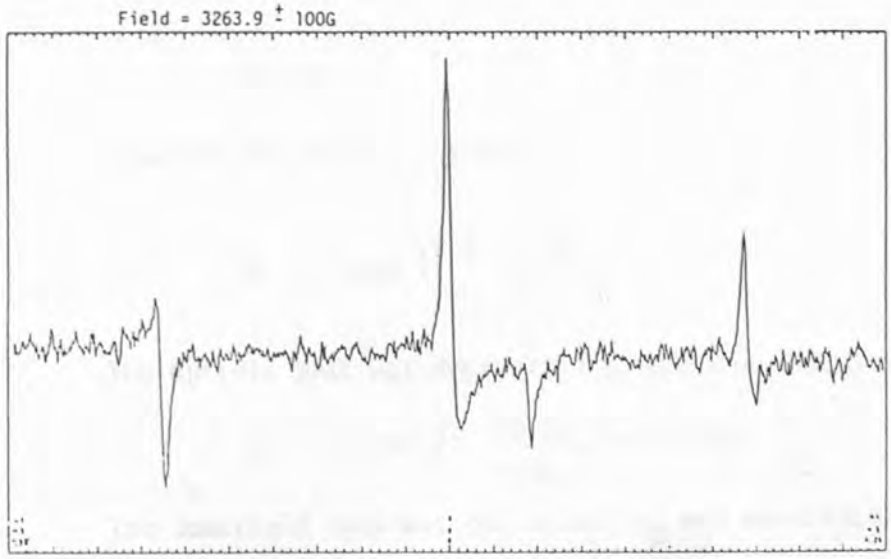

determination, that is, at 19.6°C. The sample was then reheated, this time to 272.2°C and another spectrum was run, this is shown in Fig. 3.5.

The scan of 1000G revealed no further peaks.

The signal obtained was evidently not due to Co^{IV}. To see if perhaps it was due to a lanthanide impurity from the $La(NO_3)_2.6H_2O$ the spectrum of this was run. No signal was obtained.

In order to determine what the signal was due to the g value was calculated. This was done by repeating the scan at 25.2°C with a standard of known g value present, that is, dpph.

The calculation of the g value is shown below.

The central peak has two peaks equidistant on either side, so these can be attributed to the same species.

The dpph peak overlapped with the central peak obtained from $La_{0.4}Sr_{0.6}CoO_3$, so the outer peaks were calculated from the dpph g value (g_{dpph}) and the central peak was calculated from one of these.

$$g_{dpph} = 2.00358 = g_{ref}$$

Equation 29, which is shown in section 2.2.2.6, was used.

$$g = g_{ref}\left(1 \pm \frac{B_{ab}}{B_o}\right) \qquad 29$$

The upfield peak was designated g, and was calculated

$$g_1 = 2.00358\left(1 - \frac{29.88}{3260.0}\right) = 1.9852$$

The downfield peak was designated g_2 and was calculated

$$g_2 = 2.00358\left(1 + \frac{35.75}{3260.0}\right) = 2.0256$$

The g value for the central peak was then calculated from g_1.

$$g_{central} = 1.9852 \left(1 + \frac{32.5}{3260.0}\right) = 2.0050$$

The g value for the species represented by the three peaks was thereby calculated by taking the average value of the three g values. The final g value was therefore 2.0053.

The signal was not assigned and is almost certainly due to an impurity of some sort (85). Apart from lacking the hyperfine splitting expected for Co^{IV} the signal is too small for the amount of Co^{IV} expected (85).

3.3 ADSORPTION AND DESORPTION OF SO_2 AND CO ON $La_{1-x}Sr_xCoO_3$

In this section the details of the heating and cooling procedure for preparation of each catalyst and the subsequent adsorption and desorption cycles will be reported. The consequences of exposing samples which were pre-exposed to SO_2, to CO will also be given.

Before these experiments, which were all carried out in the vacuum line are reported, the dimensions of the vacuum line will be included.

3.3.1 Calculation of the vacuum line dimensions

The volume of the gas handling side was measured by allowing 1000 cm^3 air at atmospheric pressure (760 mm Hg) into this part of the line when it was evacuated. The pressure in the line rose to 283 mm Hg. From these pressures and the initial volume the volume was calculated

$$P_1V_1 = P_2V_2$$

P_1 = 760 mm Hg

V_1 = 1000 cm^3

P_2 = 283 mm Hg

$$V_2 = \frac{760 \times 1000}{283} = 2686 \pm 7 \text{ cm}^3$$

The volume of the gas handling side was therefore 1686 cm^3 (V_g). The next step of the measurement was to isolate the 1000 cm^3 bulb and to allow the 1686 cm^3 of air at 283 mm Hg pressure into the remainder of the vacuum line. The total pressure of the vacuum line was then measured as 167 mm Hg. From these pressures and the volume the total volume of the vacuum line was measured.

$$P_2V_g = P_3V_3$$

P_2 = 283 mm Hg

V_g = 1686 cm^3

P_3 = 167 mm Hg

$$V_3 = \frac{283 \times 1686}{167} = 2857 \pm 12 \text{ cm}^3$$

The volume of the section of the vacuum line which contains the microbalance was then calculated from the difference between the total volume and that of the gas handling side

$$2857 - 1686 = 1171 \pm 14 \text{ cm}^3$$

From these volumes it was possible to calculate the pressure of SO_2 and of CO which when allowed into the gas handling side would give a pressure of 7.6 mm Hg and 15.2 mm Hg respectively in the whole vacuum line. The pressures were 12.9 mm Hg and 25.8 mm Hg respectively.

3.3.2 Calibration of the temperature in the vacuum line with that of the furnace

Obtaining reproducible results of temperatures, as calculated from the chromel-alumel thermocouple, during heating proved to be impossible.

All of the measurements were made when the vacuum was such that it was off scale on the Pirani gauge. The experiment was repeated several times, with the cold function monitored by a thermometer inside the vacuum line but distant from the furnace and outside the vacuum line.

On heating the furnace to 300^{o}C or 650^{o}C the thermocouple eventually gave agreement within 5^{o}C. The static temperatures were therefore taken as those given by the furnace. There may have been errors during TPD. This may have led to errors during calculations of desorption energies using MASS 1. The desorption energies were calculated in order to ascertain whether adsorption was physisorption or chemsorption so the errors did not affect the results considerably.

The calibration at temperatures below 300^{o}C with a mercury thermometer gave better agreement than with the thermocouple. The

temperatures were up to 20°C lower inside the vacuum line, during heating. A lower temperature inside the line during heating can be explained by the lag in heating, particularly in a vacuum.

3.3.3 SO_2 adsorption and desorption experiments

The adsorption and desorption experiments will be reported in the order in which they were carried out. This is because the results of some of the earlier runs influenced the procedure during the latter investigations.

The results of the four experiments will then be compared as this gives the most interesting picture of the work.

3.3.3.1 Adsorption of SO_2 on $La_{0.5}Sr_{0.5}CoO_3$ followed by TPD

The preparation of the catalyst by heating and cooling, the adsorption, desorption and scavenging experiments were all carried out as described in sections 2.3.2 to 2.3.3.1.2. The mass changes due to each step of the experiments are shown in Table 3.7 and graphically in Fig. 3.6.

If Table 3.7 is used as a guide to the graph of the mass changes then the effects of each step of the experiment can easily be followed.

It is evident that heating the catalyst leads to a loss of mass, adsorption causes an increase, evacuation causes a slight decrease and TPD causes a further decrease. This can be seen, for example, at points 27 to 30 on Fig. 3.6.

Table 3.7

SO_2 adsorption on $La_{0.5}Sr_{0.5}CoO_3$

Step No. in experiment	Mass of catalyst/g $\pm 5 \times 10^{-6}$	Procedure just followed
1	0.0902	Initial mass
2	0.09022	Evacuation
3	0.08383	Heated to 650°C
4	0.08511	Cooled to room temperature
5	0.08514	Before adsorption SO_2
6	0.08612	Adsorption SO_2 (r.t.)
7	0.08592	Re-evacuation
8	0.08496	TPD to 650°C
9	0.08502	Cooled to room temperature
10	0.08594	Adsorption SO_2 (r.t.)
11	0.08585	Re-evacuation
12	0.08552	TPD to 650°C
13	0.0859	Cooled to room temperature
14	0.0867	Adsorption SO_2 (r.t.)
15	0.08652	Re-evacuation
16	0.08607	TPD to 650°C
17	0.08603	Cooled to room temperature
18	0.08669	Adsorption SO_2 (r.t.)
19	0.08669	Re-evacuation
20	0.08642	TPD to 650°C
21	0.08682	Cooled to room temperature
22	0.0867	Heated to 100°C
23	0.08753	Adsorption SO_2 (100°C)
24	0.08723	Re-evacuation
25	0.08722	TPD to 650°C
26	0.08774	Cooled to room temperature
27	0.0877	Heated to 100°C

table continued

Table 3.7 (continued)

Step No. in experiment	Mass of catalyst/g $\pm$ 5 x 10^{-6}	Procedure just followed
28	0.08828	Adsorption SO_2 (100°C)
29	0.08815	Re-evacuation
30	0.08787	TPD to 650°C
31	0.08815	Cooled to room temperature
32	0.08758	Heated to 300°C
33	0.08816	Adsorption SO_2 (300°C)
34	0.08815	Re-evacuation
35	0.08802	TPD to 650°C
36	0.08831	Cooled to room temperature
37	0.08835	Left for 1 day
38	0.08825	Heated to 300°C
39	0.0885	Adsorption SO_2 (300°C)
40	0.08847	Re-evacuation
41	0.08827	TPD to 650°C
42	0.0886	Cooled to room temperature
43	0.08842	Heated to 500°C
44	0.09305	Adsorption SO_2 (500°C)
45	0.09317	Cooled to room temperature
46	0.09326	Re-evacuation
47	0.09568	Adsorption SO_2 (r.t.) and heated to 500°C
48	0.09573	Re-evacuation
49	0.09574	Before TPD
50	0.09554	TPD to 650°C
51	0.09575	Left at 650°C
52	0.09576	Cooled to 500°C
53	0.09714	Adsorption O_2 (air)
54	0.09714	Re-evacuation
55	0.09696	Heated to 650°C
56	0.0963	Allow air into system, removed from balance, re-balance and evacuate

table continued

Table 3.7 (continued)

Step No. in experiment	Mass of catalyst/g $\pm 5 \times 10^{-6}$	Procedure just followed
57	0.09579	Heat to 500°C
58	0.09599	Adsorption O_2 (air, 500°C)
59	0.0963	Heated to 650°C
60	0.09638	Cooled to 500°C
61	0.09624	Adsorption O_2 (500°C)
62	0.0962	Heated to 650°C
63	0.09626	Left at 650°C
64	0.0923	Cooled, allowed air into system, removed from balance, re-balanced and evacuated.
65	0.0919	Heated to 650°C
66	0.09206	Cooled to 500°C. Adsorption SO_2 (500°C)
67	0.09216	Re-evacuation
68	0.09201	Heated to 650°C
69	0.09217	Before adsorption O_2
70	0.09217	Adsorption O_2 (650°C)
71	0.09246	Re-evacuation
72	0.09248	Before adsorption
73	0.09224	Adsorption O_2 (650°C)
74	0.09257	Evacuation and cooled to 500°C
75	0.09229	Adsorption O_2 (500°C)
76	0.09268	Re-evacuation
77	0.09266	Heated to 550°C
78	0.0927	Left at 550°C
79	0.09237	Before adsorption O_2
80	0.09236	Adsorption O_2 (550°C)
81	0.09245	Cooled to room temperature
82	0.0926	Adsorption CO (8% CO 92% N_2, r.t.)
83	0.09259	Re-evacuation
84	0.09272	TPD to 650°C
-	0.0956	Cooled to room temperature, allowed air into system re-weighed in 4 fig. balance

FIGURE 3.6 ADSORPTION OF SO_2 ON $La_{0.5}Sr_{0.5}CoO_3$

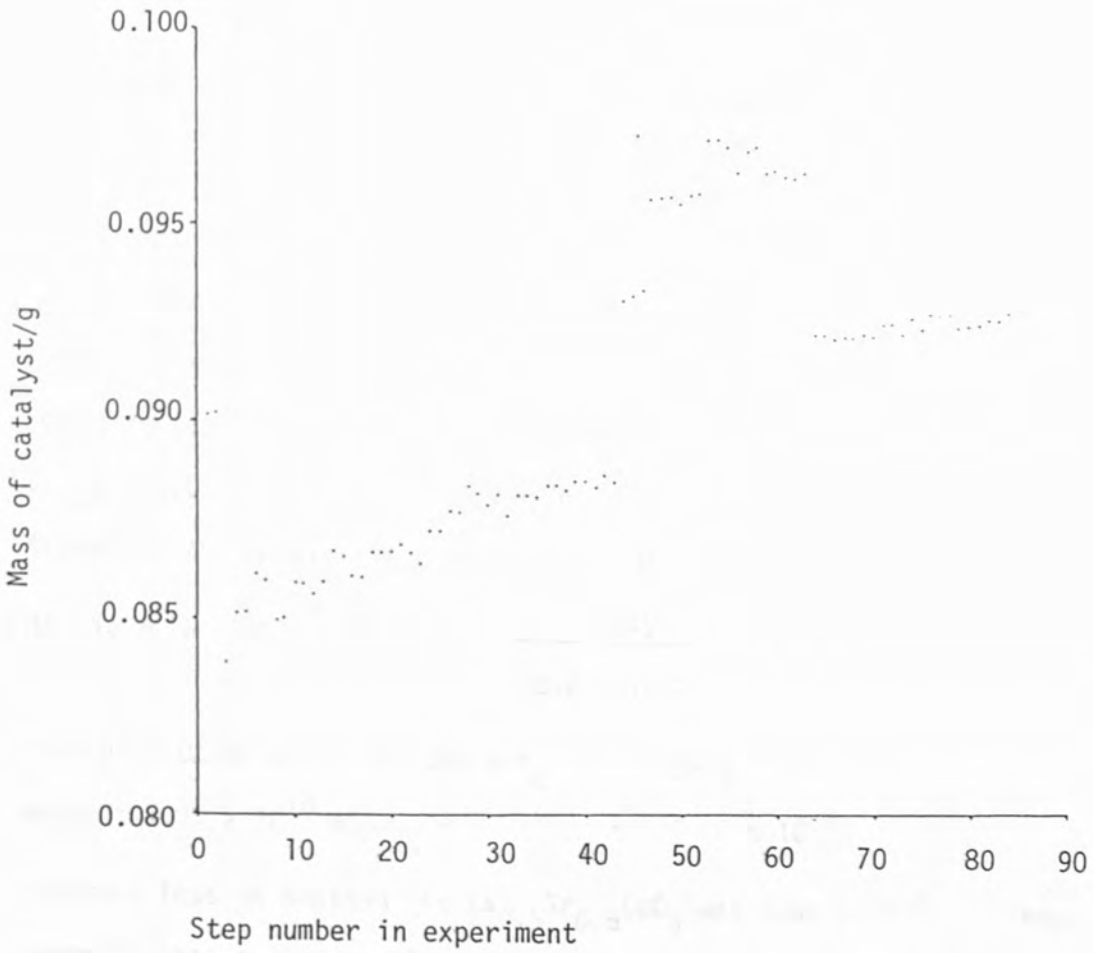

The first steps of the experiment are the evacuation and heating of the catalyst. The mass spectrum due to oxygen desorption is shown with the temperature change, in Fig. 3.7. The temperature of the first O_2 peak was 592°C. The total loss of mass due to evacuation and heating before adsorption was equivalent to 5.61% of the initial mass. This mass loss was probably due to degassing of the $La_{0.5}Sr_{0.5}CoO_3$ sample as well as loss of oxygen. The loss of mass expected from degassing was calculated. The approximation that a monolayer of N_2 was adsorbed was made. This approximation was made in order to calculate the maximum mass loss expected for desorption of air adsorbed on the surface. The surface area of an N_2 molecule was given as 16.2Å, that is, $16.2 \times 10^{-20} m^2$. The initial mass of $La_{0.5}Sr_{0.5}CoO_3$ was 0.0902 g, the specific surface area was 16.12 $m^2 g^{-1}$ therefore the total surface area was 1.45 m^2.

$$\text{No. } N_2 \text{ molecules adsorbed} = \frac{1.45}{16.2 \times 10^{-20}} = 8.95 \times 10^{18}$$

Mass of 6.02252×10^{23} molecule N_2 = 28 g

Mass of 8.95×10^{18} molecule = 4.16×10^{-4} g

The mass loss on heating the $La_{0.5}Sr_{0.5}CoO_3$ was 5.06×10^{-3} g. This suggests that oxygen was lost from the bulk of the sample, that is, lattice oxygen.

The adsorption and desorption experiments at room temperature, 100°C and 300°C are shown. The cyclical nature of the experiment is evident and it is obvious that as the temperature of adsorption is increased, the mass is increasing as TPD does not cause desorption

FIGURE 3.7 MASS SPECTROMETER SIGNAL DUE TO O_2 DESORPTION FROM $La_{0.5}Sr_{0.5}CoO_3$ AND TEMPERATURE PLOTTED AGAINST TIME

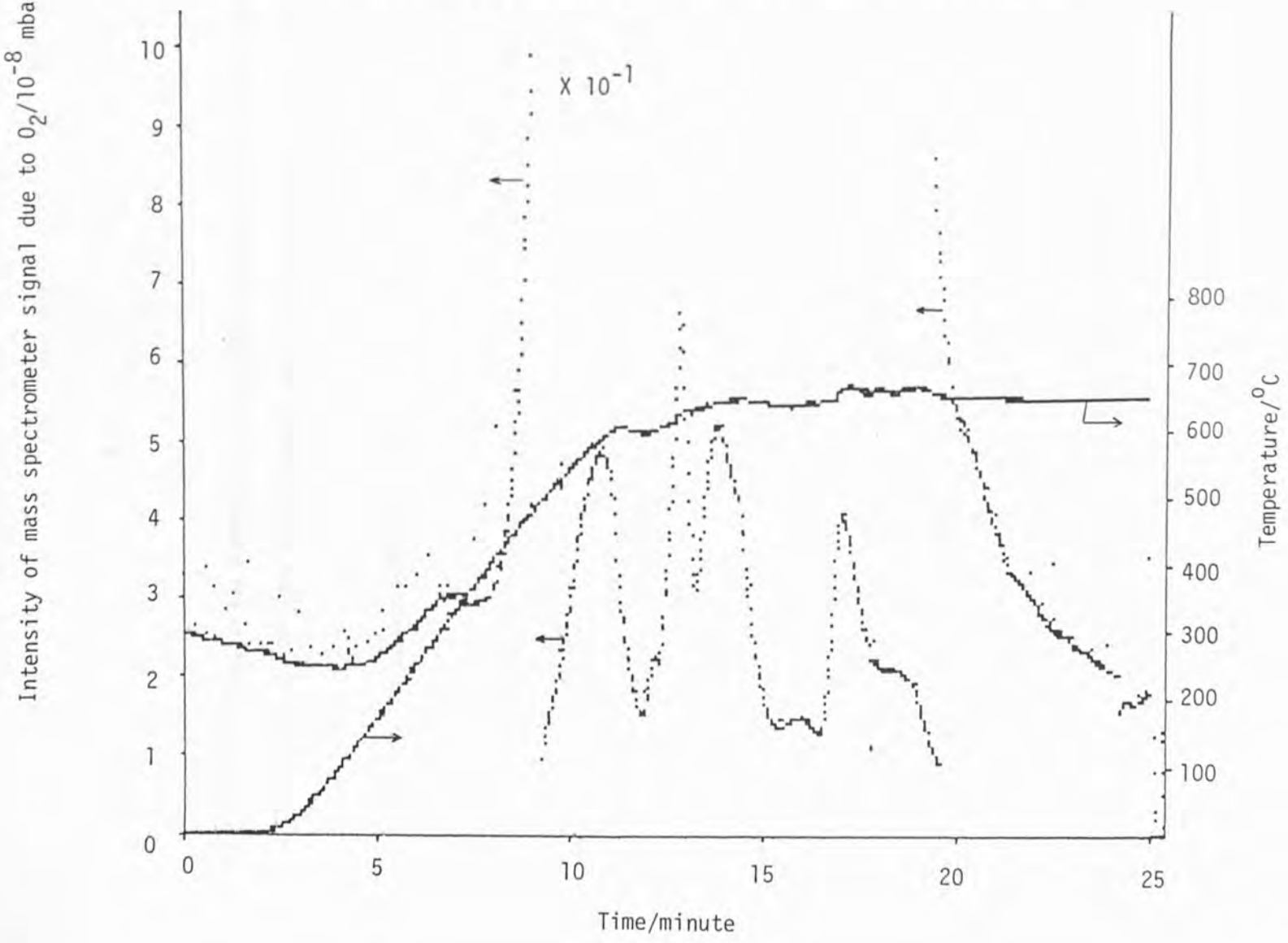

of all of the adsorption products. A steady increase in mass is therefore observed.

The first major break in the graph is at point 44 and is due to adsorption of SO_2 at 500°C. It seems that at a temperature between 300°C and 500°C sufficient energy is supplied for chemisorption, or reaction with the surface which is impossible at 300°C. The break in the adsorption of SO_2 at 500°C was due to an unavoidable delay but the adsorption was continued as shown at point 47. The total mass increase was equivalent to 12.38% of the mass before adsorption.

The remainder of the experiment was spent unsuccessfully attempting to remove the excess weight by a series of air, O_2 and CO in N_2 exposures. The loss of mass at point 64 was not a chemical loss but due to an interruption of the experiment where the catalyst was removed and then re-balanced. During the disturbance some of the sample was lost.

The results of the computation of the TPD experiments using the program MASS 1 are shown in Table 3.8.

Some of the desorptions did not produce well defined MS peaks and these were too complicated for MASS 1 to calculate the desorption energies.

Table 3.8

Desorption energies of SO_2 from $La_{0.5}Sr_{0.5}CoO_3$

Temperature of adsorption ^oC	No. species desorbed	Desorption energies/kJ mol^{-1}	F*
25	2	61.81, 78.17	0.11E-01
42	2	42.10, 53.29	0.26E-01
32	2	41.88, 49.33	0.16E-01
41	2	37.92, 49.90	0.42E-01
100	2	34.88, 62.57	0.13E-01
100	2	34.9, 49.8	-
300	1	73.49	0.14E-01
300	1	108.9	0.13-01
500	-	-	
500	-	-	

* see section 3.6

Those calculated indicate mostly chemisorption. Those below 40 kJ mol^{-1} were on the borderline of relatively strong physisorption and weak chemisorption according to Bond (83). Bond states that physisorption has a heat of adsorption of 8-20 kJ mol^{-1} and chemisorption is 40-800 kJ mol^{-1}. The activation energies are not zero and this suggests chemisorption has occurred. The mass spectrum of the TPD of SO_2 after adsorption at 42^oC and the temperature change as collected by the BBC microcomputer are shown in Fig. 3.8a. The output from the calculation of the desorption energies by MASS 1, of this data, is shown in Fig. 3.9.

FIGURE 3.8a MASS SPECTROMETER SIGNAL DUE TO SO_2 DESORPTION FROM $La_{0.5}Sr_{0.5}CoO_3$ (AFTER SO_2 ADSORPTION AT ROOM TEMPERATURE) AND TEMPERATURE PLOTTED AGAINST TIME

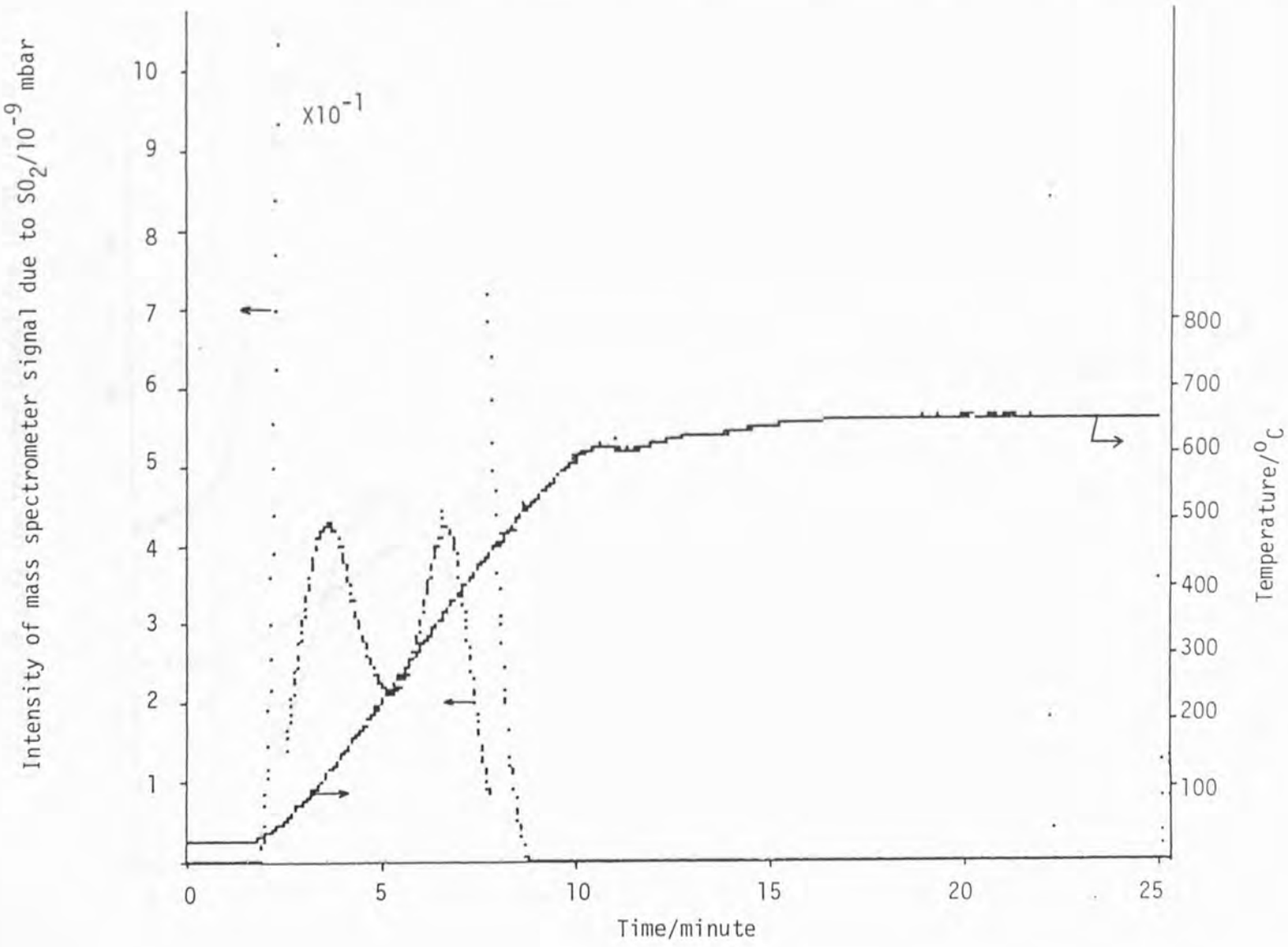

FIGURE 3.8b MASS SPECTROMETER SIGNAL DUE TO CO_2 DESORPTION FROM $La_{0.5}Sr_{0.5}CoO_3$ (AFTER CO ADSORPTION AT 300°C) AND TEMPERATURE PLOTTED AGAINST TIME

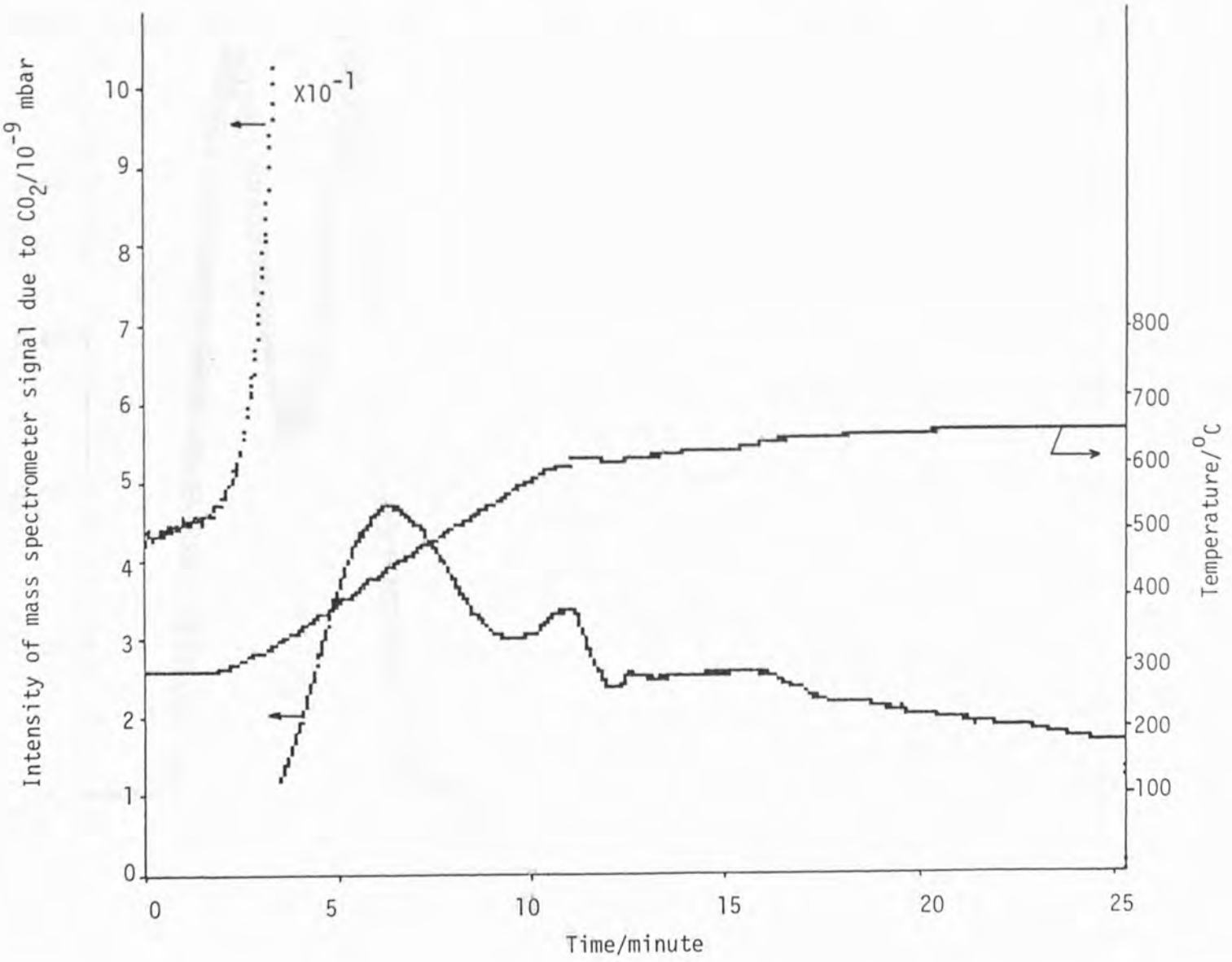

FIGURE 3.9 OUTPUT OBTAINED FROM MASS1 COMPUTER PROGRAM FOR TPD OF SO_2 FROM $La_{0.5}Sr_{0.5}CoO_3$

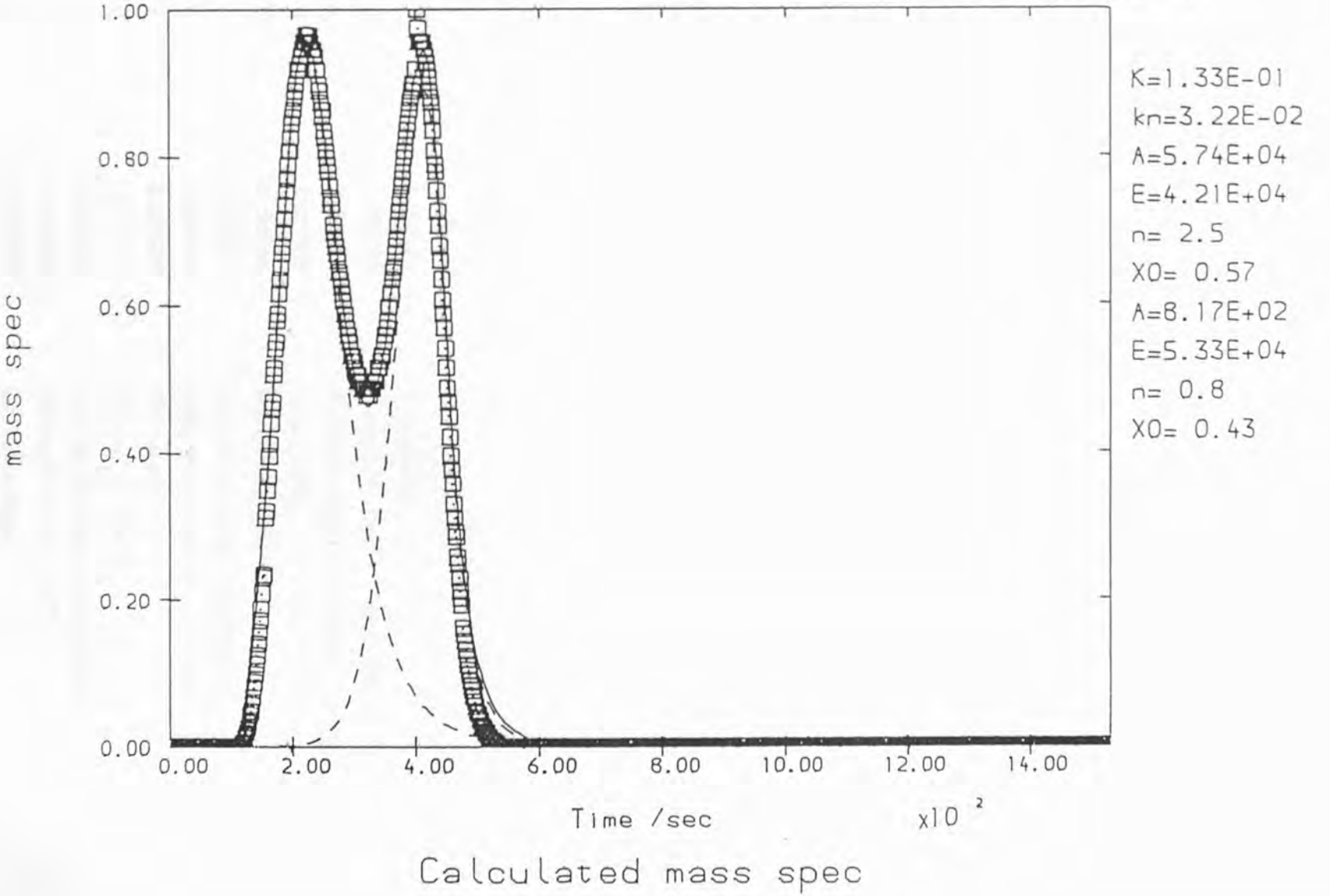

From the desorption energies it can be seen that on first exposing $La_{0.5}Sr_{0.5}CoO_3$ to SO_2 there is relatively strong chemisorption. The subsequent exposures at the lower temperatures are less strong and this may indicate a modification of the surface by the initial SO_2 adsorption. The adsorptions at 300°C are also strong. Those at 500°C are so strong that desorption is very slight and it is not possible to calculate the desorption energies.

3.3.3.2 Adsorption of SO_2 on $La_{0.3}Sr_{0.7}CoO_3$ followed by TPD

The preparation, for adsorption, of the catalyst, the adsorption, desorption and scavenging steps of the experiment are shown in Table 3.9. Each step is represented graphically in Fig. 3.10.

Table 3.9

SO_2 adsorption on $La_{0.3}Sr_{0.7}CoO_3$

Step No. in experiment	Mass of catalyst/g ± 5 x 10^{-6}	Procedure just followed
1	0.0935	Initial mass
2	0.09148	Evacuation
3	0.08243	Heated to 650°C (went off scale)
4	0.0859	Allowed up to atmospheric pressure
5	0.08586	Evacuation
6	0.08536	Heated to 650°C
7	0.0858	Cooled to room temperature
8	0.08592	Left with just rotary pump
9	0.08605	Re-evacuation
10	0.08509	Heated to 650°C
11	0.08584	Cooled to room temperature
12	0.08619	Adsorption SO_2 (r.t.)
13	0.0862	Re-evacuation
14	0.08579	TPD to 650°C

table continued

Table 3.9 (continued)

Step No. in experiment	Mass of catalyst/g ± 5 x 10^{-6}	Procedure just followed
15	0.08754	Cooled to room temperature and left with just rotary pump
16	0.08762	Re-evacuation
17	0.08763	Adsorption SO_2 (r.t.)
18	0.0871	Re-evacuation
19	0.08633	TPD to 650°C
20	0.08656	Cooled to room temperature
21	0.08678	Adsorption SO_2 (r.t.)
22	0.08672	Re-evacuation
23	0.08632	TPD to 650°C
24	0.08679	Left at 650°C
25	0.08709	Cooled to room temperature
26	0.08738	Adsorption SO_2 (r.t.)
27	0.08727	Re-evacuation
28	0.08691	TPD to 650°C
29	0.08695	Left at 650°C
30	0.08723	Cooled to room temperature
31	0.08717	Heated to 100°C
32	0.08713	Before adsoprtion SO_2
33	0.08734	Adsorption SO_2 (100°C)
34	0.08729	Re-evacuation
35	0.08696	TPD to 650°C
36	0.08706	Left at 650°C
37	0.08734	Cooled to 100°C
38	0.08763	Adsorption SO_2 (100°C)
39	0.08754	Re-evacuation
40	0.0872	TPD to 650°C
41	0.08752	Cooled to 100°C
42	0.08772	Adsorption SO_2 (100°C)
43	0.08765	Re-evacuation
44	0.08725	TPD to 650°C

table continued

Table 3.9 (continued)

Step No. in experiment	Mass of catalyst/g $\pm 5 \times 10^{-6}$	Procedure just followed
45	0.08802	Cooled to room temperature and left rotary pumping, then diff. pump led to no change
46	0.08759	Heated to 300°C
47	0.08827	Adsorption SO_2 (300°C)
48	0.08819	Re-evacuation
49	0.08805	TPD to 650°C
50	0.08812	Cooled to 300°C
51	0.08825	Adsorption SO_2 (300°C)
52	0.08825	Re-evacuation
53	0.08813	TPD to 650°C
54	0.08824	Cooled to 500°C
55	0.08825	Before adsorption SO_2
56	0.09051	Adsorption SO_2 (500°C)
57	0.09051	Re-evacuation
58	0.09051	TPD to 650°C
59	0.09052	Cooled to 500°C
60	0.09072	Adsorption SO_2 (500°C)
61	0.09072	Re-evacuation and TPD to 650°C
62	0.09116	Cooled to room temperature
63	0.09071	Heated to 600°C
64	0.09086	Before allow CO into system
65	0.09059	Allowed CO into system (600°C)
66	0.09066	Re-evacuation
67	0.09056	Heat to 650°C
68	0.09086	Cooled to room temperature and left rotary pumping
69	0.09096	Re-evacuation
70	0.09096	Allowed CO into system (r.t.)
71	0.09126	Heated to 650°C in presence of CO
72	0.09026	Re-evacuation
73	0.09026	Cooled to room temperature

table continued

Table 3.9 (continued)

Step No. in experiment	Mass of catalyst/g $\pm 5 \times 10^{-6}$	Procedure just followed
74	0.09106	Allowed CO into system (r.t.) and heated to 650°C in presence of CO
75	0.09034	Re-evacuation
76	0.09036	Cooled to room temperature
77	0.09005	Heated to 600°C
78	0.10296	Adsorption SO_2 and CO (600°C)
79	0.10316	Re-evacuation
80	0.10316	Cooled to room temperature
81	0.10306	Allowed CO into system (r.t.) and heated to 650°C in presence of CO
82	0.10276	Re-evacuation
83	0.10326	Cooled to 600°C
84	0.10316	Allowed CO into system (600°C)
85	0.10296	Re-evacuation (rotary pump)
-		Cooled to room temperature and allowed up to atmosphere pressure

The trend observed is very similar to that described for $La_{0.5}Sr_{0.5}CoO_3$. There is a considerable decrease in mass due to evacuation and heating. The loss is equivalent to 8.19% of the initial mass. The temperature of the first O_2 peak was 353°C.

The expected loss of mass due to desorption of a monolayer of N_2 was calculated for this sample in the same manner as it was for $La_{0.5}Sr_{0.5}CoO_3$ in section 3.3.3.1. The expected mass loss was

FIGURE 3.10 ADSORPTION OF SO_2 ON $La_{0.5}Sr_{0.5}CoO_3$

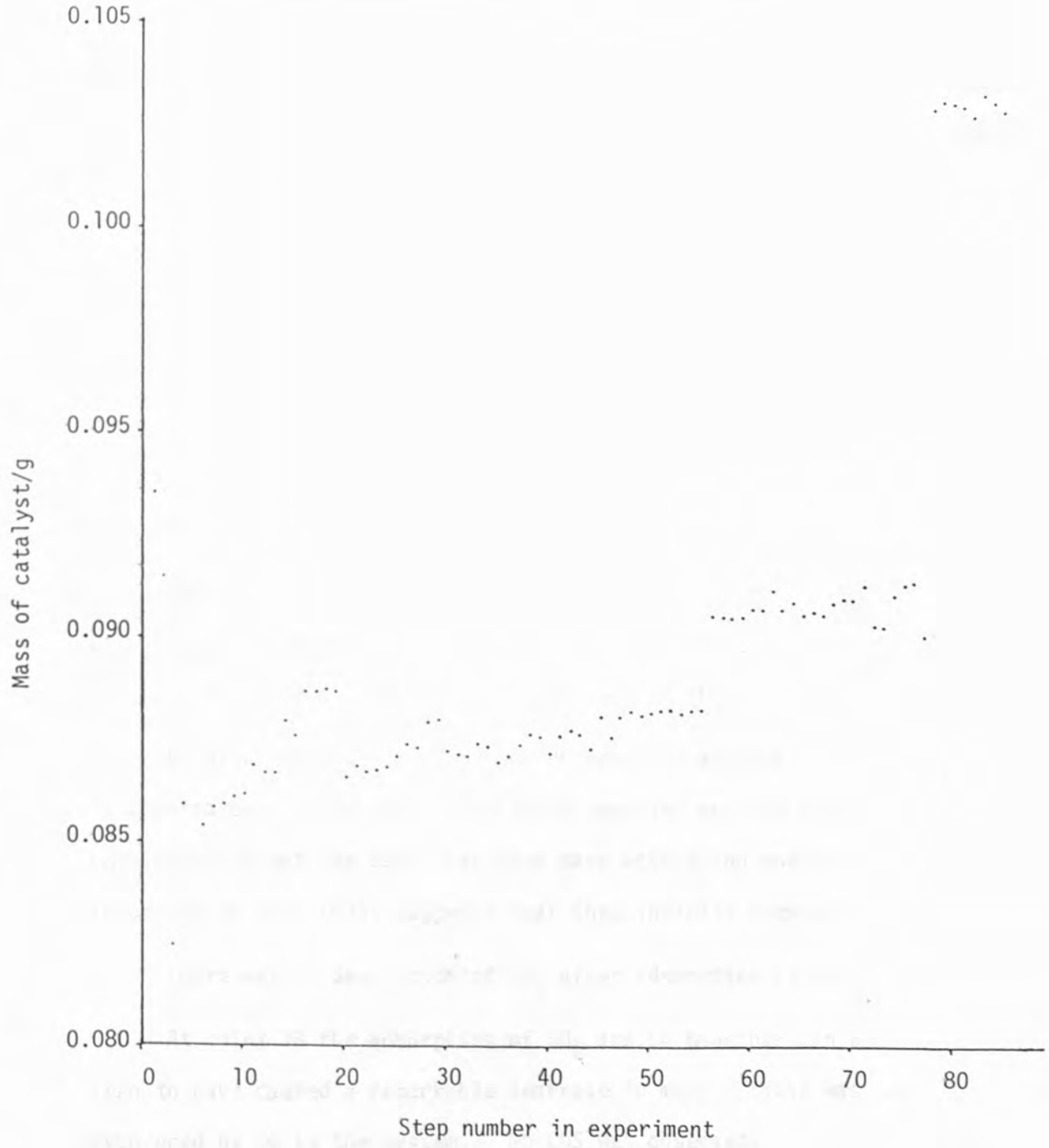

4.57×10^{-4}g and the observed loss of mass due to heating in a vacuum was 7.66×10^{-3} g. Allowing for an error in the assumption that a monolayer of N_2 may be desorbed it seems that like the $La_{0.5}Sr_{0.5}CoO_3$ sample there was evolution of lattice oxygen.

The mass of the sample increased gradually with each adsorption and TPD cycle until at 500°C adsorption is significantly greater than at the lower temperatures. The mass increase was equivalent to 5.44% of the mass before adsorption.

In this experiment 100% CO was allowed into the system to attempt to scavenge sulphur species from the catalyst surface. This was not very successful, yet after further exposure to CO and evacuation, at point 72 of Fig. 3.10 the mass did fall slightly.

The observation that the desorption energies of SO_2 from $La_{0.5}Sr_{0.5}CoO_3$ increased with adsorption temperature is repeated for $La_{0.3}Sr_{0.7}CoO_3$. This is shown in Table 3.10.

As with the $La_{0.5}Sr_{0.5}CoO_3$ experiment, it appears that the SO_2 is chemisorbed. The lower desorption energies are low for chemisorption but the fact that they have activation energies, according to Bond (83), suggests that they indicate chemisorption.

There was no desorption of SO_2 after adsorption at 500°C.

At point 78 the adsorption of SO_2 and CO together can be seen to have caused a remarkable increase in mass. This was not recovered by CO in the system. No COS was observed.

Table 3.10

Desorption energies of SO_2 from $La_{0.3}Sr_{0.7}CoO_3$

Temperature of adsorption/°C	No. species desorbed	Desorption energies/ kJ mol^{-1}	F*
41	3	38.10, 52.57, 53.23	0.28E-01
25	3	34.81, 55.20, 55.62	0.18E-01
25	3	50.00, 60.00, 70.00	0.12E-01
25	3	34.81, 55.20, 55.62	
100	2	36.22, 61.72	0.25E-01
100	2	35.86, 57.72	0.20E-01
100	2	34.29, 90.85	0.35E-01
300	1	148.7	0.14E-01
300	1	188.6	0.23E-01
500	-	-	

* see section 3.6

There was no visual evidence of sulphur deposition, however, when the sample was allowed up to atmospheric pressure it did smell of sulphur.

3.3.3.3 Adsorption of SO_2 on $La_{0.7}Sr_{0.3}CoO_3$ followed by TPD

The preparation, for adsorption, of the catalyst, the adsorption, desorption and scavenging steps of the experiment are shown in Table 3.11. Each step is represented graphically in Fig. 3.11.

Table 3.11

SO_2 adsorption on $La_{0.7}Sr_{0.3}CoO_3$

Step No. in experiment	Mass of catalyst/g ± 5 x 10^{-6}	Procedure just followed
1	0.1615	Initial mass
2	0.16143	Evacuation
3	0.1578	Heated to 650°C
4	0.16004	Cooled to room temperature and left with just rotary pump
5	0.16005	Re-evacuation
6	0.15882	Heated to 650°C
7	0.1592	Appeared to leak - re-evacuation
8	0.15936	Cooled to room temperature
9	0.15917	Heated to 650°C
10	0.15931	Cooled to 49°C
11	0.15915	Heated to 650°C
12	0.15982	Cooled to room temperature
13	0.15972	Before adsorption SO_2
14	0.16055	Adsorption SO_2 (r.t.)
15	0.16033	Re-evacuation
16	0.16949	TPD to 650°C
17	0.15955	Cooled to room temperature
18	0.15956	Before adsorption SO_2
19	0.16042	Adsorption SO_2 (r.t.)
20	0.16027	Re-evacuation
21	0.15969	TPD to 650°C
22	0.16114	Cooled to room temperature
23	0.16123	Adsorption SO_2 (r.t.)
24	0.16094	Re-evacuation
25	0.15968	TPD to 650°C
26	0.16008	Cooled to 100°C
27	0.16011	Before adsorption SO_2

table continued

Table 3.11 (continued)

Step No. in experiment	Mass of catalyst/g $\pm 5 \times 10^{-6}$	Procedure just followed
28	0.16072	Adsorption SO_2 (100°C)
29	0.16055	Re-evacuation
30	0.15988	TPD to 650°C
31	0.15997	Cooled to 100°C
32	0.16000	Isolated from pump to pump back to SO_2 cylinder and re-evacuated
33	0.16078	Adsorption SO_2 (100°C)
34	0.16060	Re-evacuation
35	0.16009	TPD to 650°C
36	0.16016	Cooled to 300°C
37	0.16025	Isolated from pump to pump back to SO_2 cylinder and re-evacuated
38	0.1608	Adsorption SO_2 (300°C)
39	0.16072	Re-evacuation
40	0.16047	TPD to 650°C
41	0.16048	Cooled to room temperature
42	0.16198	Allowed up to atmospheric pressure for 2 days
43	0.16169	Re-evacuation
44	0.16073	Heat to 650°C
45	0.16083	Cooled to 300°C
46	0.16077	Isolated from pump to pump back to SO_2 cylinder and re-evacuated
47	0.16112	Adsorption SO_2 (300°C)
48	0.16114	Re-evacuation
49	0.16099	TPD to 650°C
50	0.16112	Cooled to 500°C
51	0.16095	Isolated from pump to pump back to SO_2 cylinder and re-evacuated
52	0.1904	Adsorption SO_2 (500°C)
53	0.1914	Re-evacuation
54	0.1904	Cooled to room temperature
55	0.1904	Allowed up to atmospheric pressure
56	0.1909	At atmospheric pressure for 2 weeks

table continued

Table 3.11 (continued)

Step No. in experiment	Mass of catalyst/g $\pm$ 5 x 10^{-6}	Procedure just followed
57	0.1904	Re-evacuation
58	0.1804	TPD to 650°C
59	0.1806	Cooled to 500°C
60	0.1808	Isolated from pump to pump back to SO_2 and re-evacuated
61	0.1844	Adsorption SO_2 (500°C)
62	0.1747	Re-evacuation
63	0.1727	TPD to 650°C
64	0.1727	Cooled to 600°C
65	0.15981	Allowed CO into system (600°C) and heated to 650°C in presence of CO
66	0.15984	Re-evacuation
67	0.16182	Cooled to 600°C
68	0.16235	Isolated from pump to pump back to SO_2 and CO cylinders and re-evacuated
69	0.1699	Adsorption SO_2 and CO (600°C)
70	0.16864	Re-evacuation
71	0.1787	Cooled to room temperature
72	0.1789	Isolated from pump to pump back to CO cylinder and re-evacuated
73	0.1771	Allowed CO into system (r.t.) and heated to 650°C in presence of CO
74	0.1771	Cooled to 600°C
75	0.1771	Cooled to 500°C
76	0.1772	Re-evacuation
77	0.1771	Cooled to room temperature
78	0.1774	Allowed up to atmospheric pressure

FIGURE 3.11 ABSORPTION OF SO_2 ON $La_{0.7}Sr_{0.3}CoO_3$.

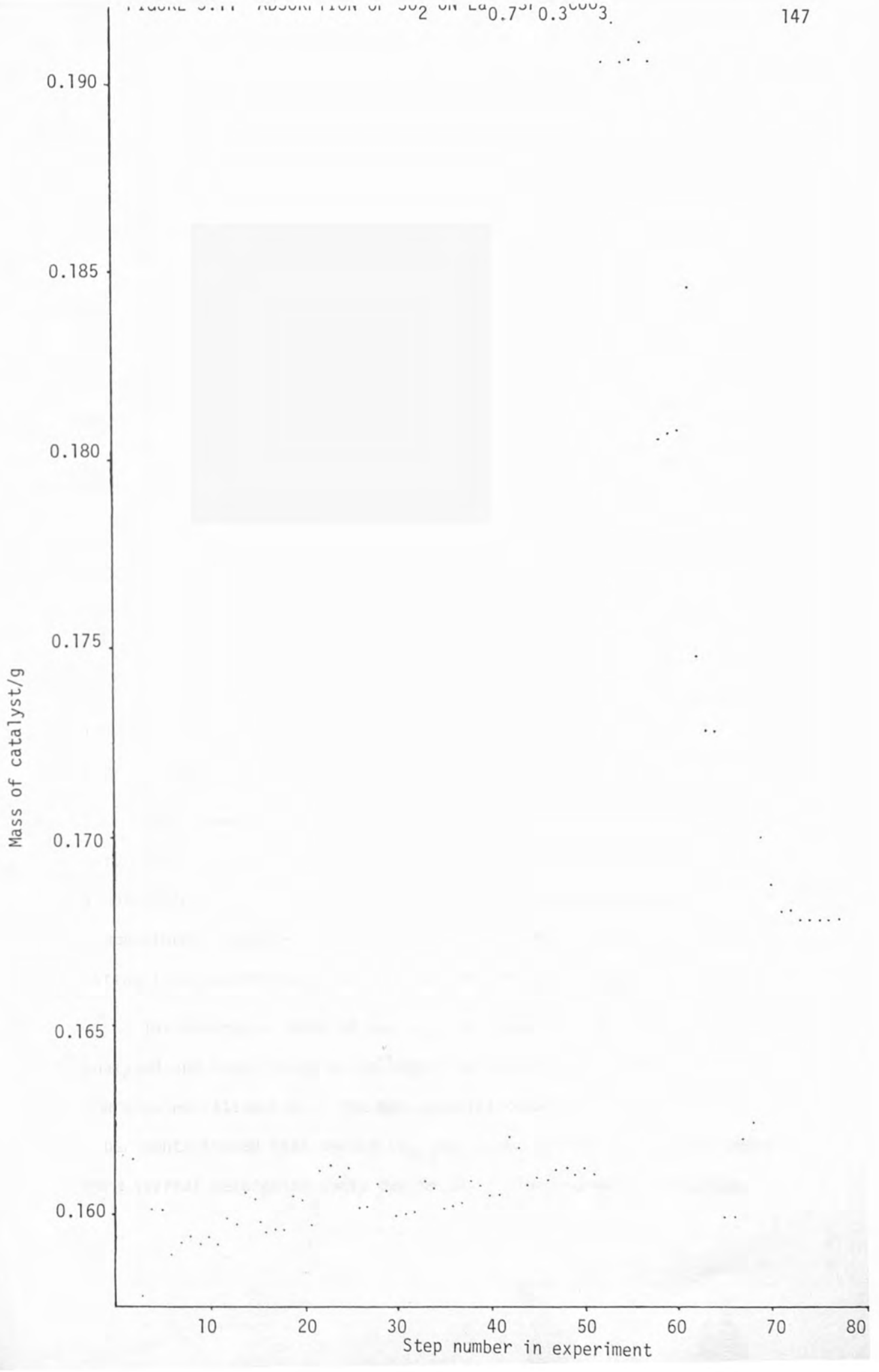

As observed previously evacuation and heating of the catalyst led to mass loss and desorption of oxygen. The loss observed was 1.10% and the temperature of the first O_2 peak was 621^{o}C.

As with the two previous samples studied the loss of mass which would be expected for desorption of a monolayer of N_2 was calculated, this was 1.20×10^{-3} g. The loss of mass due to heating the catalyst under vacuum was 1.78×10^{-3} g. It appeared that lattice oxygen was desorbed from this sample too.

The trend for adsorption of SO_2 observed during this experiment is very similar to that for $La_{0.3}Sr_{0.7}CoO_3$ and $La_{0.5}Sr_{0.5}CoO_3$. A gradual increase in mass is observed throughout the range of adsorption temperatures until adsorption at 500^{o}C caused a very big increase, equivalent to 19.21% of the mass before exposure to SO_2. The SO_2 adsorption is shown at point 52 on Fig. 3.11.

TPD, shown at point 58, removed much of the adsorbed SO_2 but heating to 650^{o}C in the presence of CO caused the mass to return to almost exactly that before the initial exposure to SO_2 at room temperature; compare points 13 and 65. The MS was set at 60 amu during this scavenging experiment but no COS was detectable.

The desorption data of the $La_{0.7}Sr_{0.3}CoO_3$ SO_2 experiment was analysed and computation using MASS 1 to calculate the desorption energies was attempted. The mass spectra obtained from the TPD experiments showed that unlike $La_{0.3}Sr_{0.7}CoO_3$ and $La_{0.5}Sr_{0.5}CoO_3$ there were several desorption peaks due to SO_2. The changes in MS scale

were more frequent and the definition of the peaks was more complicated than MASS 1 could handle.

When the SO_2 adsorptions, TPDs and scavenging reactions were completed SO_2 and CO were adsorbed together on the $La_{0.7}Sr_{0.3}CoO_3$ surface. This led to the mass increase shown at point 69 of Fig. 3.11. A small decrease in mass was obtained by heating the sample from room temperature to 650°C in CO. The mass decrease was very little but nevertheless COS was detected by the MS. The first trace of COS detected was at 283°C.

3.3.3.4 Adsorption of SO_2 on $La_{0.4}Sr_{0.6}CoO_3$ followed by TPD

The $La_{0.4}Sr_{0.6}CoO_3$ experiment was carried out in order to investigate whether a trend observed across the series of $La_{1-x}Sr_xCoO_3$ (x = 0.3, 0.5, 0.7) was real. It appeared from the earlier experiments that the total mass increase after adsorption of SO_2 at 500°C increased as La increased. The increase in mass on adsorption of SO_2 at 500°C was markedly greater than that at room temperature, 100°C or 300°C. The adsorption on $La_{0.4}Sr_{0.6}CoO_3$ was therefore only carried out at 500°C.

Each step of the experiment is detailed in Table 3.12. The steps are represented graphically in Fig. 3.12.

As with the three $La_{1-x}Sr_xCoO_3$ compounds studied previously, initial heating under vacuum led to a mass decrease. If the total mass decrease due to evacuation and heating, before adsorption, is calculated, the percentage loss of mass is 5.61%. The temperature of the first O_2 peak observed by the mass spectrometer on initial

Table 3.12

SO_2 adsorption on $La_{0.4}Sr_{0.6}CoO_3$

Step No. in experiment	Mass of catalyst/g $\pm$ 5 x 10^{-6}	Procedure just followed
1	0.1023	Initial mass
2	0.10281	Evacuation
3	0.09674	Heated to 650°C
4	0.09817	Cooled to room temperature
5	0.09717	Heated to 650°C
6	0.09713	Cooled to room temperature
7	0.09712	Heated to 650°C
8	0.098	Cooled to room temperature
9	0.09731	Heated to 500°C
10	0.1073	Adsorption SO_2 (500°C)
11	0.10685	Evacuation
12	0.10615	TPD to 650°C
13	0.10567	Cooled to room temperature
14	0.10671	Allowed up to atmospheric pressure

heating was 409°C. The mass losses and temperatures of oxygen desorption of the various $La_{1-x}Sr_xCoO_3$ catalysts will be compared in section 3.3.3.5.

The actual mass loss due to heating the $La_{0.4}Sr_{0.6}CoO_3$ sample under vacuum was 4.99 x 10^{-3} g. The desorption of a hypothetical monolayer of N_2 would have given a mass loss of 3.30 x 10^{-4}g. As with the other samples, there appeared to be evolution of lattice oxygen.

FIGURE 3.12 ADSORPTION OF SO_2 ON $La_{0.4}Sr_{0.6}CoO_3$

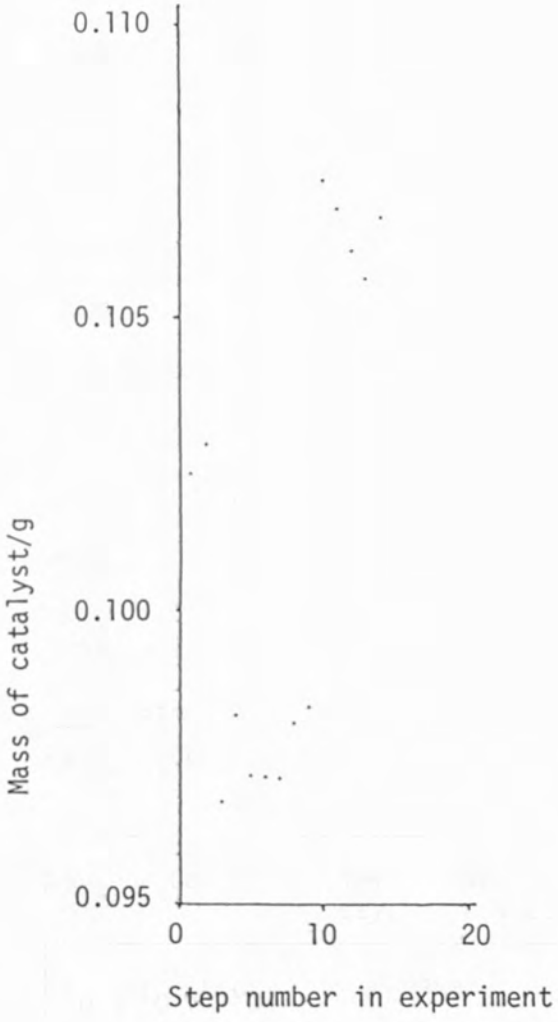

The change of mass on adsorption of SO_2 at 500°C was equivalent to 10.27% of the mass before adsorption. This mass change was compared to those of the other three catalysts investigated. The trend acorss the series was continued for the $La_{0.4}Sr_{0.6}CoO_3$ example.

3.3.3.5 Summary of oxygen desorption data from $La_{1-x}Sr_xCoO_3$

From the data recorded by the BBC microcomputer during heating, the temperatures at which O_2 was first detected by the MS, was calculated. The mass changes due to heating of the catalysts were also recorded. Each of the catalysts investigated had a different starting mass so the mass changes are recorded as percentages of the initial mass. The temperatures of initial oxygen desorption and the percentage mass losses are given in Table 3.13.

Table 3.13

Temperatures of initial oxygen desorption and mass changes on heating $La_{1-x}Sr_xCoO_3$

$La_{1-x}Sr_xCoO_3$	Temperature of oxygen desorption/°C	Percentage mass loss on heating
$La_{0.3}Sr_{0.7}CoO_3$	353	8.19
$La_{0.4}Sr_{0.6}CoO_3$	409	4.88
$La_{0.5}Sr_{0.5}CoO_3$	592	5.61
$La_{0.7}Sr_{0.3}CoO_3$	621	1.10

The temperatures and percentage mass losses shown in Table 3.13 are plotted against proportion of La in $La_{1-x}Sr_xCoO_3$ in Fig. 3.13. It is clear from Fig. 3.13 that there is a trend of greater mass loss and of oxygen desorption at lower temperatures at the lower La proportions and lesser mass losses which occurred at higher temperatures for higher La content.

3.3.3.6 Summary of SO_2 adsorption data on $La_{1-x}Sr_xCoO_3$

A trend of increasing SO_2 adsorption on $La_{1-x}Sr_xCoO_3$ with increasing La content was observed. Fig. 3.14 shows how the percentage mass of each sample increased on adsorption of SO_2 at room temperature, 100°C, 300°C and 500°C. Of particular interest, is the increase in masses at 500°C and the apparent linearity of total percentage mass increase at 500°C with La content.

3.3.3.7 Comparison of mass losses due to heating fresh $La_{1-x}Sr_xCoO_3$ and mass gains due to subsequent adsorption of SO_2

The relationships between the mass losses due to heating fresh $La_{1-x}Sr_xCoO_3$ in a vacuum and the mass gains after exposure to SO_2 are interesting. The mass changes are shown as true masses and as percentages, with the ratios of the mass gains and mass losses, in Table 3.14.

At this stage it is not possible to offer an explanation of mass changes, however, attention may be drawn to the mass gain/mass loss ratio. The initial loss of mass is not recovered for the $La_{0.3}Sr_{0.7}CoO_3$ sample. For both the $La_{0.4}Sr_{0.6}CoO_3$ and $La_{0.5}Sr_{0.5}CoO_3$ samples the gain in mass is virtually double the mass loss.

FIGURE 3.13 PERCENTAGE MASS CHANGE ON HEATING FRESH CATALYST TO 650°C IN A VACUUM AND TEMPERATURE OF FIRST OXYGEN DESORPTION PEAK AGAINST La CONTENT

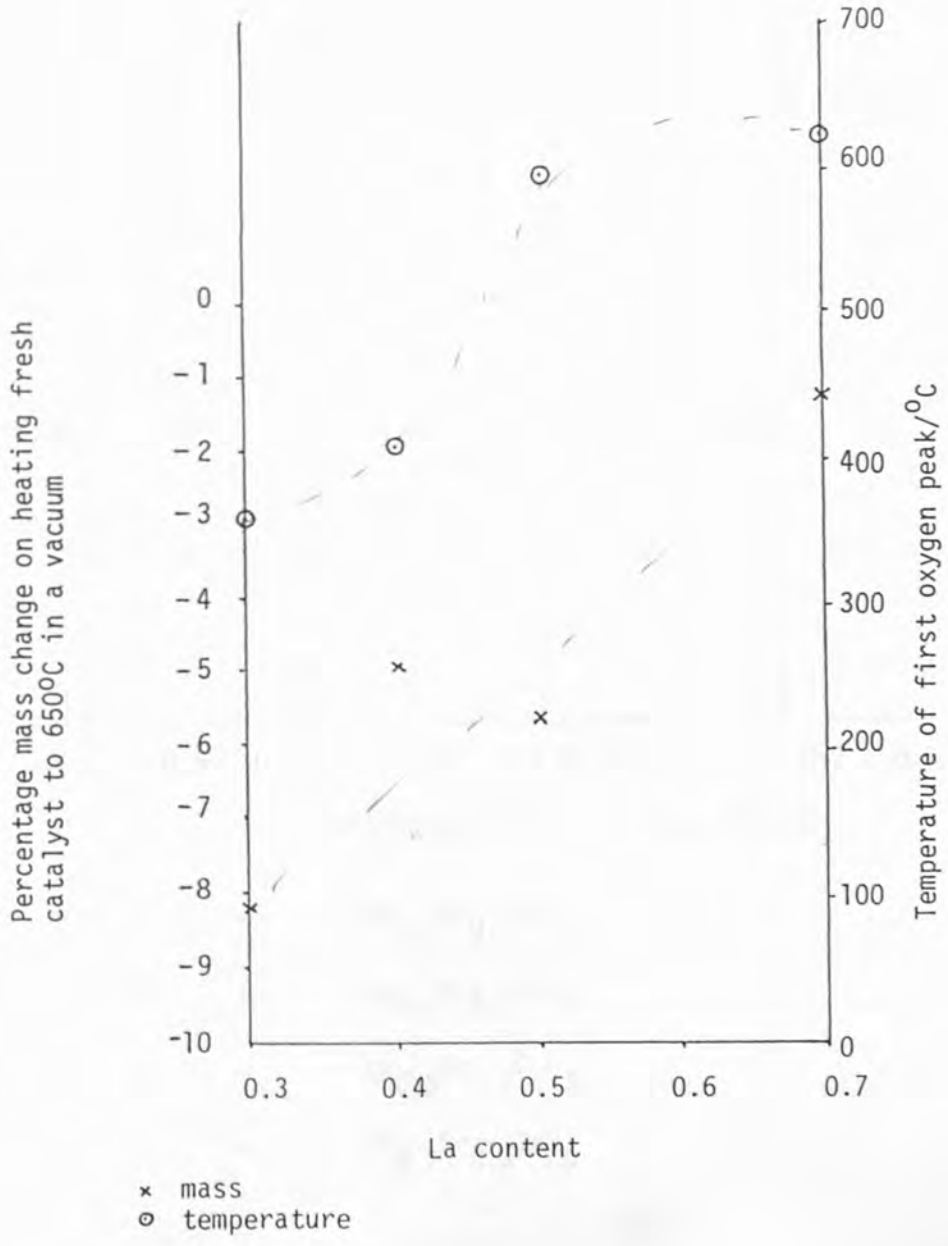

FIGURE 3.14 PERCENTAGE MASS INCREASE DUE TO ADSORPTION OF SO_2

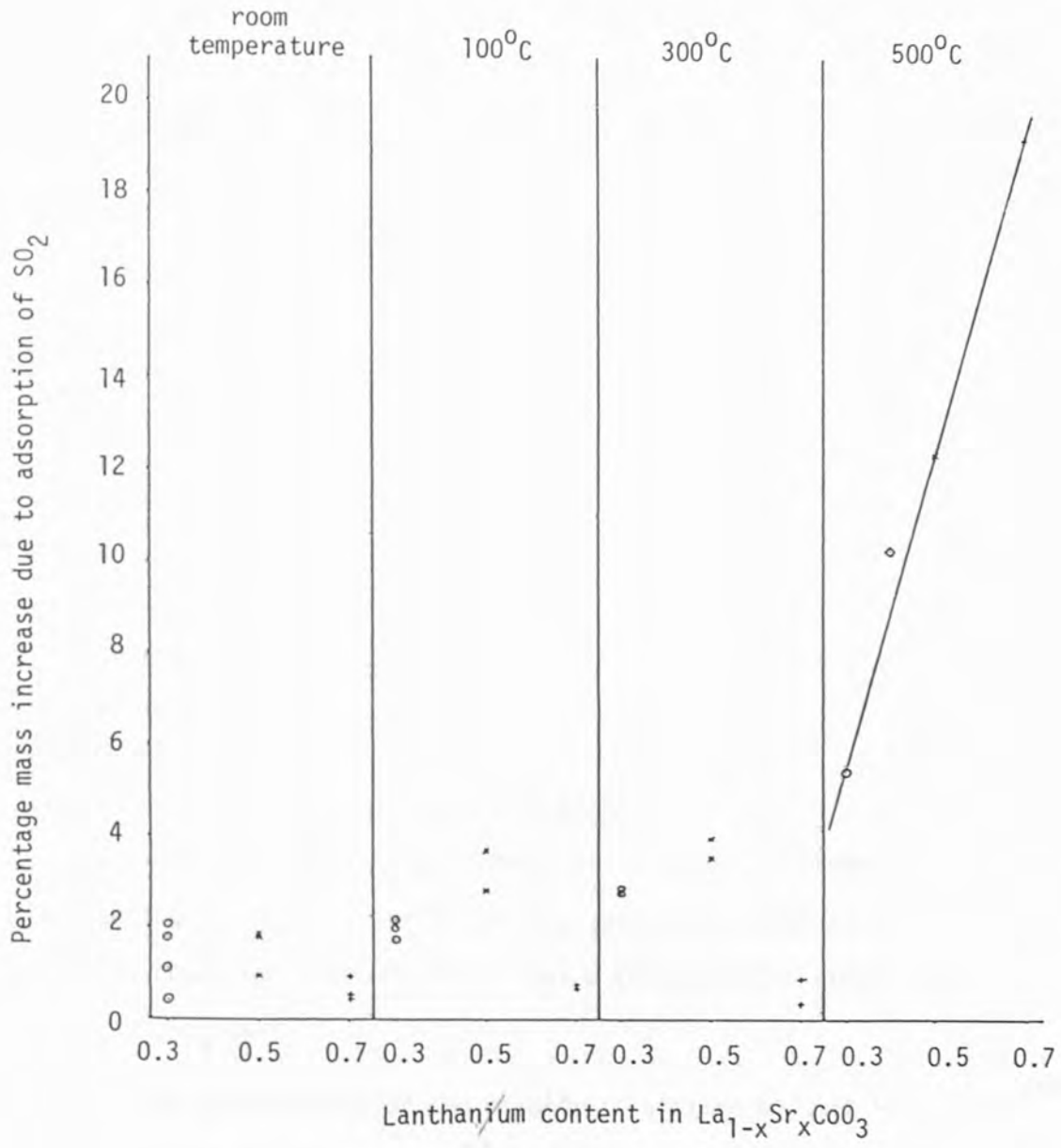

o = $La_{0.3}Sr_{0.7}CoO_3$

◇ = $La_{0.4}Sr_{0.7}CoO_3$

× = $La_{0.5}Sr_{0.5}CoO_3$

\+ = $La_{0.7}Sr_{0.3}CoO_3$

Table 3.14

Mass losses due to heating $La_{1-x}Sr_xCoO_3$ under vacuum and mass gains due to adsorption of SO_2

$La_{1-x}Sr_xCoO_3$	Initial mass/g	Mass loss/g	% Mass loss	Mass gain/g	% Mass gain.	Mass gain / Mass loss
$La_{0.3}Sr_{0.7}CoO_3$	0.0935	7.66×10^{-3}	8.19	4.67×10^{-3}	5.44	0.61
$La_{0.4}Sr_{0.6}CoO_3$	0.1023	4.99×10^{-3}	4.88	9.99×10^{-3}	10.27	2.00
$La_{0.5}Sr_{0.5}CoO_3$	0.0902	5.06×10^{-3}	5.61	0.01054	12.38	2.08
$La_{0.7}Sr_{0.3}CoO_3$	0.1615	1.78×10^{-3}	1.10	0.03068	19.21	17.24

The increase in mass observed after SO_2 adsorption on $La_{0.7}Sr_{0.3}CoO_3$ is far in excess of the mass loss.

3.3.4 CO adsorption and desorption experiments

The CO adsorption experiments are reported in order of increasing La content, apart from $La_{0.4}Sr_{0.6}CoO_3$ which was investigated last in order to check whether or not a trend existed across the $La_{1-x}Sr_xCoO_3$ series.

The presentation of the results is similar to that in section 3.3.3 for the SO_2 experiments.

Most of the CO_2 desorptions were too erratic for computation by MASS 1, for calculation of the desorption energy. The fact that CO_2 was formed indicates chemisorption and reduction of the catalyst. An example of a mass spectrum of the TPD of CO_2, after adsorption of CO is shown in Fig. 3.8b, for comparison with the SO_2 spectrum shown in Fig.3.8a.

3.3.4.1 Adsorption of CO on $La_{0.3}Sr_{0.7}CoO_3$ followed by TPD

The mass changes due to each step in the experiment are shown in Table 3.15. These steps are shown graphically in Fig. 3.15.

Table 3.15

CO adsorption on $La_{0.3}Sr_{0.7}CoO_3$

Step No. in experiment	Mass of catalyst/g $\pm 5 \times 10^{-6}$	Procedure just followed
1	0.0816	Initial mass
2	0.08147	Evacuation
3	0.07356	Heated to 650°C
4	0.07481	Cooled to room temperature
5	0.07369	Heated to 650°C
6	0.07387	Cooled to room temperature
7	0.07355	Heated to 650°C
8	0.07482	Cooled to room temperature
9	0.07478	Before adsorption CO
10	0.07517	Adsorption CO (r.t.)
11	0.0751	Re-evacuation
12	0.0737	TPD to 650°C
13	0.07465	Cooled to room temperature
14	0.07455	Isolated from pump, to pump back to CO cylinder and re-evacuated
15	0.075	Adsorption CO (r.t.)
16	0.07509	Re-evacuation
17	0.0739	TPD to 650°C
18	0.0739	Cooled to room temperature
19	0.08048	Left with just rotary pump
20	0.07999	Re-evacuation
21	0.0733	Heated to 650°C
22	0.07336	Cooled to room temperature
23	0.07339	Isolated from pump, to pump back to CO cylinder and re-evacuated.

table continued

Table 3.15 (continued)

Step No. in experiment	Mass of catalyst/g $\pm$ 5 x 10^{-6}	Procedure just followed
24	0.07366	Adsorption CO (r.t.)
25	0.07411	Re-evacuation
26	0.07341	TPD to 650°C
27	0.07392	Cooled to room temperature
28	0.07377	Heated to 100°C
29	0.07391	Adsorption CO (100°C)
30	0.07393	Re-evacuation
31	0.07345	TPD to 650°C
32	0.07337	Cooled to 100°C
33	0.07373	Adsorption CO (100°C)
34	0.07386	Re-evacuation
35	0.07335	TPD to 650°C
36	0.07351	Cooled to 100°C
37	0.0738	Adsorption CO (100°C)
38	0.0738	Re-evacuation
39	0.07347	TPD to 650°C
40	0.07365	Cooled to 300°C
41	0.07403	Adsorption CO (300°C)
42	0.07406	Re-evacuation
43	0.07359	TPD to 650°C
44	0.07407	Cooled to room temperature
45	0.07407	Left under vacuum 1 day
46	0.07475	Left with just rotary pump 1 day
47	0.07469	Re-evacuation
48	0.07374	Heated to 650°C
49	0.07385	Cooled to 300°C
50	0.0741	Adsorption CO (300°C)
51	0.07444	Re-evacuation
52	0.07402	TPD to 650°C

table continued

Table 3.15 (continued)

Step No. in experiment	Mass of catalyst/g $\pm 5 \times 10^{-6}$	Procedure just followed
53	0.07406	Cooled to 500°C
54	0.0807	Adsorption CO (500°C)
55	0.07956	Re-evacuation
56	0.07433	TPD to 650°C
57	0.07434	Cooled to 500°C
58	0.08295	Adsorption CO (500°C)
59	0.08181	Re-evacuation
60	0.07681	TPD to 650°C
61	0.07706	Cooled to 300°C
62	0.07802	Adsorption CO (300°C)
63	0.07792	Re-evacuation
64	0.07645	TPD to 650°C
65	0.07692	Cooled to room temperature
66	0.08158	Allowed up to atmospheric pressure
-	0.0815	Re-weighed in 4 fig. balance.

Examination of Fig. 3.15 with Table 3.15 for reference shows that as with the SO_2 experiments heating of the catalyst led to loss of mass, adsorption of CO led to an increase, re-evacuation led to a decrease and this continued during TPD.

Adsorption of CO at room temperature, 100°C and 300°C all led to small increases in mass. Exposure of the sample at 500°C led to a much more marked mass change. The total increase in mass after adsorption at 500°C was 5.92×10^{-3}g, that is, 7.92% of the mass before adsorption. Re-evacuation and TPD led to a return to the mass before

FIGURE 3.15 ADSORPTION OF CO ON $La_{0.3}Sr_{0.7}CoO_3$

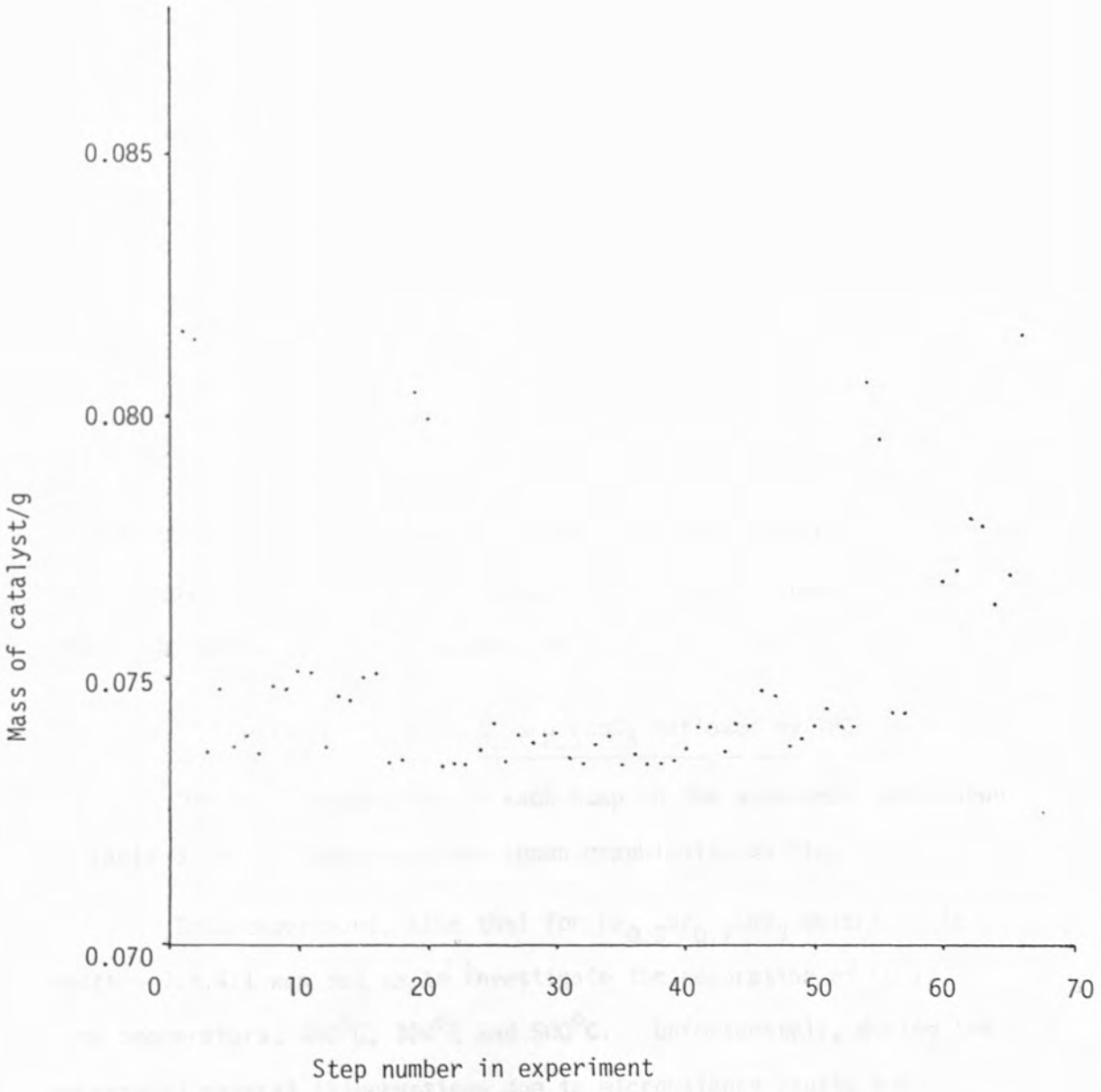

exposure after the first 500°C adsorption, but recovery was not complete after the second.

It is interesting to note that the adsorption experiments for SO_2 all indicated that adsorption of SO_2 was significantly greater at 500°C than at the lower temperatures, similarly to CO adsorption in this experiment.

It was not only adsorption of CO at 500°C that caused the mass to increase. By switching off the diffusion pump and allowing the pressure in the vacuum line to increase, adsorption from the air occurred. The result of this can be seen at point 19 of Fig. 3.15. The mass fell again when the sample was heated under vacuum. When the experiment had been completed and the sample was allowed up to atmospheric pressure the mass recovered to approximately the initial mass of fresh $La_{0.3}Sr_{0.7}CoO_3$. This suggests that oxygen removed by evacuation, heating and, or reduction by CO is re-adsorbed.

3.3.4.2 Adsorption of CO on $La_{0.5}Sr_{0.5}CoO_3$ followed by TPD

The mass changes due to each step in the experiment are shown in Table 3.16. These steps are shown graphically in Fig. 3.16.

This experiment, like that for $La_{0.3}Sr_{0.7}CoO_3$ described in section 3.3.4.1 was set up to investigate the adsorption of CO at room temperature, 100°C, 300°C and 500°C. Unfortunately, during the experiment several interruptions due to microbalance faults and power cuts meant that the $La_{0.3}Sr_{0.7}CoO_3$ sample had to be allowed up to air and removed from the vacuum line a couple of times.

Table 3.16

CO adsorption on $La_{0.5}Sr_{0.5}CoO_3$

Step No. in experiment	Mass of catalyst/g $\pm 5 \times 10^{-6}$	Procedure just followed
1	0.1718	Initial mass
2	0.17141	Evacuation
3	0.1608	Heated to 650°C (went off scale), cooled to room temperature, allowed up to atmospheric pressure and re-weighed in 4 fig. balance.
4	0.16058	Evacuation
5	0.15858	Heated to 650°C
6	0.16132	Cooled to room temperature and left just rotary pump
7	0.16012	Diff pumped and heated to 650°C
8	0.16073	Cooled to room temperature
9	0.16144	Left under vacuum 16 hr.
10	0.16018	Heated to 650°C
11	0.16031	Cooled to room temperature
12	0.16102	Adsorption CO (r.t.)
13	0.16093	Re-evacuation
14	0.16025	TPD to 650°C
15	0.16024	Cooled to room temperature (immed)
16	0.1609	Adsorption CO (r.t.)
17	0.16097	Re-evacuation
18	0.16026	TPD to 650°C
19	0.16113	Cooled to room temperature
20	0.16137	Adsorption CO (r.t.)
21	0.16131	Re-evacuation
22	0.16027	TPD to 650°C
23	0.16048	Cooled to 44°C (T furnace)
24	0.16019	Heated to 650°C
25	0.16058	Cooled to 100°C
26	0.16102	Adsorption CO (100°C)

table continued

Table 3.16 (continued)

Step No. in experiment	Mass of catalyst/g $\pm$ 5 x 10^{-6}	Procedure just followed
27	0.16104	Re-evacuation
28	0.16033	TPD to 650°C
29	0.16127	Cooled to 100°C
30	0.1612	Adsorption CO (100°C)
31	0.16118	Re-evacuation
32	0.16039	TPD to 650°C
33	0.16022	Left at 650°C
34	0.16055	Cooled to 100°C
35	0.16095	Adsorption CO (100°C)
36	0.16029	TPD to 650°C
37	0.16122	Cooled to 100°C
38	0.1612	Before adsorption CO
39	0.16118	Adsorption CO (100°C)
40	0.1612	Re-evacuation
41	0.16029	TPD to 650°C
42	0.16041	Cooled to 300°C
43	0.16065	Isolated balance from pumps before adsorption CO.
44	0.16094	Adsorption CO (300°C)
45	0.16106	Re-evacuation
46	0.16031	TPD to 650°C
47	0.16226	Left under vacuum 2 days, then just rotary pump for 1 day
48	0.1578	Fault with microbalance, catalyst removed, some lost then re-balanced
49	0.15742	Evacuation
50	0.15647	Heated to 650°C
51	0.1564	Left at 650°C
52	0.15668	Cooled to 40°C (T furnace)
53	0.15651	Heated to 650°C
54	0.15646	Cooled to 44°C (T furnace)
55	0.15651	Heated to 650°C

table continued

Table 3.16 (continued)

Step No. in experiment	Mass of catalyst/g $\pm$ 5 x 10^{-6}	Procedure just followed
56	0.15725	Left balance under vacuum but not pumped 16 hr.
57	0.15693	Heated to 650°C
58	0.15671	Cooled to 41°C (T furnace)
59	0.15695	Heated to 650°C
60	0.15672	Cooled to 44°C (T furnace)
61	0.15705	Heated to 650°C
62	0.15658	Cooled to 300°C
63	0.15755	Before adsorption CO
64	0.15724	Adsorption CO (300°C)
65	0.15771	Re-evacuation
66	0.15709	TPD to 650°C
67	0.15646	Left at 650°C
68	0.1576	Cooled to room temperature and left just rotary pump
69	0.15784	Heated to 300°C
70	0.15786	Adsorption CO (300°C, 20 mmHg)
71	0.15846	Re-evacuation
72	0.15766	TPD to 650°C
73	0.1545	Cooled to room temperature, allowed up to atmospheric pressure for 2 weeks - removed from balance
74	0.15462	Evacuation
75	0.15207	Heated to 500°C
76	0.15281	Isolated from pumps before adsorption CO
77	0.15502	Adsorption CO (500°C)
78	0.15444	Re-evacuation
79	0.14919	TPD to 650°C
80	0.15054	Cooled to room temperature, left just rotary pump 1 day and re-evacuated

table continued

Table 3.16 (continued)

Step No. in experiment		Mass of catalyst/g $\pm 5 \times 10^{-6}$	Procedure just followed
81		0.14916	Heated to 650°C
82		0.14913	Before adsorption CO
83		0.15111	Adsorption CO (500°C)
84	*	0.1496	TPD to 650°C and went off scale therefore cooled to room temperature and re-balanced.
85		0.14945	Evacuation
86		0.1468	Heated to 650°C
87		0.14679	Cooled to 500°C
88		0.15007	Adsorption CO (500°C)
89		0.14976	Re-evacuation
90		0.14768	TPD to 650°C
91		0.14939	Cooled to 500°C
92		0.14929	Isolated from pump and re-evacuated
93		0.15145	Adsorption CO (500°C)
94		0.15109	Re-evacuation
95		0.14844	TPD to 650°C
96		0.15711	Left just rotary pump 2 days then re-evacuated
97		0.15102	Heated to 650°C
98		0.15102	Cooled to 600°C
99		0.1539	Adsorption CO (600°C)
100		0.153	Left at 600°C
101		0.15173	Re-evacuation
102		0.14901	TPD to 650°C
103		0.14899	Cooled to 600°C
104		0.16009	Adsorption O_2 (600°C)
105		0.15989	Re-evacuation

* off scale

table continued

Table 3.16 (continued)

Step No. in experiment	Mass of catalyst/g $\pm 5 \times 10^{-6}$	Procedure just followed
106	0.15939	Before adsorption CO
107	0.15689	Adsorption CO ($600^{o}C$)
108	0.15393	Re-evacuation
109	0.15085	TPD to $650^{o}C$
110	0.15094	Cooled to $600^{o}C$
111	0.17769	Adsorption SO_2 ($600^{o}C$)
112	0.17769	Re-evacuation
113	0.17769	TPD to $650^{o}C$
114	0.17519	Cooled to $600^{o}C$ and adsorption CO
115	0.17219	Re-evacuation
116	0.17139	TPD to $650^{o}C$
117	0.17409	Electricity off 1½ h cooled then re-evacuated, heated to 650°C and cooled to 600°C.
118	0.17759	Adsorption CO ($600^{o}C$)
119	0.17799	Re-evacuation
120	0.17729	Cooled to room temperature
121	0.17709	Allowed up to atmospheric pressure

Any loss of material which occurred due to these distrubances was accounted for.

After the initial loss of mass due to evacuation and heating the mass followed a cyclical pattern due to heating, cooling, adsorption of CO at room temperature, $100^{o}C$ and $300^{o}C$ and desorption, this continued after the microbalance fault at point 48.

FIGURE 3.16 ADSORPTION OF CO ON $La_{0.5}Sr_{0.5}CoO_3$

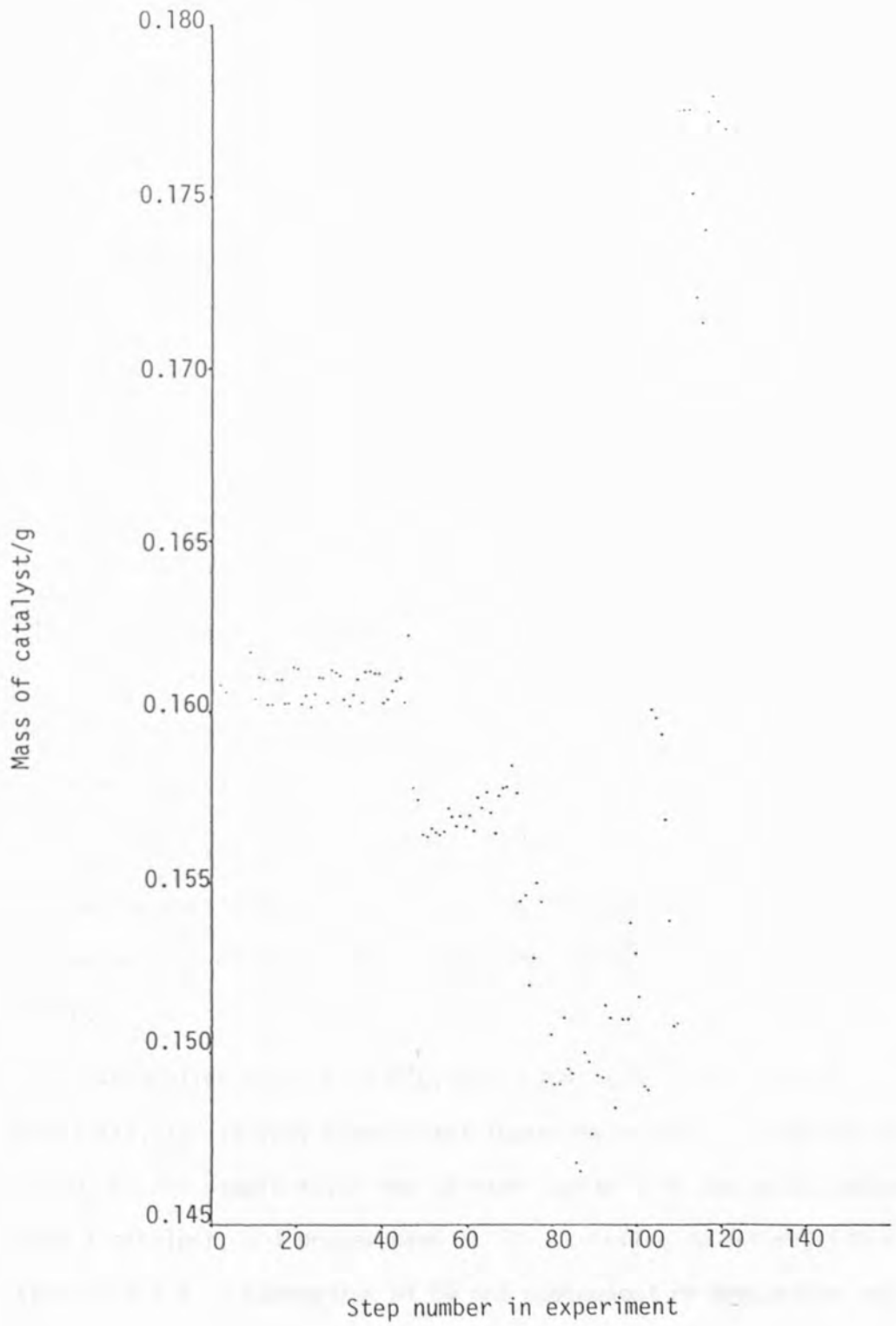

Adsorption at 500°C, shown at point 77 was greater than at the lower temperatures and this coincides with each of the previous experiments with SO_2 and with CO. If the masses due to TPD are examined throughout the experiment before CO adsorption at 500°C, it can be seen that the mass remains remarkably stable. The first adsorption of CO at 500°C gives a percentage mass increase of 1.45% which is of the order of 1% greater than the increase at the lower temperatures. The mass loss on TPD is also greater than that due to TPD at lower temperatures. The mass loss is possibly almost entirely due to oxygen being scavenged from the lattice by the adsorbed CO to form CO_2, which was then desorbed. The loss of mass due to re-evacuation and TPD was equivalent to 2.37% of the mass before adsorption. A percentage loss of 2.28% (from calculation of equivalent percentage of 1.45% 28 amu to 44 amu) minus 1.45%, that is, 0.83% would be expected if just CO_2 was being desorbed. Each time material is heated under vacuum there is likely to be desorption of gases adsorbed at lower temperatures.

Further adsorptions of CO at 500°C led to greater losses of mass on TPD, particularly at point 84 where the mass went off scale. The adsorption of CO at 600°C, point 99, is very similar to that at 500°C.

Adsorption of O_2 at 600°C, point 104, and of SO_2 at 600°C, point 111, led to very significant increases in mass. This adsorption of SO_2 on the sample after the CO experiments gave the result expected from a catalyst, not pre-exposed to CO, according to the results of section 3.3.3. Adsorption of CO and subsequent re-evacuation and TPD

did lead to a decrease in mass, not all of the mass increase due to SO_2 exposure was removed and no COS was detected.

3.3.4.3 Adsorption of CO on $La_{0.7}Sr_{0.3}CoO_3$ followed by TPD

The mass changes due to each step in the experiment are shown in Table 3.17. These steps are shown graphically in Fig. 3.17.

Table 3.17

CO adsorption on $La_{0.7}Sr_{0.3}CoO_3$

Step No. in experiment	Mass of catalyst/g $\pm 5 \times 10^{-6}$	Procedure just followed
1	0.1072	Initial mass
2	0.10728	Evacuation
3	0.10226	Heated to 650°C
4	0.10363	Cooled to room temperature
5	0.10454	Left with just rotary pump then re-evacuated
6	0.10389	Heated to 650°C
7	0.104	Cooled to room temperature
8	0.10385	Heated to 650°C
9	0.10374	Cooled to room temperature
10	0.10301	Heated to 650°C
11	0.10314	Cooled to room temperature
12	0.10298	Heated to 650°C
13	0.10343	Cooled to room temperature
14	0.10366	Adsorption CO (r.t.)
15	0.10368	Re-evacuation
16	0.10303	TPD to 650°C
17	1.10336	Cooled to room temperature
18	0.10337	Isolated from pump then re-evacuated
19	0.10357	Adsorption CO (r.t.)
20	0.10363	Re-evacuation
21	0.10307	TPD to 650°C
22	0.10307	Cooled to room temperature

table continued

Table 3.17 (continued)

Step No. in experiment	Mass of catalyst/g ± 5 x 10^{-6}	Procedure just followed
23	0.10381	Left under vacuum but the pressure increased, then re-evacuated
24	0.10321	Heated to 650°C
25	0.10322	Cooled to 100°C
26	0.10325	Isolated from pump, to pump back to CO cylinder and re-evacuated
27	0.10362	Adsorption CO (r.t.)
28	0.10366	Re-evacuation
29	0.10325	TPD to 650°C
30	0.10318	Cooled to 100°C
31	0.10351	Adsorption CO (100°C)
32	0.10356	Re-evacuation
33	0.10314	TPD to 650°C
34	0.10318	Cooled to 300°C
35	0.10321	Isolated from pump, to pump back to CO cylinder and re-evacuated
36	0.10339	Adsorption CO (300°C)
37	0.10324	Re-evacuation
38	0.10288	TPD to 650°C
39	0.10289	Cooled to 300°C
40	0.10291	Isolated from pump, to pump back to CO cylinder and re-evacuated
41	0.1032	Adsorption CO (300°C)
42	0.10319	Re-evacuation
43	0.10291	TPD to 650°C
44	0.10546	Cooled to room temperature and left just rotary pumping
45	0.10536	Re-evacuation
46	0.1021	Heated to 650°C
47	0.10225	Cooled to 300°C
48	0.10252	Isolated from pump, to pump back to CO cylinder and re-evacuated
49	0.10271	Adsorption CO (300°C)
50	0.10229	Re-evacuation and TPD to 650°C

table continued

Table 3.17 (continued)

Step No. in experiment	Mass of catalyst/g $\pm$ 5 x 10^{-6}	Procedure just followed
51	0.10229	Cooled to 500°C
52	0.10226	Isolated from pump, to pump back to CO cylinder and re-evacuated
53	* 0.09972	Adsorption CO (500°C)
54	* 0.09972	Re-evacuation and TPD to 650°C
55	0.10384	Cooled to 500°C and allowed O_2 into system
56	0.10402	Re-evacuation
57	0.10397	Isolated from pump, to pump back to CO cylinder and re-evacuated
58	* 0.09954	Adsorption CO (500°C)
59	0.0992	Re-evacuation, cooled to room temperature, allowed O_2 into system re-evacuated and allowed up to atmospheric pressure and re-balanced.
60	0.09903	Re-evacuation
61	0.09853	Heated to 650°C
62	0.09871	Cooled to room temperature
-	0.0994	Allowed up to atmospheric pressure and weighed in 4 fig. balance.

* off scale

After the initial loss of mass due to evacuation and heating the cyclical nature of the mass changes due to heating and cooling plus adsorption and desorption is visible. From about point 30 onwards a very gradual decline in mass can be seen. This is due to adsorption of CO at 100°C and above. The adsorption caused an increase in mass but the overall reaction with desorption due to evacuation and TPD caused losses in mass. The most significant loss

FIGURE 3.17 ADSORPTION OF CO ON $La_{0.7}Sr_{0.3}CoO_3$

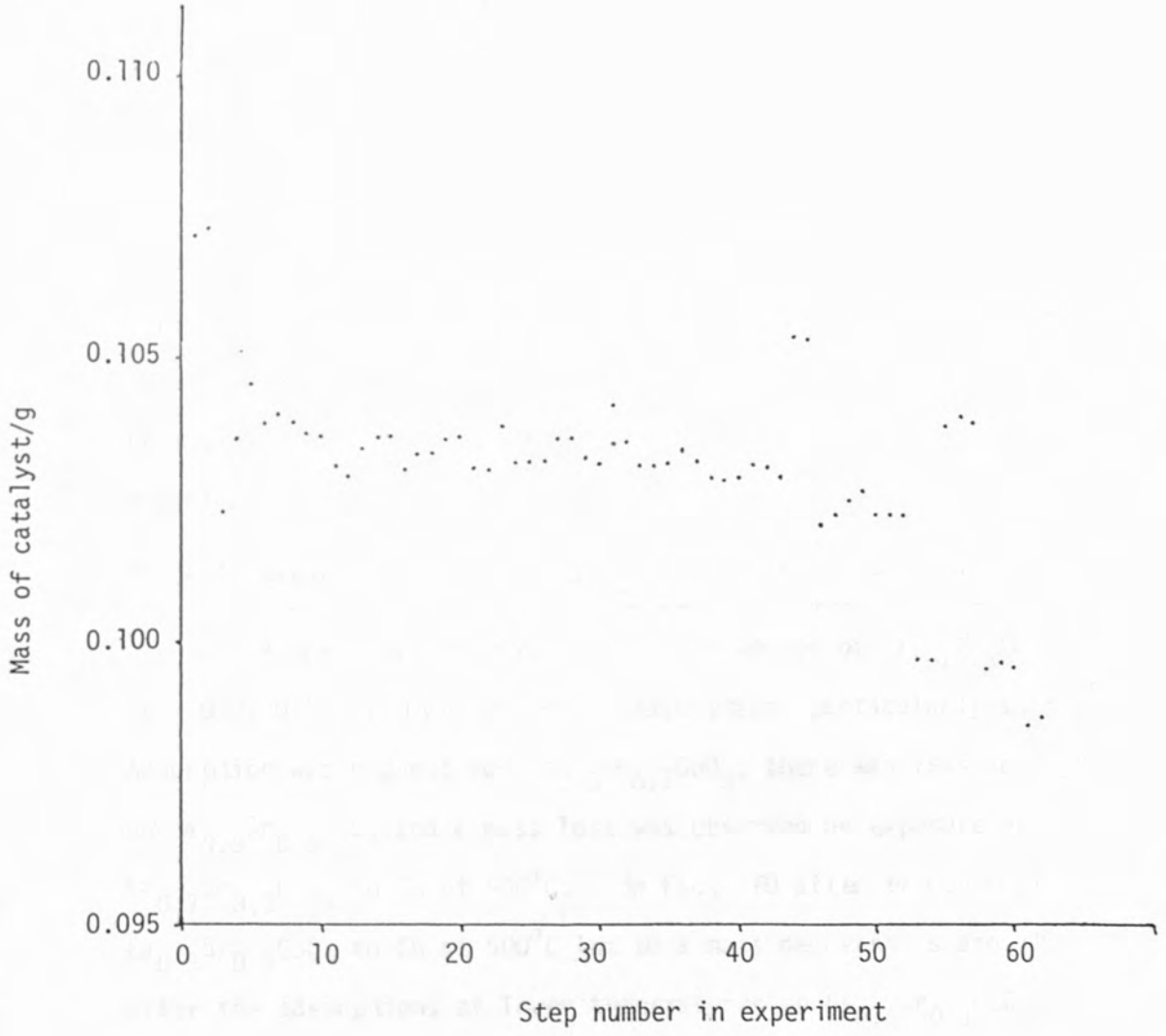

in mass was due to adsorption of CO at 500°C. The overall mass loss due to CO adsorption at point 53 was at least 3.59%. The loss of mass was sufficient to put the microbalance off scale, so the loss was in fact greater than 3.59%. Even though the mass had gone off scale the next step of the experiment, the TPD, was followed. Next, the sample was allowed to cool once more to 500°C and O_2 was allowed into the line. The mass immediately recovered. It seemed that CO had reacted with oxygen associated with the catalyst and had desorbed as CO_2.

A further adsorption of CO was allowed again at 500°C. The effect was the same as the first 500°C adsorption, the mass dropped significantly and went off scale. When O_2 was allowed into the vacuum line at room temperature the mass did not recover, nor did it increase significantly when it was allowed up to atmospheric pressure at room temperature.

3.3.4.4 Adsorption of CO on $La_{0.4}Sr_{0.6}CoO_3$ followed by TPD

A trend was observed across the series of $La_{1-x}Sr_xCoO_3$ ($x = 0.3, 0.5, 0.7$) concerning CO adsorption, particularly at 500°C. Adsorption was highest for $La_{0.3}Sr_{0.7}CoO_3$, there was less adsorption on $La_{0.5}Sr_{0.5}CoO_3$ and a mass loss was observed on exposure of $La_{0.7}Sr_{0.3}CoO_3$ to CO at 500°C. In fact TPD after exposure of $La_{0.5}Sr_{0.5}CoO_3$ to CO at 500°C led to a mass decrease as did TPD after the adsorptions at lower temperatures on $La_{0.7}Sr_{0.3}CoO_3$.

It was therefore decided to investigate a fourth perovskite-type oxide to see if the trend was real. Only exposure of

$La_{0.4}Sr_{0.6}CoO_3$ to CO at 500°C was investigated as this temperature was the most interesting in the previous experiments.

The results of each step in the experiment are shown in Table 3.18. These results are represented graphically in Fig. 3.18.

Table 3.18

CO adsorption on $La_{0.4}Sr_{0.6}CoO_3$

Step No. in experiment	Mass of catalyst/g ± 5 x 10^{-6}	Procedure just followed
1	0.09925	Initial mass
2	0.09925	Evacuation
3	0.09192	Heated to 650°C
4	0.09209	Cooled to room temperature
5	0.09192	Heated to 650°C
6	0.09189	Cooled to 500°C
7	0.09193	Isolated from pump, to pump back to CO cylinder and re-evacuated
8	0.09274	Adsorption CO (500°C)
9	0.09194	Re-evacuation
10	* 0.08786	TPD to 650°C
-	0.0892	Cooled to room temperature, allowed up to atmospheric pressure and re-weighed on 4 fig. balance

* off scale

FIGURE 3.18 ADSORPTION OF CO ON $La_{0.4}Sr_{0.6}CoO_3$

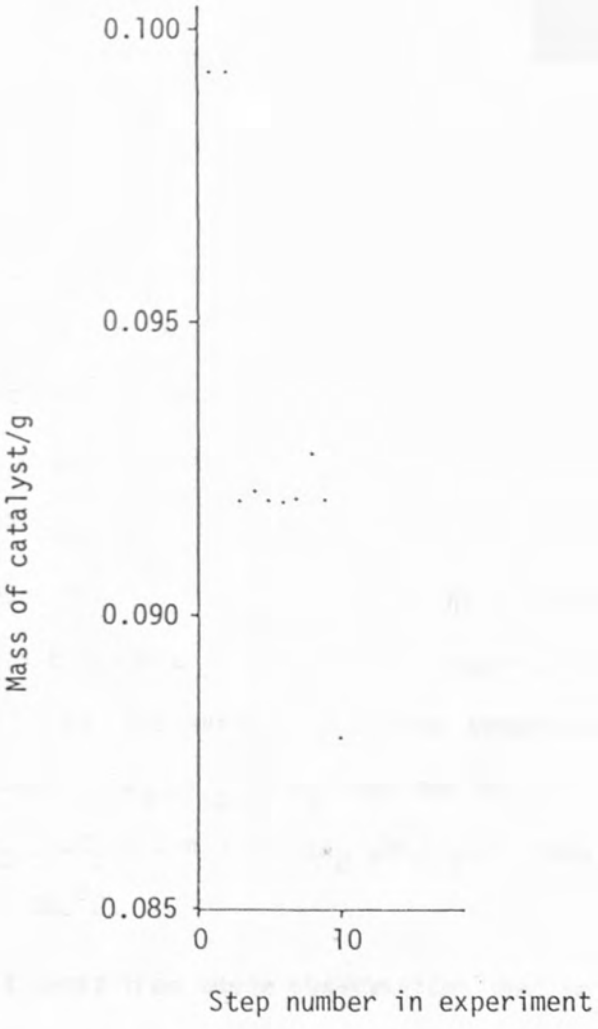

The $La_{0.4}Sr_{0.6}CoO_3$ sample lost mass on heating in a vacuum, as expected. The catalyst was heated to 650°C twice and then allowed to cool to 500°C for CO adsorption. Adsorption of CO at 500°C led to a mass increase equivalent to 0.88% of the mass before adsorption. TPD led to a loss of mass which went off the microbalance scale. This had also occurred for $La_{0.5}Sr_{0.5}CoO_3$ and $La_{0.7}Sr_{0.3}CoO_3$. From Table 3.18, it can be seen that allowing the catalyst sample up to atmospheric pressure at room temperature caused some of the mass lost due to TPD to be recovered.

3.3.4.5 Summary of CO adsorption data on $La_{1-x}Sr_xCoO_3$

For each of the samples of $La_{1-x}Sr_xCoO_3$ investigated the most significant mass changes on exposure to CO, at the temperatures studied, were at 500°C. The percentage mass changes on exposure to CO at 500°C are shown in Fig. 3.19. At low La content in $La_{1-x}Sr_xCoO_3$ there is a mass increase and at high La content there is a mass decrease.

Loss of mass after exposure to CO at room temperature was recovered by exposure to O_2. The extent of recovery of the mass changed across the series as did the temperature at which this took place. $La_{0.4}Sr_{0.6}CoO_3$ regained mass at room temperature, $La_{0.5}Sr_{0.5}CoO_3$ did not. $La_{0.7}Sr_{0.3}CoO_3$ regained mass when exposed to O_2 at 500°C.

It seems from these observations that on increasing the La content, that is, decreasing x in $La_{1-x}Sr_xCoO_3$, reduction by CO was easier and re-oxidation by pure O_2 or O_2 in air was more difficult.

FIGURE 3.19 PERCENTAGE MASS CHANGE ON EXPOSURE OF $La_{1-x}Sr_xCoO_3$ TO CO AT 500^oC PLOTTED AGAINST La CONTENT IN $La_{1-x}Sr_xCoO_3$

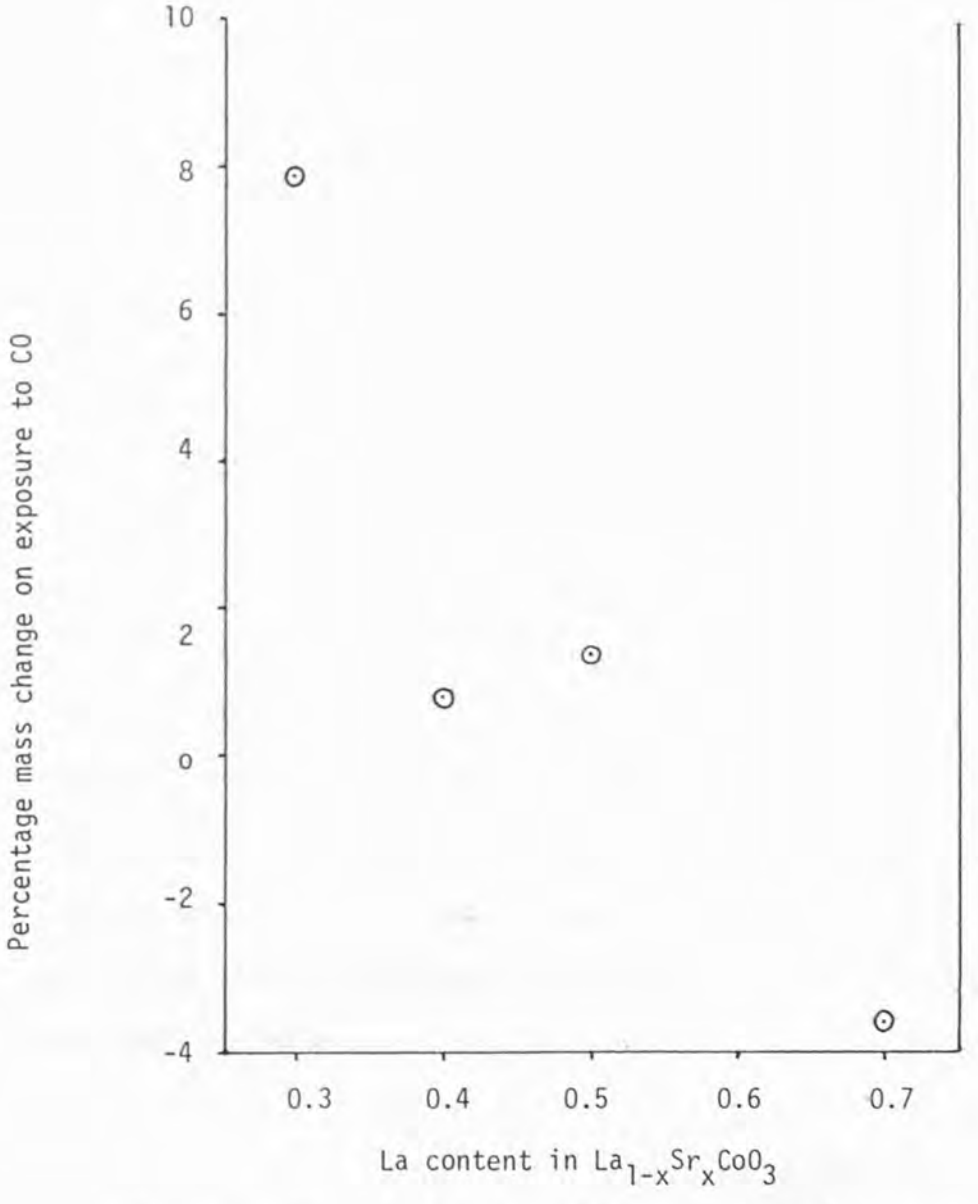

(compare with calculated δ, which represents oxygen vacancies, in Fig. 1.2 and with loss of oxygen due to heating in Fig. 3.13).

3.3.5 Simultaneous SO_2 and CO adsorption experiments

After the individual adsorptions of SO_2 and CO it was decided that $La_{1-x}Sr_xCoO_3$ should be exposed to the two gases simultaneously. Such an experiment may show if the two gases compete for sites on $La_{1-x}Sr_xCoO_3$. The experiments are representative of the initial conditions of the flow-rig experiments. The results will be presented in the order in which the experiments were carried out. This is because observations during earlier experiments influenced later procedures.

3.3.5.1 Adsorption of SO_2 and CO on $La_{0.5}Sr_{0.5}CoO_3$

The mass changes observed during this experiment are given in Table 3.19 and Fig. 3.20.

Heating of the $La_{0.5}Sr_{0.5}CoO_3$ under vacuum led to a loss of mass which casued the microbalance reading to go off scale. Allowing the catalyst up to atmospheric pressure was sufficient to bring the mass back on to the scale. Oxygen was probably lost and replaced from oxygen in the atmosphere. The counterweight was decreased so that if there were further mass decreases the mass would remain on scale. The mass did decrease further due to heating to 650^oC.

Adsorption of SO_2 and CO at 600^oC led to a percentage mass increase equivalent to 23.98% of the mass before adsorption. This was greater than the combined mass increases of SO_2 and CO adsorbed separately at 500^oC.

Table 3.19

SO_2 and CO adsorption on $La_{0.5}Sr_{0.5}CoO_3$

Step No. in experiment	Mass of catalyst/g $\pm 5 \times 10^{-6}$	Procedure just followed
1	0.1293	Initial mass
2	0.12854	Evacuation
3	0.12851	Before heated to 650°C
4	* 0.12337	Heated to 650°C went off scale
5	0.12432	Cooled to room temperature and allowed up to atmospheric pressure, mass increased on to microbalance scale (Sample re-balanced)
6	0.12391	Evacuated
7	0.11971	Heated to 650°C
8	0.11996	Cooled to 600°C
9	0.12013	Before adsorption SO_2 and CO
10	0.14894	Adsorption SO_2 and CO (600°C)
11	0.15084	Tried to heat to 650°C at 10% of the maximum heating rate temperature started to decrease, re-evacuated and cooled to room temperature
12	0.13334	Allowed CO into system at room temperature and heated to 650°C, cooled to 600°C
13	0.13359	Cooled to room temperature
14	0.13339	Re-evacuated
15	0.13459	Left just rotary pumping
16	0.13484	Re-evacuated
17	0.13299	Heated to 650°C
18	0.13309	Cooled to 600°C
19	0.14984	Adsorption SO_2 and CO (600°C)
20	0.14394	Re-evacuated
21	0.13544	Allowed CO into system at 600°C
22	0.13694	Re-evacuated and cooled to room temperature and allowed up to atmospheric pressure
-	0.1373	Re-weighed on 4-fig balance.

* off scale

FIGURE 3.20 ADSORPTION OF SO_2 and CO ON $La_{0.5}Sr_{0.5}CoO_3$

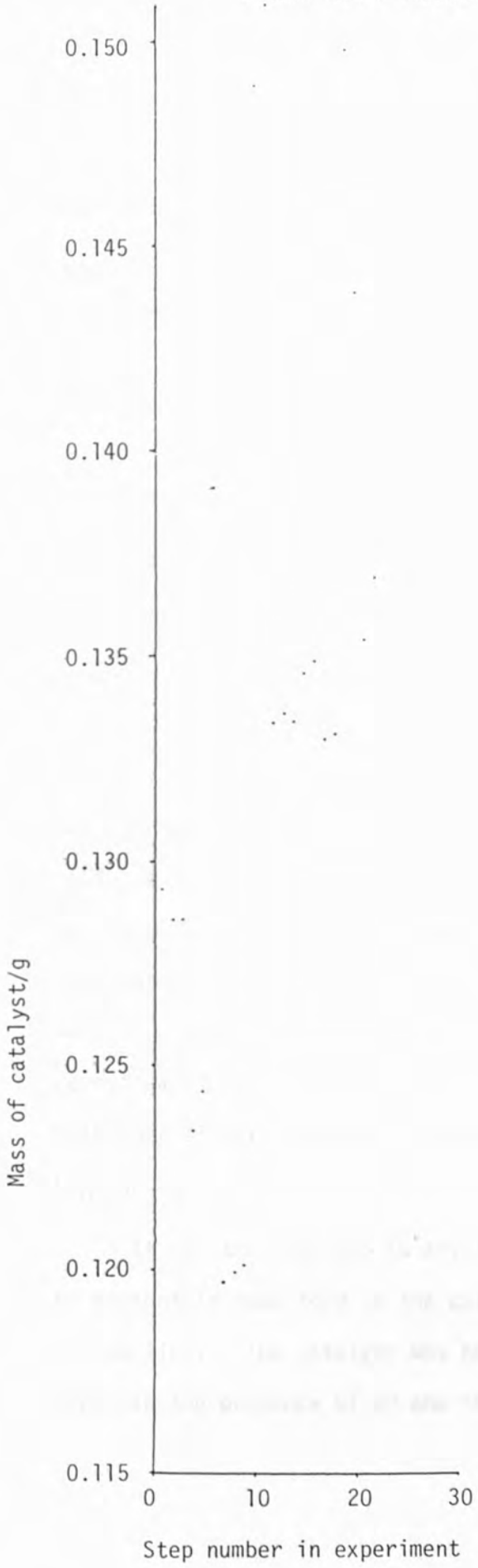

During the adsorption of SO_2 and CO the needle valve to the MS was opened slightly and SO_2, CO_2 and COS were looked for. This was complicated by the fact that each of the gases was present in such different amounts that different scales were required for their detection. The MS was set on its scan mode and the scale was changed manually so that SO_2 and CO_2 could be followed and COS was sampled occasionally. The SO_2 was observed to decrease slowly and CO_2 increased slowly too. COS showed slight increases in partial pressure each time it was sampled.

It was decided to heat the $La_{0.5}Sr_{0.5}CoO_3$ in the presence of SO_2 and CO to see if further adsorption occurred at the higher temperatures. The temperature controller was set at 10% of the maximum heating rate so that increased adsorption or desorption could be followed easily with temperature change. The 10% input was insufficient to maintain the temperature of 600^{o}C so the temperature fell. Initially, a fault with the temperature controller was suspected and it was switched off. The vacuum line was re-evacuated and the sample was allowed to cool to room temperature. A further slight increase in mass occurred on cooling the $La_{0.5}Sr_{0.5}CoO_3$.

It was then decided to try to scavenge any sulphur which may be present in some form on the catalyst, by allowing CO into the vacuum line. The catalyst was heated from room temperature to 650^{o}C in the presence of CO and this led to a considerable decrease

in mass although the mass did not go down to that before adsorption. During heating to 650°C , COS was detected at 275°C.

The adsorption of SO_2 and CO was repeated at 600°C and the mass increase that resulted was partly removed by heating from 600°C to 650°C in the presence of CO.

When the catalyst was removed there was sulphur on the inside of the cooling jacket above the furnace. This sulphur production supports the evidence for the catalysis of the reaction between SO_2 and CO to give elemental sulphur and CO_2, given by the MS observations during adsorption of SO_2 and CO.

The sulphur, which has a boiling point of 444°C, would have been present as a gas at the temperature of adsorption, particularly at the low pressure of the experiments. The cooling jacket would have caused condensation of the sulphur.

3.3.5.2 Adsorption of SO_2 and CO on $La_{0.3}Sr_{0.7}CoO_3$

The results of this experiment are shown in Table 3.20 and they are displayed graphically in Fig. 3.21.

Heating to 650°C in a vacuum led to a loss of mass due to degassing and apparent loss of lattice oxygen. When the mass had settled at 600°C the $La_{0.3}Sr_{0.7}CoO_3$ was exposed to SO_2 and CO. The immediate mass increase was equivalent to 33.63%. This was greater than the combined mass increases of SO_2 and CO adsorbed separately at 500°C. Heating the $La_{0.3}Sr_{0.7}CoO_3$ from room temperature to 650°C in the presence of CO restored the mass to close to that of the fresh catalyst. During heating COS was detected by the MS.

Table 3.20

SO_2 and CO adsorption on $La_{0.3}Sr_{0.7}CoO_3$

Step No. in experiment	Mass of catalyst/g $\pm 5 \times 10^{-6}$	Procedure just followed
1	0.0378	Initial mass
2	0.0378	Evacuation
3	0.0326	Heated to 650°C
4	0.03303	Cooled to room temperature
5	0.0338	Left just rotary pump for 2 days
6	0.03374	Re-evacuation
7	0.03308	Heated to 650°C
8	0.03327	Cooled to room temperature
9	0.03296	Heated to 650°C
10	0.03295	Cooled to 600°C
11	0.04403	Adsorption SO_2 and CO (600°C)
12	0.04343	Re-evacuation
13	0.04343	Cooled to room temperature
14	0.03697	Allowed CO into system (r.t.) and heated to 650°C in presence of CO
15	0.03697	Cooled to 612°C in presence of CO
16	0.03685	Cooled to room temperature in presence of CO
17	0.03692	Re-evacuation
18	0.03728	Heated to 650°C
19	0.03727	Cooled to 600°C
20	0.05013	Adsorption SO_2 and CO (600°C)
21	0.04168	Re-evacuation
22	0.03703	Allowed CO into system (600°C) and heated to 650°C in presence of CO
23	0.03707	Re-evacuation and cooled to 600°C
24	0.05153	Adsorption SO_2 and CO (600°C)
25	0.04258	Re-evacuation
26	0.03724	Allowed CO into system at 600°C and heated to 650°C in presence of CO
27	0.03727	Re-evacuation and cooled to room temperature
28	0.03707	Heated to 650 °C

table continued

Table 3.20 (continued)

Step No. in experiment	Mass of catalyst/g $\pm 5 \times 10^{-6}$	Procedure just followed
29	0.03707	Cooled to room temperature
30	0.03717	Allowed up to atmospheric pressure
-	0.0368	Re-weighed to 4-fig balance

The COS was first detected at 622°C. After the mass had settled again at 600°C, the adsorption was repeated. The mass increase after the second exposure to SO_2 and CO at 600°C led to an increase in mass greater than the first. The mass was once again decreased by exposure to CO, this time at 600°C, and heating in CO to 650°C. The adsorption and recovery of the mass was then repeated once more.

During the heating of the $La_{0.3}Sr_{0.7}CoO_3$ in the presence of CO, each time there was production of COS.

There was also production of sulphur. As observed for the $La_{0.5}Sr_{0.5}CoO_3$ experiment, there was sulphur condensed on the cooling jacket above the furnace in which the catalyst was suspended. It seems likely that the reaction between SO_2 and CO was catalysed by the $La_{0.3}Sr_{0.7}CoO_3$, as sulphur is one of the expected products.

3.3.5.3 Adsorption of SO_2 and CO on $La_{0.7}Sr_{0.3}CoO_3$

The mass changes which occurred during this experiment are shown in Table 3.21. The masses are displayed graphically in Fig. 3.22.

FIGURE 3.21 ADSORPTION OF SO_2 AND CO ON $La_{0.3}Sr_{0.7}CoO_3$

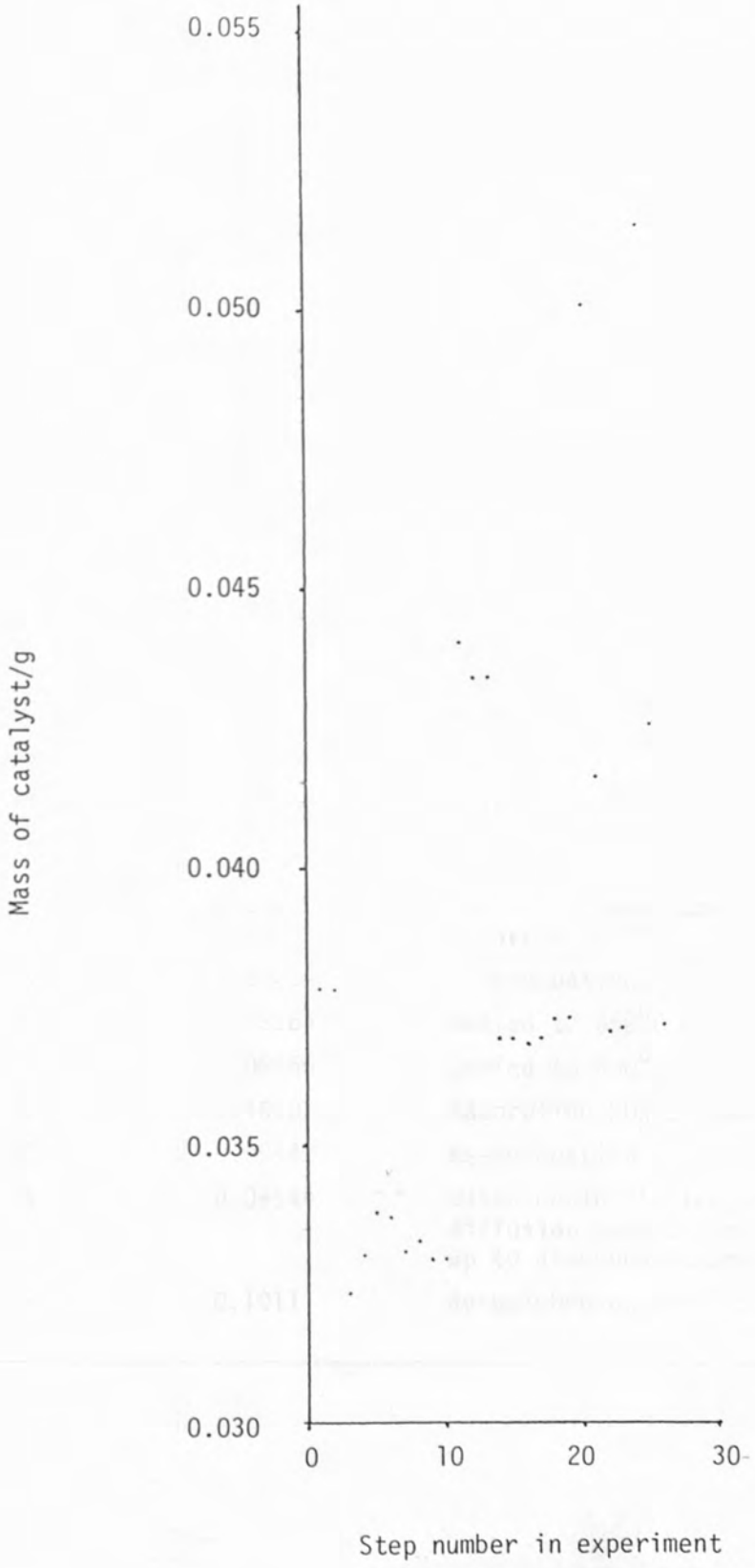

Table 3.21

SO_2 and CO adsorption on $La_{0.7}Sr_{0.3}CoO_3$

Step No. in experiment	Mass of catalyst/g $\pm 5 \times 10^{-6}$	Procedure just followed
1	0.0889	Initial mass
2	0.08856	Evacuation
3	0.08391	Heated to 650°C
4	0.08523	Cooled to room temperature
5	0.0841	Heated to 650°C
6	0.08507	Cooled to room temperature
7	0.08399	Heated to 650°C
8	0.0853	Cooled to room temperature
9	0.08419	Heated to 650°C
10	0.0842	Cooled to 600°C
11	0.10606	Adsorption SO_2 and CO (600°C)
12	0.10361	Re-evacuation
13	0.10356	Cooled to room temperature
14	0.08982	Allowed CO into system at room temperature and heated to 650°C in the presence of CO
15	0.09026	Cooled to room temperature in the presence of CO
16	0.09024	Re-evacuation
17	0.08964	Heated to 650°C
18	0.08965	Cooled to 600°C
19	0.10107	Adsorption SO_2 and CO (600°C)
20	0.09942	Re-evacuation
21	0.09944	Water cooler failed and mercury from diffusion pump boiled away. Allowed up to atmospheric pressure
-	0.1011	Re-weighed on 4-fig balance

FIGURE 3.22 ADSORPTION OF SO_2 AND CO ON $La_{0.7}Sr_{0.3}CoO_3$

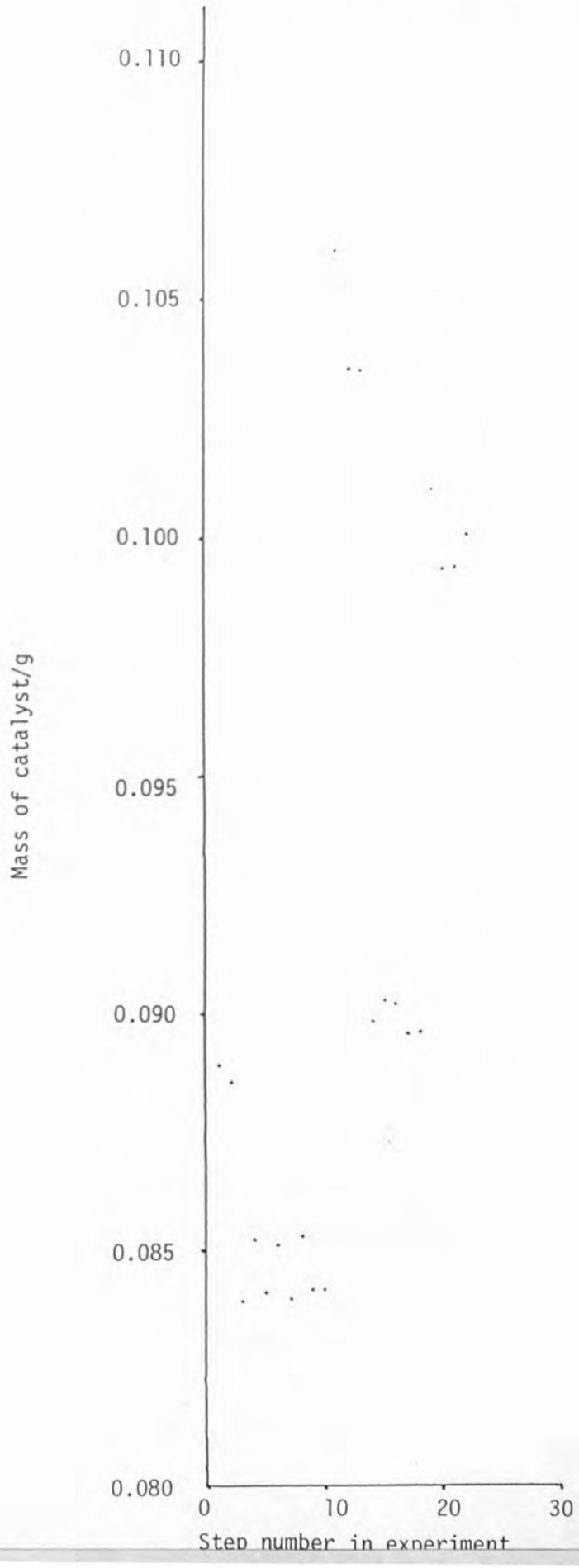

The initial mass loss due to evacuation and heating under vacuum can easily be seen from Fig. 3.22. Next, the heating and cooling cycles are evident by the alternate increases and decreases in mass.

Exposure of $La_{0.7}Sr_{0.3}CoO_3$ to SO_2 and CO at 600°C, led to a mass increase equivalent to 25.96% of the mass before adsorption. As with the previous SO_2 and CO adsorption experiments, it appears that a reaction must have occurred and not just adsorption on the surface of the catalyst.

The experiment with CO was repeated to see if the mass decreased and COS was produced. CO was allowed into the vacuum line at room temperature; it was noted that this produced no change in mass. The catalyst was then heated to 650°C in the presence of CO and the mass did fall. During heating the MS detected COS. At 286°C the needle on the MS started to flicker, then it came on to the 10^{-10} mbar scale at 350°C.

The adsorption of SO_2 and CO was repeated at 600°C and once again a significant increase in mass was observed. The removal of this excess mass, which was observed after second adsorptions in previous experiments, was not attempted due to a fault with the water pressure which destroyed the diffusion pump.

When the $La_{0.4}Sr_{0.6}CoO_3$ sample was removed from the rig and the cooling jacket was examined it was observed that as in the previous SO_2 and CO adsorption experiments there was sulphur on the cooling jacket.

3.3.5.4 Adsorption of SO_2 and CO on $La_{0.4}Sr_{0.6}CoO_3$

The resultant mass changes of each step of the experiment are shown in Table 3.22. Each step is shown on a graph in Fig. 3.23.

Table 3.22

SO_2 and CO adsorption on $La_{0.4}Sr_{0.6}CoO_3$

Step No. in experiment	Mass of catalyst/g $\pm 5 \times 10^{-6}$	Procedure just followed
1	0.1091	Initial mass
2	0.10914	Evacuation
3	0.10375	Heated to 650°C
4	0.10458	Cooled to room temperature
5	0.10355	Heated to 650°C
6	0.10379	Cooled to room temperature
7	0.10387	Heated to 650°C
8	0.10471	Cooled to room temperature
9	0.104	Heated to 650°C
10	0.10423	Cooled to 600°C
11	0.10426	Isolated from pump, to pump back to SO_2 and CO cylinders and re-evacuated
12	0.12593	Adsorption SO_2 and CO (600°C)
13	0.12593	Re-evacuation
14	0.12553	Cooled to room temperature
15	0.10658	Allowed CO into system (r.t.) and heated to 650°C in presence of CO
16	0.10659	Cooled to room temperature in presence of CO
17	0.10494	Re-evacuation
18	0.10485	TPD to 650°C
19	0.10486	Cooled to 600°C
20	0.10485	Isolated from pump, to pump back to SO_2 and CO cylinders and re-evacuated

table continued

Table 3.22 (continued)

Step No. in experiment	Mass of catalyst/g ± 5 x 10^{-6}	Procedure just followed
21	0.1052	Isolated from pump, to pump away excess CO from gas handling side of vacuum line
22	0.11532	Adsorption SO_2 and CO (600°C)
23	0.11412	Re-evacuation
24	0.11177	Allowed CO into system (600°C) and heated to 650°C in presence of CO
25	0.11167	Re-evacuation
26	0.11177	Cooled to 600°C
27	0.11157	Allowed CO into system (600°C) led to no change so increased P_{CO} to 44 mm Hg.
28	0.11137	Cooled to room temperature in presence of CO
29	0.11087	Heated to 650°C in presence of CO
30	0.11107	Cooled to room temperature and re-evacuated
-	0.1151	Allowed up to atmospheric pressure and re-weighed on 4 fig. balance

It can be seen from Table 3.22 and Fig. 3.23 that heating $La_{0.4}Sr_{0.6}CoO_3$ under vacuum leads to a mass decrease, adsorption of SO_2 and CO causes a very substantial increase of mass and subsequent heating in the presence of CO causes a mass decrease.

Mass increase due to SO_2 and CO adsorption is equivalent to 20.78% of the mass before adsorption. During heating from room temperature in the presence of CO the MS detected COS. The temperature at which COS was detected was 350°C.

FIGURE 3.23 ADSORPTION OF SO_2 AND CO ON $La_{0.4}Sr_{0.6}CoO_3$

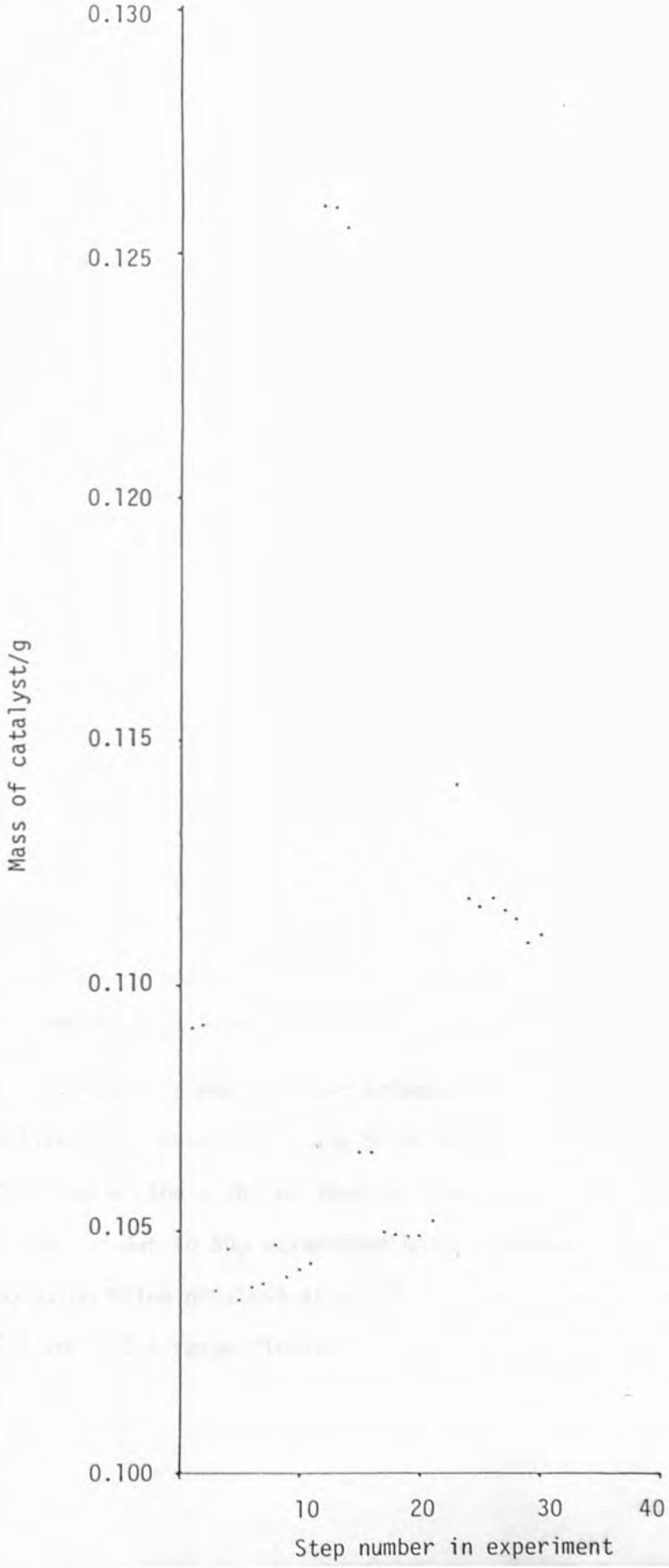

Further adsorption of SO_2 and CO was allowed, at 600°C. Instead of heating in the presence of CO from room temperature to 650°C, the sample was heated from 600°C to 650°C. There was some mass loss but not to the extent of the previous 'scavenging reaction' with CO. Cooling to room temperature with the CO still in the system and further heating to 650°C led to further mass loss.

As with the other $La_{1-x}Sr_xCoO_3$ samples studied, when the catalyst was removed sulphur was observed on the cooling jacket above the furnace. Once again it seems that the reaction between SO_2 and CO has been catalysed.

3.3.5.5 Summary of simultaneous SO_2 and CO adsorption data on $La_{1-x}Sr_xCoO_3$

For each of the samples of $La_{1-x}Sr_xCoO_3$ which were exposed to SO_2 and CO there were large increases in mass. These mass increases were always greater than the sum of the mass changes due to individual adsorption of SO_2 and CO at 500°C. The percentage mass changes and the sums of those due to SO_2 and CO separately are shown in Fig. 3.24.

A comparison may be drawn between the summation and the actual simultaneous adsorption. The mass increases are greatest at either end of the x values studied, that is, at x = 0.3 and x = 0.7. This may be due to SO_2 adsorption being greatest at x = 0.3 and CO adsorption being greatest at x = 0.7, as was revealed in sections 3.3.3 and 3.3.4 respectively.

FIGURE 3.24 PERCENTAGE MASS INCREASES DUE TO EXPOSURE OF $La_{1-x}Sr_xCoO_3$ TO SO_2 AND CO INDIVIDUALLY AND SIMULTANEOUSLY PLOTTED AGAINST La CONTENT IN $La_{1-x}Sr_xCoO_3$

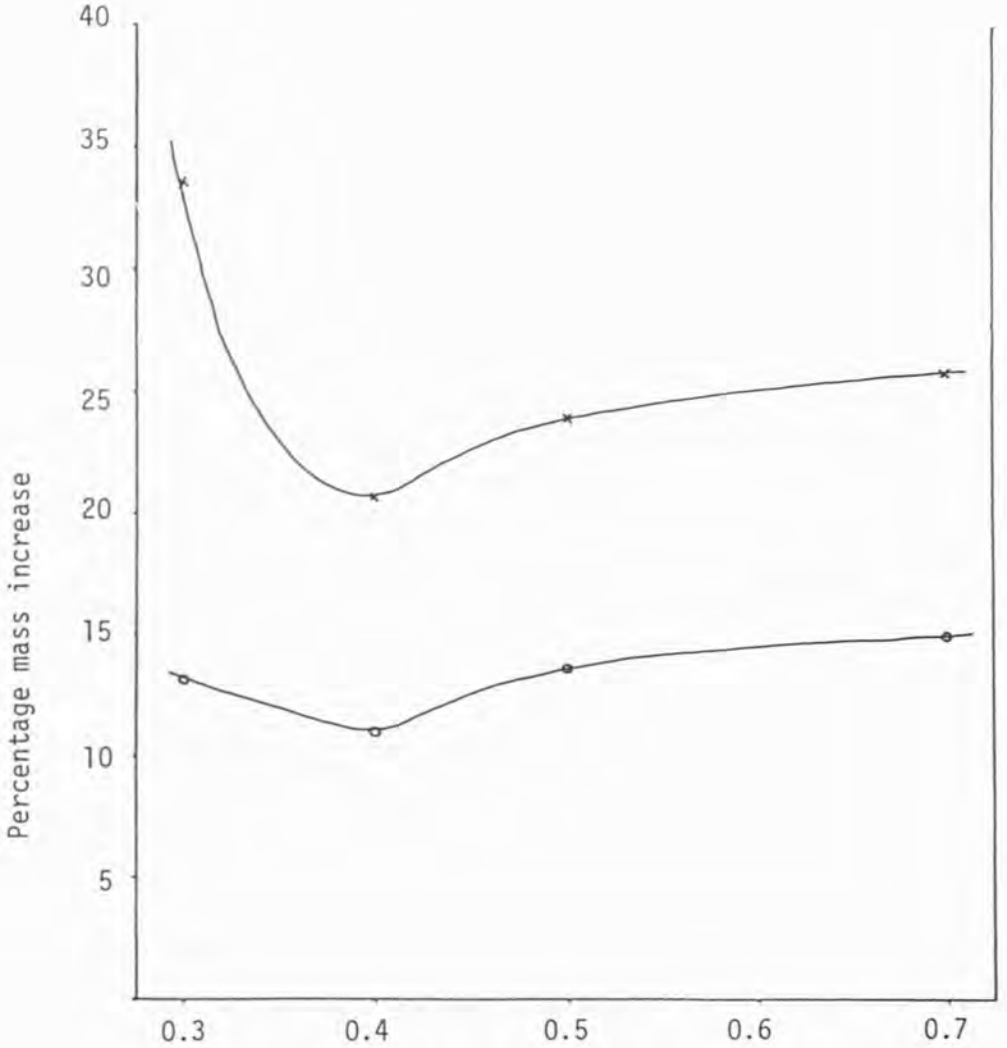

x Percentage mass increases due to adsorption of SO_2 and CO simultaneously at 600°C

o Sum of percentage mass increases due to adsorption of SO_2 and CO individually

The excess mass is not thought to be due to the fact that the combined adsorption was at 600°C, while the individual adsorptions were at 500°C. There is positive evidence in the form of sulphur condensed on the cooling jacket and CO_2 and COS detected by the MS, to indicate that the reaction shown in equations 1 and 2 and reproduced below have occurred.

$$SO_2 + 2CO \rightleftharpoons \frac{1}{x} S_x + 2CO_2 \qquad 1$$

$$CO + [S] \longrightarrow COS \qquad 2$$

The use of [S] to represent the sulphur source does not define what the source is.

Reduction of the masses after adsorption of SO_2 and CO, by CO is always greater if there is heating from room temperature to 650°C in CO than from 600°C to 650°C in CO.

3.3.6 Summary of the results of adsorption of SO_2 and CO individually and simultaneously on $La_{1-x}Sr_xCoO_3$

The purpose of this section is to show, in the form of tables, the main observations of the adsorption reactions. The observations include percentage mass changes and whether or not sulphur was produced or if COS was produced after scavenging reactions with CO. The results are shown in Tables 3.23, 3.24 and 3.25.

Table 3.23

Percentage mass changes on adsorption of SO_2 and CO individually and simultaneously

$La_{1-x}Sr_xCoO_3$	Adsorption SO_2 (500°C) % mass change	Adsorption CO (500°C) % mass change	Adsorption SO_2 and CO (600°C) % mass change
$La_{0.3}Sr_{0.7}CoO_3$	5.44	7.92	33.63
$La_{0.4}Sr_{0.6}CoO_3$	10.27	0.88	20.78
$La_{0.5}Sr_{0.5}CoO_3$	12.38	1.45	23.98
$La_{0.7}Sr_{0.3}CoO_3$	19.21	at least 3.59	25.96

Table 3.24

Evidence for sulphur production on $La_{1-x}Sr_xCoO_3$ exposed to SO_2

$La_{1-x}Sr_xCoO_3$	Adsorption SO_2 (500°C)	Adsorption SO_2 and CO (600°C
$La_{0.3}Sr_{0.7}CoO_3$	X	✓
$La_{0.4}Sr_{0.6}CoO_3$	X	✓
$La_{0.5}Sr_{0.5}CoO_3$	X	✓
$La_{0.7}Sr_{0.3}CoO_3$	X	✓

✓ denotes presence of sulphur (condensed on cooling jacket)

X denotes no sulphur observed

Table 3.25

Evidence for COS production during scavenging of sulphur species by CO on $La_{1-x}Sr_xCoO_3$ exposed to SO_2

$La_{1-x}Sr_xCoO_3$	Adsorption SO_2 (500°C)	Adsorption SO_2 and CO (600°C)
$La_{0.3}Sr_{0.7}CoO_3$	X	✓
$La_{0.4}Sr_{0.6}CoO_3$	X	✓
$La_{0.5}Sr_{0.5}CoO_3$	X	✓
$La_{0.7}Sr_{0.3}CoO_3$	X	✓

✓ denotes MS evidence for COS

X denotes no COS detection

3.3.7 Control experiment - SO_2 and CO adsorption on the silica balance pan with no $La_{1-x}Sr_xCoO_3$

SO_2 and CO were allowed into the vacuum line in the absence of $La_{1-x}Sr_xCoO_3$ on the balance pan.

Adsorption of SO_2 at room temperature produced a mass change of 0.07 mg. Considering the results of the SO_2 adsorption and TPD experiments, this was regarded as being insignificant. Fig. 3.25 shows the TPD of SO_2 from glass. The amount is very small compared to TPD after the room temperature adsorption of SO_2 on $La_{0.5}Sr_{0.5}CoO_3$ shown in Fig. 3.8. The desorbed SO_2 is barely on

FIGURE 3.25 MASS SPECTROMETER SIGNAL DUE TO SO_2 DESORPTION FROM SILICA BALANCE PAN IN VACUUM LINE, IN ABSENCE OF $La_{1-x}Sr_xCoO_3$ (AFTER ADSORPTION OF SO_2 AT ROOM TEMPERATURE) AND TEMPERATURE PLOTTED AGAINST TIME

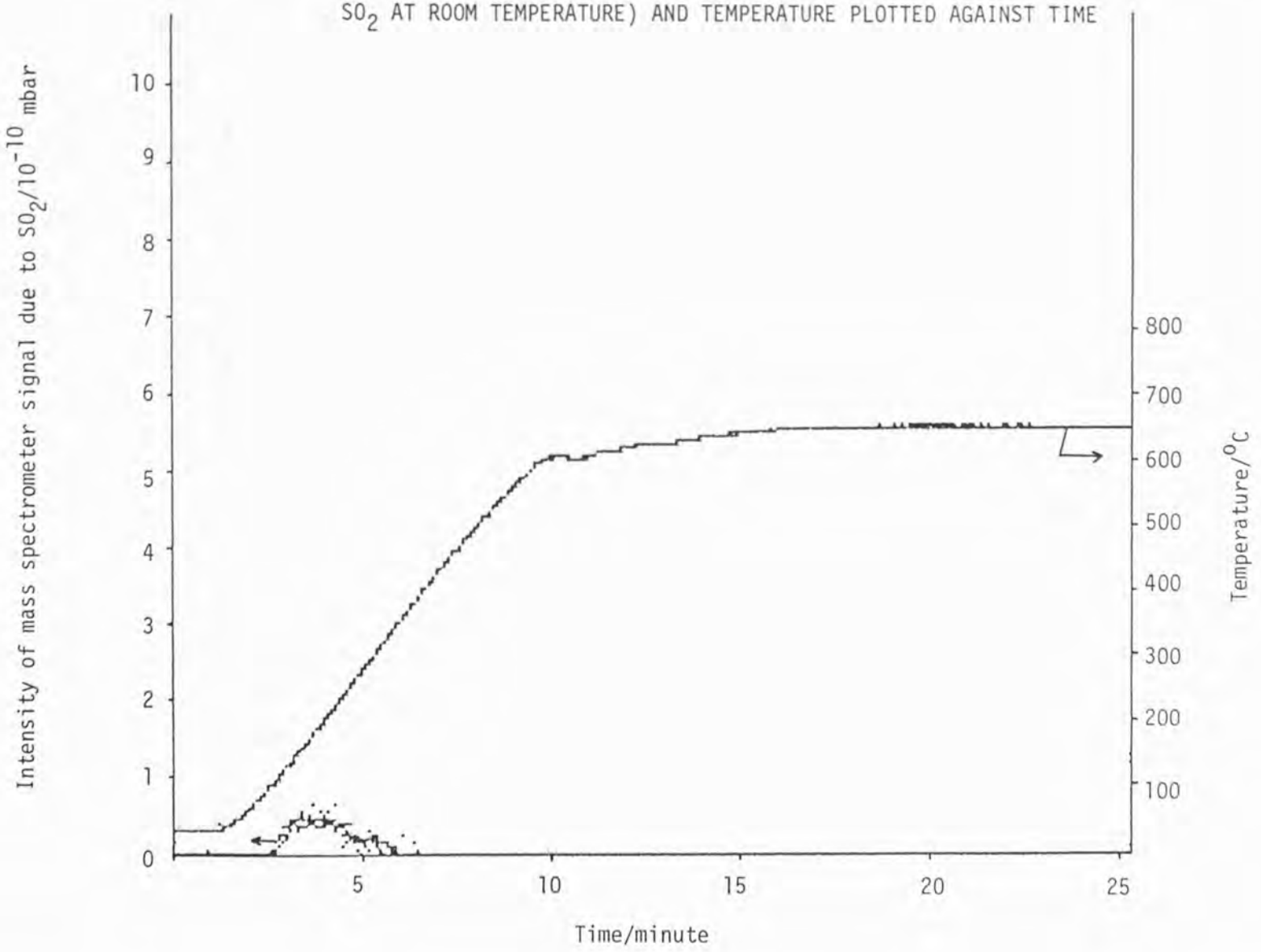

the 10^{-10} mbar scale, that from $La_{0.5}Sr_{0.5}CoO_3$ is high on the 10^{-9} mbar scale.

Exposure to CO of the balance pan at room temperature produced no change in mass.

Any mass changes observed during the experiments were therefore considered to be due to adsorption by $La_{1-x}Sr_xCoO_3$.

3.4 SO_2 AND CO FLOW-RIG EXPERIMENTS

The flow-rig experiments are described in section 2.4.2. $La_{1-x}Sr_xCoO_3$ (x = 0.3, 0.5, 0.7) was studied to see which was the most efficient catalyst for removal of SO_2 and CO to produce elemental sulphur and CO_2.

In this section the removal of SO_2 and production of CO_2 and sometimes COS, under various temperatures, SO_2:CO ratios and flow rates for each catalyst will be reported.

3.4.1 Flow-rig investigation of $La_{0.3}Sr_{0.7}CoO_3$

The results of the flow-rig investigation of $La_{0.3}Sr_{0.7}CoO_3$ are given in Table 3.26. The conditions of each experiment are shown plus the percentages of SO_2, CO and COS. Comments about the change in percentage of SO_2 during heating and the behaviour of COS during cooling to room temperature are included.

Table 3.26

Flow-rig investigation of $La_{0.3}Sr_{0.7}CoO_3$

Flow rate SO_2/ cm^3min^{-1}	Flow rate CO/ cm^3min^{-1}	% SO_2	% CO	Total flow rate /cm^3min^{-1}	Equilibrium SO_2 % before heating	Temperature experiment /°C	Equilibrium SO_2% at temperature experiment	Equilibrium CO_2% at temperature experiment	Equilibrium COS % at temperature experiment	Increase SO_2% on initial heating	Increase or appearance of COS during cooling
1	2	1	2	100	0.94	500	-	1.78	0.04		✓
1	2	1	2	100	0.97	550	I	1.84	0.05	[✓]	[✓]
1	2	1	2	100	↓	600	0.07	1.90	0.10		
1	2	1	2	100		650	0.07	1.80	I		
1	1	1	1	100	1.00	500	0.73	0.63	-	[✓]	[✓]
1	1	1	1	100	↓	550	0.71	0.63	-		
1	1	1	1	100	1.00	600	0.77	0.53	-	[✓]	
1	1	1	1	100	↓	650	0.77	0.60	-		
1	4	1	4	100	1.00	500	-	1.92	0.96	[✓]	
1	4	1	4	100	↓	550	-	1.94	0.92		
1	4	1	4	100	1.02	600	I	2.07	0.80	[✓]	
1	4	1	4	100	↓	650	I	2.03	0.56		
1	2	1	2	50	1.00	500	0.33	1.29	-		[✓]
1	2	1	2	50	↓	550	0.25	1.32	-		
1	2	1	2	50	0.94	600	0.26	1.10	-	[✓]	[✓]
1	2	1	2	50	↓	650	0.27	1.13	-		
1	4	1	4	50	0.83	500	-	1.71	0.48	✓	
1	4	1	4	50	0.71	550	-	1.68	0.52	[✓]	
1	4	1	4	50	↓	600	-	1.79	0.53		
1	4	1	4	50	0.73	650	-	1.74	0.49	✓	✓

I = intermittent

↓ shows how many temperatures were investigated without interruption

If the SO_2:CO ratios are compared it can be seen that for the stoichiometric ratio at 100 cm^3 min^{-1} total flow rate, there is virtually complete removal of SO_2, CO_2 is produced and there is some COS production, this increases with increasing temperature. For the stoichiometric ratio at 50 $cm^3 min^{-1}$ less of the SO_2 was removed but no COS was produced.

When equal amounts of SO_2 and CO were passed over the catalyst there was insufficient CO to react with all of the SO_2. No COS was produced indicating that the CO formed CO_2 preferentially to COS at the temperatures investigated.

When there was an excess of CO, that is 1% SO_2 and 4% CO virtually all of the SO_2 was removed at the shorter contact time and all of the SO_2 was removed at the longer contact time. The excess CO, however, was then available for production of COS.

It was noticed that almost every time that the gas flow was set up the outlet of SO_2 increased for the first or second reading during heating, that is, before there was evidence of CO_2 and perhaps COS to show that the reaction had started. This increase in outlet percentage of SO_2 is thought to be due to SO_2 which was adsorbed at room temperature being desorbed during heating.

An interesting observation which was made throughout the $La_{0.3}Sr_{0.7}CoO_3$ experiment was that COS production appeared to increase, or even start during cooling of the catlayst under the stream of SO_2 and CO in N_2. These peaks in COS production tended

to occur below 400°C. The temperature at which each sample was taken was noted but samples were not taken at the exact same temperatures each time the catalyst was cooled.

None of the conditions studied gave a completely satisfactory result.

3.4.2 Flow-rig investigation of $La_{0.5}Sr_{0.5}CoO_3$

The conditions and results of the flow-rig investigation of $La_{0.5}Sr_{0.5}CoO_3$ are given in Table 3.27.

As with the $La_{0.3}Sr_{0.7}CoO_3$ catalyst the stoichiometric mixture appears to give the best result, but not complete removal of gas phase sulphur. The low contact time study, that is, when the total flow rate was 100 cm^3min^{-1} gave total removal of SO_2 but a small amount of COS was produced. The longer contact time, given by a flow rate of 50 cm^3min^{-1} gave incomplete removal of SO_2 but no COS was produced.

A deficiency of CO for complete reaction of the SO_2 was provided in the 1% SO_2 and 1% CO reaction. The removal of SO_2 was favoured to COS production. Not all of the SO_2 was removed but no COS was detected.

Excess CO removed all SO_2 except at 650°C for a total flow rate of 50 cm^3min^{-1}. The excess CO after reaction with SO_2 then appeared to react with either elemental sulphur, or a sulphur species formed with the catalyst and COS was produced at both flow rates.

Table 3.27

Flow-rig investigation of $La_{0.5}Sr_{0.5}CoO_3$

Flow rate SO_2/ cm^3min^{-1}	Flow rate CO/ cm^3min^{-1}	% SO_2	% CO	Total flow rate /cm^3min^{-1}	Equilibrium SO_2 % before heating	Temperature experiment /°C	Equilibrium SO_2 % at temperature experiment	Equilibrium CO_2 % at temperature experiment	Equilibrium COS % at temperature experiment	Increase SO_2% on initial heating	Increase or appearance of COS during cooling
1	2	1	2	100	0.62	500	-	1.90	0.02	✓	✓
1	2	1	2	100	0.52	550	-	1.82	0.02		✓
1	2	1	2	100	0.62	600	-	1.83	0.02	✓	✓
1	2	1	2	100	0.62	650	-	1.82	0.02	✓	✓
1	1	1.14	1.14	87.5	0.65	500	0.51	0.68	-	[✓	[✓
1	1	1.14	1.14	87.5	↓	550	0.49	0.66	-		
1	1	1.14	1.14	87.5	↓	600	0.50	0.66	-		
1	1	1.14	1.14	87.5	↓	650	0.50	0.68	-		
1	1	1	1	100	↓	650	0.50	0.64	-	]	]
1	4	1	4	100	0.62	500	-	2.02	0.87	[✓]	
1	4	1	4	100	↓	550	-	2.03	0.92		
1	4	1	4	100	0.61	600	-	2.10	0.72	[✓	[✓
1	4	1	4	100	↓	650	-	2.02	0.61	]	]
1	2	1	2	50	0.58	500	*	1.22	-		✓
1	2	1	2	50	0.60	550	*	1.15	-	[✓	[✓
1	2	1	2	50	↓	600	*	1.16	-	]	]
1	2	1	2	50	0.92	650	0.38	1.13	-	✓	✓
1	4	1	4	50	0.77	500	-	1.73	0.46		
1	4	1	4	50	↓	550	-	1.82	0.48		
1	4	1	4	50	0.73	600	-	1.87	0.61	[✓	
1	4	1	4	50	↓	650	I	2.14	0.50	]	

* peaks appear but no % given

I intermittent

↓ shows how many temperatures were investigated without interruption

The increase in SO_2 percentage on initial heating of the catalyst, thought to be due to desorption was observed for $La_{0.5}Sr_{0.5}CoO_3$, similarly to $La_{0.3}Sr_{0.7}CoO_3$.

The increase or new appearance of COS observed on cooling $La_{0.3}Sr_{0.7}CoO_3$ in the gas flow was observed again for $La_{0.5}Sr_{0.5}CoO_3$.

3.4.3 Flow-rig investigation of $La_{0.7}Sr_{0.3}CoO_3$

The conditions and results from the flow-rig investigation of $La_{0.7}Sr_{0.3}CoO_3$ are shown in Table 3.28.

The stoichiometric ratio of SO_2 and CO at 100 cm^3min^{-1} total flow rate gave virtually complete removal of SO_2 and very little COS production. COS production appeared to increase as the temperature was increased. At the longer contact time, that is, when the flow rate was 50 cm^3min^{-1}, all of the SO_2 was removed, however, there was COS production at each of the four temperatures studied.

When there was a deficiency of CO not all of the SO_2 was removed and no COS was produced.

Excess CO for the stoichiometric reaction led to removal of all SO_2 but production of COS occurred at all of the temperatures investigated at both flow rates. At the faster flow rate there was more CO_2 and COS produced than at the slower flow rate. During cooling the production of COS increased further for the experiment at the faster flow rate. The COS production did not increase at the slower flow rate which had low COS production.

Table 3.28

Flow-rig investigation of $La_{0.7}Sr_{0.3}CoO_3$

Flow rate SO_2/ cm^3min^{-1}	Flow rate CO/ cm^3min^{-1}	% SO_2	% CO	Total flow rate /cm^3min^{-1}	Equilibrium SO_2 % before heating	Temperature experiment /°C	Equilibrium SO_2 % at temperature experiment	Equilibrium CO_2 % at temperature experiment	Equilibrium COS % at temperature experiment	Increase SO_2% on initial heating	Increase or appearance of COS during cooling
1	2	1	2	100	0.93	500	0.04	1.84	-		[✓]
1	2	1	2	100	↓	550	I	1.84	-		
1	2	1	2	100	0.93	600	-	1.86	I	[✓]	[✓]
1	2	1	2	100	↓	650	I	1.83	0.03		
1	1	1	1	100	0.92	500	0.66	0.69	-	[✓]	[✓]
1	1	1	1	100	|	550	0.64	0.69	-		
1	1	1	1	100	|	600	0.67	0.71	-		
1	1	1	1	100	↓	650	0.67	0.70	-		
1	4	1	4	100	1.00	500	-	2.00	0.94		[✓]
1	4	1	4	100	|	550	-	2.06	0.93		
1	4	1	4	100	|	600	-	2.22	0.77		
1	4	1	4	100	↓	650	-	2.04	0.64		
1	2	1	2	50	1.00	500	0.38	1.16	-	[✓]	[✓]
1	2	1	2	50	↓	550	0.34	1.17	-		
1	2	1	2	50	0.83	600	0.13	1.23	-		[✓]
1	2	1	2	50	↓	650	0.22	1.21	-		
1	4	1	4	50	0.70	500	-	1.63	0.62	[✓]	
1	4	1	4	50	|	550	-	1.69	0.65		
1	4	1	4	50	|	600	-	1.80	0.61		
1	4	1	4	50	↓	650	-	1.78	0.47		

I = intermittent

↓ shows how many temperatures were investigated without interruption

The percentage of SO_2 in the outlet increased on initial heating of the $La_{0.7}Sr_{0.3}CoO_3$ sample, as it did during the $La_{0.3}Sr_{0.7}CoO_3$ and $La_{0.5}Sr_{0.5}CoO_3$. This was possibly due to desorption of SO_2 which was adsorbed on exposure of the sample to SO_2 at room temperature.

3.4.4 Summary of the flow-rig experiments

The catalytic efficiencies of the three $La_{1-x}Sr_xCoO_3$ compounds investigated were in general very similar. The results are summarized in Table 3.29. The best results were for the SO_2:CO ratio of 1:2 at a flow rate of 100 cm^3min^{-1}. These results are compared in Table 3.30.

Table 3.29

(a) Summary of 100 cm^3min^{-1} flow rate experiments

Composition of gas flow	SO_2 removed	CO_2 formed	COS formed
1% SO_2 1% CO	X	✓	X
1% SO_2 2% CO	*	✓	≠ ✓
1% SO_2 4% CO	✓	✓	✓

* see Table 3.30 ≠ not for $La_{0.7}Sr_{0.3}CoO_3$ at 500°C and 550°C

Table 3.29 (continued)

(b) Summary of 50 $cm^3 min^{-1}$ flow rate experiments

Composition of gas flow	SO_2 removed	CO_2 formed	COS formed
1% SO_2 2% CO	X	✓	X
1% SO_2 4% CO	✓	✓	✓

Table 3.30

Summary of the data obtained for the 1% SO_2 and 2% CO experiments with a total flow rate of 100 cm^3 cm^{-1}

$La_{1-x}Sr_xCoO_3$	500°C	550°C	600°C	650°C
$La_{0.3}Sr_{0.7}CoO_3$	✓	I	X	X
$La_{0.5}Sr_{0.5}CoO_3$	✓	✓	✓	✓
$La_{0.7}Sr_{0.3}CoO_3$	X	I	✓	I

✓ = SO_2 removed

I = intermittent SO_2 observed

X = significant amount of SO_2 remaining

shaded = COS produced

Table 3.29 gives an overall impression of the effect of changing the SO_2:CO ratio on removal of SO_2 and production of COS. A deficiency of CO neither removes all SO_2 or forms COS whereas an excess of CO both removes SO_2 and produces the unwanted COS. The stoichiometric ratio of SO_2:CO as 1:2, therefore deserves closer scrutiny.

Table 3.30 summarizes the results obtained for 1% SO_2 and 2% CO at a total flow rate of 100 cm^3min^{-1}. The most efficient $La_{1-x}Sr_xCoO_3$ catalyst appears from this Table, to be $La_{0.7}Sr_{0.3}CoO_3$ at 550°C. This is if an intermittent SO_2 outlet but no COS is acceptable.

3.4.5 Control experiment - SO_2 and CO flow-rig experiment with no $La_{1-x}Sr_xO_3$

The control experiment was carried out with no $La_{1-x}Sr_xCoO_3$ present, as described in section 2.4.2.3.

Throughout the temperature range investigated for the 1% SO_2 and 2% CO mixture and during the 1% SO_2 and 4% CO mixture study, gas samples were analysed regularly by the G.C. The SO_2 content of the outlet gas remained at 1% and there was no trace of CO_2 or COS. No sulphur was condensed in the ice bath.

3.5 PROPERTIES OF USED $La_{1-x}Sr_xCoO_3$

In this section the results of XRD, ESCA and conductivity measurements made on $La_{1-x}Sr_xCoO_3$ samples which were used in the vacuum line and flow rig experiments will be reported.

3.5.1 Bulk properties of $La_{1-x}Sr_xCoO_3$ after exposure to SO_2 and CO, determined by XRD

The $La_{1-x}Sr_xCoO_3$ samples were investigated in four different experiments. These were SO_2 adsorption, CO adsorption, simultaneous SO_2 and CO adsorption and the flow-rig experiments. The XRD results will be divided into these groups.

Unknown peaks were identified by the d values, which were calculated from the 2θ values using the wavelength of the X-radiation. The d values for sulphur and oxygen compounds of La, Sr and Co and of the elements themselves were looked up, to compare with the experimental results.

A list of the 2θ and d values of interest is given in Appendix 2.

3.5.1.1 XRD of $La_{1-x}Sr_xCoO_3$ exposed to SO_2 in the vacuum line

The major peaks obtained from XRD of samples exposed to SO_2 are recorded in Table 3.31.

From the XRD information it appears that there has been some reaction of SO_2 with the $La_{1-x}Sr_xCoO_3$. On first looking at Table 3.31 it seems that exposure of $La_{1-x}Sr_xCoO_3$ to SO_2 leads to production of $SrSO_4$. $SrSO_4$ was not detected on $La_{0.4}Sr_{0.6}CoO_3$ or $La_{0.7}Sr_{0.3}CoO_3$.

Table 3.31

XRD signals of $La_{1-x}Sr_xCoO_3$ after exposure to SO_2 (λ = 1.542 Å)

A $La_{0.3}Sr_{0.7}CoO_3$ *		B $La_{0.4}Sr_{0.6}CoO_3$		A $La_{0.5}Sr_{0.5}CoO_3$		A $La_{0.7}Sr_{0.3}CoO_3$ *	
2θ/intensity	assignment	2θ/intensity	assignment	2θ/intensity	assignment	2θ/intensity	assignment
27.2s	$SrSO_4$	11.7vw		26.2w		26s	La_2O_2S
28.5m		18.2vw		27.4m	$SrSO_4$	28.8s	La_2O_2S
30.2s	$SrSO_4$	28.7w		28.2vw		30s	Co_4S_3/SrS
31.9s		31.8s		29w		31m	Co_3S_4
32.9m	$SrSO_4$	33.2s	perovskite	30.2m	$SrSO_4$	36.8s	La_2O_2S
33.5s	perovskite	36.7m		33vs	perovskite	42.7m	SrS
36.7s		38.5w		37m		45s	La_2O_2S
37.2w	42.6s	42.6s		44.5w		47.6sb	La_2O_2S
42.6s		47.8s	perovskite	45.2w		50.1w	Co_4S_3
44.6m		57.9m		47.7m	perovskite	50.7w	Co_4S_3
47.8w	perovskite	58.7m	perovskite	50.6w		52.3s	Co_4S_3
59vw	perovskite	65.1m		NO XRD AT HIGHER 2θ VALUES		59w	

* = exposed to SO_2 and CO after the SO_2 exposures and before XRD s = strong m = medium w = weak

vs = very strong vw = very weak A = Philips PW1010 X-ray diffractometer used

sb = strong and broad B = Philips PW1710 X-ray diffractometer used

2θ error = ± 0.05°

It must be borne in mind that XRD is a bulk technique and therefore if the reaction only occurred at the surface there may be insufficient product to be detected by this method.

There appears to be sulphidation of $La_{0.7}Sr_{0.3}CoO_3$ and it appears to have lost its perovskite-type structure. It may no longer be called $La_{0.7}Sr_{0.3}CoO_3$. The perovskite-type structure of $La_{0.3}Sr_{0.7}CoO_3$, exposed to SO_2 and CO, like the $La_{0.7}Sr_{0.3}CoO_3$ was, appears to be weak, which suggests that a significant amount of it has reacted too. The $La_{0.4}Sr_{0.6}CoO_3$ and $La_{0.5}Sr_{0.5}CoO_3$ have retained their perovskite-type structure.

Each of the samples have peaks which have not been assigned. The reason for this is that many of the probable species present, have close 2θ values or are only represented by perhaps two out of three strong peaks so positive identification of species proves to be impossible.

3.5.1.2 XRD of $La_{1-x}Sr_xCoO_3$ exposed to CO in the vacuum line

The major peaks obtained from XRD of samples exposed to CO are recorded in Table 3.32.

The perovskite structure is evident, with the three most strong peaks of the $La_{1-x}Sr_xCoO_3$ present.

$La_{0.5}Sr_{0.5}CoO_3$ has evidence of $SrSO_4$. This sample was exposed to SO_2 after the CO experiment and shows the same result as those exposed to SO_2 only, described in section 3.5.1.1.

It appears that CO alone causes no permanent change to the perovskite-type structure.

Table 3.32

XRD signals of $La_{1-x}Sr_xCoO_3$ after exposure to CO

(λ = 1.542 Å) (no XRD available for $La_{0.3}Sr_{0.7}CoO_3$)

B $La_{0.4}Sr_{0.6}CoO_3$		A $La_{0.5}Sr_{0.5}CoO_3$		A $La_{0.7}Sr_{0.3}CoO_3$	
2θ/intensity	assignment	2θ/intensity	assignment	2θ/intensity	assignment
13vw		27.2m		19.2vw	
16.3vw		28-29mb		24.5w	
28.2vw		30.1m	$SrSO_4$	27.7vw	
31.7s		31.7m		28.5w	
33.2m	perovskite	33s	perovskite	33.8s	
38.5m		36.7s		33.3s	perovskite
39.8vw		42.7s	$SrSO_4$	43.1m	perovskite
44.4m		44.5m		44.2m	
44.7m		45.3m		44.5m	
48.7w	perovskite	47.5m	perovskite	47.6m	
65.1w		59w	perovskite	58.3m	perovskite
78.3w		62.3m		66vw	
		70.7w		76vw	
		75w		79vw	

s = strong m = medium w = weak

vs = very strong vw = very weak mb = medium and broad

A = Philips PW1010 X-ray diffractometer used

B = Philips PW1710 X-ray diffractometer used

error in 2θ = $\pm$ 0.05°

3.5.1.3 XRD of $La_{1-x}Sr_xCoO_3$ exposed to SO_2 and CO in the vacuum line

The results of the XRD examinations of the samples exposed to SO_2 and CO simultaneously, in the vacuum line are given in Table 3.33.

Table 3.33

XRD signals of $La_{1-x}Sr_xCoO_3$ after exposure to SO_2 and CO in the vacuum line (λ = 1.542 Å) (no XRD available for $La_{0.7}Sr_{0.3}CoO_3$)

A $La_{0.3}Sr_{0.7}CoO_3$		B $La_{0.4}Sr_{0.6}CoO_3$		A $La_{0.5}Sr_{0.5}CoO_3$	
2θ/intensity	assignment	2θ/intensity	assignment	2θ/intensity	assignment
15.6w		25.8m	SrS	13.6vw	
25.7m	SrS	28.6m		15.5vw	
27.8vw		29.8s	SrS/Co_4S_3	25.8m	SrS
28.7m		31.3m		27.2vw	
29.9s	SrS/Co_4S_3	38.5m	$LaS_{1.75-1.80}$	28.7s	
31.3w		39.7w	Co_4S_3	29.9s	SrS/Co_4S_3
36.6w		42.5m	SrS	31.3w	
39vw		44.7m	$LaS_{1.75-1.80}$	35.6vw	
39.7vw	Co_4S_3	47.6m		36.6w	
41w		50.3w	Co_4S_3	39.7w	Co_4S_3
42.7m	SrS	52.2s	Co_4S_3	42.6w/m	SrS
45w		52.7w		42.9w/m	
47.2w		54vw		44.8m	
47.7w		65.1w		47.6w	
49.6w		69.9w		50.4w	
50.4w	Co_4S_3			52.4m	Co_4S_3
52.3m	Co_4S_3				
70w					

s = strong m = medium w = weak vs = very strong vw = very weak
A = Philips PW1010 X-ray diffractometer used
B = Philips PW1710 X-ray diffractometer used
error in 2θ = $\pm$ 0.05°

The first important observation from the XRD results, is that the perovskite-type structure no longer exists. It appears that the SO_2 and CO have reacted with the $La_{1-x}Sr_xCoO_3$ and sulphides of La, Sr and Co have been formed. This agrees with the observation of $La_{0.7}Sr_{0.3}CoO_3$ exposure to SO_2 and CO after the SO_2 experiment described in section 3.5.1.1.

As with the other specimens examined, not all of the peaks have been assigned. The unassigned peaks include some of the strongest signals, such as around $2\theta = 28.7$.

The powder diffraction manual (80) was consulted and a list of possible compounds containing mixtures of La, Sr, Co, O and S, with strong peaks around this value was made. The compounds included $La_2O_2(SO_4)$, La_2O_2S, La_4SrO_7, $La_2Sr_2O_5$ and SrO_2. The 2θ values of these are given with other values of interest and relevance, in Appendix 2. There may be a mixture of these compounds present which overlap at around $2\theta = 28.7$. This would make identification using ratios of peak sizes difficult.

3.5.1.4 XRD of $La_{1-x}Sr_xCoO_3$ exposed to SO_2 and CO in the flow rig apparatus

The results of the XRD examinations of the $La_{1-x}Sr_xCoO_3$ samples exposed to SO_2 and CO in the flow-rig apparatus are given in Table 3.34.

The peaks which represent the $La_{1-x}Sr_xCoO_3$ perovskite-type structure were no longer visible after the flow-rig experiments. The SO_2 and CO appear to have reacted with the $La_{1-x}Sr_xCoO_3$ and sulphides have been formed.

Table 3.34

XRD of $La_{1-x}Sr_xCoO_3$ after exposure to SO_2 and CO in the flow-rig apparatus (λ = 1.542 Å)

B $La_{0.3}Sr_{0.7}CoO_3$		B $La_{0.5}Sr_{0.5}CoO_3$		B $La_{0.7}Sr_{0.03}CoO_3$	
2θ/intensity	assignment	2θ/intensity	assignment	2θ/intensity	assignment
22.5w	Co_4S_3				
25.2w		25.8m	SrS	14.1vw	
26m	SrS	26s		25.2s	
28.8m		28.8s		25.8m	
30s	SrS	30s	SrS	28.8s	
31w	$LaS_{1.75-1.80}$	31m		30.1w	
32.5w	CoS_2	32.5w		31.1w	$LaS_{1.75-1.80}$
35.5w		35.6w	$CoS_{1.097}$	32.6s	CoS_2/Co_3S_4
36.3w	CoS_2	36.6m		35.7w	CoS_2
38.1w	$LaS_{1.75-1.80}$	38.6w	$CoS_{1.097}$	36.6m	
38.6w		42.7m	SrS	38.7m/s	CoS_2/ $LaS_{1.75-1.80}$
42.8s	SrS	45m		45.1m	
44.9w	$LaS_{1.75-1.80}$	47.3m	Co_3S_4	46.6m	
46.4w	Co_4S_3				
47.2w		47.9w		47.3m	
50.5w	Co_4S_3	52.5m		48.9w	
52.9w		54.1w		52.6w	
54.9w		55.3w	$CoS_{1.097}$	53.4w	
55.2w	CoS_2			65.8m	
70.1w					

s = strong m = medium w = weak

vs = very strong vw = very weak

B = Philips PW1710 X-ray diffractometer used.

error in 2θ = $\pm$ 0.05°

Not all of the peaks have been assigned. The main peak which has not been assigned is around $2\theta = 28.8$. This was found with the other samples exposed to SO_2 and CO. This peak may be due to a combination of two or more compounds containing some or all of the elements La, Sr, Co, O and S. Some examples of these are given in section 3.5.1.3.

3.5.1.5 Summary of the XRD results of the $La_{1-x}Sr_xCoO_3$ samples exposed to SO_2 and CO individually and simultaneously in the vacuum line and flow rig apparatus

The evidence relating to the perovskite-type structure of all of the samples examined may be summarised in Table 3.35.

Table 3.35

XRD evidence for the perovskite structure of fresh and used $La_{1-x}Sr_xCoO_3$

$La_{1-x}Sr_xCoO_3$	Fresh	SO_2 adsorption	CO adsorption	SO_2 and CO adsorption	SO_2 and CO flow-rig
$La_{0.3}Sr_{0.7}CoO_3$	✓	* ✓ weak	✓	X	X
$La_{0.4}Sr_{0.6}CoO_3$	✓	✓	✓	X	X
$La_{0.5}Sr_{0.5}CoO_3$	✓	✓	≠ ✓	X	X
$La_{0.7}Sr_{0.3}CoO_3$	✓	* X	✓	X	X

✓ = evidence for perovskite-type structure

X = no evidence for perovskite-type structure

* = exposure to SO_2 and CO after SO_2 adsorption

≠ = exposure to SO_2 after CO adsorption

In general the XRD results did not show differences due to changing La:Sr ratios. The XRD experiments were not quantitative. It is interesting to note that there are not high proportions of La compounds detected at, for example, $La_{0.7}Sr_{0.3}CoO_3$ and large proportions of Sr compounds at, for example, $La_{0.3}Sr_{0.7}CoO_3$. The only sulphate species observed in the samples exposed to SO_2 only, was $SrSO_4$.

It appears that SO_2 reacts with the $La_{1-x}Sr_xCoO_3$ to produce $SrSO_4$, but the perovskite-type structure is maintained.

CO does not appear to alter the perovskite-type structure or to react with $La_{1-x}Sr_xCoO_3$ to leave any solid product.

SO_2 and CO together appear to have a similar effect on the $La_{1-x}Sr_xCoO_3$ whether in a static system such as the vacuum line where the sample has or has not been pre-exposed to SO_2, or in a gas flow where at the most they make up a total of 5% of the gas. The perovskite-type structure is destroyed and sulphides are formed. Other compounds comprised the elements which make up $La_{1-x}Sr_xCoO_3$ and sulphur appear to be formed. The only positive identification of one of these was La_2O_2S in the product of SO_2 and CO adsorption on $La_{0.7}Sr_{0.3}CoO_3$ which had been pre-exposed to SO_2. The X-ray diffraction pattern of the product of this experiment is shown in Fig. 3.26.

FIGURE 3.26 XRD SPECTRUM OF PRODUCTS OF EXPOSURE OF $La_{0.7}Sr_{0.3}CoO_3$ to SO_2 INDIVIDUALLY AND THEN TO SO_2 AND CO SIMULTANEOUSLY

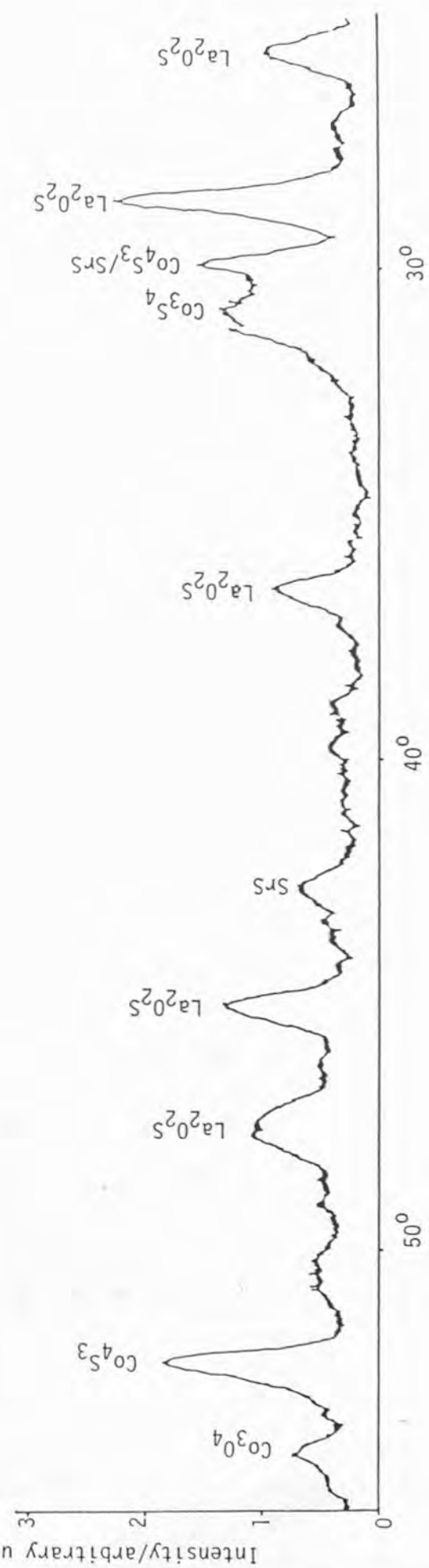

3.5.2 Surface properties of $La_{1-x}Sr_xCoO_3$ after exposure to SO_2 and CO, determined by ESCA

The fresh catalysts and those used in the flow-rig apparatus were investigated using ESCA. $La_{0.4}Sr_{0.6}CoO_3$ was not studied in the flow-rig apparatus so the sample from the simultaneous adsorption of SO_2 and CO was investigated. The binding energies obtained from the used catalysts are shown in Table 3.36.

Table 3.36

Binding energies of $La_{1-x}Sr_xCoO_3$ after exposure to SO_2 and CO

	Binding energy/eV			
Energy level	$La_{0.3}Sr_{0.7}CoO_3$ Flow-rig	$La_{0.4}Sr_{0.6}CoO_3$ Vacuum line	$La_{0.5}Sr_{0.5}CoO_3$ Flow-rig	$La_{0.7}Sr_{0.3}CoO_3$ Flow-rig
$La3d_{5/2}$	836.4	836.1	834.6	836.5
$Sr3d_{5/2}$	133.5	133.3	133.2	133.7
$Co2p_{3/2}$	779.2	778.5	778.8	778.8
	781.4 *	780.8 *	781.6 *	781.8 *
O1s	531.8	531.6	532.1	532.2
S2p	160.6	161.1	160.7	161
	166.1	166	166.8	167.1
	167.5	167.5	168.4	168.4

* = shoulder b.e. error = $\pm$ 0.3 eV

On comparison of Table 3.36 with Table 3.5, which shows the binding energies of fresh $La_{1-x}Sr_xCoO_3$, it can be seen that the number of species of some of the elements have changed. This is illustrated in Table 3.37.

Table 3.37

Number of species of each element distinguished by ESCA before and after exposure to SO_2 and CO

	Number of species detected							
Energy level	$La_{0.3}Sr_{0.7}CoO_3$		$La_{0.4}Sr_{0.6}CoO_3$		$La_{0.5}Sr_{0.5}CoO_3$		$La_{0.7}Sr_{0.3}CoO_3$	
	Fresh	Flow rig	Fresh	Vacuum line	Fresh	Flow rig	Fresh	Flow rig
$La3d_{5/2}$	1	1	1	1	1	1	1	1
$Sr3d_{5/2}$	1	1	1	1	1	1	1	1
$Co2p_{3/2}$	1	2	1	2	1	2	1	2
O1s	2	1	2	1	2	1	2	1
S2p	0	3	0	3	0	3	0	3

There appears to be very little change of binding energies of La and Sr. La and Sr only exist in the oxidation states + 3 and + 2 respectively. If changes have occurred in the chemical environment they are not reflected in changes of the La and Sr spectra.

The Co spectra of the $La_{1-x}Sr_xCoO_3$ exposed to SO_2 and CO shows evidence of two Co species. The Handbook of X-ray Photoelectron Spectroscopy (81) gives the binding energies for 36 Co compounds and

the relationship between binding energy and oxidation state is shown to be not straightforward. There is a vague increase in binding energy with oxidation state. A Co compound not represented in the handbook could not easily be identified by its binding energy. The lower binding energy observed during the ESCA measurements may be divalent Co and the higher binding energy may be trivalent Co. If the claim made in section 3.2.4, that there is only one Co peak produced for fresh $La_{1-x}Sr_xCoO_3$, in spite of there being trivalent and tetravalent Co present is true, then it appears that the surface structure, at least of $La_{1-x}Sr_xCoO_3$ has altered and produced at least two Co compounds in each of the specimens studied.

There is just one binding energy for oxygen in the used specimens. The fresh $La_{1-x}Sr_xCoO_3$ gave spectra showing two oxygen species and these were tentatively attributed to lattice oxygen and adsorbed oxygen. The higher binding energy species appears to have remained whereas the lower binding energy species has disappeared.

There are three sulphur species detected by ESCA. The S2p spectrum for $La_{0.5}Sr_{0.5}CoO_3$ after the flow-rig experiment is shown in Fig. 3.27. Reference to the ESCA handbook (81) gives the impression that the largest peak, which has the lowest binding energy is due to sulphur in the form of sulphide. The highest binding energy peak appears to be due to sulphate species. The smallest peak with the binding energy a little lower to that of the sulphate may, according to the example given in the handbook (81), be due to sulphite.

FIGURE 3.27 ESCA SPECTRUM OF THE SULPHUR SPECIES PRESENT AFTER $La_{0.5}Sr_{0.5}CoO_3$ HAS BEEN EXPOSED TO SO_2 AND CO IN THE FLOW RIG EXPERIMENTS

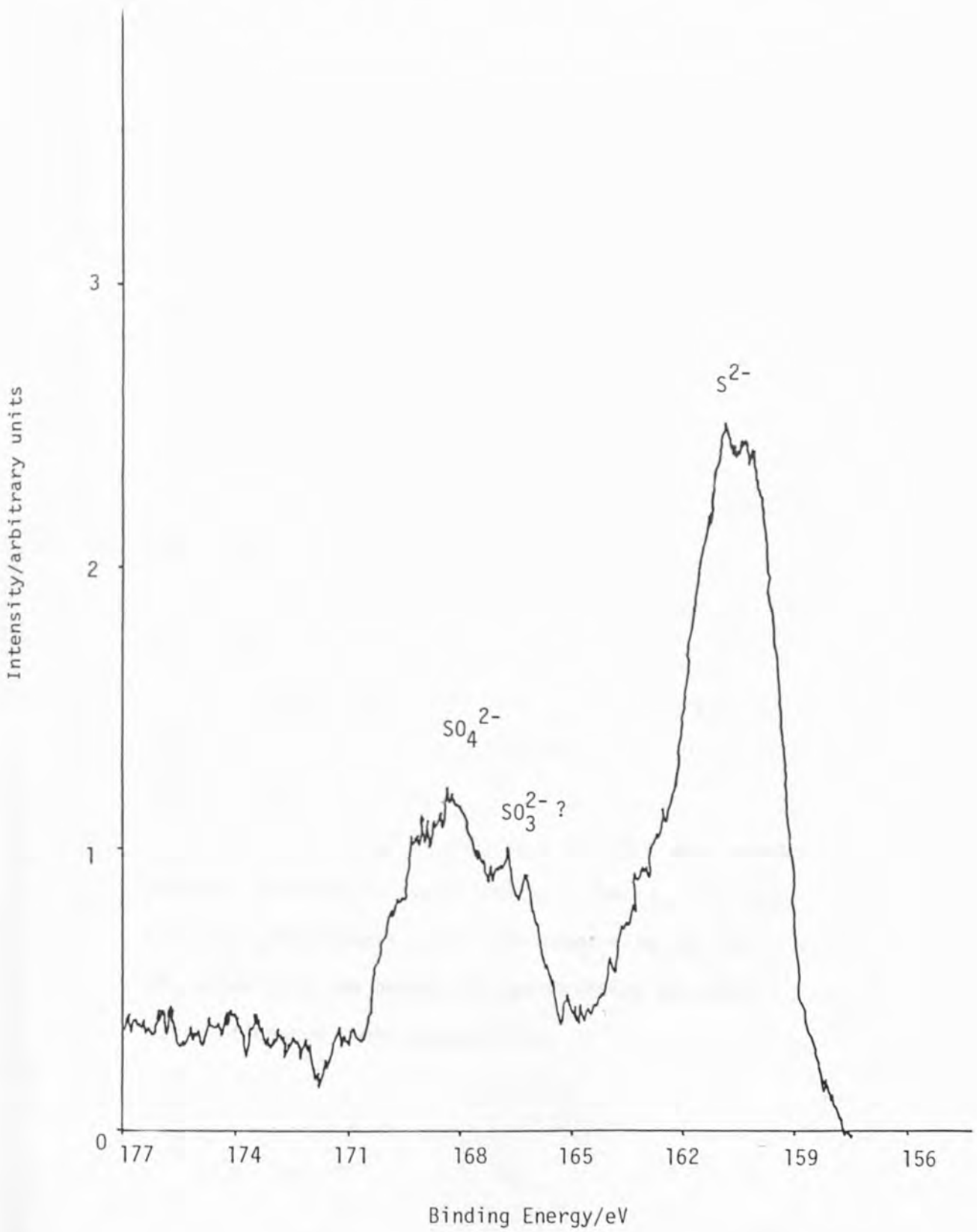

The sensitivity of the binding energy of S in various SO_4^{2-} environments is not clear, there may be sulphates of two of the metals present or another unknown sulphur species not represented in the handbook.

The ESCA studies show that the surface of the catalyst has been significantly altered by exposure to SO_2 and CO. Co appears to have been involved in a reaction and at least three different sulphur species are present on the used catalyst surface.

3.5.3 Conductivities of $La_{1-x}Sr_xCoO_3$ after exposure to SO_2 and CO

The conductivities of the $La_{1-x}Sr_xCoO_3$ samples were measured after exposure to SO_2, CO and SO_2 with CO in the vacuum line and SO_2 with CO in the flow-rig apparatus. The results of these measurements are given in Table 3.38.

The conductivity measurements may be compared to those of the fresh catalysts in Table 3.6.

It appears that the interactions of SO_2 and CO with $La_{1-x}Sr_xCoO_3$ lead to changes in the structure which are sufficient to influence the conductivity.

All of the $La_{1-x}Sr_xCoO_3$ samples which were exposed to SO_2 showed a decrease in conductivity. The $La_{0.3}Sr_{0.7}CoO_3$ and $La_{0.7}Sr_{0.3}CoO_3$ samples were both exposed to SO_2 and CO after the SO_2 experiment and before the conductivity was measured and this may have influenced their conductivity.

Table 3.38

Conductivities of $La_{1-x}Sr_xCoO_3$ after exposure to SO_2 and CO

	Conductivity/$\Omega^{-1}m^{-1}$			
$La_{1-x}Sr_xCoO_3$	SO_2 adsorption	CO adsorption	SO_2 and CO adsorption	SO_2 and CO flow-rig
$La_{0.3}Sr_{0.7}CoO_3$	v. high resistance *	0.516	124.4	24.88
$La_{0.4}Sr_{0.6}CoO_3$	4.5×10^{-6}	v. high resistance	2.43×10^{-5}	
$La_{0.5}Sr_{0.5}CoO_3$	7.34×10^{-3}	5.42×10^{-6} ≠	1.53×10^{-3}	0.23
$La_{0.7}Sr_{0.3}CoO_3$	1.93×10^{-2} *	8.22×10^{-6}	v. high resistance	0.37

* exposed to SO_2 and CO after the SO_2 experiment

≠ exposed to SO_2 after CO experiment

The $La_{0.3}Sr_{0.7}CoO_3$ exposed to CO showed virtually no change in conductivity. The other samples on which CO was adsorbed, including the $La_{0.5}Sr_{0.5}CoO_3$ which was exposed to SO_2 after the CO experiment, all had lower conductivities than the fresh samples.

The samples exposed to SO_2 and CO in the vacuum line, had lower conductivities than the fresh catalysts, except in the case of $La_{0.3}Sr_{0.7}CoO_3$ whose conductivity had increased by about 300 times its original value. The $La_{0.7}Sr_{0.3}CoO_3$ differed from the other $La_{1-x}Sr_xCoO_3$ samples because after adsorption of SO_2 and CO the scavenging of sulphur species by CO was not attempted.

Those samples exposed to SO_2 and CO in the flow-rig apparatus showed the smallest changes in conductivity. The $La_{0.3}Sr_{0.7}CoO_3$ conductivity increased around 60 fold. The conductivities of $La_{0.5}Sr_{0.5}CoO_3$ and $La_{0.7}Sr_{0.3}CoO_3$ decreased around 80 fold and 50 fold respectively.

3.6 ERRORS

Many of the experiments, such as the adsorption and TPD of SO_2 were extremely time consuming and consequently were only carried out once. Due to the lack of duplication of results it was impossible to calculate standard deviations. Errors have, however, been estimated and these are included in the tables of results.

There was no means of calculating the error of the desportion energies, however, the parameter F, which is the standard deviation of the calculated points is a guide. F^2 is represented by equation 30.

$$F^2 = \sum_{i}^{N} (S_{calculated} - S_{experimental})^2/(N-2) \qquad 30$$

S = MS signal N = number of data points

The values of F are given in Tables 3.8 and 3.10.

In the flow-rig experiments steady state readings were obtained and the standard deviations of the percentage values in the outflow were calculated to be about 1.5% of the mean value.

CHAPTER 4

DISCUSSION

In this chapter the results related in Chapter 3 will be discussed and where it is relevant, comparison will be made to previous work reported in the literature.

The characterization of the fresh $La_{1-x}Sr_xCoO_3$ requires very little discussion.

Explanation of the mass changes observed during the adsorption and TPD experiments will be attempted. The characteristics of the fresh and used catalysts will be referred to, to assist the elucidation of the mechanisms which took place.

The flow-rig results will also be explained with reference to the changes to the catalysts' properties before and after the experiments.

The explanations of the adsorption and desorption experiments and the flow-rig experiments will be used to suggest a mechanism for the reaction between SO_2 and CO to give sulphur and CO_2.

4.1 DECOMPOSITION OF $Co(NO_3)_2.6H_2O$, ONE OF THE INGREDIENTS IN THE PREPARATION OF $La_{1-x}Sr_xCoO_3$

$Co(NO_3)_2.6H_2O$ is one of the ingredient nitrates used in the preparation of $La_{1-x}Sr_xCoO_3$ for the experiments described in this thesis. $Co(NO_3)_2.6H_2O$ was decomposed as described in section 2.1.1. The resultant mass changes and evolution of gases during decomposition are reported in section 3.1.

The experiment was carried out twice and the results were very similar in each instance.

The loss of mass on evacuation may be due to water of crystallization being removed. A mass loss of 30.9% would be equivalent to that expected if $5H_2O$ molecules per $Co(NO_3)_2.6H_2O$ were evolved.

As can be seen from Fig. 3.1 H_2O was also detected during heating; this may be the final H_2O being removed but it is likely that the loss of mass due to evacuation was in part due to degassing of the $Co(NO_3)_2.6H_2O$. Less than $5H_2O$ may be included in the 31.2% and 29.6% mass losses.

The final solid product is possibly an oxide of cobalt. From a starting compound $Co(NO_3)_2.6H_2O$, disregarding adsorbed gases from the atmosphere a mass loss of 72.4% would give Co_3O_4, 71.5% would give Co_2O_3 and 74.2% would give CoO. The actual loss of mass was 71.1% for both of the samples studied. This agrees most closely with Co_2O_3. The mass losses expected for production of the other oxides, however, are so similar that when degassing is considered a positive identification of the oxide or oxides produced, by mass loss alone, is not possible.

Fig. 3.1 shows the relative abundances of gases evolved towards the end of the decomposition experiment, as collected by the MS. Background pressures of H_2O, N_2, O_2 and CO_2 will be included in their signals. Products of decomposition detected at this point include NO and possibly H_2O and O_2. The presence of NO explains the blue/green ring observed in the liquid N_2 trap during the decomposition of the nitrates of La, Sr and Co. The MS evidence also reinforces

the evidence for NO as a decomposition product, given by the production of NO_2, on allowing the freeze drying apparatus up to atmospheric pressure, as described in section 2.1.

The O_2 reading was higher than the background reading on the 10^{-9} mbar scale normally observed. The drop in the amount of O_2 observed in relation to the other gases shown in Fig. 3.1 may be due to O_2 falling back to its background level or of decomposition products, especially NO increasing.

Tabulated melting point data (86) indicates that $Co(NO_3)_2.6H_2O$ loses $3H_2O$ at 55°C at atmospheric pressure. At the time when the first pressures were recorded to give the relative amounts shown in Fig. 3.1, the temperature was already 150°C, and the pressure was considerably lower than atmospheric, that is, about 3.5×10^{-6} mbar. It therefore seems likely that H_2O was evolved from the $Co(NO_3)_2.6H_2O$.

The evidence of mass loss and evolution of NO and H_2O support the theory that the nitrates first decompose to give oxides as expected and that it is from these, that the perovskite-type compounds are derived.

4.2 CHARACTERIZATION OF FRESH $La_{1-x}Sr_xCoO_3$

The surface area measurements of $La_{1-x}Sr_xCoO_3$ indicate the efficiency of the freeze-drying method for the production of catalysts of a relatively high area to volume ratio.

The density of $La_{0.4}Sr_{0.6}CoO_3$ was measured. The density and specific surface area were used together to calculate the radii of particles. From this data the areas were calculated by assuming

that the particles were spherical. The number of unit cells at the surfaces were cacculated from the known area of a unit cell. This proved useful in section 4.3.2 when the apparent number of SO_2 molecules adsorbed, calculated from the mass increase was examined in relation to the number of unit cells at the surface of the catalyst, to see if there was any correlation. The calculations are shown in section 4.3.2.

The XRD measurements provided the assurance that the perovskite-type structure had actually been achieved by the freeze-drying and calcination process.

The ESCA analyses provided binding energies of the electrons of the surface atoms, which could be compared with those of the surfaces after exposure to SO_2 and CO.

The conductivity measurements proved that the $La_{1-x}Sr_xCoO_3$ was indeed a semiconductor as stated in the literature (49). They could be compared with those of the used catalysts.

The e.s.r. spectrum of $La_{0.4}Sr_{0.6}CoO_3$ did not provide the spectral pattern which would be expected for Co^{IV}. The analysis for Co^{IV} was both to show the presence of Co^{IV} in $La_{1-x}Sr_xCoO_3$ and from academic interest, as the e.s.r. spectrum of this species has proven difficult to obtain. Buffat et al (87) claim to have done the first complete characterization of isolated six-coordinated Co^{IV} ions in an oxide lattice. They have synthesized $Sr_{0.5}La_{1.5}Li_{0.5}Co_{0.5}O_4$ and measured its e.s.r. spectrum at 4.2K. They claim that their spectrum is that of Co^{IV} and that g values of $2.32 \leq g_{\perp} \leq 2.55$, $g_{\parallel} < 0.85$, which were obtained agreed with a $g_{\perp}$ value

obtained by other workers, Townsend and Hill (88) for Co^{IV} in $Al_2O_3:Co^{4+}, Mg^{2+}$.

4.3 THE ADSORPTION AND DESORPTION EXPERIMENTS

The desorption of oxygen due to evacuation and heating, the SO_2 experiments, CO experiments and SO_2 and CO experiments will be discussed.

4.3.1 Desorption of oxygen from fresh $La_{1-x}Sr_xCoO_3$

The desorption of oxygen from $La_{1-x}Sr_xCoO_3$ appears to be easier on increasing the proportion of La in the catalyst, that is, on decreasing value of x. At low La proportions the desorption of oxygen occurs at lower temperatures and in greater amounts than at high La proportions. This trend suggests that the tendency of the catalyst to lose oxygen increases on decreasing La or increasing x. Earlier workers such as Yamazoe et al (17), Sieyama et al (22), Nakamura et al (24) and Misono and Nitadori (25), also found that reducibility as measured by reaction with CO increased as x increased. In some instances the earlier workers were looking at pre-adsorbed and lattice oxygen. The $La_{1-x}Sr_xCoO_3$ samples in the present work had been calcined in air at 550^oC and stored in air, so they too may have adsorbed oxygen but they certainly lost not only adsorbed oxygen but lattice oxygen during heating under vacuum. The method by which this was calculated is shown in section 3.3.3.1.

Sieyama et al (22) state that the $La_{1-x}Sr_xCoO_3$ compounds which have high numbers of oxygen vacancies are able to accommodate oxygen from the gas phase and that such sorbed oxygen tends to be more reactive than lattice oxygen. The change in the number of oxygen

vacancies with proportion of La in $La_{1-x}Sr_xCoO_3$ was calculated and is shown in Fig. 1.2 in section 1.3.1.1. The number of oxygen vacancies, expressed as δ, was calculated for the compounds used in the present work. This was done by working out how much oxygen loss was required from the $La_{1-x}Sr_xCoO_3$ lattice to maintain charge neutrality if it is assumed that δ = 0 when all of the Co is trivalent and when Sr is present substituted for La, then tetravalent Co is present. The amounts of tetravalent Co for each La:Sr ratio studied is taken from work by Jonker and van Santen (18). An example of the calculation is shown in Fig. 1.2. The formulae for $La_{1-x}Sr_xCoO_3$, as calculated by this method, for the catalysts studied are $La_{0.3}Sr_{0.7}CoO_{2.82}$, $La_{0.4}Sr_{0.6}CoO_{2.95}$, $La_{0.5}Sr_{0.5}CoO_{2.96}$ and $La_{0.7}Sr_{0.3}CoO_3$. The greatest number of oxygen vacancies does coincide with the greatest loss of oxygen observed during heating and this supports the reports made by Sieyama et al (22). The percentage mass losses expected if each vacancy was filled by an oxygen atom and these were desorbed, was calculated. The calculated percentage losses were 1.37% for $La_{0.3}Sr_{0.7}CoO_3$, 0.37% for $La_{0.4}Sr_{0.6}CoO_3$, 0.29% for $La_{0.5}Sr_{0.5}CoO_3$ and as $La_{0.7}Sr_{0.3}CoO_3$ appears to have no oxygen vacancies there would be no desorption from oxygen vacancy sites. The observed percentage mass losses are greater than those expected if there was desoprtion from oxygen vacancy sites.

The desorption of oxygen referred to by Sieyama et al (22), was in a helium atmosphere whereas the desorption referred to in this thesis was under vacuum. The conditions are different but both may

be conducive to oxygen desorption due to the low partial pressure of oxygen in the first and the low overall pressure in the second.

It is not clear why the compounds with high oxygen vacancies should be expected to adsorb more oxygen. Their charge neutrality is in fact maintained by the multivalent nature of Co, which compensates for the lack of oxygen. The oxygen rich compound may be thermodynamically more stable.

4.3.2 Adsorption of SO_2 on $La_{1-x}Sr_xCoO_3$

The graph of total mass increase due to adsorption of SO_2 after exposure at 500°C, in Fig. 3.14, shows that adsorption increases as La in $La_{1-x}Sr_xCoO_3$ increases. The increase in mass is virtually linear with increase in La content.

To ascertain what the mass increases depended on their relationship with various properties of the catalysts were investigated.

The specific surface areas, which are shown in Table 3.2 do not share the same relationship of linearity with La content of the mass changes. This suggests that either the adsorption or indeed reaction, suggested by some of the relatively high mass changes, is not a surface phenomena nor is it due to an evenly distributed surface feature.

The conductivities of the $La_{1-x}Sr_xCoO_3$ samples are shown in Table 3.6. These do not vary with La content as SO_2 adsorption does and this suggests that SO_2 adsorption is not proportional to conductivity. This does not rule out the possibility that the semiconducting properties of the $La_{1-x}Sr_xCoO_3$ samples are important. It appears, however, that the conductivity of the samples exposed to SO_2 falls dramatically after exposure. This may be due to the formation of $SrSO_4$. XRD shows that the perovskite-type structure is

still present yet there may be sufficient $SrSO_4$ to decrease the conductivity of the samples significantly.

Fig. 1.2 in section 1.3.1.1 shows how Co^{IV} content changes in $La_{1-x}Sr_xCoO_3$ ($0 \leq x \leq 1$) as presented by Jonker and van Santen (18) and the calculated value of δ which is proportional to oxygen vacancies. Neither of these features of $La_{1-x}Sr_xCoO_3$ change linearly with La content, even within the range studied in this work.

It appears that the mass changes observed are related to La content or Sr content of the catalysts or to a relationship between these two. Bearing in mind the magnitude of the mass changes the possibility of chemical reactions having occurred cannot be ruled out.

The mass changes can be examined to see if the mechanism which caused them may be made clearer. It is interesting to look at the relationship between the mass losses due to heating under vacuum and the subsequent increases in mass due to SO_2 adsorption in this context. This relationship is shown in Table 3.14.

It has already been suggested, above, that the SO_2 adsorption reaction is not proportional to the surface area of $La_{1-x}Sr_xCoO_3$. Table 4.1 shows the relationship between the number of unit cells at the catalyst surfaces and the number of SO_2 molecules equivalent to the increase in mass after exposure to SO_2. The initial mass was chosen as a measure of the surface area because the number of unit cells was not expected to change during heating.

The method for calculating the number of unit cells at the surface is shown for $La_{0.4}Sr_{0.6}CoO_3$ using equations 31, 32 and 33. The assumption that the particles are spherical is made.

$$r_{particle} = \frac{3}{s.s.a.\ \rho}$$

$r_{particle}$ = radius of a particle 31

s.s.a. $La_{0.4}Sr_{0.6}CoO_3$ = 11.23 m^2g^{-1}

$$r_{particle} = \frac{3}{11.23 \times 4.03 \times 10^6}$$

$$= 6.63 \times 10^{-8}m$$

$A_{particle} = 4\pi r^2$ 32

$A_{particle}$ = area of a particle

$A_{particle} = 4\pi(6.63 \times 10^{-8})^2$

$= 5.52 \times 10^{-14}m^2$

Area of 1 g (s.s.a.) = 11.23 m^2g^{-1}

$\therefore$ Area of 0.1023 g = 1.15 m^2g^{-1}

Area of unit cell = $(3.81 \times 10^{-10})^2$ = $1.45 \times 10^{-19}m^2$

$(3.81 \times 10^{-10}$ = length of 1 side of unit cell (84))

No. unit cells at surface = $\frac{\text{Total area}}{\text{Area unit cell}}$ 33

$$= \frac{1.15}{1.45 \times 10^{-19}}$$

$$= 7.93 \times 10^{18}$$

Table 4.1 shows that there are more SO_2 molecules adsorbed than there are unit cells at the surface. In fact there are 4, 12.5, 10 and 10 times as many SO_2 molecules adsorbed as surface unit cells for $La_{0.3}Sr_{0.7}CoO_3$, $La_{0.4}Sr_{0.6}CoO_3$, $La_{0.5}Sr_{0.5}CoO_3$ and $La_{0.7}Sr_{0.3}CoO_3$, respectively.

Table 4.1

The number of unit cells at the surface of $La_{1-x}Sr_xCoO_3$ and the number of SO_2 molecules which would give a mass increase equivalent to that observed on exposure to SO_2

$La_{1-x}Sr_xCoO_3$	Initial mass/g	Surface area/m^2	No. unit cells at the surface	No. SO_2 molecules adsorbed	No. unit cell / No. SO_2 molecules
$La_{0.3}Sr_{0.7}CoO_3$	0.0935	1.59	1.10×10^{19}	4.39×10^{19}	0.25
$La_{0.4}Sr_{0.6}CoO_3$	0.1023	1.15	7.93×10^{18}	9.40×10^{19}	0.08
$La_{0.5}Sr_{0.5}CoO_3$	0.0902	1.45	1×10^{19}	9.92×10^{19}	0.10
$La_{0.7}Sr_{0.3}CoO_3$	0.1615	4.18	2.88×10^{19}	2.89×10^{20}	0.10

Area of a unit cell, exposed at the surface, if flat (length of one side = 3.81 Å (84)) = $1.45 \times 10^{-19} m^2$

Even considering inherent errors in this calculation, this appears to indicate that a reaction beyond the surface has occurred.

Table 3.14 shows that all of the mass lost during heating of $La_{0.3}Sr_{0.7}CoO_3$ was not replaced on exposure to SO_2.

The mass increase on exposure of both $La_{0.4}Sr_{0.6}CoO_3$ and $La_{0.5}Sr_{0.5}CoO_3$ to SO_2 was virtually double the mass loss due to heating under vacuum. Knowing that the atomic mass of S is double that of O, then without further consideration two possible explanations of the doubling of the mass changes may be made. The first explanation

is that every oxygen atom desorbed is replaced by a sulphur atom. The second explanation is that for every two oxygen atoms desorbed there is one SO_2 molecule adsorbed. If the former explanation was correct then the presence of sulphide may be evident from XRD and, or ESCA. If the latter explanation was true then either of these techniques may be expected to show the presence of sulphate.

The increase in mass observed for the $La_{0.7}Sr_{0.3}CoO_3$ after exposure to SO_2 is far in excess of the mass loss. Bearing in mind the explanations postulated above for $La_{0.4}Sr_{0.6}CoO_3$ and $La_{0.5}Sr_{0.5}CoO_3$ mass changes a similar explanation may be offered in this instance except that the reactivity of the $La_{0.7}Sr_{0.3}CoO_3$ with SO_2 must be greater than that of the other $La_{1-x}Sr_xCoO_3$ compounds

A theoretical calculation to work out the change in mass expected, if all of the lattice oxygen in $La_{0.7}Sr_{0.3}CoO_3$ was replaced by sulphur, was made.

The molecular mass of $La_{0.7}Sr_{0.3}CoO_3$ is 230.41 a.m.u., according to calculations made from the Co^{IV} graph by Jonker and van Santen (18), there are no oxygen vacancies in $La_{0.7}Sr_{0.3}CoO_3$. The percentage mass which is oxygen is 20.83%. If all of the oxygen is replaced by sulphur the molecular mass would be 278.71 a.m.u. The increase in mass due to the substitution would be 20.96% of the molecular mass of $La_{0.7}Sr_{0.3}CoO_3$. If there is replacement of oxygen by sulphur in the $La_{0.7}Sr_{0.3}CoO_3$ sample, then it appears to be almost complete, because the mass increase is 19.21%.

On the other hand, there may be formation of sulphates. The mass increase is not large enough to suggest that the perovskite-type oxide reacted completely to give a sulphate or the individual

sulphates of La, Sr and Co. Discounting any change in the oxidation state of Co, a hypothetical change to $La_{0.7}Sr_{0.3}Co(SO_4)_3$ which is equivalent in mass terms to the formation of the sulphates, would produce a mass increase of 104.16%. If, for example, the Sr was leached from the perovskite-type lattice as $SrSO_4$, a mass increase of 11.46% may be expected if the remaining oxygen maintained a neutral complex of the La and Co. If formation of sulphate did occur then this sort of mechanism seems most probable. The increase in mass, for $La_{0.7}Sr_{0.3}CoO_3$, from the initial mass, as opposed to that after evacuation and heating, was 17.89%. It seems that if there is sulphate formation, that it is a sulphate of La, Sr or Co or a combination of these. Leaching of all of the La, trivalent Co or tetravalent Co would give a higher percentage mass increase than Sr. It would be expected that if complete reaction of Sr occurred that the mass changes for $La_{1-x}Sr_xCoO_3$, where x = 0.5, 0.6 and 0.7, would be higher than for $La_{0.7}Sr_{0.3}CoO_3$. They were considerably less.

The possibility of the formation of perovskite sulphides, as opposed to perovskite oxides was considered. There was no literature evidence found which suggested that sulphidation of an oxide perovskite produced a sulphide perovskite. The sulphide perovskites were formed by heating mixtures of sulphides for several weeks (89), reaction of CS_2 with oxides (90) and by growing single crystals by a flux method (91). Takahashi et al (92) have published XRD data for $LaCoS_3$. The major peaks which this gives are not present in the correct size ratios on the diffraction patterns of any of the used catalysts in this work.

Whatever the explanation for the increases in mass on adsorption of SO_2 is, it appears, in the absence of other evidence, that there is a reaction of SO_2 with the bulk of the $La_{1-x}Sr_xCoO_3$ and that its extent is proportional to the La content of the catalyst.

XRD studies of the $La_{1-x}Sr_xCoO_3$ samples after SO_2 adsorption provided further evidence for the explanation of the mass changes observed.

The XRD patterns for $La_{0.3}Sr_{0.7}CoO_3$ and $La_{0.5}Sr_{0.5}CoO_3$ showed good evidence for $SrSO_4$. The $La_{0.7}Sr_{0.3}CoO_3$ sample had evidence for sulphides of Sr and Co and La_2O_2S. Ln_2O_2S is known for the lanthanide metals; it is closely related to Ln_2O_3(93). This sample had been exposed to SO_2 and CO simultaneously, after the SO_2 adsorption experiments and before the XRD measurements were made. It is therefore not clear if there was sulphate formation, for which there is now no evidence because of a further reaction due to the SO_2 and CO exposure. The $La_{0.3}Sr_{0.7}CoO_3$ sample was also exposed to SO_2 and CO after the SO_2 adsorption experiments but this did not lead to the formation of sulphides and La_2O_2S. The peak near $2\theta = 28^o$ which was strong in the $La_{0.7}Sr_{0.3}CoO_3$ signal and medium or strong in the SO_2 and CO adsorption experiments but which was weak or very weak in the SO_2 only adsorptions was present and was of medium intensity. This may indicate the presence of one of the compounds including some of La, Sr, Co, O and S mentioned in section 3.5.1.3. Further evidence for changes to the $La_{0.3}Sr_{0.7}CoO_3$ is the weakness of the perovskite signal which suggests that some of the $La_{0.3}Sr_{0.7}CoO_3$ structure has been destroyed during the vacuum line experiments.

The lack of evidence for sulphate on the $La_{0.4}Sr_{0.6}CoO_3$ is surprising. The specific surface area of the $La_{0.4}Sr_{0.6}CoO_3$ was slightly lower than the other samples but not significantly so. The reaction did appear to penetrate the surface of the compound but the bulk may have been insufficiently changed for the XRD measurements to detect sulphate. An ESCA analysis of the surface would have provided a useful clue about any permanent changes to the $La_{0.4}Sr_{0.6}CoO_3$ which encountered the SO_2.

It seems from the mass and XRD results that SO_2 reacts with $La_{1-x}Sr_xCoO_3$ and that $SrSO_4$ is formed in sufficient amounts for detection by XRD but not so much that the perovskite structure of the $La_{1-x}Sr_xCoO_3$ was destroyed. Even exposure to SO_2 after the CO experiment with $La_{0.5}Sr_{0.5}CoO_3$ produced $SrSO_4$ and retained the perovskite structure.

Raccah and Goodenough (94) suggest that the Co^{IV} sites formed because of the presence of Sr^{2+} ions in $La_{1-x}Sr_xCoO_3$, remain adjacent to those Sr^{2+} ions. It may be that this arrangement makes the Sr^{2+} particularly reactive, with respect to the other cations, so $SrSO_4$ is produced.

To ascertain which of the sulphates of either La, Sr or Co would be most easily formed in terms of their thermodynamic properties, the free energies of formation of those with sufficient available data were calculated from their oxides, using equation 34.

$$\Delta G_f^{\ominus} \text{ products} - \Delta G_f^{\ominus} \text{ reactants} = \Delta G_f^{\ominus} \text{ reaction} \qquad 34$$

The oxides were used to represent $La_{1-x}Sr_xCoO_3$ and the data available was sparse and is shown in Table 4.2.

Table 4.2

Free energies of formation of some strontium, cobalt and sulphur compounds

Compound	$\Delta G_f^{\ominus}$/kJ mol^{-1}
SrO	-562.3
$SrSO_4$	-1341.0
CoO	-214.2
Co_3O_4	-795.0
$CoSO_4$	-782.4
SO_2	-300.4
*O_2	0.0

* The source of oxygen is assumed to be elemental, but it is probably lattice oxygen in the perovskite-type structure.

$$SrSO_4 + SO_2 + \tfrac{1}{2}O_2 \longrightarrow SrSO_4$$

$\Delta G_f^{\ominus}$ reaction = -1341.0 - (-562.3 + -300.4) = 1478.3

$$CoO + SO_2 + \tfrac{1}{2}O_2 \longrightarrow CoSO_4$$

$\Delta G_f^{\ominus}$ reaction = -782.4 - (-214.2 + -300.4) = -267.6

$$\tfrac{1}{3}\,Co_3O_4 + SO_2 + \tfrac{1}{3}\,O_2 \longrightarrow CoSO_4$$

$\Delta G_f^{\ominus}$ reaction = -2347.2 - (-795.0 + -901.2) = -217.0

In the above theoretical calculations the free energy of formation per mole of sulphate formed from SrO, CoO and Co_3O_4 is -478.3, -267.6 and 217.0 kJ, respectively. This suggests that in thermodynamic terms $SrSO_4$ is the most likely sulphate species to be formed. This is of course assuming that the reactivity of the Sr, Co and O in the oxides have the same relative values of those in the perovskite. This may not be the case particularly if Sr^{2+} has the reactivity in $La_{1-x}Sr_xCoO_3$ suggested by Raccah and Goodenough (94).

4.3.3 Adsorption of CO on $La_{1-x}Sr_xCoO_3$

The graph of total mass change due to adsorption of CO after exposure at 500°C in Fig. 3.19 shows that at low La content in $La_{1-x}Sr_xCoO_3$ there is an increase in mass on exposure to CO but where there is a high La content there is evidence of mass loss. The extent of the loss was not measured because it caused the microbalance reading to go off scale.

Unlike the SO_2 adsorption experiments the mass changes across the $La_{1-x}Sr_xCoO_3$ series do not appear to vary linearly with the La content. It appears that the mechanism is not the same across the range.

To ascertain what the mass changes were dependent on, their relationships with various properties of the catalysts were investigated.

The specific surface areas of the $La_{1-x}Sr_xCoO_3$ samples are shown in Table 3.2. They do not appear to have a direct relationship with the mass changes observed.

The conductivities of the $La_{1-x}Sr_xCoO_3$ samples are shown in Table 3.6. They do not appear to be the factors governing the mass changes. In fact the conductivities of each of the $La_{1-x}Sr_xCoO_3$ samples, except $La_{0.3}Sr_{0.7}CoO_3$ were greatly reduced after the CO experiments. XRD showed that the perovskite-type structure still remained but the removal of oxygen by the reaction of CO with the catalyst appears to have been sufficient to reduce the conductivity. Arakawa et al (95) investigated the use of $LaCoO_3$ as a gas sensor for CO, among other gases. They measured the conductivity of $LaCoO_3$ in the presence of CO between 25°C and 500°C. The conductivity decreased in the presence of CO. XRD measurements before and after exposure showed the perovskite-type structure remained intact. They described the reaction as that shown in equation 35.

$$CO_{(g)} + O^{2-}{}_{(s)} \longrightarrow CO_2 + 2e^- \qquad 35$$

(s) = surface

Viswanathan and George (27) also reported a decrease in conductivity of $LaCoO_3$ in the presence of CO.

In this work the conductivity measurements were all made in air but recovery may not have been complete. In this work the mass loss by $La_{0.3}Sr_{0.7}CoO_3$ was regained so permanent reduction may not have taken place and the conductivity was retained.

The graphs shown in Fig. 1.2 in section 1.3.1.1 indicate that the percentage of Co^{IV} is not a controlling factor but the presence of oxygen vacancies may influence the interaction between CO and $La_{1-x}Sr_xCoO_3$. Voorhoeve et al (11) emphasize the importance of oxygen vacancies with respect to catalytic activity. If the oxygen vacancies, represented by δ in Fig. 1.2 are examined in conjunction with the CO adsorption results a theory may be postulated.

The $La_{0.3}Sr_{0.7}CoO_3$ sample has the greatest number of oxygen vacancies of the four $La_{1-x}Sr_xCoO_3$ compounds investigated. CO adsorption was carried out after evacuation and heating so adsorbed oxygen evolved by this treatment will have been desorbed. The reducibility of compounds with low La content and high value of x (that is, Sr content), appears to be highest, as found in this work by oxygen desorption and quoted in the literature (17, 22, 24, 25). It therefore seems that perhaps the CO adsorbed at 500°C may have filled some of the oxygen vacancies and stabilized the lattice in this way. Chemisorption of CO may therefore be strong.

Tascon and Gonzalez-Tejuca (33) state that CO is adsorbed on oxygen sites yet in the present work adsorption of CO is greatest where according to Jonker and van Santen (18) the oxygen vacancy numbers would be expected to be greatest.

$La_{0.4}Sr_{0.6}CoO_3$ and $La_{0.5}Sr_{0.5}CoO_3$ have some oxygen vacancies and these like the $La_{0.3}Sr_{0.7}CoO_3$ may adsorb CO and not readily release further oxygen from the lattice for desorption of CO_2.

The loss of mass from $La_{0.7}Sr_{0.3}CoO_3$ on exposure to CO at 500^oC may be explained by the abundance of oxygen present in $La_{0.7}Sr_{0.3}CoO_3$. According to Fig. 1.2 $La_{0.7}Sr_{0.3}CoO_3$ has no oxygen vacancies. The discussion of oxygen loss from $La_{0.7}Sr_{0.3}CoO_3$ during evacuation and heating in section 4.3.1 suggested that its reducibility was low and therefore little oxygen was lost during heating. It may be that heating alone is insufficient to remove much oxygen but if the activation energy is available for the reaction of CO with lattice oxygen and its subsequent desorption,then this may occur. Viswanathan and George (27) state that the ease of oxidation of CO is related to the ease of removal of oxygen, whether it is adsorbed or lattice oxygen.

A further indication that CO may replace oxygen lost from $La_{1-x}Sr_xCoO_3$ during heating under vacuum may be found by looking at Figs. 3.15, 3.16, 3.17 and 3.18, with reference to Tables3.15, 3.16, 3.17 and 3.18 respectively. Fig. 3.15 in particular shows how either exposure to oxygen, by allowing the sample up to atmospheric pressure, or exposure to CO led to the recovery of the mass lost by heating in a vacuum. According to mass evidence $La_{0.3}Sr_{0.7}CoO_3$ is not permanently changed by CO adsorption. Lattice oxygen may be removed both by heating in a vacuum or by desorption of CO as CO_2. It seems that this oxygen is replaced by either allowing air or pure oxygen into the system.

Yamazoe (17) noted that heating of $La_{1-x}Sr_xCoO_3$ with pre-adsorbed oxygen gave an increase of desorption as x increased. This suggests that adsorption of oxygen increased with x, as adsorption of CO did in

the present work, possibly because of the increase in oxygen vacancies.

Voorhoeve et al (96) state that pre-reduction of perovskite-type oxides leads to better binding of CO. Oxygen vacancies may not necessarily represent reduction of a surface but they may indicate a lower oxidation state so this observation is in agreement with those of CO adsorption in this work.

The postulation made above, about CO replacing lattice oxygen must be reconciled with the reducibility across the range of $La_{1-x}Sr_xCoO_3$ compounds discussed in section 4.3.1. It seems that the reactivity of $La_{1-x}Sr_xCoO_3$ with CO may have a conflicting trend to the reducibility in terms of removal of oxygen by evacuation and heating, even though CO adsorbing on $La_{1-x}Sr_xCoO_3$ and desorbing as CO_2 is reduction. It must be borne in mind that the reduction discussed in section 4.3.1 has already taken place before CO adsorption and it is possible that it was limited by charge compensation, probably by Co, which may also limit the CO_2 desorption.

The work of Sieyama et al (22) is cited in section 1.3.1.1. The reactivity of oxygen in $La_{1-x}Sr_xCoO_3$ was studied and the total reactivity of oxygen was defined as the product of the specific reactivity and the amount of oxygen desorbed, which is not thought to be lattice oxygen. It was found that the total reactivity peaked between $x = 0.2$ and $x = 0.4$, that is, at $La_{0.7}Sr_{0.3}CoO_3$. This agrees with the observations of CO adsorption on $La_{1-x}Sr_xCoO_3$ reported in this thesis.

Nakamura et al (24) looked at oxidation of CO over $La_{1-x}Sr_xCoO_3$ in the presence of O_2 as opposed to scavenging of oxygen from the lattice. They found that the rate of oxidation increased to x = 0.2 and was very slow for x values greater than x = 0.4. Pre-oxidation of the surface aided the oxidation of CO. Pre-oxidation was also noted as an aid to the catalytic oxidation of CO by $La_{1-x}Sr_xCoO_3$ by George and Viswanthan (23).

It appears, therefore, and unsurprisingly that availability of oxygen associated with the $La_{1-x}Sr_xCoO_3$ is the over-riding factor for oxidation of CO in the presence of $La_{1-x}Sr_xCoO_3$. It seems that $La_{0.7}Sr_{0.3}CoO_3$ may be one of the best catalysts in the series for this reaction, at atmospheric pressure it has no oxygen vacancies and evacuation and heating do not lead to loss of much oxygen so it seems that $La_{0.7}Sr_{0.3}CoO_3$ is the best source of oxygen for the oxidation of CO. Indeed it would be of interest to measure the mass changes on exposure of $La_{1-x}Sr_xCoO_3$ to CO, when no pre-evacuation and consequent removal of oxygen, had taken place. It would be interesting to compare such an experiment with the loss of oxygen due to evacuation and heating and the further change caused by exposure to CO.

The overall mass changes which occurred on exposure to CO at 500^oC were not the only results of interest from the CO adsorption experiments. Some of the details of the experiments gave more information about $La_{1-x}Sr_xCoO_3$.

It seems that the mass losses due to TPD of CO_2 were recovered by exposure to oxygen. It is of interest to note that for

$La_{0.4}Sr_{0.6}CoO_3$ exposure to oxygen at room temperature was sufficient to give a mass increase. Exposure to oxygen of $La_{0.5}Sr_{0.5}CoO_3$ did not give a mass increase. Exposure of $La_{0.7}Sr_{0.3}CoO_3$ at 500°C did, however, lead to an increase in mass. From these observations it may be deduced that re-oxidation of $La_{1-x}Sr_xCoO_3$ decreases as La content increases. A higher temperature was required at lower x values. This disagrees with the observation of Nakamura et al (24) that re-oxidation decreased with increase of x.

Of interest too, is the observation that after exposure to CO of $La_{0.7}Sr_{0.3}CoO_3$ at 500°C and the consequent loss of mass, TPD after evacuation yielded CO_2. It may be the case that there are at least two CO_2 adsorption species. These forms of CO_2 may be distinguished by their desorption energies. The data from TPD of CO_2 from the $La_{1-x}Sr_xCoO_3$ samples was too complex for MASS1, the computer program, to calculate energies of desorption. An example of the MS output from CO_2 desorption after CO adsorption is shown in Fig. 3.8a. It is likely that there are several sites for CO adsorption. Tascon and Gonzalez-Tejuca (33) after adsorption of CO on $LaCoO_3$ observed two adsorbed species. It seems possible that the mass loss due to exposure of $La_{0.7}Sr_{0.3}CoO_3$ to CO may be due to CO_2 being formed on a site with a low energy of desorption. The CO_2 observed after TPD may be from a site where it has a higher energy of desorption. Tascon and Gonzalez-Tejuca followed the adsorption of the CO species and noted that when adsorption at the higher temperature took place the coverage exceeded a monolayer. The increased desorption energies may then be partly due to diffusion of CO_2 through the lattice.

The temperature at which Tascon and Gonzalez-Tejuca noted that CO adsorption led to greater than monolayeral coverage is 375^{o}C. This falls between 300^{o}C and 500^{o}C, the temperatures between which the mass changes due to exposure to CO changed most dramatically in the present work.

It seems probable that during exposure to CO at 500^{o}C that mass loss did not only occur for the $La_{0.7}Sr_{0.3}CoO_3$ sample but that this mechanism operated on the other samples too, just as the adsorption was shown by TPD to have occurred on the $La_{0.7}Sr_{0.3}CoO_3$. It seems likely that just as the overall loss of mass from $La_{0.7}Sr_{0.3}CoO_3$ conceals the CO adsorption the overall increase in mass may conceal a mass loss which could also be taking place.

Hayward and Trapnell (97) state that some oxides adsorb CO reversibly and others adsorb it irreversibly. $La_{1-x}Sr_xCoO_3$ appears to belong to the latter group, however, the evidence for more than one type of adsorption site does leave the doubt that reversible adsorption may be occurring, undetected because of the inability to distinguish between CO and N_2 with the MS.

The calculated percentage reduction expressed in terms of oxygen associated with CO to give CO_2, is shown for each of the $La_{1-x}Sr_xCoO_3$ samples, in Table 4.3. The amount of oxygen removed due to reaction with CO is calculated by working out the mass of oxygen required to oxidize all of the adsorbed CO to CO_2, if the mass increase is attributed to CO adsorption. The mass of oxygen obtained by this calculation is then expressed as a percentage of the mass before adsorption. This number is then termed the percentage reduction.

Table 4.3

The calculated percentage reduction of $La_{1-x}Sr_xCoO_3$ by CO exposure at 500°C

$La_{1-x}Sr_xCoO_3$	% mass change	actual mass change/g	calculated % reduction
$La_{0.3}Sr_{0.7}CoO_3$	+7.92	5.92×10^{-3}	4.53
$La_{0.4}Sr_{0.6}CoO_3$	+0.88	8.1×10^{-4}	0.50
$La_{0.5}Sr_{0.5}CoO_3$	+1.45	2.21×10^{-3}	0.82
$La_{0.7}Sr_{0.3}CoO_3$	-4.09	4.23×10^{-3}	4.09

According to Table 4.3 the reducibility of $La_{1-x}Sr_xCoO_3$ is greatest at high and low values of x and is lowest at x = 0.5 and x = 0.6. It seems unlikely that the 'calculated % reduction' represents the full extent of reduction by CO.

At 500°C the reaction between CO and $La_{1-x}Sr_xCoO_3$ indicates that the reactivity of oxygen in $La_{1-x}Sr_xCoO_3$, for reaction with CO, increases with increasing La content.

Apart from the reactivity of oxygen with respect to CO, it is interesting to note that lanthanide compounds with CO tend to be unstable (98) so an increase in La content might be less likely to adsorb CO.

The XRD patterns of the $La_{1-x}Sr_xCoO_3$ samples exposed to CO appear to indicate no permanent change in the bulk perovskite-type structure, in spite of the suggestion by Hayward and Trapnell (97) that the oxidation of CO is most reasonably accomplished by decomposition of the surface. There appears to be sufficient oxygen

available to deem decomposition unnecessary. Creighton and White (99) suggest that all chemisorbed CO will be oxidized to CO_2 if there is excess oxygen available. It appears that any oxygen lost during CO_2 production is replaced on exposure to atmospheric oxygen. This agreed with the observation of Nakamura et al (30), that the perovskite structure is restored by re-oxidation. Arakawa et al (100) studied the reduction of $LaCoO_3$ by H_2 and found that the perovskite-type structure was maintained under these conditions. The crystal structure changed from rhombohedral to cubic. This agrees with the observations by Askham et al (16) that increasing the Sr content and hence introducing oxygen vacancies led to the structure changing from a rhombohedral to a cubic perovskite-type structure.

One of the $La_{1-x}Sr_xCoO_3$ samples, that is, $La_{0.5}Sr_{0.5}CoO_3$ had been exposed to SO_2 after the CO adsorption experiment, it showed XRD evidence of $SrSO_4$ in the bulk.

4.3.4 Simultaneous adsorption of SO_2 and CO on $La_{1-x}Sr_xCoO_3$

The percentage mass changes due to simultaneous adsorption of SO_2 and CO at 600°C and the sums of individual mass changes due to exposure of SO_2 and CO separately at 500°C, are shown in Fig. 3.24. It can immediately be seen that the sums of the individual mass increases follow the trend of the mass changes due to simultaneous adsorption. The sums of the individual mass changes are lower than the mass change due to exposure to the two gases together.

On first consideration, it would appear that the trend in mass changes can be explained similarly to those for individual SO_2 and CO exposure. At low La proportions, that is, $La_{0.3}Sr_{0.7}CoO_3$, adsorption of CO at 500°C produces the highest mass increase in the series. At high La proportions, that is, $La_{0.7}Sr_{0.3}CoO_3$, adsorption of SO_2 produces the highest mass increase in the series. This would appear to explain the trough in the mass changes at $La_{0.4}Sr_{0.6}CoO_3$ and $La_{0.5}Sr_{0.5}CoO_3$.

The mechanisms working on the individual adsorption experiments may indeed be operating during the simultaneous adsorption experiments, but it appears from the increased mass changes, the observation of elemental sulphur production, the COS production after CO exposure and the XRD patterns that there are other processes occurring.

First of all, the mass increases are greater than the sums of the mass changes after exposure to the same pressures of SO_2 and CO individually. The temperature of adsorption of the simultaneously adsorbed gases is admittedly 100°C higher than that where individual adsorption was attempted. The fact that the two gases are there together and are known to react, in the presence of $La_{0.5}Sr_{0.5}CoO_3$, to produce sulphur and CO_2 and to cause sulphidation of the catalyst (12), leads to the notion that the effect of SO_2 and CO together is not additive but synergistic. It appears that the reaction between SO_2 and CO producing sulphur and CO_2 may have taken place.

Evidence for the above supposition is available with the presence of elemental sulphur being clearly visible after adsorption of SO_2 with CO.

Hibbert and Tseung (12) attributed the ability of CO to react with sulphur in the used $La_{0.5}Sr_{0.5}CoO_3$ catalyst to the presence of sulphides which were formed during the reaction between the SO_2 and CO. Passing CO over the $La_{1-x}Sr_xCoO_3$ samples after adsorption of SO_2 and CO in this work also produced COS. The catalysts exposed to only SO_2 did not yield COS on exposure to CO afterwards so this too suggests that the effects of the two gases was not simply additive.

The evidence of COS production suggesting that the catalyst is different after adsorption of SO_2 from after adsorption of SO_2 and CO is strongly enforced by comparing the XRD patterns of the two sets of catalysts. The catalysts exposed to SO_2 in the absence of CO show evidence of sulphate formation, in fact, the presence of $SrSO_4$ is evident. Those catalysts exposed to SO_2 and CO together show evidence of sulphidation. Several sulphides of Co have been recognized plus SrS and $LaS_{1.75-1.80}$. There are also XRD peaks which have not been assigned. At this stage it could not be concluded whether the sulphur in the COS was from elemental sulphur which may have been retained in the catalyst sample or from one of the sulphide or unassigned species.

The $La_{0.4}Sr_{0.6}CoO_3$ sample which had been exposed to SO_2 and CO in the vacuum line was examined by ESCA. This surface analysis showed the presence of sulphide, sulphate and a third sulphur peak which may have been sulphite but which was not elemental sulphur. This appears to eliminate elemental sulphur as a sulphur species likely to contribute sulphur for COS production because it simply is not there. It may be argued that although the sulphur is produced at the catalyst surface and then removed because of the

high temperatures which exceed the boiling point of sulphur, it may also be removed by CO at the surface and COS may then be produced. The argument against elemental sulphur as a source of sulphur for COS may then be reinforced by looking at the vacuum line experiments. The COS production by exposure to CO, only occurred when there was no in situ production of elemental sulphur. Any which had been previously formed would have already been removed due to the temperature.

The presence of sulphate on the $La_{0.4}Sr_{0.6}CoO_3$ surface suggests that the mechanism which produced $SrSO_4$ on the catalysts exposed to SO_2 only is still operating in the presence of CO. Two possibilities which exist are that sulphate is formed and the CO then scavenges the oxygen from the sulphate to produce CO_2 and elemental sulphur or the alternative reaction between SO_2 and CO is happening in opposition to the reaction which produces sulphate and so this is only produced in small amounts. These possibilities are discussed in section 4.4.1.

4.3.5 COS production by scavening of sulphur by CO

The source of sulphur for the production of COS has already been discussed in section 4.3.4. No conclusion was drawn about what sulphur compound provided the sulphur for COS production but it seems unlikely that it was either elemental sulphur because according to ESCA results it does not appear to be present on the catalyst surfaces of those samples from which COS has been produced, or sulphate because when it is the only sulphur species present there is no COS production.

The only other type of sulphur which has been positively identified in the bulk and on the surface was sulphide and it seems likely that this provided the sulphur for COS production.

Although there was no production of COS, exposure to COafter SO_2 led to mass changes which followed a trend similar to that when $La_{1-x}Sr_xCoO_3$ samples were exposed to CO only. When CO was allowed into the system after exposure of $La_{0.3}Sr_{0.7}CoO_3$ to SO_2 at 500°C and heated to 650°C there was a small increase in mass and this was followed by a similar decrease on re-evacuation. These mass changes can be seen at points 74 and 75 of Fig. 3.10. On the other hand exposure of $La_{0.7}Sr_{0.3}CoO_3$ to CO after SO_2 adsorption led to a very significant mass loss. This can be seen at point 65 in Fig. 3.11. As no COS was produced and there was no XRD evidence for the removal of oxygen from $SrSO_4$ to give sulphites or sulphides, both of these mass changes may be attributed to reduction of the catalyst itself, in the manner suggested for the CO experiments discussed in section 4.3.3.

Two starting temperatures for scavenging of sulphur by CO were used, that is, room temperature and 600°C, the temperature of SO_2 and CO adsorption. The CO was allowed into the system after evacuation and the catalyst was then heated to 650°C, from either room temperature or 600°C.

There consistently appeared to be a greater loss of mass from the samples cooled to room temperature then exposed to CO and heated in CO to 650°C than those heated from 600°C to 650°C in CO. This could not be explained by the fact that it took longer to heat the catalysts from room temperature than from 600°C. Each sample was left at 650°C

until the mass reached an equilibrium value. It seems therefore that the mass loss was dependent on the presence of CO at a particular temperature or range of temperatures. The temperatures at which COS was first detected by the MS was noted. These temperatures are given in Table 4.4.

Table 4.4

Temperatures of formation of COS during scavenging of [S] by CO from $La_{1-x}Sr_xCoO_3$ exposed to SO_2 and CO simultaneously

$La_{1-x}Sr_xCoO_3$	Temperature of first COS detection/^oC
$La_{0.3}Sr_{0.7}CoO_3$	612
$La_{0.4}Sr_{0.6}CoO_3$	350
$La_{0.5}Sr_{0.5}CoO_3$	275
$La_{0.7}Sr_{0.3}CoO_3$	*286/350

*MS flickered from 286^oC (10^{-10} mbar scale)

With the exception of $La_{0.3}Sr_{0.7}CoO_3$ COS production started before the temperature reached 600^oC, the starting temperature of the other scavenging reaction.

At the higher temperatures there may be a conflict between CO adsorption on the catalyst surface and CO reaction and subsequent desorption as COS from the surface. Although the XRD results indicate that the bulk of the $La_{1-x}Sr_xCoO_3$ had altered significantly, CO

adsorption may yet be highest on the still so called '$La_{0.3}Sr_{0.7}CoO_3$' sample, as it was for adsorption at 500°C as reported in section 3.3.4.5. If the hypothesis that the COS was formed by reaction of CO with sulphides of Co, Sr or La is correct, it seems unlikely that there should be any difference between the temperature of first detecting COS particularly when there is an excess of CO present for adsorption. There is no evidence from the XRD results to suggest that a sulphide present in all of the other $La_{1-x}Sr_xCoO_3$ samples examined was absent from the $La_{0.3}Sr_{0.7}CoO_3$ sample or vice versa. The size of the $La_{0.3}Sr_{0.7}CoO_3$ sample may offer the true explanation of why COS was not detected until the temperature had reached 612°C. The initial mass of $La_{0.3}Sr_{0.7}CoO_3$ was 0.0378 g, that is, 34.6%, 29.2% and 42.5% of the initial masses of $La_{0.4}Sr_{0.6}CoO_3$, $La_{0.5}Sr_{0.5}CoO_3$ and $La_{0.7}Sr_{0.3}CoO_3$ respectively. The initial amount of COS produced may have been insufficient for detection until there had been a build up in the system even though the percentage mass increase on SO_2 and CO exposure was highest. Such a lag in detection time would be surprising as it was noted that during TPD, when the vacuum line was being pumped, detection of SO_2 or CO_2 was simultaneous with mass loss due to their desorption. The sensitivity of the MS was good.

Apart from the detection of COS at 612°C from the $La_{0.3}Sr_{0.7}CoO_3$ sample the others produced COS between 275°C and 350°C. It appears that this temperature range is sufficient to provide the activation energy required for the reaction between CO and whichever of the sulphides that may be involved in the reaction to produce COS. A recent edition of the Chemical Rubber Company data book (86) did not contain much thermodynamic data for the sulphides of La, Sr and Co.

Those represented had at least good thermal stability. The melting points quoted were in excess of 1000°C for CoS and in excess of 2000°C for La_2S_3 and SrS. Speculation about which of the sulphides, if there is just one, provides the sulphur for COS production can only be made on the evidence from XRD of which sulphides are present. This assumes that the sulphide in question has not been consumed during the COS production. The sulphides present in each of the catalysts exposed to SO_2 and CO in the vacuum line are SrS and Co_4S_3.

4.4 THE FLOW-RIG EXPERIMENTS

The flow-rig experiments represented the trial of the three $La_{1-x}Sr_xCoO_3$ samples studied as catalysts for the reduction of SO_2 by CO to provide elemental sulphur and CO_2, under various conditions. The characterization experiments and the adsorption and TPD experiments were all preliminary to the flow-rig experiments. The purpose of the preliminary work was to provide explanations for the flow-rig experiments. Tables 3.29 and 3.30 summarize the results.

4.4.1 The mechanism of the reaction between SO_2 and CO to give elemental sulphur and CO_2

For each of the catalysts studied, that is, $La_{0.3}Sr_{0.7}CoO_3$, $La_{0.5}Sr_{0.5}CoO_3$ and $La_{0.7}Sr_{0.3}CoO_3$ the overall effect of changing the percentage of CO relative to SO_2 was very similar and on the whole predictable. The stoichiometric ratio, that is, 1% SO_2 and 2% CO gavethe best removal of SO_2, but some COS was formed. Excess of CO, that is, 1% SO_2 and 4% CO tended to give complete removal of SO_2

and the formation of COS was observed. Deficiency of CO, that is, 1% SO_2 and 1% CO not surprisingly left unreacted SO_2 in the outlet gas.

There is little explanation required for the removal or not of SO_2, in terms of SO_2:CO ratio, the stoichiometric ratio is evidently the best, however, there is sufficient production of COS to eliminate the unscrupulous use of just any of the $La_{1-x}Sr_xCoO_3$ compounds to catalyse the reaction shown in equation 1 and reproduced below.

$$SO_2 + 2CO \rightleftharpoons 1/x\ S_x + 2CO_2 \qquad 1$$

On first observation of Table 3.29a and Table 3.29b it seems that CO has two possible reactions which it can take part in. The first of these reactions is the reduction of SO_2 giving the products elemental sulphur and CO_2, that is, the desired reaction. The second possibility appears to be the reaction of the CO with a sulphur compound present on or in the catalyst. The discussion in section 4.3.5 of sulphur species available for reaction with CO to produce COS may be applied to the $La_{1-x}Sr_xCoO_3$ samples used in the flow-rig too. The XRD and ESCA results are comparable in each case. This observation, in conjunction with the production of sulphur in the vacuum line supports the theory that the experiment with simultaneous adsorption of SO_2 and CO in the vacuum line is comparable to at least the initial stages of the flow-rig experiment. Watanabe (101) had found magnetic differences between samples in vacuum and oxygen conditions. These differences did not seem to affect the reaction.

Initially, it appears that the reaction of the CO with SO_2 is favoured and when the SO_2 is all removed, then the excess CO

scavenges sulphur to form COS. This idea is supported by the 1% SO_2 and 1% CO experiment with a total flow rate of 100 cm^3min^{-1}. Not all of the SO_2 is removed but there is no COS production. The two 1% SO_2 and 4% CO experiments also support this theory. All of the SO_2 is removed and there is also COS production. The stoichiometric mixture in the experiment with a total flow rate of 50 cm^3min^{-1} appears to give the final proof required to show that the reduction of SO_2 is favoured. Doubt is cast on the theory, however, by the stoichiometric mixtures with the total flow rate of 100 cm^3min^{-1}. In each part of this experiment except for $La_{0.7}Sr_{0.3}CoO_3$ at 500°C and 550°C there was COS production. Table 3.30 summarizes the results of this investigation.

An explanation of the different results obtained at the two flow rates must be attempted. The results must be explained in terms of the effect of the contact times on the ability of the two mechanisms to take place.

The mechanism of the SO_2 reduction and accompanying oxidation of CO has not yet been discussed. It has been shown by the adsorption and TPD experiments that SO_2 can be adsorbed on $La_{1-x}Sr_xCoO_3$ and hence be removed to some extent from a stream of SO_2 in the absence of CO. The products of elemental sulphur and of sulphides of La, Sr and Co expected in the presence of CO are, however, not formed. Another product found, which is also formed on the surface of $La_{1-x}Sr_xCoO_3$ after exposure to SO_2 and CO is sulphur in the form of sulphate. The adsorption and TPD experiments have indicated that the carbon product is CO_2 both in the presence and absence of SO_2. They have shown that CO exposure produces COS after exposure to SO_2 and CO.

The presence of sulphate on the surface of used catalysts, as shown by ESCA, but not in the bulk, as shown by XRD, suggests that the mechanism of SO_2 reaction with the surface to produce $SrSO_4$ is still occurring in the presence of CO. It is not, however, clear whether the formation of elemental sulphur is due to the reduction of sulphate by CO or if it is due to the reaction between CO and physisorbed or chemisorbed SO_2. The fact that the only sulphate characterized by XRD was $SrSO_4$ and that sulphides of La, Sr and Co are observed leads to the tentative suggestion that there is a reaction between CO and adsorbed SO_2, yet as it is known that SrS can be formed by reduction of $SrSO_4$ by H_2 (102), reduction by CO may also be considered as a possibility. Reduction of SO_2 may be simultaneous to or followed by the production of the sulphides observed and of elemental sulphur. The reaction with adsorbed SO_2 suggests that the reduction of SO_2 is suprafacial unlike the intrafacial reduction of NO by CO described by Voorhoeve et al (36). The CO_2 formation is probably then due to a combination of reduction of $La_{1-x}Sr_xCoO_3$ and of adsorbed SO_2. The oxygen provided by the re-oxidation of $La_{1-x}Sr_xCoO_3$ for the redox reaction postulated by Nakamura et al (24) is provided here by SO_2.

The above explanation does not, however, explain the absence of sulphate from the bulk of the used catalysts and the $La_{1-x}Sr_xCoO_3$ samples exposed to SO_2 and CO simultaneously. A possible explanation of this may be a difference in the sensitivities of XRD and ESCA. If there is conflict between the formation of sulphate and sulphide there may be insufficient sulphate formed for detection by XRD.

Even the ESCA analyses showed that the abundance of sulphide was significantly greater than that of sulphate.

It, therefore, appears that there are at least three reactions in which CO may be involved. These include reduction of $La_{1-x}Sr_xCoO_3$ to produce CO_2, reduction of SO_2 to produce CO_2 and reaction with a metal sulphide to produce COS. From the flow-rig experiments it is not clear whether reduction of $SrSO_4$ is taking place or if little $SrSO_4$ is being formed due to the SO_2/CO reaction predominating. Reference to the vacuum line experiments gives a solution which suggests that $SrSO_4$ is not reduced by CO. In section 4.3.5 it is stated that the sulphur products expected if reduction of $SrSO_4$ by CO took place are not detected. These products may include COS, $SrSO_3$, SrS or elemental sulphur. $SrSO_4$ is still detected by XRD after exposure to an excess of CO so it seems that none of the suggestedreduction reactions take place.

The XRD analyses of the used flow-rig catalysts indicate that the perovskite structure of the original compound no longer exists. The solid products of the reaction of $La_{1-x}Sr_xCoO_3$ are in the main sulphides. This is also true for the samples exposed to SO_2 and CO in the vacuum line for relatively short times. It seems that the $La_{1-x}Sr_xCoO_3$ compounds are rapidly sulphided.

The importance of the perovskite-type structure for catalytic activity must be examined. It is doubtful that the actual structure is vital in terms of, for example, atomic distances, for adsorption of reactant gases, if the sulphides formed do not curtail the catalytic reactivity. Madgavkar and Vogel (55) looked at the catalytic

combustion of HC and CO and they emphasize the use of the perovskite-type structure in their work.

Voorhoeve et al (103) say that the geometrical distortions of the basic perovskite cube and unimportant for the catalytic reduction of NO. Section 1.3.1.2 introduces catalytic properties of perovskite-type compounds. It seems also that the fresh $La_{1-x}Sr_xCoO_3$ compounds investigated in the present work which have the perovskite-type structure are catalytically active yet these properties are also evident in the sulphided catalysts.

There is no XRD evidence of oxide being present. This of course means that one of the CO_2 oxygen sources is unavailable relatively quickly. This may be a factor which would cause the COS production to increase, on the other hand the reduction of SO_2 might increase.

At the slower flow rate, that is 50 cm^3min^{-1}, the contact time between the SO_2 and CO, on the catalyst surface is evidently longest, consequently the CO is unavailable for COS production. Not all of the SO_2 is removed, however, and this may be because the surface is blocked by adsorbed SO_2.

At the lower contact time and higher flow rate the SO_2 is passing through the catalyst bed more quickly but this is not the only factor which needs to be taken into consideration. At the higher contact times the SO_2 adsorption sites may be saturated. At the lower contact time the adsorptivity of the catalyst must be taken into account. The graph of percentage mass increase due to exposure of SO_2 against La content of $La_{1-x}Sr_xCoO_3$ is shown in Fig. 3.14. It is clear that

the total amount of SO_2 adsorbed increases with La content. $La_{0.7}Sr_{0.3}CoO_3$ had the highest La content of $La_{1-x}Sr_xCoO_3$ compounds studied and it showed a very considerable increase in mass. The opposite trend appears to be true for CO adsorption on $La_{1-x}Sr_xCoO_3$ and this is shown in Fig. 3.19. Fig. 3.24 shows the mass changes when $La_{1-x}Sr_xCoO_3$ is exposed to both SO_2 and CO. Perhaps the catalyst which adsorbs much SO_2 and little CO is best. The CO can then react with the SO_2 saturated surface to produce sulphur and CO_2, but not with the sulphides or the perovskite surface. This may explain why there is COS production during the experiments where stoichiometric mixtures of SO_2 and CO are used, except when $La_{0.7}Sr_{0.3}CoO_3$ is used as a catalyst at 500°C and 550°C. On examination of the TPD data from $La_{0.7}Sr_{0.3}CoO_3$ after SO_2 adsorption the first adsorption yields three peaks, they are at 508-518°C, 569°C and 645°C, the second adsorption yields two peaks at 569 – 574°C and 649 – 654°C. This may even explain why there was COS production during the experiments at 600°C and 650°C. The SO_2 may have been less strongly held at these temperatures and the CO may then have reacted with the metal sulphides to produce COS instead of CO_2.

As with the experiments with the stoichiometric mixtures of SO_2 and CO where the contact time was long, the $La_{0.7}Sr_{0.3}CoO_3$ surface may have become saturated with SO_2, so some SO_2 was present in the outlet gases. This appeared to be the best compromise though, because COS is a more acute poison than SO_2, and an environmental application for removal of SO_2 gave the impetus for this work.

$La_{0.7}Sr_{0.3}CoO_3$ appears to be the best catalyst for the reduction of SO_2 by CO. It is interesting to note here that Iehisha et al (14) found that $La_{0.7}Sr_{0.3}CoO_3$ was the best of the $La_{1-x}Sr_xCoO_3$ series in the role of oxide cathode for a CO_2 laser. Its activity is attributed to its adsorption and desorption properties. Such properties are discussed in detail with reference to SO_2 and CO in this chapter.

Another explanation for the incomplete removal of SO_2 from the gas stream over $La_{0.7}Sr_{0.3}CoO_3$ may be the poor adsorptivity of $La_{0.7}Sr_{0.3}CoO_3$ for CO.

The results of the $La_{0.3}Sr_{0.7}CoO_3$ and $La_{0.5}Sr_{0.5}CoO_3$ experiments with respect to SO_2 and COS in their outlet gases may be explained in terms of their relative adsorptivities of SO_2, the contact time of SO_2 and CO with the catalyst, the reactivity of CO with SO_2 and the metal sulphides and the temperatures of the experiments.

It seems that the availability of SO_2 on the catalyst surface is vitally important. If the SO_2 is there in the abundance required for complete reaction with CO then it seems that this is the preferred reaction. None of the flow-rig experiments showed COS production in the absence of some removal of SO_2.

4.4.2 The role of the catalyst in the reduction of SO_2 by CO

The control experiment which was reported in section 3.4.5 showed that in the absence of $La_{1-x}Sr_xCoO_3$ no reaction took place between SO_2 and CO to produce elemental sulphur, CO_2 or COS, at the temperature reported.

The description of possible mechanisms discussed in section 4.4.1 indicate a clear role for a material which will adsorb SO_2 and CO sufficiently well to allow the desired reaction to take place. SO_2 appears to have two modes of action, these are reaction with the surface to form $SrSO_4$ or mere adsorption. CO appears to have three modes of action and these are reduction of the $La_{1-x}Sr_xCoO_3$, reduction of SO_2 or reaction with one or more metal sulphide, formed as a consequence of the SO_2 reduction, to form COS.

It seems that a material which will favour the reduction of SO_2 as desired will be a good adsorbent of SO_2 and because of the number of options open to CO, perhaps a poorer adsorbent of this gas. $La_{0.7}Sr_{0.3}CoO_3$ appears to satisfy both of these criteria.

SO_2 adsorption appears to vary linearly with increasing La in $La_{1-x}Sr_xCoO_3$. It is not clear what the specific property of this relationship between SO_2 adsorption and La content which is important.

The $La_{1-x}Sr_xCoO_3$ samples are all semiconductors and although their conductivity is not directly related to La content it may be an important quality in itself. SO_2 has lone pairs of electrons (98) and these may help to facilitate the adsorption of the gas on the $La_{1-x}Sr_xCoO_3$ samples, which are p type semiconductors. Greenwood and Earnshaw (104) and Durrant and Durrant (105) show the lone pairs on the sulphur and Greenwood and Earnshaw show various modes of adsorption of SO_2 through the S and O atoms. Cotton and Wilkinson (98) state that SO_2 forms many complexes with a number of transition metals. The Co in $La_{1-x}Sr_xCoO_3$ may be instrumental in the adsorption of SO_2.

This idea is supported by the presence of cobalt sulphides but is put in some doubt by the direct relationship between La content and SO_2 adsorption which does not exist with Co.

George and Viswanathan (106) state that the rare earth cations play an important role in the magnetic and electric, hence conductivity,properties in $LnCoO_3$ type oxides. It appears therefore that the role of La is important, if the conductivity plays a role in the catalytic activity of $La_{1-x}Sr_xCoO_3$.

The conductivities of the catalysts after the flow-rig experiments had changed remarkably little during their exposure to SO_2 and CO. The conducting properties of the sulphur compounds produced by reaction of SO_2 and CO with the $La_{1-x}Sr_xCoO_3$ catalysts were searched for. SrS is a semiconductor and LaS, which was the nearest compound to $LaS_{1.75-1.80}$ which could be found, is a metallic conductor (86). Values of conductivities for cobalt sulphides were not found.

The fact that the catalysts conduct may be crucial to their efficiency.

The fact that each of the used catalysts no longer has the perovskite-type structure but appears to consist of a mixture of sulphides, sulphates and other less clearly defined metal/oxygen/sulphur species which possibly include sulphite, leads to the question of whether $La_{1-x}Sr_xCoO_3$ is really the catalyst.

It appears that the catalyst is efficient both at the start of the exposures to SO_2 and CO and after many hours of exposure. This suggests that either the catalyst becomes sulphided extremely quickly or a property of $La_{1-x}Sr_xCoO_3$ is carried through the chemical

changes which it undergoes. During heating of the fresh $La_{1-x}Sr_xCoO_3$ SO_2 removal, CO_2 formation and COS formation occur simultaneously. The reactions appeared to start at temperatures above 400^oC, bearing in mind that temperatures at which samples were taken were noted but these were not identical for each experiment.

Hibbert and Tseung (12) suggest that all of the initial removal of SO_2 may be attributed to sulphidation of the catalyst. It may be inferred from this that the catalyst is actually a sulphided compound. Sulphides of Sr and Co were detected in their work. Kelly (107) also observed formation of Sr and Co sulphides. He suggests that there must be considerable sulphide formation before COS is produced. Khalafalla and Haas (108) studied the use of an Fe/CrO_3 catalyst for the SO_2 reduction reaction and stated that COS production did not occur until all of the Fe had been converted to FeS. The simultaneous disappearance of SO_2 and appearance of CO_2 and COS disagrees with the observations of Khalafalla and Haas. It appears that as soon as there is sulphide present then COS production may occur. It is suggested in section 4.4.1 that this will occur unless the surface is saturated with SO_2 in which case reduction of this by CO will occur.

The question of what is catalysing the reduction of SO_2 to elemental sulphur and oxidation of CO to CO_2 remains.

The catalyst has evidently changed yet it has maintained its catalytic efficiency.

Another change of the catalyst, which has not yet been discussed is the presence of two oxygen species on the fresh $La_{1-x}Sr_xCoO_3$ surface and the presence of only one oxygen species on the used catalysts.

Reference to Table 3.5 in section 3.2.4 shows that for $La_{0.3}Sr_{0.7}CoO_3$, $La_{0.4}Sr_{0.6}CoO_3$ and $La_{0.5}Sr_{0.5}CoO_3$ the lower binding energy peak was a mere shoulder of the main oxygen peak. The $La_{0.7}Sr_{0.3}CoO_3$ sample had two clear oxygen peaks. Yamazoe (17) has looked at the ESCA spectra of $La_{1-x}Sr_xCoO_3$ after O_2 adsorption. Yamazoe assigned the lower binding energy peak to lattice oxygen and the higher binding energy peak to adsorbed oxygen. This suggests that in the present work there is least adsorbed oxygen on $La_{0.7}Sr_{0.3}CoO_3$, this agrees with the observations of Yamazoe which show an increase in oxygen adsorption on increasing x. The two peaks seen by Yamazoe may represent the same oxygen species as those observed in this work. The lower binding energy peak observed by Yamazoe was, however, about 528 eV, that is, lower than either of the peaks observed in this work and the higher binding energies observed by Yamazoe are closer to the lower binding energies recorded here.

It is only the fact that there are two peaks present in the two data sets which suggests that they represent the same oxygen species.

After the flow-rig experiments, only the peak of the higher binding energy oxygen species is remaining. It may be possible that if there is adsorbed oxygen on $La_{1-x}Sr_xCoO_3$ at the low pressures at which ESCA operates, that it could be present on the products of the reaction of SO_2 and CO. If this was the case then the higher binding energy peak may be assigned to adsorbed oxygen. This would agree with Yamazoe's interpretation of ESCA studies of $La_{1-x}Sr_xCoO_3$, except that the values would be of the order of 1 eV different between the

two data sets. 1eV is about the accuracy expected for ESCA measurements.

It must also be borne in mind that the $La_{1-x}Sr_xCoO_3$ samples examined by Yamazoe were pre-exposed to an oxygen atmosphere whereas those in the present work were exposed to the laboratory atmosphere. Perhaps the relative absorptivities of the fresh and used catalysts for oxygen should be measured.

The detection of sulphur in the form of SO_4^{2-} on the surface, by ESCA, suggests that the oxygen in SO_4^{2-} would also be detected. The relative sensitivies of O1s and S2p in ESCA are very close, they are 0.861 and 0.706 respectively. The O1s binding energy for the only sulphate quoted in the Handbook of X-ray Photoelectron Spectroscopy (81), that is, Na_2SO_4, is 531.9 eV which is close to the O1s binding energy of the used catalyst. This suggests that it is in fact $SrSO_4$ which is being detected. The evidence against this is that the peak has similar binding energies to one of the original peaks observed for the fresh $La_{1-x}Sr_xCoO_3$ catalysts.

If the oxygen species detected by ESCA, on the used catalyst is from $SrSO_4$ then it seems likely that the type of oxygen on the surface is not very important for the SO_2 reduction and CO oxidation reaction, as this is not the form the oxygen is present as in the catalytically active fresh catalyst. If, however, the O1s peak represents adsorbed oxygen then the increase in catalytic activity for oxidation of CO reported by George and Viswanathan (23) and Nakamura (24) may be supported. These earlier workers did not have SO_2 as a source of oxygen. The oxygen, if adsorbed O_2,should in

fact have been absent from the flow rig experiments as the SO_2 and CO flowed through the catalysts in O_2 free N_2.

Sis et al (9) have shown that in a reducing atmosphere $LaCoO_3$ (x = 1) breaks down to La_2O_3, Co and oxygen, via La_2O_3, Co_2O_3 Co_3O_4, CoO and Co. Both La_2O_3 (109, 110) and Co_2O_3(12) have been shown to catalyse the reduction of SO_2 by CO, but not very efficiently. The oxides produced by the decomposition of $LaCoO_3$ in a reducing atmosphere may be the equivalents of the sulphide compounds produced when the particular reducing atmosphere is a mixture of SO_2 and CO.

The mixture of cobalt sulphides formed may be a consequence of the temperatures used. Trotman-Dickenson (111) states that Co_3S_4 is stable until 650°C, then CoS_2 and $Co_{1-x}S$ compounds are formed.

4.4.3 Changes in catalytic activity observed on changing the reaction temperature

The temperatures at which the reactions were studied were 500°C, 550°C, 600°C and 650°C. Samples of the outlet gases were also analysed during heating and cooling of the catalysts in the presence of the gas flow. The changes due to the temperature changes will be discussed in the order in which they occurred.

On initial heating, the first or second sample taken always showed a slight increase in SO_2 output. This was attributed, in section 3.4.1 to desorption of SO_2 adsorbed at room temperature.

The next observation was a fall in SO_2 output, which was accompanied by CO_2 production and COS production for those experiments where COS was produced. This always occurred above 400°C.

Speculation may be made about why at this temperature the reactions producing these changes in gas outlet should occur. First of all the decrease in SO_2 will be examined. The decrease in SO_2 may merely be due to adsorption of the gas on $La_{1-x}Sr_xCoO_3$ at this temperature. Reference to Fig. 3.14 will show that adsorptivity of $La_{1-x}Sr_xCoO_3$ for SO_2 appears to increase very dramatically between 300°C and 500°C. Adsorption at 300°C is minimal compared to that at 500°C. At a temperature between 300°C and 500°C there is sufficient energy for an activated adsorption which does not readily occur at lower temperatures.

The production of CO_2 may also be explained by the increased adsorption and reaction of CO on the catalyst surface, also between 300°C and 500°C. The adsorption results are given in section 3.3.4. The fact that SO_2 is also present provides another source of oxygen for the CO oxidation.

The appearance of COS may be a consequence of the adsorption of the SO_2 and CO gases.

The coincidence of the changes in trend of adsorption of SO_2 and CO on $La_{1-x}Sr_xCoO_3$ with temperature suggests that a change in the $La_{1-x}Sr_xCoO_3$ takes place.

Sis et al (9) looked at the change in the magnetic properties of $LaCoO_3$, that is, x = 1, with temperature. They found that trivalent Co existed predominately in the low spin state below 125°C. Above this temperature the high spin state of trivalent Co became more abundant and at 375°C a rapid increase in high spin Co^{3+} occurred due to long range ordering at this temperature. Goodenough (112)

emphasizes the importance of Co^{3+} in the conductivity of $La_{1-x}Sr_xCoO_3$. The change in the adsorptivity and catalytic activity of $La_{1-x}Sr_xCoO_3$ may be related to conductivity. If this is the case then the conductivity measurements made at room temperature may be invalid for the reaction conditions.

Goodenough (112) states that as Sr is introduced into the $La_{1-x}Sr_xCoO_3$ lattice, that is, as x increased, then the amount of Co^{3+} decreases and Co is present as Co^{3+}, Co^{III} and Co^{IV}. The present work appears to support the observations of earlier workers such as Nakamura et al (24), that higher Sr content gives poorer catalytic activity. So it seems that two sets of conditions that favour higher Co^{3+} content also favour high catalytic activity. These conditions are high La content in $La_{1-x}Sr_xCoO_3$ and temperatures above 400^oC.

The cause of the increase in high spin trivalent Co, that is, Co^{3+}, at high temperatures is probably due to the electrons of trivalent Co having sufficient energy to move into the high spin configuration.

Goodenough (112) states that the decrease is Co^{3+} is accompanied by an increase in Co^{III} and Co^{IV}. If it can be assumed that at the temperatures at which the Co^{3+} abundance increases, that the Co^{III} and Co^{IV} abundances decrease then the change may be attributed to or may cause the loss of oxygen from the lattice which has been observed, in this work. A loss of negatively charged oxygen, accompanied by a change from tetravalent to trivalent Co would conserve charge neutrality in the $La_{1-x}Sr_xCoO_3$ lattice.

Tseung and Bevan (56) have examined the use of $La_{1-x}Sr_xCoO_3$ as a reversible oxygen electrode. An electrode of course must be able to conduct electricity and Tseung and Bevan attribute the activity of $La_{1-x}Sr_xCoO_3$ to trivalent Co.

Referring again to the production of COS, the minimum temperature for this reaction has in fact been shown to be lower than 400°C in several conditions in this work and by other workers, including Bazes et al (35). The first appearance of COS during heating may therefore be attributed to the adsorption of SO_2 and CO which provided the necessary ingredients for the reaction, by allowing the formation of sulphides.

The changes in the amounts of SO_2, CO_2 and COS observed once the temperatures at which the reactions occur are reached, with temperature have not yet been discussed.

It must be assumed that the relative rates of adsorption, reaction and desorption change and the activities of the three catalysts studied change for various reasons. The rate of COS production will, for example, change with the availability of sulphide for reaction with CO and with the availability of other reactions which may involve the CO. Changes in the catalyst, apart from involving the charge, magnetic and oxidation states of Co will include sulphiding of the catalyst.

Reference to Table 3.30 in section 3.4.4 shows that for the stoichiometric mixture with a total flow rate of 100 cm^3min^{-1} at the four steady state temperatures studied, the overall effect for $La_{0.5}Sr_{0.5}CoO_3$ is similar. For $La_{0.3}Sr_{0.7}CoO_3$ removal of SO_2 was best at the lower temperatures and for $La_{0.7}Sr_{0.3}CoO_3$ it was best at the higher temperatures. This agrees with the postulation above that

high La content and high temperatures are important, but this assumes that $La_{1-x}Sr_xCoO_3$ is the catalyst. Yet the XRD and ESCA evidence points to the catalytic activity of sulphides of Sr and Co. Sulphidation of La is much less prevalent, even at high La contents. Perhaps the La content is more important than the temperature once the threshold temperature has been attained. The high Sr content catalysts may have more sulphide content and this may explain their higher COS production.

During cooling of the catalyst samples, the still flowing outlet gases were sampled and analysed. The SO_2 content of the gas increased as the temperature dropped and the CO_2 content decreased thus indicating that the catalytic reduction of SO_2 and oxidation of CO was decreasing as the temperature decreased. The COS output, however, often increased or even appeared in an experiment where COS was not produced at temperatures below 400°C and often continued below 250°C. The instances of these observations are shown in Tables 3.26, 3.27 and 3.28.

The temperature required for COS production appears to be below that where CO_2 is produced. COS is probably not produced at these low temperatures during heating because the sulphide has not yet been formed by SO_2 adsorption and subsequent reduction of the SO_2 by CO. The production of COS during the sulphur scavenging reactions by CO, in the vacuum line experiments started at lower temperatures than during the flow rig experiments. This is probably because of the presence of the sulphur source for the production of COS before the introduction of CO. The CO used during the scavenging reaction is probably not involved to any great extent in the reduction of any sulphur species to a form where it will then react with CO to form COS. The fact that

the sulphur species required for COS production is already present may not be the only reason for the detection of COS at lower temperatures in the vacuum line. The methods of detection of COS in the two experiments are different. The MS used in the vacuum line experiments may be expected to detect COS in smaller quantities than the G.C. used during the flow-rig experiments. The appearance of COS at a lower temperature in the vacuum line may therefore give a false impression because of the different sensitivities of the COS detectors.

4.4.4 Relative oxidizibilities of the reactants, including $La_{1-x}Sr_xCoO_3$

The reaction being studied in this thesis is the reduction of SO_2 by CO using $La_{1-x}Sr_xCoO_3$ as a catalyst, it is shown in equation 1.

$$SO_2 + 2CO \rightleftharpoons 1/x\ S_x + 2CO_2 \qquad 1$$

Evacuation and subsequent heating of $La_{1-x}Sr_xCoO_3$ causes loss of oxygen from the lattice, this is a form of reduction of the catalyst.

The reaction of SO_2 with $La_{1-x}Sr_xCoO_3$ to produce $SrSO_4$ may be interpreted as a reduction of the catalyst, by virtue of the fact that the SO_2 is oxidized. The reaction of CO with the surface produces CO_2 and other workers (33) claim to have detected CO_3^{2-} on $LaCoO_3$, so CO may be said to reduce the catalyst.

In the presence of both of the reactants the catalyst is being reduced by both SO_2 and CO. Adsorbed SO_2 is also thought to be reduced to elemental sulphur by CO.

These reactions are represented diagramatically in terms of relative oxidizibilities in Fig. 4.1.

Fig. 4.1 is vastly oversimplified. It does not consider the form of the reaction reduced catalyst. It does, however, imply that the reaction shown in equation 1 is a suprafacial reaction which is made possible by the adsorption of SO_2 and subsequent adsorption of CO. The identity of the catalyst is not specified and the final remark is that it is a compound or compounds capable of adsorbing SO_2 and CO and it may be $La_{1-x}Sr_xCoO_3$ and sulphides of La, Sr and Co.

4.5 CATALYTIC PROPERTIES OF METAL SULPHIDES

In the earlier sections of this chapter it has been suggested that sulphides of La, Sr and Co may be acting as catalysts for the reduction of SO_2 by CO. This section discusses that possibility in the light of other work where sulphides are used as catalysts.

A literature search revealed that the major uses of sulphide catalysts were in the petroleum and associated industries. Sulphide catalysts are used for hydrogenation of many organic substances; for cracking and reforming of combustible raw materials; for synthesis of sulphur compounds and their desulphurization; isomerization reactions; dehydrogenation reactions; oxidation reactions; polymerization reactions and for some reactions of simple sulphur compounds (113).

The role of the sulphide catalyst appears to be varied and wide which is interesting because as Weisser and Landas (114) point out, in the initial development of catalysts sulphur was carefully removed because it often acted as a catalyst poison.

FIGURE 4.1 SUGGESTED MECHANISMS EXPRESSED IN TERMS OF THE RELATIVE OXIDIZIBILITIES OF THE REACTANTS INCLUDING $La_{1-x}Sr_xCoO_3$

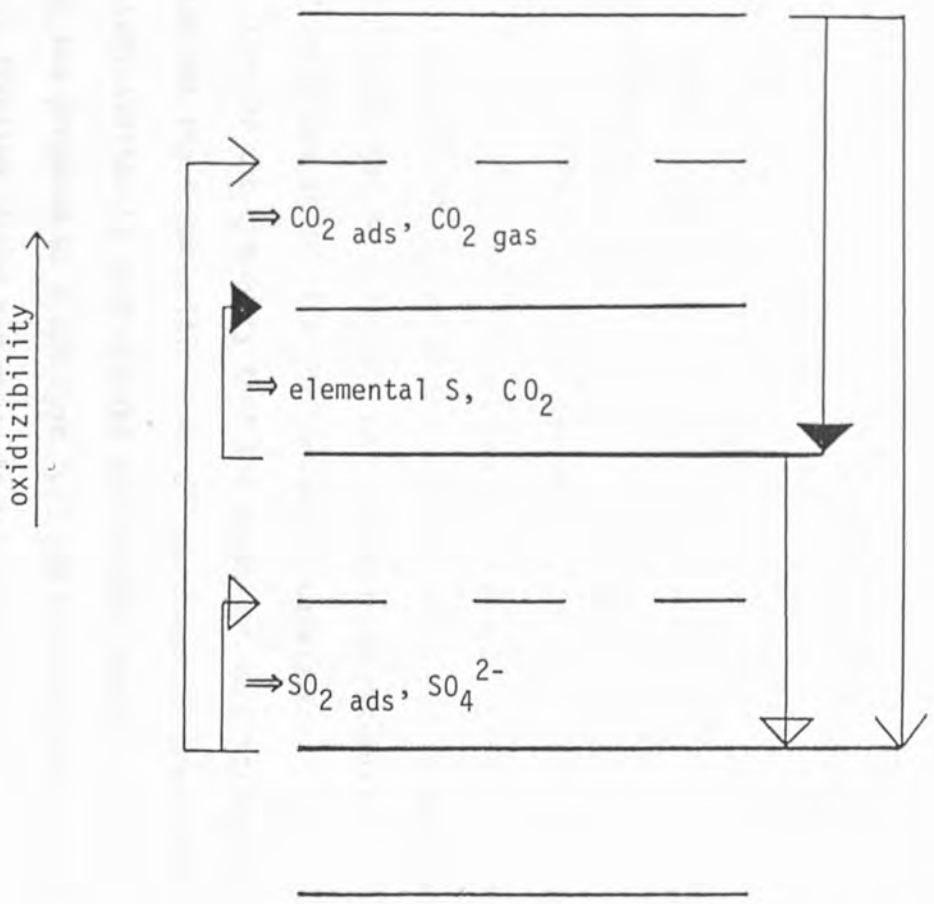

Grange (115), in his review of catalytic hydrodesulphurization makes some very interesting comments about sulphide catalysts, which are of interest with respect to this work. Grange notes that the view of the catalysts used in hydrodesulphurization has changed considerably in recent years. It seems that the catalysts which were charged to the reactors were in the oxidic form. During their catalytic lifetime they became sulphided to various extents. Some people suspected that the active phase of the catalyst was in fact the sulphided form. Much of the oxidic form remained so the fact that the oxidic form was only a transient active phase was not discovered. It seemed that the oxidic form appeared to be very reactive initially because it rapidly removed sulphur from, for example, thiophene. This removal of sulphur was because the oxidic form of the catalyst was becoming sulphided. Much of the work was with Co-Mo sulphides. It was found that under the working conditions sulphidation was thermodynamically favoured. Evidence that the sulphides were in fact the catalysts was obtained by XRD, which showed their presence. Experimental evidence included introduction of oxides to the reactor, which led to abnormal behaviour which changed as sulphidation increased and carefully unsupported sulphides acted like the industrial catalysts.

The story of the discovery that the sulphides were acting as catalysts and not the fresh oxidic forms of the compounds prepared as such is very similar to that related during this thesis. $La_{1-x}Sr_xCoO_3$ was prepared as a catalyst, yet XRD revealed that during its catalytic lifetime it was converted to sulphides of the constituent metals. The initial activity of the catalysts were high and remained so. The original catalytic activity may have been due

to sulphidation of the catalysts and the later activity to the properties of the sulphides.

Furimsky (116),in his review of the role of sulphides in hydrodesulphurization, emphasizes the importance of the conductivities of the catalysts. It appeared that in one of the examples he examined, that the catalytic activity was due to a synergistic effect of two sulphides. There seemed to be an interaction between MoS_2 and Co_9S_8 which involved electron transfer between the two sulphides.

Conductivity was also considered to be of importance in the work presented in this thesis.

In Grange's (115) review he referred to the sulphidation of catalysts and its extent. Sometimes there was not evidence for discrete sulphides but perhaps only one or two oxide ions may be replaced by sulphide, and these might bridge Mo and Co. If this sort of reaction occurred in the work presented in this thesis it might explain the difficulty in assigning some of the XRD peaks.

The importance of methods of preparation of sulphide catalysts is emphasized. Weisser and Landas (114) state that most often, preparation of some of the most active sulphide catalysts is by conversion of the respective oxides. The sulphidation is usually preceded by reduction by H_2.

A parallel may be drawn here, with the sulphides prepared in this work. They are reduced by CO.

Weisser (113) states that sulphidation is usually by mercaptans or CS_2 at temperatures around 400^oC. Grange (115) quotes temperatures of this range, that is, about 350^oC to 400^oC where sulphidation occurs

of oxidic catalysts during use. Even these temperatures, coincide with the start of catalytic activity in the present work. This reinforces the suggestions made throughout this chapter about the role of the catalyst and how changes in the catalyst at this temperature range may allow the activity to occur. This of course does not explain the vacuum line experiments, where sulphidation did not take place except that there was no reducing agent such as CO but a change in $La_{1-x}Sr_xCoO_3$ may take place, which allows SO_2 adsorption, CO adsorption/reaction and sulphidation. The sulphides quoted by Grange (115) and Weisser (113) are not those found in this work, but they do quote sulphides of several metals including Co, Mo and W so temperatures where sulphidation can occur may be similar for many metals.

Grange (115) states that catalytic activity depends on the temperature of sulphidation. He states, for example, that Co/Mo catalysts sulphided at 600^{o}C show the highest activity for hydrogenolysis. Trotman-Dickenson (111) quotes examples of how sulphides change their stoichiometry with temperature.

The sulphide catalysis reactions referred to above bear little relation to reduction of SO_2 yet simple reactions have been observed too. Weisser (113) refers to hydrogenation of SO_2 using FeS as a catalyst. This is like the iron/chromia catalysts referred to in section 1.4 (71). Also sulphide catalysis of the oxidation of H_2S by SO_2 to elemental sulphur was referred to as was the conversion of CO to CH_3OH. These involve SO_2 and CO separately so they would appear

to at least adsorb on to their respective catalysts.

It must also be remembered that earlier workers (12, 107) noted the presence of sulphides in the used catalysts although they attributed no catalytic activity to them. Hibbert and Tseung (68) noted that when Cu was studied as a catalyst for the SO_2/CO reaction, that sulphidation tended to occur. This is another example of where the sulphide is the most stable compound under the reaction conditions.

Further research into sulphides as catalysts and the behaviour of sulphides under the experimental conditions of the present work is required.

CHAPTER 5

CONCLUSIONS AND SUGGESTIONS FOR FURTHER WORK

CONCLUSIONS

1 There is a tendency for $La_{1-x}Sr_xCoO_3$ to lose oxygen by evacuation and heating, this increases as x increases or La content decreases.

2 Lattice oxygen is desorbed by evacuation and heating of $La_{1-x}Sr_xCoO_3$.

3 There is more than one type of SO_2 adsorption.

4 Adsorption of SO_2 at 500^oC is significantly greater than at room temperature, 100^oC and 300^oC.

5 Adsorption of SO_2 on $La_{1-x}Sr_xCoO_3$ under vacuum, increases as La content increases.

6 SO_2 is adsorbed beyond the surface of $La_{1-x}Sr_xCoO_3$.

7 The adsorptivity of SO_2 on $La_{1-x}Sr_xCoO_3$ is proportional to the La content but not to Co^{3+}, Co^{III}, Co^{IV} or oxygen vacancies.

8 There is XRD evidence that $SrSO_4$ is formed by reaction of SO_2 with $La_{1-x}Sr_xCoO_3$.

9 The perovskite-type structure of $La_{1-x}Sr_xCoO_3$ survives its reaction with SO_2.

10 Reaction of $La_{1-x}Sr_xCoO_3$ with SO_2 causes its conductivity to decrease.

11 There is more than one type of CO adsorption.

12 CO reacts with oxygen in $La_{1-x}Sr_xCoO_3$ to form CO_2, which is then desorbed. This seems to occur most readily when there are few oxygen vacancies and little oxygen has been desorbed by evacuation and heating, that is, at high La content.

13 Re-oxidizibility of $La_{1-x}Sr_xCoO_3$, reduced by reaction with CO increases with x, that is, decreases with increasing La content. As the La content increases then higher temperatures are required for re-oxidation.

14 $La_{1-x}Sr_xCoO_3$ reduced by CO and subsequently partly or fully re-oxidized, retained its perovskite-type structure.

15 Unless $La_{1-x}Sr_xCoO_3$ which has been reduced by reaction with CO, is completely re-oxidized, its conductivity is less than fresh $La_{1-x}Sr_xCoO_3$.

16 $La_{1-x}Sr_xCoO_3$ exposed to SO_2 and CO simultaneously becomes sulphided. Sulphides of La, Sr and Co are formed.

17 The reaction between SO_2 and $La_{1-x}Sr_xCoO_3$ which produces $SrSO_4$ continues to occur in the presence of CO, alongside the sulphidation of the catalyst.

18 SO_2 is reduced to elemental sulphur and CO is oxidized to CO_2 when the two gases are together in the presence of $La_{1-x}Sr_xCoO_3$.

19 A stoichiometric mixture of SO_2 and CO gives the most efficient conversion of the two gases to elemental sulphur and CO_2. Excess of CO leads to a side reaction which produces COS.

20 The source of sulphur for the production of COS is one or more of the metallic sulphides, formed by the reaction of SO_2 and CO with $La_{1-x}Sr_xCoO_3$.

21 After the scavenging of sulphur from the sulphide or sulphides no metallic La, Sr or Co was detected.

22 $SrSO_4$ does not react with CO to produce SrS and COS.

23 Elemental sulphur is not a source of sulphur for the production of COS.

24 It appears that $La_{0.7}Sr_{0.3}CoO_3$ is the best catalyst, of the $La_{1-x}Sr_xCoO_3$ samples studied, for the SO_2 reduction and CO oxidation.

25 The catalytic properties of $La_{0.7}Sr_{0.3}CoO_3$ may be attributed to its relatively high adsorptivity of SO_2 and relatively low adsorptivity of CO.

26 The SO_2 reduction and CO oxidation appears to be suprafacial, that is, the CO directly reduces the SO_2 without involving the catalyst surface in a chemical reaction.

27 $SrSO_4$ is not an intermediate in the reaction. Elemental sulphur is not produced if $La_{1-x}Sr_xCoO_3$ initially exposed to SO_2 only is subsequently exposed to CO.

28 After exposure of $La_{1-x}Sr_xCoO_3$ to SO_2 and CO simultaneously, the catalyst no longer retained its perovskite-type structure.

29 The continuation of the catalytic reaction after the sulphidation of the surface and loss of the perovskite-type structure, suggests that $La_{1-x}Sr_xCoO_3$ and the metal sulphide mixture both possess the catalytic properties required for the catalysis.

30 The catalysts appear to retain their conductivity after the flow-rig experiments but not after simultaneous adsorption of SO_2 and CO in the vacuum line.

31 The best compromise of experimental conditions appears to be 500^oC or 550^oC with a flow rate of 100 cm^3min^{-1} using $La_{0.7}Sr_{0.3}CoO_3$ as a catalyst with 1% SO_2 and 2% CO in N_2. This removes virtually all SO_2 and no COS is produced.

32 COS production in the absence of SO_2 removal from the SO_2 and CO stream, was never observed.

33 The La content of the catalyst and the temperature range which favours high catalytic activity also favours the formation of trivalent cobalt in the Co^{3+} state. The presence of Co^{3+} is favoured at temperatures greater than 400^oC (9).

SUGGESTIONS FOR FURTHER WORK

1 Measurement of the mass changes after the exposure of fresh $La_{1-x}Sr_xCoO_3$ to CO, may provide more information about the oxygen associated with the perovskite-type oxide. By comparison of these changes with the mass changes due to evacuation and heating under vacuum and those after subsequent exposure to CO, it could be deduced whether the oxygen removed by evacuation and heating would be removed by CO in the absence of these steps.

2. Investigation of the actual temperature at which sulphidation of the $La_{1-x}Sr_xCoO_3$ occurs and comparison of it to that of the start of the SO_2/CO reaction may show whether a sulphide species is the actual catalyst. A problem with this is that the SO_2 concentration does fall due to adsorption on $La_{1-x}Sr_xCoO_3$ and reaction with it to produce $SrSO_4$, as well as sulphide formation. Also CO_2 is produced in the absence of the SO_2/CO reaction by the reduction of $La_{1-x}Sr_xCoO_3$ by CO. The concentration of SO_2 and CO would need to be monitored continuously and not intermittently, as in the present work, in order to detect changes due to the starting of the sulphidation reaction or reactions.

3 Each of the sulphides of La, Sr and Co which were produced by reaction of SO_2 and CO with $La_{1-x}Sr_xCoO_3$ could be investigated separately and as mixtures, for their catalytic properties, by passing SO_2 and CO over them. This would ascertain which of the sulphides were catalytically active although it would not eliminate the possibility of $La_{1-x}Sr_xCoO_3$ being catalytically active too. Adsorption and desorption of SO_2 and CO, within the range of temperature studies here, may be of interest in this context too.

4 In order to discover which of the sulphides produced from $La_{1-x}Sr_xCoO_3$, provide the sulphur for COS production, these could be exposed to CO separately and as mixtures. COS formation could be detected mass spectrometrically, as in the present work.

5 It would be of interest to measure the XRD pattern of the catalysts exposed to SO_2 and CO simultaneously both after re-evacuation and then again after scavenging by CO, to see if any of the sulphides were consequently removed. A quantitative measurement of the amount of each sulphide before and after CO scavenging would be useful.

6 Measurement of the conductivity of the cobalt sulphides formed by the reaction of SO_2, CO and $La_{1-x}Sr_xCoO_3$ would be of interest. This is considering that LaS (93, 98) and SrS (86) both have conducting properties and that the catalyst retains its conductivity after the flow-rig experiments and consequent sulphidation.

7 The conductivities of the catalysts used were measured at room temperature. Measurement of the conductivities at the reaction temperatures may give a more accurate picture of the reaction conditions.

8 The $La_{1-x}Sr_xCoO_3$ samples exposed to SO_2 and CO individually were not examined by ESCA. Such analysis would be of interest for comparison with the fresh catalysts and those exposed to SO_2 and CO simultaneously.

9 To find out more about the nature of oxygen species, observed by ESCA, on the fresh and used catalysts, the relative adsorptivities of these with respect to oxygen could be measured.

10 Examination of the $La_{1-x}Sr_xCoO_3$ after various running times of the flow-rig experiments by XRD may show whether or not the simultaneous adsorptions of SO_2 and CO in the vacuum line represented the initial stages of the flow-rig experiments.

11 Exposure of $La_{1-x}Sr_xCoO_3$ which contained ^{18}O, to SO_2, followed by TPD may give some useful information about the nature of SO_2 adsorption. SO_2 is chemisorbed and subsequently desorbed by heating in a vacuum. It is not known whether or not adsorption is dissociative.

12 Carrying out the SO_2 and CO flow-rig experiments using ^{18}O containing $La_{1-x}Sr_xCoO_3$, may give further information about their interaction with the catalyst. Continuous monitoring of $C^{16}O_2$ and $C^{16}O^{18}O$ as well as SO_2 and COS may be done by mass spectrometry. If there is no reaction of CO with $La_{1-x}Sr_xCoO_3$ then the rate of production of $C^{16}O_2$ ought to be twice the rate of SO_2 removal. If $C^{16}O^{18}O$ production occurred then it would be of interest to see if this declined as the catalyst became sulphided and if SO_2 removal and, or COS production consequently increased.

APPENDIX 1

MASS1

```
      PROGRAM KINETIC
      IMPLICIT REAL *8 (A-H,O-Z)
C
C
C                 Solves the kinetic equation
C
C            -  d(alpha)                                  n
C               ---------    =    A exp( E )       alpha
C                  dt                  (RT )
C
C           Where T = f(t), for A, E and n (V1..3)
C
C           S (mass spec. signal) and T data are give at
C           different times (t) where
C
C                   dS/dt  =   A' d(alpha)/dt - k'S
C
C           alpha is the fractional coverage of the species.
C
C           A maximum of 4 different species may be processed.
C
C             INPUT DATA
C             ==========
C
C     card 1                    TITLE --- One line title
C
C     card 2                     INTER --- Number of interpolation points.
C
C     card 3    (2a3)            FIT  --- FIT if fitting experimental data
C                                         else if trying single point calc
C
C                                TEK  --- TEK if at Tektronix terminal
C
C     card 4          COL1,COL2,COL3 --- 0-16 for colours of titles,
C                                        experimental points and fitted lines
C                                        respectively.  This card is always
C                                        read but only considered if TEK=.T.
C                                        Uses COLOUR() in CHEMLIB and is for
C                                        the TELEDATA XSA.Set = 16 if using
C                                        different plotting device.
C
C     card 5                SCALE(6) --- The unknown parameters are scaled
C                                        by these factors before minimising.
C                                        1 = Mass spec multiplying factor
C                                        2 = kn, the pumping rate constant
C                                        3 = LOG(Arrhenius fact* scale)
C                                        4 = Activation energy (J/mol)
C                                        5 = n, the order of reaction
C                                        6 = x0, the initial fractional
C                                             coverage.
C
C     card 6                    NDATA --- Number of data points
C
C     cards 7           TIM,TEMP,S    --- Mass spec reading (S) and
C                                         temperature (TEMP) at time TIM
C
C
C           Version 2.0
C
C           Values of S and T are interpolated throughout the range
C           using E01BAF and E02BBF unless NDATA=INTER.
C           Minimisation by E04JAF.
C
C           Tektronix compatible, DIMFILM routines added.
C
C                                                        dbh 6/84
C
          REAL *4 RX(2500),RY(2500),RZ(2500), HOLD(200,4)
          REAL *4 XG(200),YTEMP(200),YALP(200), YDIF(200)
      DIMENSION TIM(2500),TEMP(2500)
      DIMENSION S(2500), V(18), F(18)
      COMMON /FITS/ X(2500),Y(2500),Z(2500),ND
      COMMON /FIT1/ STOT(2500),SCAL(2500,4),TEMPE(2500),
     1         SINT(2500),DS(2500),DSALPHA(2500),ALPHA(2500,4)
     2        ,DALPHA(2500,4),INTER
       COMMON /FIT2/ DELT, TMAX(4), TMIN(4), NSPEC
       COMMON /FIT3/ TEK
      COMMON /FIT4/ SCALE(6)
```

```
      CHARACTER *80 FMT(8)
      CHARACTER *80 INFILE, TITLE
      CHARACTER DUMMY
      CHARACTER *3 ANS1,ANS2,AFIT,ATEK
      INTEGER COL1,COL2,COL3
      LOGICAL FIT, TEK, YES
      PARAMETER (AFIT='FIT', ATEK='TEK')
C
C
C
      fmt(1) = '(''A='', 1pe8.2)'
      fmt(2) = '(''E='', 1pe8.2)'
      fmt(3) = '(''n= '', f3.1)'
      fmt(4) = '(''XO= '', f4.2)'
      fmt(7) = '(''K='', 1pe8.2)'
      fmt(8) = '(''kn='', 1pe8.2)'
      WRITE(*,'(//'' Name of data file : '',$)')
      READ(*,'(A80)')INFILE
      OPEN(5,STATUS='OLD',FILE=INFILE)
      READ(5,'(Q,A)')LTITLE, TITLE
      READ(5,*)INTER
      READ(5,'(2A3)')ANS1,ANS2
      TEK=.FALSE.
      FIT=.FALSE.
      IF (ANS1 .EQ. ATEK .OR. ANS2 .EQ. ATEK) TEK=.TRUE.
      IF (ANS1 .EQ. AFIT .OR. ANS2 .EQ. AFIT) FIT=.TRUE.
      READ(5,*)COL1, COL2, COL3
      READ(5,*)SCALE
      READ(5,*) NDATA
      READ(5,*)(TIM(I),TEMP(I),S(I),I=1,NDATA)
C
C             Scale mass spec data to a max of 1.
C
      SCS=S(1)
      DO I=2,NDATA
            IF(S(I) .GT. SCS) SCS=S(I)
      ENDDO
      WRITE(6,'(///1X,A80)') TITLE
      ND=NDATA
      WRITE(6,'(/'' FIT is '',L2,''  TEK is '',L2)')FIT,TEK
      WRITE(6,'(/'' INTER is '', i5)') INTER
      DO I=1,ND
            X(I)= S(I)/SCS
            Y(I)=TIM(I) - TIM(1)
            Z(I)=TEMP(I) + 273.18
          RX(I) = X(I)
          RY(I) = Y(I)
          RZ(I) = Z(I)
      ENDDO
      DELT = (Y(ND) - Y(1))/ DFLOAT(INTER-1)
      CALL INTERPOL
C
C             Numerically differentiate interpolated Mass spec signal
C             SINT(I) =>  DS(I).
C
      TIME= Y(1) - DELT
      DO I= 1,INTER
            IFAIL = 0
            DS(I) = (SINT(I+1)-SINT(I))/DELT
      ENDDO
      IF (TEK) THEN
            XSTEP = MAX(1., real(INTER)/200.)
            NSTEP = MIN(200,INTER)
            D = DELT * XSTEP
            TIME = Y(1) - D
            J= 0
            XI=0.
             DO K=1, NSTEP
                   XI= XI+ XSTEP
                   I = XI
                   TIME = TIME + D
                   J = J + 1
                   XG(J) = TIME
                   YTEMP(J) = TEMPE(I)
                   YALP(J)  = SINT(I)
                   YDIF(J)  = DS(I)
            ENDDO
            CALL CAM35MM
```

```
          write(6,'(1x,a)')char(29)
          write(6,'(1x,a)')char(12)
              CALL NOCHECK
              CALL GRSLIDE
             CALL XAXIS(0.,RY(ND))
             CALL YAXIS(RZ(1),RZ(ND))
              CALL UPDATE
              CALL COLOUR(COL3)
              CALL BOUNDS(0.,100.,0.,80.)
              call symht(3.0)
              CALL GRAPHIC(XG,YTEMP,NSTEP)
              CALL UPDATE
              IF ( ND .LT. 200)THEN
                      CALL COLOUR(COL2)
                      CALL PTPLOT(RY,RZ,ND,3)
                      CALL UPDATE
              ENDIF
              CALL COLOUR(COL1)
              CALL TITLEU(TITLE(1:LTITLE))
              CALL GRFDEF('Interpolated temperatures','Time /sec',
     1        'Temperature /K', 3)
              CALL UPDATE
              CALL WAIT
              CALL NEWFRAM
              CALL BOUNDS(0.,100.,0.,80.)
              call symht(3.0)
             CALL XAXIS(0.,RY(ND))
             CALL YAXIS(0.,1.)
              CALL UPDATE
              CALL COLOUR(COL3)
              CALL GRAPHIC(XG,YALP,NSTEP)
              CALL UPDATE
              IF ( ND .LT. 200)THEN
                      CALL COLOUR(COL2)
                      CALL PTPLOT(RY,RX,ND,3)
                      CALL UPDATE
              ENDIF
              CALL COLOUR(COL1)
              CALL TITLEU(TITLE(1:LTITLE))
              CALL GRFDEF('Interpolated S','Time /sec',
     1        'S',3)
              CALL UPDATE
              CALL OFFTOXY(0,0)
              CALL WAIT
              CALL NEWFRAM
              CALL BOUNDS(0.,100.,0.,80.)
              call symht(3.0)
              CALL XAXIS(0.,RY(ND))
              CALL AUTOY
              CALL UPDATE
              CALL COLOUR(COL3)
              CALL GRAPHIC(XG,YDIF,NSTEP)
              CALL UPDATE
              CALL COLOUR(COL1)
              CALL TITLEU(TITLE(1:LTITLE))
              CALL GRFDEF('Differential of S','Time /sec',
     1        'dS/dt',3)
              CALL UPDATE
         write(6,'(1x,a)')char(31)
         write(6,'(1x,a)')char(24)
        ENDIF
 999    WRITE(*,'('' Number of species ? '',$)')
        READ(*,*) NSPEC
C
C                Number of variables = 4*species +2[mass spec variables]
C                                      -1 (initial coverage summs to 1)
        NVAR= 4*NSPEC +1
        WRITE(*,'(/'' Guesses for variables''  /
     1  '' Mass spec scaling constant ''/
     2  '' Rate constant for pump '')')
        READ(*,*) F(1),F(2)
        XT = 0.00
        DO I=1,NSPEC
                NST= (I-1)*4 + 3
                NFIN = NST +3
                WRITE(*,'(/'' Species  '',I1)') I
                WRITE(*,'('' Mimimum and maximum temperatures ? '',$)')
                READ(*,*)TMIN(I),TMAX(I)
```

```
            IF (I.LT. NSPEC)THEN
                    WRITE(*,'(
     1              /'' Pre-exponential factor (s-1)''/
     2              '' Activation energy (J)''/
     3              '' n '' / '' XO '' )')
                    READ(*,*) (F(J), J=NST,NFIN)
                    XT = XT + F(NFIN)
            ELSE
                    IF( XT .GE. 1.00)THEN
                            WRITE(*,'(//'' Error in XO ''/
     1                      5(e10.4,2x))') (F(j), j=6,nspec,4),xt
                            STOP1
                    ENDIF
                    WRITE(*,'(
     1              /'' Pre-exponential factor (s-1)''/
     2              '' Activation energy (J)''/
     3              '' n '' )')
                    READ(*,*)(F(J),J=NST,NVAR)
            ENDIF
        ENDDO
        CALL CONVERT(NSPEC,F,V)
        CALL FITSIM(V,NVAR,FIT)
        CALL RESTORE(NSPEC,F,V)
        CALL CALCURVE(F,NVAR,SIGMA)
        WRITE(6,'(//10X,''Simplex has converged''/2x,''Function= '',
     1          G10.4/(2X,''Variable('',I2,'') = '',G10.4/))')SIGMA,
     2                  (I,F(I),I=1,NVAR)
        IF(NO .LT. 50)THEN
            WRITE(6,'(///5X,''TIME'',10X,''    S exptl'',10x,
     1              ''   S  calc'',10x,''Difference'')')
            JSTART = 1
            DO 2 I=1,NO
                    DO J=JSTART,INTER
                            TIME = Y(1) + OFLOAT(J-1)*DELT
                            IF (Y(I) .LT. TIME)THEN
                                    IAN = INEAR(J,Y(I),TIME)
                                    DIF = X(I)-STOT(IAN)
                             WRITE(6,'(2X,G10.4,7X,G10.4,11X,G10.4,
     1                        10X,G10.4)') Y(I),X(I),STOT(IAN),DIF
                                    JSTART = J
                                    GOTO 2
                            ENDIF
                    ENDDO
2           CONTINUE
        WRITE(6,'(//10X,''Simplex has converged''/2x,''Function= '',
     1          G10.4/(2X,''Variable('',I2,'') = '',G10.4/))')SIGMA,
     2                  (I,F(I),I=1,NVAR)
        ENDIF
        IF (TEK) THEN
            TIME = Y(1)
            J= 0
            XI = 0.
             DO K=1, NSTEP
                    XI=XI + XSTEP
                    I = XI
                    J = J + 1
                    YALP(J) = STOT(I)
                    DO IJ=1,NSPEC
                            HOLD(J,IJ)= SCAL(I,IJ)
                    ENDDO
            ENDDO
            CALL WAIT
            CALL NEWFRAM
            write(6,'(1x,a)')char(29)
            write(6,'(1x,a)')char(12)
            CALL BOUNDS(0.,100.,0.,80.)
            call symht(3.0)
            CALL XAXIS(0.,AY(NO))
            CALL YAXIS(0.,1.)
            CALL UPDATE
            CALL COLOUR(COL3)
            CALL GRAPHIC(XG,YALP,NSTEP)
            CALL DASH
            DO J=1,NSPEC
                    DO K=1,NSTEP
                            YTEMP(K)=HOLD(K,J)
                    ENDDO
                    CALL GRAPHIC(XG,YTEMP,NSTEP)
```

```
              ENDDO
              CALL DASHOFF
              CALL UPDATE
                      CALL COLOUR(COL2)
                      CALL PTPLOT(RY,RX,ND,3)
                      CALL UPDATE
              CALL COLOUR(COL1)
              CALL TITLEU(TITLE(1:LTITLE))
              CALL GRFDEF('Calculated mass spec','Time /sec',
     1        'mass spec',3)
              CALL UPDATE
              CALL SYMHT(2.0)
              ST=65.
              DO I=1,2
                      ST=ST-3.
                      CALL OFFTOXY(87.,ST)
                      CALL NUM(F(I),FMT(6+I),.TRUE.)
              ENDDO
              F(NVAR+1)=ALPHA(1,NSPEC)
              DO I=1,NSPEC
                      DO J=1,4
                              ST=ST-3.
                              CALL OFFTOXY(87.,ST)
                              CALL NUM(F(4*I+J-2),FMT(J),.TRUE.)
                      ENDDO
              ENDDO
              CALL UPDATE
              write(6,'(1x,a)')char(31)
              write(6,'(1x,a)')char(24)
      ENDIF
      IF (YES('Another guess') ) GOTO999
      IF(TEK) CALL ENDFILM
      STOP
      END
      FUNCTION DIFS(T)
C
C             Calculates the value of the mass spec signal at time T
C             for differential routine
C
      IMPLICIT REAL *8 (A-H,O-Z)
      COMMON /FIT1/ STOT(2500),SCAL(2500,4),TEMPE(2500),
     1       SINT(2500),DS(2500),DSALPHA(2500),ALPHA(2500,4)
     2       ,DALPHA(2500,4),INTER
       COMMON /FIT2/ DELT, TMAX(4), TMIN(4), NSPEC
      I =  NINT(T/DELT) + 1
      I = MIN(I,INTER)
      S = SINT(I)
      RETURN
      END
      SUBROUTINE RESTORE(NSPEC,V,Q)
C
C             Takes scaled variables (Q) and returns them to their proper
C             values(V). NSPEC is number of species.
C
      IMPLICIT REAL *8 (A-H,O-Z)
      COMMON /FIT4/ SCALE(6)
      DIMENSION V(18), Q(18)
      V(1) = Q(1)/ SCALE(1)
      V(2) = Q(2)/ SCALE(2)
      DO I=1,NSPEC
              J=4*(I-1)+3
              V(J) = 10.D0**(Q(J)/SCALE(3))
              V(J+1) = Q(J+1)/SCALE(4)
              V(J+2) = Q(J+2)/SCALE(5)
              IF(I.LT.NSPEC) V(J+3) = Q(J+3)/SCALE(6)
      ENDDO
      RETURN
      END
      SUBROUTINE CONVERT(NSPEC,V,Q)
C
C             Scales variables (V) to Q for use in minimisation
C             routine.
C
      implicit real *8 (a-h,o-z)
      COMMON /FIT4/ SCALE(6)
      DIMENSION V(18), Q(18)
      Q(1) = V(1) * SCALE(1)
      Q(2) = V(2) * SCALE(2)
```

```
      DO I=1,NSPEC
              J= 4*(I-1)+3
              Q(J) = LOG10(V(J))*SCALE(3)
              Q(J+1) = V(J+1)*SCALE(4)
              Q(J+2) = V(J+2)*SCALE(5)
              IF(I.LT.NSPEC) Q(J+3) = V(J+3)*SCALE(6)
      ENDDO
      RETURN
      END
      SUBROUTINE FITSIM(VAR,NVAR,FIT)
      IMPLICIT REAL *8 (A-H,O-Z)
C
C                 Fitting routine which calls FUNCT1 and FUN
C
C                  LOGICAL FIT is true if fitting routine used
C                                 false for a single set of data to be tried
C
       LOGICAL FIT
      DIMENSION VAR(NVAR)
      DIMENSION W(2000), BU(18), BL(18), QBU(18), QBL(18), IW(20)
      COMMON /FITS/ X(2500),Y(2500),Z(2500),NO
      COMMON /FIT1/ STOT(2500),SCAL(2500,4),TEMPE(2500),
     1        SINT(2500),DS(2500),DSALPHA(2500),ALPHA(2500,4)
     2        ,DALPHA(2500,4),INTER
       COMMON /FIT2/ DELT, TMAX(4), TMIN(4), NSPEC
      EXTERNAL FUNCT1
C
C               Set upper and lower bounds. QBU,QBL are real values
C
      IB=0
      QBL(1)=0.000100
      QBU(1)=5.00
      QBL(2)=1.0-6
      QBU(2)=1.00
      DO I=1,NSPEC
              J= 4*(I-1) + 3
              QBL(J)= 1.01
              QBU(J)= 1.014
              QBL(J+1) = 1.04
              QBU(J+1) = 1.06
              QBL(J+2) = 0.00
              QBU(J+2) = 2.500
              QBL(J+3) = 0.01
              QBU(J+3) = 0.99
      ENDDO
      CALL CONVERT(NSPEC,QBU,BU)
      CALL CONVERT(NSPEC,QBL,BL)
      IFAIL = 1
      LW= NVAR*(NVAR-1)/2 + 12*NVAR
      LIW= NVAR +2
C
C                     Minimise using E04JAF
C
      IF (FIT) THEN
              CALL E04JAF(NVAR,IB,BL,BU,VAR,F,IW,LIW,W,LW,IFAIL)
              IF (IFAIL .NE. 0)THEN
                      WRITE(*,'('' Warning: IFAIL = '',i2)') IFAIL
              ENDIF
      ELSE
              CALL FUNCT1(NVAR,VAR,SIMFUN)
              F=SIMFUN
      ENDIF
      RETURN
      END
      SUBROUTINE FUNCT1(N,VAR,SIMFUN)
C
C               Sum of the squares of the errors in
C               (dS/dt - k'S) experimental and calculated where
C               S is the amplitude of the mass spectrometer signal
C
      IMPLICIT REAL *8 (A-H,O-Z)
      COMMON /FITS/ X(2500),Y(2500),Z(2500),NO
      COMMON /FIT1/ STOT(2500),SCAL(2500,4),TEMP(2500),
     1        SINT(2500),DS(2500),DSALPHA(2500),ALPHA(2500,4)
     2        ,DALPHA(2500,4),INTER
       COMMON /FIT2/ DELT, TMAX(4), TMIN(4), NSPEC
      DIMENSION VAR(N),V(18),Q(18)
       PARAMETER(R=8.314300)
```

```
      GOL = LOG(10.DO)
      SIMFUN=1.020
C
C                     Restore scaled variables
C
      DO I=1,N
            Q(I)=VAR(I)
      ENDDO
      CALL RESTORE(NSPEC,V,Q)
C
C           Set initial alpha's for each species
C
      NSPEC1=NSPEC-1
      INT1 = INTER -1
      IF(NSPEC .GT. 1)THEN
            XT=0.DO
            DO J=1,NSPEC1
                  ALPHA(1,J) = V(4*(J-1)+6)
                  XT =XT + ALPHA(1,J)
            ENDDO
            IF (XT .GT. 1.1DO) RETURN
            ALPHA(1,NSPEC) = MAX(0.DO,1.DO-XT)
      ELSE
      ALPHA(1,1)= 1.DO
      ENDIF
C
C           Loop over interpolated data points
C
      SIMFUN=0.DO
      DO I=1,INT1
C
C                     Experimental function    SFN
C                     (dS/dt - k'S)
C
            SFN = DS(I) + V(2)*SINT(I)
C
C                     Calculated function is DSALPHA / V(1)
C
            DSALPHA(I)= 0.DO
            DO J= 1,NSPEC
C                           Calculate increment in alpha (DALPHA)
C                           for tmin<T<tmax and alpha>1.e6
C
                  IF (TEMP(I) .LT. TMAX(J) .AND. TEMP(I) .GT.
     1            TMIN(J) .AND. ALPHA(I,J) .GT. 1.D-6) THEN
                        JFOUR = 4*(J-1)
                        DALPHA(I,J)= -V(JFOUR+3)*EXP(-V(JFOUR+4)
     1                  /(R*TEMP(I)))* ALPHA(I,J)**V(JFOUR+5)
                  ELSE
                        DALPHA(I,J) = 0.DO
                  ENDIF
                  ALPHA(I+1,J) = ALPHA(I,J) + DALPHA(I,J)*DELT
                  DSALPHA(I) = DSALPHA(I) + DALPHA(I,J)
            ENDDO
            SIMFUN = SIMFUN + (-DSALPHA(I)/V(1) - SFN)**2
            F = SIMFUN
      ENDDO
      SIMFUN = SQRT(SIMFUN/FLOAT(INT1))
      RETURN
      END
       SUBROUTINE INTERPOL
      IMPLICIT REAL *8 (A-H,O-Z)
C
C           Interpolates INTER values of S and TEMP through
C           experimental values
C           If INTER = ND then just copy over values from
C           X,Z to SINT and TEMPE
C
      COMMON /FITS/ X(2500),Y(2500),Z(2500),ND
      COMMON /FIT1/ STOT(2500),SCAL(2500,4),TEMPE(2500),
     1       SINT(2500),DS(2500),DSALPHA(2500),ALPHA(2500,4)
     2       ,DALPHA(2500,4),INTER
       COMMON /FIT2/ DELT, TMAX(4), TMIN(4), NSPEC
       DIMENSION WK(616), SPLINE(104), SPLINE2(104)
      n=nd
      IF (INTER .GT. ND) THEN
C
C           Calculate spline for SINT
```

```
C
              IFAIL = 0
              CALL E01BAF(N,Y,X,SPLINE,SPLINE2,104,WK,616,IFAIL)
              TIME=Y(1)
              SINT(1)=X(1)
              SINT(INTER)=X(N)
              INTR=INTER-1
              DO I=2,INTR
                     TIME = TIME + DELT
                     CALL E02BBF(N+4,SPLINE,SPLINE2,TIME,SINT(I),
     1               IFAIL)
              ENDDO
C
C                            Now for temperature
C
              CALL E01BAF(N,Y,Z,SPLINE,SPLINE2,104,WK,616,IFAIL)
              TEMPE(1) = Z(1)
              TEMPE(INTER)=Z(N)
              TIME=Y(1)
              DO I=2,INTR
                     TIME = TIME + DELT
                     CALL E02BBF(N+4,SPLINE,SPLINE2,TIME,TEMPC(I),
     1               IFAIL)
              ENDDO
       ELSE
              DO I=1,INTER
                     TEMPE(I) = Z(I)
                     SINT(I) = X(I)
              ENDDO
       ENDIF
       RETURN
       END
       FUNCTION INEAR(I,TEXPT,TINTER)
       IMPLICIT REAL *8 (A-H,O-Z)
        COMMON /FIT2/ DELT, TMAX(4), TMIN(4), NSPEC
       INEAR = I
       IF (ABS(TEXPT-TINTER) .LT. DELT/2.DO) RETURN
            INEAR = I-1
       RETURN
       END
       SUBROUTINE CALCURVE(V,NV,SIGMA)
C
C              Calculates the mass spec amplitude vs time curve
C              given the optimised values of the variables V(NV).
C
C              SCAL(data,species) are the individual values
C              STOT(data) are the summed values to be compared with the
C                        experimental values (SINT).
C              SIGMA is the deviation of these values.
C
       IMPLICIT REAL *8 (A-H,O-Z)
       COMMON /FIT1/ STOT(2500),SCAL(2500,4),TEMPE(2500),
     1        SINT(2500),DS(2500),DSALPHA(2500),ALPHA(2500,4)
     2        ,DALPHA(2500,4),INTER
       COMMON /FIT2/ DELT, TMAX(4), TMIN(4), NSPEC
       DIMENSION V(NV)
       INT1 = INTER-1
       DINT1 = INT1
       SUM=0.DO
       STOT(1)=0.DO
C
C              Initialise calculated points
C
       DO J=1,NSPEC
              SCAL(1,J)=0.DO
       ENDDO
       DO I=1,INT1
              STOT(I+1)=0.DO
              DO J=1,NSPEC
                     SCAL(I+1,J) = SCAL(I,J) - DALPHA(I,J)/V(1)*DELT
     1                                        - SCAL(I,J)*V(2)*DELT
                     SCAL(I+1,J)=MAX(SCAL(I+1,J),0.DO)
                     STOT(I+1) = STOT(I+1) + SCAL(I+1,J)
              ENDDO
              SUM = SUM + (STOT(I+1) - SINT(I+1))**2
       ENDDO
       SIGMA = SQRT(SUM/DINT1)
       RETURN
       END
```

APPENDIX 2

XRD DATA

Some of the data consulted in order to assign XRD peaks

La	d	3.06_x	1.60_x	1.89_9					
	2θ	29.19	57.62	48.15					
La	d	3.04_x	1.60_x	2.86_8					
	2θ	29.38	57.62	31.28					
La	d	3.23_x	2.86_7	2.27_5					
	2θ	27.62	32.28	39.71					
La_2Co_3O	d	2.65_x	2.58_x	2.45_6					
	2θ	33.83	34.78	36.68					
La_2O_3	d	2.98_x	1.97_6	2.28_6					
	2θ	29.99	46.08	39.53					
La_2O_3	d	3.27_x	2.00_4	2.83_4					
	2θ	27.28	45.35	31.62					
La_2O_3	d	2.91_x	2.89_5	1.92_5					
	2θ	30.73	30.95	47.35					
$La_2O_2S_2$	d	1.73_4	2.97_3	3.05_x	2.21_3	1.77_3	2.10_3	1.33_3	4.00_2
	2θ	52.93	30.09	29.28	40.84	51.65	43.08	70.86	22.23
$La(NO_3)_3.6H_2O$	d	6.70_x	4.71_x	5.99_6					
	2θ	13.22	18.84	14.79					
$LaCoO_3$	d	2.71_x	2.68_x	1.91_8					
	2θ	33.01	33.44	47.61					
$La_2(SO_4)_3$	d	6.50_x	2.61_7	2.65_7					
	2θ	13.62	34.36	33.83					
$La_{1.75\text{-}1.80}S$	d	2.37_x	2.03_8	2.90_7					
	2θ	37.97	44.64	30.84					

La_2S_3	d	3.55_x	3.52_8	2.64_8					
	2θ	25.09	25.30	33.96					
$LaS_{1.94}$	d	2.38_x	2.93_9	2.75_7					
	2θ	37.80	30.51	32.56					
La_2S_3	d	3.59_x	3.52_8	2.55_7					
	2θ	24.80	25.30	35.20					
$La_2O_2(SO_4)$	d	3.12_x	1.91_7	1.44_6	2.30_6	1.82_5	1.76_5	1.74_4	1.14_4
	2θ	28.61	80.77	64.74	39.17	50.13	51.96	52.60	85.11
La_2O_2S	d	3.12_x	2.02_8	3.46_7	2.46_7	3.49_6	1.92_6	2.30_2	6.91_1
	2θ	28.61	44.88	25.75	36.53	25.53	47.35	39.17	12.81
La_4SrO_7	d	3.10_x	3.05_6	2.99_x	3.41_5	1.99_4	2.28_4	2.30_3	1.95_3
	2θ	28.80	29.28	29.89	26.14	45.59	39.53	39.17	46.58
$La_2Sr_2O_5$	d	3.11_x	3.02_x	2.44_8	3.16_6	2.32_4	1.66_4	2.90_3	2.61_3
	2θ	28.71	29.58	36.84	28.24	38.82	55.35	30.84	34.36
SrO_2	d	3.13_9	2.00_5	2.52_x	1.87_x	3.30_4	1.29_4	1.57_3	1.55_3
	2θ	28.52	45.35	35.63	48.70	27.02	73.41	58.82	59.66
SrO_2	d	2.52_x	3.13_9	2.00_5					
	2θ	36.63	28.52	45.35					
$Sr(NO_3)_2$	d	4.48_x	2.35_7	2.25_5					
	2θ	19.82	38.30	40.08					
SrS_2O_7	d	3.46_x	3.19_8	2.91_8					
	2θ	25.75	27.97	30.73					
$SrSO_4$	d	3.62_x	2.54_4	2.17_1					
	2θ	24.59	35.34	41.62					

SrS_3O_{10}	d	3.46_x	3.27_x	3.19_x					
	2θ	25.75	27.28	27.97					
$SrSO_4$	d	2.97_x	3.30_x	2.73_6					
	2θ	30.09	27.02	32.81					
SrS	d	3.01_x	2.13_5	3.48_3					
	2θ	29.68	42.44	25.60					
SrS	d	2.13_5	3.48_3	3.01_x	1.74_2	1.81_1	1.35_1	1.50_1	1.23_1
	2θ	42.44	25.60	29.68	52.60	50.42	69.66	61.86	77.63
Co	d	2.05_x	1.77_4	1.25_3					
	2θ	22.09	25.82	38.08					
Co_2O_3	d	2.87_x	2.33_x	1.78_x					
	2θ	31.17	28.65	51.33					
Co_2O_3	d	1.78_x	2.87_x	2.33_x	3.21_9	1.63_9	1.39_9	1.57_5	0.00_1
	2θ	51.33	31.17	38.65	27.80	56.46	67.38	58.82	
$Co(NO_3)_2$	d	4.29_x	3.32_5	2.23_5					
	2θ	20.71	26.85	40.45					
$Co(NO_3)_2.6H_2O$	d	5.82_x	3.28_x	3.15					
	2θ	15.22	27.19	28.34					
$Co(NO_3)_2.6H_2O$	d	4.60_x	3.29_8	2.19					
	2θ	19.30	27.11	41.23					
$CoS_{1.097}$	d	1.93_x	1.68_6	2.52_4					
	2θ	47.08/954.63		35.69					
$CoS_{1.035}$	d	1.95_x	1.69_4	2.93_2					
	2θ	46.57	54.28	30.51					

CoS_2	d	2.75_x	2.46_6	1.66_6				
	2θ	32.61	36.52/355.34					
Co_3S_4	d	2.83_x	1.67_8	2.36_7				
	2θ	31.67	54.98	38.13				
$CoSO_4$	d	3.53_x	2.61_7	2.65_7				
	2θ	25.23	34.36	33.83				
$CoSO_4.7H_2O$	d	4.87_x	3.76_8	4.82_6				
	2θ	18.22	23.66	18.41				
$CoSO_4.4H_2O$	d	4.46_x	5.44_9	3.94_5				
	2θ	19.91	16.29	22.57				
$CoSO_4.6H_2O$	d	4.38_x	4.02_6	5.45_3				
	2θ	20.27	22.11	16.26				
Co_4S_3	d	1.81_x	1.98_6	4.08_3				
	2θ	50.42	45.83	21.8				
Co_4S_3	d	1.76_x	2.99_7	2.28_7	1.01_x	1.91_7	1.30_7	1.24_7	1.15_7
	2θ	51.96	29.88	39.52	99.52	47.62	72.75	76.89	84.20
Co_4S_3	d	1.76_x	1.69_9	1.94_x	1.01_g	1.03_x	1.27_9	1.12_9	2.54_8
	2θ	51.96	54.29	46.83	99.52	96.93	74.76	87.01	35.34
Co_4S_3	d	1.69_9	1.94_x	1.76_x	1.01_g	1.03_x	1.27_9	1.12_9	2.54_8
	2θ	54.29	46.83	51.96	99.52	96.93	74.76	87.01	35.34
$(Co,Fe,Ni)_9S_8$	d	1.76_x	1.92_8	3.01_x	5.75_6	2.88_6	1.02_6	2.29_5	1.30_5
	2θ	51.96	47.35	14.84	15.41	31.06	98.20	39.35	72.75
Co_6S_5	d	1.76_x	3.00_8	1.91_8	1.01_g	1.29_8	1.15_8	1.04_8	2.28_7
	2θ	51.96	29.78	47.61	99.52	73.41	84.20	95.69	39.53
Co_9S_6	d	1.76_x	2.99_6	1.92_2	1.01_x	1.29_4	1.24_4	1.15_4	1.04_4
	2θ	51.96	29.89	47.35	99.52	73.41	76.89	84.20	95.69
Al	d	2.34_x	2.02_5	1.22_2					
	2θ	38.48	44.88	78.39					

REFERENCES

1. Royal Commission on Environmental Pollution, Tenth Report, 1984, HMSO.

2. Central Electricity Generating Board, 1986, Video *Acid Rain*.

3. Fry, G., I. Muniz and A. Semb, 1986, *New Scientist, 106,* (1501), 46.

4. Liemkuehler, J. Ger. Offen. DE 3,335,947 (C1 B01D53/34) 11 Apr 1985, Appl. 04 Oct 1983, 15 pp.

5. Mitsubishi Heavy Industries Ltd., Jpn Kokai Tokkyo Koho JP 60 78,622 [85 78,622] (C1 B01D53/34) 04 May 1985, Appl 83/186961 07 Oct. 1983 6 pp.

6. Margraf, A. Ger. Offen. DE 3,341,689 (C1 B01D53/34) 30 May 1985, Appl 18 Nov 1983 5 pp.

7. Krigmont, H.V., H.H. Haaland; H.W. Spencer III; J.L. Stern and R.J. Trisconi GER. DE 3,429,221 (C1 B01D53/34) 18 Apr 1985, US Appl. 537,125 29 Sep. 1983 22 pp.

8. Cross, M. 1984, *New Scientist, 104,* (1424), 6.

9. Sis, L.B., G.P. Wirtz and S.C. Sorenson, 1973, *J. Appl. Phys., 44,* 5553.

10. Happel, J., M.A. Hnatow, L. Bajars and M. Kundrath, 1975, *Ind. Eng. Chem., Prod. Res. Dev., 14,* 154.

11. Voorhoeve, R.J.H., J.P. Remeika and L.E. Trimble,1955 in *The Catalytic Chemistry of Nitrogen Oxides,* Eds. Klimisch, R.L. and J.G. Larson, Plenum, New York.

12. Hibbert, D.B. and A.C.C. Tseung, 1979, *J. Chem. Biotechnol., 29,* 713.

13. Vondrák, J. and L. Doležal, 1984, *Electrochemica Acta., 29,* 477.

14. Iehisha, N., K. Fukaya, K. Matsuo, N. Horiuchi and N. Karute, 1986, *J. Appl. Phys., 59,* 317.

15. Voorhoeve, R.J.H., D.W. Johnson, J.P. Remeika and P.K. Gallagher, 1977, *Science, 195,* 827.

16. Askham, F., I. Fankuchen and R.J. Ward, 1950 *J. Am. Chem. Soc., 72,* 3799.

17. Yamazoe, N., Y. Teraoka and T. Seimyama, 1981, *Chem. Lett.,* 1767.

18. Jonker, G.H. and J.H. van Santen, 1953, *Physica, 19,* 120.

19. Goodenough, J.B., 1966, *J. Appl. Phys., 37,* 1415.

20. Yakel, H.L., 1955, *Acta. Crystallogr., 8,* 394.

21. Gai, P.L. and C.N.R. Rao, 1975, *Mater. Res. Bull., 10,* 787.

22. Sieyama, T., N. Yamazoe and K. Eguchi, 1985, *Ind. Eng. Chem. Prod. Res. Dev., 24,* 19.

23. George, S. and B. Viswanathan, 1983, *React. Kinet. Catal. Lett., 22,* 411.

24. Nakamura, T., M. Misono and Y. Yoneda, 1981, *Chem. Lett.,* 1589.

25. Misono, M. and T. Nitadori, 1985, in *Adsorption and Catalysis on Oxide Surfaces,* Studies in Surface Science and Catalysis 21, Eds. Che, M. and G.C. Bond, Elsevier, Amsterdam.

26. Tseung, A.C.C., S. Saigal and H.L. Bevan, 1974, Final Report, Research Grant Report, SRC, SRC Ref. B/SR/9426.

27. Viswanathan, B. and S. George, 1984, *Ind. J. Technol., 22,* 348.

28. Iwamoto, M., Y. Yuda, N. Yamazoe and T. Seiyama, 1978, *J. Phys. Chem., 82,* 2564.

29. Nakamura, T., M. Misono, T. Uchijima and Y. Yoneda, 1980, *Nippon Kagaku Kaishi, 11,* 1679.

30. Nakamura, T., M. Misono and Y. Yoneda, 1983, *J. Catal., 83,* 151.

31. Nakamura, T., M. Misono, and Y. Yoneda, 1982, *Bull. Chem. Soc. Jpn., 55,* 394.

32. Voorhoeve, R.J.H., J.P. Remeika, P.E. Freeland and B.T. Matthias, 1972, *Science, 177,* 353.

33. Tascon, J.M.D. and L. Gonzalez-Tejuca, 1980, *Z. Phys. Chem.* (Weisbaden), *121,* 63.

34. Ihava Chemical Industries Ltd. Patent No. 2 146 664 France 6 Apr 1973 - in Ref. 12.

35. Bazes, J.G.I., L.S. Caretto and K. Nobe, 1975, *Ind. Eng. Chem. Prod. Res. Dev., 14,* 264.

36. Voorhoeve, R.J.H., J.P. Remeika and L.E. Trimble, 1976, *Annals New York Academy of Sciences, 272,* 3.

37. Sorenson, S.G., J.A. Wronkiewicz, L.B. Sis and G.P. Wirtz, 1974, *Amer. Ceram. Soc. Bull., 53,* 446.

38. Mars, P. and D.W. van Krevelen, 1954, *Chem. Eng. Sci., 3,* 41.

39. Lauder, A. US Patent No. 3 897 367 29 Jul. 1975.

40. Bauerle, G.L., N.T. Thomas and K. Nobe, 1972, *Chem. Eng. J., 4,* 199.

41. Sekido, S., H. Tachibana and Y. Ninomiya, Eur. Pat. Appl. EP 89 199 (C1 B01J23/02) 21 Sep. 1983 JP Appl. 82/39 797 12 Mar 1982, 33 pp.

42. Chauvin, C., C. Michel, D.E. Williams and B.C. Tofield, 1985, *Mater. Chem. Phys., 13,* 197.

43. Teraoka, Y., H.M. Zhang, S. Furukawa and N. Yamazoe, 1985, *Chem. Lett.,* 1743.

44. Yamazoe, N., S. Furukawa, Y. Teraoka and T. Seiyama, 1982, *Chem. Lett.,* 2019.

45. Ishigaki, T., S. Yamauchi, J. Mizusaki and K. Fueki, 1984, *J. Solid State Chem., 54,* 100.

46. Teraoka, Y., H.M. Zhang, S. Furukawa and N. Yamazoe, 1985, *Chem. Lett.*, 1367.

47. Tascon, J.M.D. and L. Gonzalez-Tejuca, 1980, *React. Kinet. Catal. Lett., 15,* 185.

48. Fierro, J.L.G. and L. Gonzalez-Tejuca, 1984, *J. Catal., 87,* 126.

49. Meadowcroft, D.B., 1970, *Nature, 226,* 847.

50. Gallagher, P.K., D.W. Johnson, E.M. Vogel and F. Schrey, 1975, *Mater. Res. Bull., 10,* 623.

51. Johnson, D.W., P.K. Gallagher, G.K. Wertheim and E.M. Vogel, 1977, *J. Catal., 48,* 87.

52. Yao, Y.F.Y., 1975, *J. Catal., 36,* 266.

53. Croat, J.J. and G.G. Tibbetts, 1976, *Science, 194,* 318.

54. Tachibana, K., K. Yamamura and S. Sekido, Jpn. Kokai Tokkyo Koho JP 60,225 643 [85, 225, 643] (Cl B01J23/28) 09 Nov. 1985, Appl. 84/84, 352, 25 Apr 1984 4 pp.

55. Madjavkar, A.M. and R.F. Vogel US US 4363361 (Cl 166-256; B01D53/B4) 14 Dec 1982 Appl. 245 529 19 Mar 1981 7 pp.

56. Tseung, A.C.C. and H.L. Bevan, 1973, *Electroanalytical Chemistry and Interfacial Electrochemistry, 45,* 429.

57. Winter, E.R.S., 1966, *J. Catal., 6,* 35.

58. Tseung, A.C.C., B.S. Hobbs and A.D.S. Tantram, 1970, *Electrochim. Acta., 15,* 473.

59. Matsuki, K. and H. Kamadu, 1986, *Nippon Kagaku Kaishi, 2,* 107.

60. Viswanathan, S. and A. Charkey, 1985, *Proc. Intersoc. 20th Energy Convers. Eng. Conf.,* 2.21-2.26.

61. Kobussen, A.G.C. and G.H.J. Broers, 1981, *J. Electroanal. Chem., Interfacial Electrochem., 126,* 221.

62. Perrault, G.G. and J. Reby, 1978, *C.R. Hebd. Seances Acad. Sci., Ser C, 286,* 67.

63. Dautzenberg, F.M., J.E. Nader and A.J.J. van Ginneken, 1971, *Chem. Eng. Prog., 67,* 86.

64. Querido, R. and W.L. Short, 1973, *Ind. Eng. Chem. Process Des. Develop., 12,* 10.

65. Okay, V.C. and W.L. Short, 1973, *Ind. Eng. Chem. Process Des. Develop., 12,* 291.

66. Mohadi, M.F., The catalytic reduction of sulphur dioxide to elemental sulphur in wet stack gases - unpublished report Dept. Chem. Eng., Univ. of Calgary, Canada.

67. Quinlan, C.W., V.C. Okay and J.R. Kittrell, 1973, *Ind. Eng. Chem. Process Des. Develop., 12,* 107.

68. Hibbert, D.B. and A.C.C.Tseung,1978, *J. Chem. Soc. Faraday Trans.* I, 74, 1981.

69. Quinlan, C.W., V.C. Okay and J.R. Kittrel, 1973, *Ind. Eng. Chem. Process Des. Develop., 12,* 359.

70. Goetz, V.N., A. Sood and J.R. Kittrell, 1974, *Ind. Eng. Chem. Process Des. Develop., 13,* 110.

71. Khalafalla, S.E. and L.A. Haas, 1975, *Adv. in Chem., 139,* 60.

72. Sood, A. and J.R. Kittrell, 1974, *Ind. Eng. Chem. Prod. Res. Develop., 13,* 180.

73. George, Z.M. and R.W. Tower, 1977, *Reprints of the Canadian Symposium on Catalysis, 5,* 492.

74. Tseung, A.C.C. and H.L. Bevan, 1970, *J. Mater. Sci., 5,* 604.

75. Hibbert, D.B. and A.C.C. Tseung, 1979, *J. Mater. Sci., 14,* 2665.

76. Kelly, J., D.B. Hibbert and A.C.C. Tseung, 1978, *J. Mater. Sci., 13,* 1053.

77. Micromeritics Surface Area Analyser - Instruction Manual, 1979, Micromeritics Instrument Corporation, Norcross, Georgia.

78. Brunauer, S., P.H. Emmett and E. Teller, 1938, *J. Am. Chem. Soc., 60,* 309.

79. Atkins, P.W., 1978, *Physical Chemistry,* Oxford University Press, Oxford.

80. Selected Powder Diffraction Data for Minerals, 1974, 1st Edition, Joint Committee on Powder Diffraction Standards, Ed. L.G. Berry Pennsylvania.

81. Wagner, C.D., W.M. Riggs, L.E. Davis and J.F. Moulder Ed. G.E. Muilenberg, 1978, Handbook of X-ray Photoelectron Spectroscopy, Perkin Elmer Corp. Minnesota.

82. Adams, J.Q., S.W. Nicksic and J.R. Thomas, 1966, *J. Chem. Phys., 45*, 654.

83. Bond, G.C., 1974, *Heterogeneous Catalysis Principles and Applications*, Oxford Chemistry Series, Clarendon Press, Oxford.

84. Hibbert, D.B. and A.C.C. Tseung, Unpublished Data.

85. Sales, K., Private Communication.

86. Chemical Rubber Company, 1985-6, Handbook of Chemistry and Physics 66th Edition, C.R.C. Press, Cleveland Ohio.

87. Buffat, B., G. Demazeau, M. Pouchard, J.M. Dance and P. Hagenmuller, 1983, *J. Solid State Chem., 50*, 33.

88. Townsend, M.G. and O.F. Hill, 1965,*Trans. Faraday Soc., 61*, 2597 - in Ref. 87.

89. Hahn, H. and V. Mutschke, 1956, *Z. anorg. Chem. 288*, 269.

90. Clearfield, A., 1963, *Acta. Crystallogr., 16*, 135.

91. Gardner, R.A., M. Vlasse and A. Wold, 1967, *Proc. Second International Conf. of Solid Compounds of Transition Elements*, Enschende, Netherland p.64.

92. Takahashi, T., T. Oka, O. Yamada and K. Ametani, 1971, *Mater. Res. Bull. 6* 173.

93. Trotman-Dickenson, A.F. (Ed.) 1973, *Comprehensive Inorganic Chemistry, 2,* Pergamon Press, Oxford.

94. Raccah, P.M. and J.B. Goodenough, 1968, *J. Appl. Phys., 39,* 1209.

95. Arakawa, T., K. Hiroshiand S. Jiro, 1985, *J. Mater. Sci., 20,* 1207.

96. Voorhoeve, R.J.H., L.E. Trimble, S. Nakajima and E. Banks, 1982, in *Catalysis Under Transient Conditions,* A.C.S. Symposium Series 178, Eds. Bell, A.T. and L.L. Hegedus.

97. Hayward, D.O. and B.M.W. Trapnell, 1964, *Chemisorption* Butterworths, London.

98. Cotton, F.A. and G. Wilkinson, 1980, Advanced Inorganic Chemistry. A Comprehensive Text, John Wiley and Sons, New York.

99. Creighton, J.R. and J.M. White in *Catalysis Under Transient Conditions,* A.C.S. Symposium Series 178, Eds. Bell, A.T. and L.L. Hegedus.

100. Arakawa, T., N. Ohara and J. Shiokawa, 1984, *Chem. Lett.* 1467.

101. Watanabe, H.J., 1957, *J. Phys. Soc. Japan, 12,* 515 in Goodenough, J.B., 1958, *J. Phys. Chem. Solids, 6,* 287.

102. Trotman-Dickenson, A.F. (Ed.), 1973, *Comprehensive Inorganic Chemistry, 1,* Pergamon Press, Oxford.

103. Voorhoeve, R.J.H., J.P. Remerka, L.E. Trimble, A.S. Cooper, F.J. Disalvo and P.K. Gallagher, 1975, *J. Solid State Chem., 14,* 395.

104. Greenwood, N.N. and A. Earnshaw, 1984, *Chemistry of the Elements,* Pergamon Press, Oxford.

105. Durrant, P.J. and B. Durrant, 1970, *Introduction to Advanced Inorganic Chemistry,* Longman, London.

106. George, S. and B. Viswanathan, 1983, *J. Colloid. Interface. Sci. 95,* 322.

107. Kelly, J., Private Communication.

108. Khalafalla, S.E. and L.A. Haas, 1972, *J. Catal., 24,* 121.

109. Seo, G., S. Kwon and H. Park, 1984, *Hwahak Konghak, 22,* 141.

110. Seo, G., S. Kwon, G. Lim and C. Cho, 1984, *Hwahak Konghak, 22,* 161.

111. Trotman-Dickenson, A.F. (Ed.), 1973, *Comprehensive Inorganic Chemistry, 3,* Pergamon Press, Oxford.

112. Goodenough, J.B., 1958, *J. Phys. Chem. Solids, 6,* 287.

113. Weisser, O., 1962, *Int. Chem. Eng., 56,* 1222.

114. Weisser, O., and S. Landas, 1973, *Sulphide Catalysts, their Properties and Applications,* Pergamon, New York.

115. Grange, P., 1980, *Catal. Rev. Sci. Eng., 21,* 135.

116. Furimsky, E. 1980, *Catal. Rev. Sci. Eng., 22,* 371.